AD_____

Award Number: DAMD17-98-1-8614

TITLE: Mechanisms of Virus-Induced Neural Cell Death

PRINCIPAL INVESTIGATOR: Kenneth L. Tyler, M.D.

CONTRACTING ORGANIZATION: University of Colorado Health Sciences Center
Denver, Colorado 80262

REPORT DATE: September 2002

TYPE OF REPORT: Annual

PREPARED FOR: U.S. Army Medical Research and Materiel Command
Fort Detrick, Maryland 21702-5012

DISTRIBUTION STATEMENT: Approved for Public Release;
Distribution Unlimited

REPORT DOCUMENTATION PAGE

Form Approved
OMB No. 074-0188

1. AGENCY USE ONLY (Leave blank)	2. REPORT DATE	3. REPORT TYPE AND DATES COVERED
	September 2002	Annual (15 Aug 01 -14 Aug 02)

4. TITLE AND SUBTITLE
Mechanisms of Virus-Induced Neural Cell Death

5. FUNDING NUMBERS
DAMD17-98-1-8614

6. AUTHOR(S):
Kenneth L. Tyler, M.D.

7. PERFORMING ORGANIZATION NAME(S) AND ADDRESS(ES)
University of Colorado Health Sciences Center
Denver, Colorado 80262

E-Mail:
Ken.Tyler@UCHSC.edu

8. PERFORMING ORGANIZATION REPORT NUMBER

9. SPONSORING / MONITORING AGENCY NAME(S) AND ADDRESS(ES)
U.S. Army Medical Research and Materiel Command
Fort Detrick, Maryland 21702-5012

10. SPONSORING / MONITORING AGENCY REPORT NUMBER

11. SUPPLEMENTARY NOTES

12a. DISTRIBUTION / AVAILABILITY STATEMENT
Approved for Public Release; Distribution Unlimited

12b. DISTRIBUTION CODE

13. Abstract

Virtually all known neurotropic viruses are capable of killing infected cells by inducing a specific pattern of cell death known as apoptosis, yet the mechanisms by which this occurs and its relevance to human disease remain largely unknown. We have shown that apoptosis is an important feature of human CNS viral infections including herpes simplex virus and cytomegalovirus encephalitis, and PML. We have used reovirus infection of cultured cells and animals as an experimental model system to explore mechanisms of apoptosis, and the effects of perturbing apoptosis on viral pathogenesis. Reovirus apoptosis is characterized by involvement of death receptors and their ligands and is associated with sequential activation of caspase cascades. In non-neuronal cells apoptosis requires augmentation by mitochondrial pro-apoptotic factors including cytochrome *c* and Smac/DIABLO for its full expression, however in neurons the mitochondrial pathway appears to be activated only at late times post-infection and less robustly than in non-neuronal cells. Infection is also associated with selective activation of mitogen activated protein kinase cascades and the resulting up-regulation of specific sets of transcription factors and their associated genes. Studies are currently underway to investigate the effects both in vitro and in vivo of inhibiting specific pathways involved in reovirus-induced apoptosis and testing the efficacy of these interventions as potential novel strategies for anti-viral therapy.

14. SUBJECT TERMS
virus, encephalitis, apoptosis, cell death, neurons

15. NUMBER OF PAGES
123

16. PRICE CODE

17. SECURITY CLASSIFICATION OF REPORT	18. SECURITY CLASSIFICATION OF THIS PAGE	19. SECURITY CLASSIFICATION OF ABSTRACT	20. LIMITATION OF ABSTRACT
Unclassified	Unclassified	Unclassified	Unlimited

Table of Contents

INTRODUCTION (Subject, Purpose, Scope of the Research)

The clinical manifestations of viral infection result from the capacity of viruses to damage or kill cells in different organs. Two distinct patterns of cell death, necrosis and apoptosis can be distinguished based on a variety of biochemical and morphological criteria. Apoptotic cell death is characterized by diminution in cell size, membrane blebbing, and compaction, margination and fragmentation of nuclear DNA. DNA fragmentation occurs predominantly at internucleosomal regions resulting in the generation of pathognomonic DNA 'ladders' when DNA from apoptotic cells is subjected to agarose gel electrophoresis.

Most apoptotic processes are triggered by the activation of caspases, a family of cellular cysteinyl proteases. Caspases can be hierarchically ordered into initiator enzymes which trigger the proteolytic activation of downstream effector enzymes. Effector caspases in turn act on a variety of cellular substrates to induce the morphological changes characteristic of apoptosis. Individual initiator caspases are associated with different cellular organelles involved in extrinsic or intrinsic pathways of cell death. In the extrinsic pathway, death is mediated by the binding of apoptosis inducing ligands such as TRAIL, TNF, or FasL to their cognate cell surface "death receptors". This binding triggers the activation of death-receptor associated initiator caspases including caspase 8 and 10 through a death-inducing signal complex (DISC). Intrinsic death signals appear to act predominantly through their effect on either the mitochondrion, or the Golgi/ER system. Mitochondrial death signals result in the release of a variety of pro-apoptotic factors including cyctochrome *c,* AIF, and Smac/DIABLO. Although the actions of mitochondrial pro-apoptotic factors are diverse, two important pathways

include apoptosome-mediated activation of the initiator caspase 9 triggered by cytosolic release of cytochrome *c,* and potentiation of caspase activity by the inhibition of cellular inhibitor of apoptosis proteins (IAPs) mediated by their binding to Smac/DIABLO. The subject and purpose of this research project is to study the cellular mechanisms by which viruses induce apoptotic cell death.

PROGRESS REPORT

This is the fourth annual progress report on this research project. Seventeen papers have been published or accepted for publication in 2001-2002 (see Reportable Outcomes). Reprints of all published papers have been included as an appendix. The technical reporting requirements for this grant specify that journal publications can be substituted for detailed descriptions of specific aspects of the research. However, to facilitate review of this report, we have also briefly summarized the key research findings in these papers in the text. Reference numbers in text refer to papers listed in Reportable Outcomes. Accomplishments are reviewed below and keyed to the specific aims/statement of work (SOW) as outlined in the original research application and subsequent expansions.

Original SOW 1: Is apoptosis a general feature of human viral encephalitis?

Bringing progress on this aim up to the level of accomplishment achieved on other components of the SOW was a major priority during this reporting period. We have two papers in press in ***Journal of Infectious Disease*** and ***Archives of Neurology*** (13,14) directly related to this aim, and three additional papers published or in press in ***Brain Pathology, Journal of Clinical Virology,*** and ***Annals of Neurology*** (4, 10, 15) related

to additional studies performed as part of our characterization of this material. We initially began with studies of apoptosis in brain tissue of patients with herpes simplex virus (HSV) and cytomegalovirus (CMV) encephalitis (13). These two infections were initially selected because HSV encephalitis represents the most common cause of severe sporadic focal encephalitis in the U.S., and CMV encephalitis is the most common congenital neurological infection in humans. We have shown in both cases that apoptosis is an important feature of encephalitis caused by these viruses, that it occurs almost exclusively in area of viral infection, and that it is present only during the acute phase of infection, and not in long-term survivors of acute infection. Apoptosis could be detected both in virally infected cells (direct apoptosis) and in uninfected cells in close proximity to infected cells (bystander apoptosis). We subsequently expanded our studies to examine apoptosis in brain tissue from patients with progressive multifocal leukoencephalopathy (PML). PML has become one of the most important opportunistic viral CNS infections, due largely to its prevalence in patients with AIDS. We found that apoptosis occurred almost exclusively in JC virus-infected oligodendrocytes at the periphery of demyelinating lesions in PML. Apoptosis was not detected in the 'bizarre' astrocytes that are characteristic of PML, nor in neurons. This result is consistent with the fact that JCV infection in astrocytes is abortive (non-productive) and that the virus fails to infect neurons. These studies (13, 14) represent the first demonstration that apoptosis occurs in the CNS in these key human viral encephalitides, and the first demonstration that apoptosis is an important mechanism of CNS injury in viral infections other than HIV.

An essential prelude to these studies was the accurate characterization of diagnosis in cases selected for further study. Our experience obtaining and characterizing

this material lead to two additional publications (4,10) as well as a third study describing the use of quantitative PCR to categorize different forms of CNS infection caused by Epstein-Barr virus, a related herpesvirus (15).

Expanded SOW Aim 1.1: Cellular apoptotic pathways activated in human viral apoptosis.

We have already initiated these studies, which essentially involve immunohistochemical (IHC) determination of which caspases are activated in brain tissue inn human HSV and CMV encephalitis. We have shown that activated caspase 3 can be detected in areas of apoptosis in brain tissues from patients with CMV and HSV encephalitis, and correlated theses results with detection of apoptosis by TUNEL and the presence of inflammatory cells (using CD3 as a marker) (13, 14).

Expanded SOW Aim 1.2: Examine apoptotic pathways and the effects of inhibiting apoptosis in a murine encephalitis model.

In previously reported work supported by this grant we have shown that apoptosis occurs in the CNS in a murine model of reovirus-induced apoptosis (Oberhaus et al. J. Virol. 71:2100-2106, 1997). We have also shown that apoptosis in the heart can be prevented by the administration of calpain inhibitors (1). These studies form the basis for this expansion of the original SOW. We have now extended our studies of CNS apoptosis to show that we can detect activated caspase 3 in apoptotic cells in the murine CNS, and have used co-labeling to correlate infected (antigen positive) and apoptotic cells, and to identify the predominant apoptotic cell type as neurons (11). Having established the basic features of this model, we are now testing the effects of treating mice with a cell permeable pan-caspase inhibitor, and are examining the pathogenesis of reovirus

encephalitis in caspase 3 deficient mice (courtesy of Dr. Richard Flavell at Yale University).

Expanded SOW Aim 1.3: Examine changes in gene expression in a murine model of CNS encephalitis in which apoptotic injury is critical to pathogenesis. In work supported by this grant, we have used large scale oligonucleotide arrays (Affymetrix GeneChips) to examine changes in the expression of mRNAs for cell cycle regulatory genes following reovirus-infected HEK cells (8). We are currently analyzing changes in expression of mRNAs for apoptosis-related genes. We are also analyzing the transcription factor requirements for individual virus-regulated genes (see below Expanded SOW 2.3). We believe that these studies will provide the conceptual framework for the more complex analysis that is required for the brain tissue studies.

Original SOW 2.0: Is the ceramide/sphingomyelin pathway involved in reovirus-induced apoptosis? As noted in our previous progress reports this aim was expanded based on work accomplished to identify cellular pathways involved in reovirus-induced apoptosis. Accomplishments are now discussed under the expanded SOW objectives.

Expanded SOW 2.1 & 2.2: Identify cellular pathways leading to the activation of NF-κB and JNK/c-JUN in reovirus-infected cells.

We have previously shown in work supported by this grant that reovirus infection is associated with the activation of NF-κB (Connolly et al., J. Virol. 74:2981-2989, 2000). We have recently shown that reovirus infection also leads to the selective activation of mitogen activated protein kinase pathways including both the ERK and JNK pathways (5). ERK activation is a transient early event induced by both the prototype

reovirus serotype 1 (T1L) and serotype 3 (T3D) strains. By contrast, JNK activation occurs predominantly with reovirus T3D rather than T1L. We have used reassortant reoviruses (T1L x T3D) to identify the reovirus S1 gene as the primary determinant of the capacity of reoviruses to activate JNK. We have also shown that JNK activation is associated with activation of the JNK-dependent transcription factor c-Jun, and that there is a significant correlation between the capacity of reoviruses to activate the JNK/c-Jun pathway and their capacity to induce apoptosis (5). We have recently begun to examine reovirus-induced apoptosis in mouse embryo fibroblasts (MEFs) derived from mice with targeted gene disruptions in individual JNK isoforms. We have also begun studies of the effects on apoptosis in both HEK cells and primary neuronal cultures of inhibiting JNK activation with pharmacologic inhibitors and through use of an adenovirus vector expressing a DN-c-Jun.

Expanded SOW 2.3: NF-κB and c-Jun regulated genes involved in apoptosis

In collaboration with Dr. Gary Johnson in the UCHSC Department of Pharmacology and UCHSC Cancer Center and Dr. Imran Shah in the Bioinformatics Group of the Gene Expression Core Facility at UCHSC, we are trying to determine whether we can identify patterns of transcriptional regulation that might provide a common theme for the induction of genes following reovirus infection. This study involves (a) identifying all genes up-regulated following reovirus infection in HEK cells (done), (b) using GenBank (www.ncbi.nlm.nih.gov) and other sources to obtain ~1000 kb of nucleotide sequence upstream of the initial start codon of these reovirus-regulated genes (done), (c) using TRANSFAC (http://transfac.gbf.de/TRANSFAC) a transcription factor database, and TRANSPATH (http://193.175.244.148/) a signal transduction pathway

database and other databases containing information about promoter binding sequences to identify the pattern and order of transcription factor binding sites in genes up-regulated following reovirus infection compared to non-altered control genes (in progress). These studies when completed should enable us to identify key transcription factor motifs involved in reovirus-induced alterations in host cell gene expression.

Expanded SOW 2.4: Identify the role of the mitochondrion in reovirius-induced apoptosis. We have recently shown that reovirus infection in HEK cells is associated with release of mitochondrial pro-apoptotic factors including cytochrome *c* (9) and Smac/DIABLO (12). Cytochrome *c* forms part of the apoptosome involved in activation of the mitochondrial-related initiator caspase, caspase 9. We have also shown that caspase 9 is activated following reovirus infection (9, 12). Cytochrome *c* is not the only mitochondrial pro-apoptotic factor release following reovirus infection. We have recently shown that infection is also associated with the release of Smac/DIABLO. This protein facilitates apoptosis by binding to cellular inhibitor of apoptosis (IAP) proteins that act to inhibit caspase activation. Binding of Smac/DIABLO to IAPs prevents their inhibition of caspase activity, thereby augmenting apoptosis. We have shown that, consistent with the release of Smac/DIABLO, reovirus infection is associated with a selective down-regulation of specific cellular IAPs including XIAP, cIAP1, and survivin (12). We have also shown, using cells expressing a dominant negative form of caspase 9, that is likely Smac/DIABLO mediated events rather than caspase 9 activation that plays a critical role in augmenting reovirus-induced apoptosis. We have also shown, using cells stably expressing Bcl-2, that in HEK cells mitochondrial augmentation is critical for the full expression of reovirus-induced apoptosis. Apoptosis is dramatically inhibited in cells

expressing Bcl-2, and this inhibition is associated with reduction in the release of mitochondrial pro-apoptotic factors including cytochrome *c* and Smac/DIABLO and in inhibition of associated downstream events including caspase 9 activation and down-regulation of IAPs (9, 12).

Interestingly, our studies of reovirus-induced apoptosis in primary neuronal cultures suggest that mitochondrial pathways may be less important in these cells then in non-neuronal cells (see below, Expanded SOW 3.1) (11).

Expanded SOW 2.5: Identify the mechanism by which reovirus infection sensitizes cells to killing by TRAIL. We have previously shown in work supported by this grant, that reovirus-induced apoptosis in non-neuronal cells involves the apoptosis-inducing ligand TRAIL and its associated death receptors, DR4 and DR5 (Clarke et al., J Virol 74:8135-8139, 2000). We have recently extended these observations to show that reovirus-induced killing of a wide variety of human cervical, breast, and lung cancer derived cell lines is due to apoptosis, and is also mediated by TRAIL (6). Reovirus infection and TRAIL act synergistically to induce apoptosis, and reovirus infection sensitizes cells to killing by TRAIL. As part of these studies we have established that up-regulation of both caspase 8 and activation of the transcription-factor NF-κB are required for this process (6,7). We are currently in the process of investigating the mechanism for the increased activity, including investigation of the levels of cellular IAPs (whose down-regulation could enhance caspase 8 activity), and the potential role of mitochondrial factors in this process.

Original SOW 3.0: Is reovirus apoptosis associated with aberrant regulation of cell cycle progression and does this dysregulation occur in post-mitotic neurons?

We have previously shown in work supported by this grant that reovirus infection is associated with dysregulation of cell cycle, and the induction of G2/M cell cycle arrest (Poggioli et al., J. Virol. 74:9562-9570, 2000). We have recently expanded these studies by investigating the effects of reovirus infection on key G2/M checkpoint regulatory kinases. We have shown that infection is associated with inhibition of the G2/M checkpoint kinase $p34^{cdc2}$, and that this in turn may result from up-regulation of $p34^{cdc2}$ kinases including chk1 and wee1, and inhibition of the activity of the $p34^{cdc2}$ phosphatase, CDC25C (3). We have also used oligonucleotide microarrays to identify the set of genes involved in cell cycle regulation whose expression is either up- or down-regulated following reovirus infection (8) (see Expanded SOW 1.3). The studies supported by this grant have now made reovirus-induced cell G2/M arrest one of the best characterized models of virus-induced cell cycle perturbation.

Expanded SOW 3.1: Evaluate apoptotic pathways in both primary and continuous neuronal cell lines.

We have examined apoptotic pathways activated following reovirus infection in both mouse neuroblastoma (NB41A3) and primary cortical neuronal cultures (11). The pathways we have identified to date in neuronal cultures are similar too but not identical to those we have identified in non-neuronal cells (see above and refs. 9, 12). In Both neurons and non-neuronal cultures apoptosis involves cell surface death receptors. However, in neurons, in contrast to HEK cells, we have evidence that both TNF and FasL in addition to TRAIL may play a role in apoptosis (11). In all cell types examined to date, infection is followed by caspase 8 activation which can be detected using antibodies specific for the activated form of caspase 8 (11). In HEK cells, mitochondrial pro-

apoptotic factors play a critical role in augmenting death-receptor initiated apoptosis (see ref. 9, 12). By contrast, in neurons release of mitochondrial cytochrome *c* into the cytoplasm occurs only at low levels at late times following infection (11). Consistent with this result, caspase 9 activation occurs at only low levels, and peptide inhibitors with relative specificity for caspase 9 (Ac-LEHD-CHO) are less effective then caspase 8 (Ac-IETD-CHO), caspase 3 (Ac-DEVD-CHO), or pan-caspase inhibitors (Ac-ZVAD-CHO) in blocking reovirus-induced neuronal apoptosis.

Expanded SOW 3.2: Identify the role of reovirus σ1s protein in reovirus-induced cell cycle dysregulation.

We have recently found that the reovirus σ1s protein contains a classical nuclear localization signal (NLS). We have created a plasmid that allows for expression of σ1s coupled both to green fluorescent protein (GFP) and to the protein pyruvate kinase (PK). Because its size exceeds the limits for passive diffusion into the nucleus, the transfected fusion protein GFP-PK does not enter the nucleus unless it is actively transported. We have shown that coupling the σ1s protein to this construct (σ1s-GFP-PK) allows for nuclear transport, establishing that σ1s contains a functional NLS. We have subsequently generated a construct in which the putative σ1s NLS, encompassing a highly arginine and lysine (KR) rich set of amino acids at positions #14-21, has been deleted. The resulting construct $\sigma 1s_{\Delta NLS}$-GF-PK) is no longer transported to the nucleus. This indicates that region of σ1s between AAs 14-21 is necessary for the nuclear localization of σ1s.

The σ1s protein also contains a putative nuclear export sequence (NES) encompassing AAs 75-84. We have recently created a deletion encompassing this region. Initial studies suggest that the $\sigma 1s_{\Delta NES}$-GFP-PK construct remains localized to the

nucleus of transfected cells, suggesting that the NES in σ1s, like the NLS, is functional.

Studies are currently underway to identify the nuclear import and export proteins and mechanisms utilized by σ1s. Studies are also underway to transfect cells with σ1s-GFP, identify and sort transfected cells by FACS based on their expression of GFP, and then analyze specific biological perturbations such as cell cycle arrest in this population of cells.

Reviews covering work encompassed in many parts of the SOW have been published or are currently in press in ***Trends in Microbiology*** (2), ***Virology*** (16) and ***Apoptosis*** (17).

KEY RESEARCH ACCOMPLISHMENTS:

SOW 1

*Apoptosis is an important feature of CNS injury in human CNS viral infections including herpes simplex virus and cytomegalovirus encephalitis and progressive multifocal leukoencephalopathy (PML).

*Apoptosis in human CNS viral infections is associated with activation of caspase 3

*Apoptosis is a major feature of reovirus-induced encephalitis in mice, and is associated with activation of caspase 3. Apoptosis occurs predominantly in neurons, both those that are virus-infected (direct apoptosis) and in cells in proximity to infected cells (bystander apoptosis).

*Apoptosis is a major mechanism of myocardial injury in an in vivo model of viral myocarditis, is associated with calpain activation, and can be inhibited by treatment of

mice with calpain inhibitor.

SOW 2

*Reovirus infection results in selective activation of mitogen associated protein kinase (MAPK) pathways including the extracellular related kinase (ERK) and c-Jun-N-terminal kinase (JNK) pathways.

* Reovirus activation of JNK is associated with downstream activation of the JNK-dependent transcription factor c-Jun, and this activation correlates with the capacity of viral strains to induce apoptosis.

*Differences in the capacity of reovirus strains to activate JNK are determined by the viral S1 gene.

*Reovirus-induced apoptosis in non-neuronal cells is initiated by death-receptor activation, but requires augmentation by mitochondrial apoptotic pathways for its full expression.

*Reovirus-induced activation of caspase 8 results in the cleavage of the Bcl-2 family protein Bid, and cleaved Bid translocates to the mitochondrion and activates mitochondrial apoptotic pathways.

*Mitochondrial pro-apoptotic factors released following reovirus infection include both cytochrome *c* and Smac/DIABLO but not apoptosis inducing factor (AIF).

*Activation of mitochondrial apoptotic pathways is associated with the subsequent down-regulation of cellular IAPs including XIAP, cIAP1, and survivin and this down-regulation is blocked by stable over-expression of Bcl-2 or DN-FADD.

*Reovirus-induced oncolysis of human cervical, breast, and lung cancer cell lines results from apoptosis induction and is mediated by the apoptosis-inducing ligand TRAIL.

* Reovirus infection can sensitize cancer kills to killing by TRAIL, and this process involves up-regulation of the death-receptor associated initiator caspase, caspase 8.

*TRAIL induced killing of cancer cell lines involves down-regulation of cellular inhibitor of apoptosis proteins (IAPs).

SOW 3

*Reovirus-induced inhibition of cell cycle regulation and induction of G2/M arrest is mediated by the σ1s protein and is associated with inhibition of the key G2/M regulatory kinase $p34^{cdc2}$.

*Reovirus infection results in the selective up-regulation of specific sets of genes involved in the control and regulation of cell cycle progression.

*Reovirus σ1s protein contains functional nuclear localization and nuclear export sequences.

*Reovirus induced apoptosis in neurons involves pathways that are similar to but not identical with those identified in non-neuronal cells. Although both pathways involve death-receptors, release of mitochondrial pro-apoptotic pathways appears to be a later and less robust feature of neuronal apoptosis compared to apoptosis in non-neuronal cells.

REPORTABLE OUTCOMES

Publications (Papers marked with an * are included in the appendix. Other papers listed have been accepted for publication but are currently in manuscript rather than page proof form. Copies of page proofs or reprints of these papers will be included in subsequent annual reports, but can be provided earlier upon request.)

*1. DeBiasi R, Edelstein C, Sherry B, **Tyler KL**. Calpain inhibition protects against virus induced apoptotic myocardial injury J Virol 75:351-361, 2001.

*2. **Tyler KL**, Clarke P, DeBiasi RL, Kominsky D, Poggioli G. Reovirus and the host cell. Trends Microbiol 9:560-564, 2001.

*3. Poggioli GJ, Dermody TS, **Tyler KL**. Reovirus-induced σ1s-dependent G2/M cell cycle arrest is associated with inhibition of $p34^{cdc2}$. J Virol 75:7429-7434, 2001.

*4. DeMasters BK, DeBiasi R, **Tyler KL.** Polymerase chain reaction as a diagnostic adjunct in herpesvirus infections of the nervous system. Brain Pathol.11:452-464, 2001.

*5. Clarke P, Meintzer SM, Widmann C, Johnson GL, **Tyler KL.** Reovirus infection activates JNK-dependent transcription factor c-Jun. J. Virol. 75:11275-11283, 2001.

*6. Clarke P, Meintzer SM, Spalding AC, Johnson GL, **Tyler KL.** Caspase-8 dependent sensitization of cancer cells to TRAIL-induced apoptosis following reovirus infection. Oncogene 20:6910-6919, 2001.

*7. Spalding AC, Jotte RM, Scheinman RI, Geraci MW, Clarke P, Tyler KL, Johnson GL. TRAIL and inhibitors of apoptosis are opposing determinants for NF-κB-dependent, genotoxin-induced apoptosis of cancer cells. Oncogene 21:260-271, 2002.

*8. Poggioli GJ, DeBiasi RL, Bickel, R., Bickel R, Jotte R, Spalding A, Johnson GL, **Tyler KL**. Reovirus-induced alterations in gene expression related to cell cycle regulation. J Virol. 76:2585-2594, 2002.

*9. Kominsky D, Bickel RJ, **Tyler KL**. Reovirus induced apoptosis requires both death-receptor- and mitochondrial-mediated caspase-dependent pathways of cell death. Cell Death and Differentiation 9:926-933, 2002.

*10. DeBiasi RL, Kleinschmidt-DeMasters BK, Weinberg A, **Tyler KL.** Use of PCR for the diagnosis of herpesvirus infections of the central nervous system. J Clin Virol 25:S5-S11, 2002.

11. Richardson-Burns S, **Tyler KL.** Reovirus induced neuronal apoptosis is mediated by caspase 3 and is associated with the activation of death receptors. J Neurovirol (MS# 02-235, in press), 2002.

12. Kominsky D, Bickel R, **Tyler KL.** Reovirus induced apoptosis requires mitochondrial release of Smac/DIABLO and involves reduction of cellular inhibitor of apoptosis protein levels. J. Virol. (MS# JVI 912-02, in press, 2002).

13. DeBiasi RL, Kleinschmidt-DeMasters BK, Richardson-Burns S, **Tyler KL**. Herpes simplex virus and cytomegalovirus encephalitis in humans are associated with CNS apoptosis. J Infect Dis (MS#02-0541, In Press), 2002.

14. Richardson-Burns S, DeBiasi R, Kleinschmidt-DeMasters BK, **Tyler KL.** Progressive multifocal leukoencephalopathy is associated with apoptosis of infected oligodendrocytes in the CNS of AIDS and non-AIDS patients. Arch Neurol (MS#NOC20215, In Press), 2002.

*15. Weinberg A, Li S, Palmer M, **Tyler KL**. Use of quantitative CSF PCR in the analysis of Epstein-Barr virus infections of the central nervous system. Ann Neurol (MS#200200341, In Press), 2002.

16. Kominsky D, **Tyler KL.** Cellular mechanisms of virus-induced apoptosis. Virology (In press), 2002.

17. Clarke P, DeBiasi RL, Hoyt C, Kominsky D, Meintzer S, Richardson-Burns S, **Tyler KL**. Mechanisms of reovirus-induced apoptosis. Apoptosis (In press, 2002).

Selected Abstracts/Presentations at National and International Meetings

Kominsky D, Bickel R, **Tyler KL**. Reovirus infection induces both extrinsic death receptor- and intrinsic mitochondrial-mediated pathways of apoptosis. American Society for Virology, 20th Annual Meeting, Madison, WI, July 21-5, 2001.

Clarke P, Meintzer SM, Widmann C, Johnson GL, **Tyler KL.** Reovirus infection results in the activation of c-Jun N-terminal kinase (JNK) and the JNK-stimulated transcription factor c-Jun. American Society for Virology, 20th Annual Meeting, Madison, WI, July 21-5, 2001.

DeBiasi RL, Poggioli GJ, Bickel R, Kominsky D, Jotte RM, Johnson GJ, **Tyler KL.** Reovirus infection results in altered transcription of genes related to cell cycle, apoptosis and DNA repair including BRCA-1, GADD45 and regulators of Bcl-2. American Society for Virology, 20th Annual Meeting, Madison, WI, July 21-5, 2001.

Richardson-Burns S, Clarke P, **Tyler KL**. Reovirus infection induces neuronal apoptosis. American Society for Virology, 20th Annual Meeting, Madison, WI, July 21-5, 2001.

Tyler KL, Kominsky D, Richardson-Burns S, Clarke P. Mechanisms of virus-induced cell death. American Neurological Association, 126th Annual Meeting, Chicago, IL, September 30-October 3, 2001.

Richardson-Burns S, **Tyler KL.** Reovirus induces apoptosis in primary neuronal cultures and neuroblastoma-derived cell lines. Society for Neuroscience 31st Annual Meeting, San Diego, CA, Nov. 10-15, 2001.

DeBiasi RL, Sherry B, Johnson G, **Tyler KL.** Apoptotic Signaling in Viral Myocarditis. St. Jude/Pediatric Infectious Disease Society, Pediatric Microbial Research Conference, Nashville, TN Feb 21-23, 2002.

Clarke P, Meintzer S, **Tyler KL.** NF-κB mediates the release of TRAIL from reovirus-infected cells and the onset of virus-induced apoptosis. Keystone Conference: NF-κB: Bench to bedside, Keystone, CO Feb 25-Mar 3, 2002.

DeBiasi RL, Kleinschmidt-DeMasters B, Richardson-Burns S, **Tyler KL**. Human herpes simplex encephalitis is associated with CNS apoptosis. 54th Annual Meeting of the American Academy of Neurology, Denver, CO, April 14-19, 2002.

Richardson-Burns S, Kleinschimdt-DeMasters B, DeBiasi R, **Tyler KL**. Neuronal apoptosis in human herpes simplex and cytomegalovirus encephalitis and progressive multifocal leucoencephalitis. 2002 Annual Meeting of the American Association of Neuropathologists, Denver, CO, June 20-23, 2002.

Richardson-Burns S, Kominsky DJ, **Tyler KL.** Reovirus-induced neuronal apoptosis predominantly involves death receptor rather than mitochondrial-mediated apoptotic pathways. American Society for Virology, 21st Annual Meeting, Lexington, KY July 20-24, 2002.

Clarke P, Meintzer S, **Tyler KL.** Phosphorylation and degradation of IκBα in reovirus-infected cells. American Society for Virology, 21st Annual Meeting, Lexington, KY July 20-24, 2002.

DeBiasi RL, Sherry B, **Tyler KL**. Apoptosis occurs in reovirus-infected primary cardiac myocytes and caspase inhibition is protective *in vitro* and *in vivo*. American Society for Virology, 21st Annual Meeting, Lexington, KY July 20-24, 2002.

Selected Invited Presentations (Kenneth L. Tyler, M.D.)

2001. Gordon Conference: Animal Cells and Viruses. Mechanisms of virus-induced apoptosis in vitro and in vivo: lessons from the reovirus system.

2001. Faculty, Review and Update in Neurobiology for Neurosurgeons, Marine Biological Laboratory, Woods Hole, MA.

2002. Microbiology, Immunology, and Cancer Biology Seminar Series, University of Minnesota: Mechanisms of virus-induced cell death *in vitro* and *in vivo*.

2001.Dept. of Neurology, Dartmouth University Medical School, Neurology/Neurosurgery Grand Rounds

2002. Dept. of Neurology, University of Massachusetts Medical Center Neurology Grand Rounds. Herpes simplex virus infections of the CNS in the PCR era.

2002. Faculty, Course on Neurovirology (Recurrent and chronic meningitis and encephalitis), 53rd Annual Meeting American Academy of Neurology, Denver, CO

2002. Faculty, Infections of the Nervous System (Acute encephalitis), 53rd Annual Meeting American Academy of Neurology, Denver, CO

2002. International Herpes Management Forum (IHMF), CNS Workshop. HSV encephalitis in older children and adults, and Mollaret's meningitis. Denver, CO

CONCLUSIONS

Due in significant part to support provided by this grant, reoviruses have become one of the best understood models of virus-induced apoptosis. Viral genes and proteins involved in induction of apoptosis have been identified. The caspase activation pathways involved in apoptosis have been defined in both neuronal and non-neuronal cells, as has the role of specific mitochondrial pro-apoptotic factors. The capacity of the virus to activate specific MAPK cascades and their associated transcription factors has been characterized, and studies are currently underway to establish the entire network of genes that are up-regulated following viral infection. The importance of apoptosis in a variety of in vivo models of infection including encephalitis and myocarditis has been established, and studies are currently underway to determine whether key apoptotic

pathways identified in vitro are also active in vivo. Targeted interventions that modulate apoptosis and enhance cell survival in vitro are being tested for efficacy as novel anti-viral strategies in vivo. The importance of apoptosis as a mechanism of CNS injury has also been established in a variety of key human viral infections, providing added significance to its study in both cell culture and experimental models of infection.

JOURNAL OF VIROLOGY, Jan. 2001, p. 351–361 Vol. 75, No. 1
0022-538X/01/$04.00+0 DOI: 10.1128/JVI.75.1.351–361.2001

Calpain Inhibition Protects against Virus-Induced Apoptotic Myocardial Injury

ROBERTA L. DEBIASI,[1,2,3] CHARLES L. EDELSTEIN,[4] BARBARA SHERRY,[5] AND KENNETH L. TYLER[2,3,4,6]*

Departments of Pediatric Infectious Diseases,[1] Neurology,[2] Medicine,[4] and Microbiology and Immunology,[6] University of Colorado Health Sciences Center, and Denver Veterans Affairs Medical Center,[3] Denver, Colorado 80262, and Department of Microbiology, College of Veterinary Medicine, North Carolina State University, Raleigh, North Carolina 27606[5]

Received 23 May 2000/Accepted 14 September 2000

Viral myocarditis is an important cause of human morbidity and mortality for which reliable and effective therapy is lacking. Using reovirus strain 8B infection of neonatal mice, a well-characterized experimental model of direct virus-induced myocarditis, we now demonstrate that myocardial injury results from apoptosis. Proteases play a critical role as effectors of apoptosis. The activity of the cysteine protease calpain increases in reovirus-infected myocardiocytes and can be inhibited by the dipeptide alpha-ketoamide calpain inhibitor Z-Leu-aminobutyric acid-CONH(CH_2)3-morpholine (CX295). Treatment of reovirus-infected neonatal mice with CX295 protects them against reovirus myocarditis as documented by (i) a dramatic reduction in histopathologic evidence of myocardial injury, (ii) complete inhibition of apoptotic myocardial cell death as identified by terminal deoxynucleotidyltransferase-mediated dUTP-biotin nick end labeling, (iii) a reduction in serum creatine phosphokinase, and (iv) improved weight gain. These findings are the first evidence for the importance of a calpain-associated pathway of apoptotic cell death in viral disease. Inhibition of apoptotic signaling pathways may be an effective strategy for the treatment of viral disease in general and viral myocarditis in particular.

The mechanisms by which viruses produce cytopathic effects in their host cells are not well understood. Such knowledge is essential to an understanding of viral pathogenesis and development of novel antiviral therapies. Apoptosis is a mechanism of active cell death distinct from necrosis, characterized by DNA fragmentation, cell shrinkage, and membrane blebbing without rupture (26). Apoptosis plays a critical role in many physiologic (28, 74), as well as infectious and noninfectious, pathologic conditions (72). Viruses may either promote or inhibit apoptosis as a strategy to maximize pathogenicity in their hosts (40, 54, 67). Several viruses, including adenovirus, poxviruses, herpesviruses, and human papillomavirus, proliferate and evade host immune responses by interfering with programmed cell death (1, 19, 31, 68). Many other viruses, such as human immunodeficiency virus, human T-cell leukemia virus, influenza virus, measles virus, rubella virus, poliovirus, human herpesvirus 6, Sindbis virus, and reoviruses, cause cytopathic effect by induction of apoptosis in their target cells (11, 14, 21–23, 34, 40, 42, 50, 70).

We have used reovirus-induced apoptosis as an experimental model system to study the viral and cellular mechanisms involved in apoptotic cell death (39). Reoviruses are nonenveloped viruses that contain a genome of segmented, double-stranded RNA. Infection of cultured fibroblasts and epithelial cells with reoviruses induces apoptosis. Reoviral strains differ in the efficiencies with which they induce this cellular response, and these differences are determined by the viral S1 gene (44, 69). Apoptosis also occurs following reovirus infection in vivo and colocalizes with areas of pathologic injury (38, 39). This finding suggests that apoptosis is an important mechanism of tissue damage in reoviral infection.

Reovirus strain 8B is a reassortant reovirus that efficiently produces myocarditis in infected neonatal mice (55, 58). Damage has been shown to be a direct effect of viral infection of myocardiocytes (60). This damage differs from that of several other models of viral myocarditis (such as coxsackievirus and murine cytomegalovirus) in which secondary inflammatory responses, or lymphocyte recognition of viral or self-antigens on myocardial cells, may be the predominant cause of cardiac damage (12, 17, 20, 30, 46). SCID mice infected with reovirus 8B develop myocarditis, and passive transfer of reovirus-specific immune cells is protective, rather than harmful, to 8B-infected mice (58, 60). This finding indicates that immune mechanisms contribute to amelioration rather than induction of reovirus-induced viral injury (60). However, the mechanism by which direct myocardial injury occurs is not well characterized. Since tissue damage occurs by apoptosis in other in vivo models of reoviral infection (38), and apoptosis has been suggested in some models of viral myocarditis (6, 25), we wished to determine if reoviral myocarditis occurs as a result of apoptotic cell injury and, if so, whether manipulation of known signaling pathways preceding apoptosis is protective.

Protease cascades appear to play critical roles as effectors of apoptosis, as with the cysteine proteases caspases and calpain (10, 32, 41, 62, 79). Caspases are the most extensively investigated members of this class of protease and have been implicated in a wide variety of apoptotic models. However, the role of calpain in apoptosis has been recognized recently. Calpain is a calcium-dependent neutral cysteine protease that is ubiqui-

* Corresponding author. Mailing address: Department of Neurology (B-182), University of Colorado Health Sciences Center, 4200 E. 9th Ave., Denver, CO 80262. Phone: (303) 393-2874. Fax: (303) 393-4686. E-mail: Ken.Tyler@UCHSC.edu.

tous in the cytosols of many cell types (35, 63). Calpains have recently been implicated in several models of apoptosis, including dexamethasone-induced thymocyte apoptosis (65), neuronal cell apoptosis (36), neutrophil apoptosis (64), ischemia-induced rat liver apoptosis (27, 61), myonuclear apoptosis in limb-girdle dystrophy (3), and chemical hypoxia-induced apoptosis of rat myocytes (8). We have recently shown that reovirus-induced apoptosis in vitro is preceded by increased cellular calpain activity and is inhibited by two classes of calpain inhibitors (13).

We now show that reovirus 8B-induced myocarditis occurs by apoptosis. Calpain activity increases in cardiomyocytes following infection with reovirus 8B, and calpain inhibition reduces myocardial injury and morbidity in infected mice. This is evidence that interference with apoptotic signaling pathways may prove of benefit as a therapeutic strategy in the treatment of viral infection in general and viral myocarditis in particular.

MATERIALS AND METHODS

Virus. Reovirus 8B is an efficiently myocarditic reovirus that has been previously characterized (58). 8B stocks were subjected to plaque assay three times and passaged twice in mouse L cells prior to use.

Mice. Swiss-Webster (Taconic) mouse litters were housed in individual filter-topped cages in an American Association for Laboratory Animal Care-accredited animal facility. All animal procedures were performed under protocols approved by the appropriate institutional committees.

Mouse inoculations. Two-day-old Swiss-Webster (Taconic) mice were intramuscularly inoculated with 1,000 PFU of 8B reovirus in the left hind limb (20-μl volume). Mock-infected mice received gel saline vehicle inoculation (equal volume) (137 mM NaCl, 0.2 mM $CaCl_2$, 0.8 mM $MgCl_2$, 19 mM H_3BO_3, 0.1 mM $Na_2B_4O_7$, 0.3% gelatin).

Histologic analysis. At 7 days postinfection, mice were sacrificed and hearts were immediately immersed in 10% buffered formalin solution. After being mounted as transverse sections, hearts were embedded in paraffin and sectioned to 6 μm in thickness. For quantification of degree of myocardial injury, hematoxylin- and eosin-stained midcardiac sections (at least six per heart) were examined at a ×125 magnification by light microscopy and scored blindly. Scoring was performed using a previously validated system (58), with scores ranging from 0 to 4 (0, no lesions; 1, one or a few small lesions; 2, many small or a few large lesions; 3, multiple small and large lesions; and 4, massive lesions). Twenty-three to 24 mice were scored from each group.

DNA fragmentation. The presence of internucleosomal DNA cleavage in myocardial tissue was investigated by phenol-chloroform extraction of DNAs from 8B-infected and mock-infected hearts and precipitation in 95% ethyl alcohol. The DNA was then end labeled with 5 μCi of [^{32}P]dGTP using 10 U of terminal transferase (M187; Promega Corporation), resolved by electrophoresis on a 2% agarose gel, fixed in 5% acetic acid–5% methanol, dried, and scanned on a Instant Imager (Packard Instrument Company).

TUNEL. Evaluation of fragmented DNA was performed by terminal deoxynucleotidyltransferase (TdT)-mediated dUTP-biotin nick end labeling (TUNEL), as previously described (38). Paraffin-embedded cardiac midsections were prepared by removing paraffin with xylene and then rehydrating them in 100, 95, and then 70% ethanol solutions. After digestion in proteinase K solution (Boehringer Mannheim) for 30 min at 37°C, slides were pretreated in 0.3% H_2O_2 in phosphate-buffered saline for 15 min at room temperature and then washed. The TdT labeling reaction was carried out under coverslips in a humidified chamber for 1 h at 37°C with TdT and digoxigenin 11-dUTP. (Boehringer Mannheim). The reaction was stopped with SSC (1× SSC is 0.15 M NaCl plus 0.015 M sodium citrate) buffer. After being blocked in 2% bovine serum albumin for 10 min, sections were probed with Vectastain ABC (avidin DH and biotinylated enzyme; Vector Laboratories) for 1 h at room temperature, and then visualized with a diaminobenzadine peroxidase substrate kit (Vector Laboratories). Negative and positive controls were used with all reactions.

Viral-antigen stain. Cardiac midsections were prepared as noted above. Following the hydrogen peroxide incubation, slides were blocked in 2% normal goat serum for 30 min at room temperature. Sections were then incubated in rabbit polyclonal anti-reovirus type 3 Dearing antiserum as the primary antibody (gift of Terence Dermody, Vanderbilt University) at a dilution of 1:1,000 for 1 h at 37°C. Biotinylated goat anti-rabbit antibody was used as the secondary antiserum (1:200 dilution in 2% normal goat serum) for 30 min at 37°C. Sections were probed and visualized as noted above.

Calpain activity in myocytes. The determination of the presence of calpain-specific spectrin (fodrin) breakdown products (150- and 145-kDa doublet) by immunoblotting was used as an assay of calpain activity (36). Mouse primary cardiac myocyte cultures were prepared as previously described (5). Cells were plated at 1.6×10^6 cells/well in 24-well plates and incubated for 48 h. Cells were then infected with reovirus strain 8B (multiplicity of infection [MOI], 20, in Dulbecco modified Eagle medium [DMEM]) or mock infected (DMEM) and then incubated at 37°C. Mock-infected cells were harvested at 48 h. 8B-infected cells were harvested at 24, 48, and 72 h postinfection. Cell lysates were prepared by sonication in lysis buffer (15 mM Tris [pH 7.4], 10 mM EDTA, 0.1% NP-40, 20% glycerol, 50 mM β-mercaptoethanol, 50 μg of pepstatin per ml, 100 μg of leupeptin per ml, 1 mM phenylmethylsulfonyl fluoride), and the cytoplasmic fractions were run on a 7.5% polyacrylamide gel. Protein loading for these gels (25 μg/well) was normalized by protein concentration analysis of cell lysates. Following transfer (15 V overnight), the nitrocellulose membrane was blocked in 5% nonfat dried milk–Tris normal saline for 2 h, probed with anti-fodrin mouse monoclonal antibody (ICN) at a dilution of 1:1,000 for 1.5 h, and then washed. Membranes were then incubated in anti-mouse immunoglobulin G horseradish peroxidase-linked whole antibody (Amersham) at a dilution of 1:1,000, as the secondary antibody. After the membranes were washed, ECL Plus (Amersham) was used for detection.

In additional experiments, primary cardiac myocytes were infected with 8B reovirus (using the method described above) with and without pretreatment in CX295 (100 μM). Cell lysates were prepared and analyzed for calpain activity by immunoblotting as described above.

Specificity of the calpain inhibitor CX295. *Z*-Leu-aminobutyric acid-CONH(CH_2)3-morpholine (CX295) is a dipeptide alpha-ketoamide compound which inhibits calpain at the active site (kindly provided by Gary Rogers at Cortex Pharmaceuticals, Inc.). To determine the efficacy of CX295 as a calpain inhibitor, 10 μg of purified μ-calpain (porcine RBC; Calbiochem) was added to the preferred fluorogenic calpain substrate sucrose-Leu-Tyr-amino-methyl-coumarin (SLY-AMC) in the presence and absence of CX295 (100 μM), as well as in the presence of the pan-caspase inhibitor *Z*-D-DCB (100 μM). The calpain assay was performed as previously described (16). Proteolytic hydrolysis of the substrate by purified calpain liberates the highly fluorescent AMC moiety. Fluorescence at a 380-nm excitation and 460-nm emission was quantified with a Hitachi F2000 spectrophotometer. An AMC standard curve was determined for each experiment. Calpain activity was expressed in picomoles of AMC released per minute of incubation time per microgram of purified calpain.

To determine the specificity of CX295 as a calpain inhibitor, 10 ng of purified caspase 3 (Upstate) was added to the preferred fluorogenic caspase-3 substrate DEVD-AMC in the presence and absence of the pan-caspase inhibitor *Z*-D-DCB (100 μM), as well as CX295 (100 μM). In addition, 57 ng of purified caspase-1 (provided by Nancy Thornberry, Merck) was added to the preferred fluorogenic caspase-1 substrate YVAD-AMC in the presence and absence of *Z*-D-DCB, as well as CX295. The caspase activity assay was performed as previously described (16). Caspase activity was expressed as picomoles of AMC released per minute of incubation time per nanogram of purified caspase. Experiments were all performed in triplicate.

Calpain inhibition in vivo. For calpain inhibition experiments, animals received daily intraperitoneal injections of either active CX295 (70 mg/kg of body weight in a 50-μl volume) or its inactive saline diluent. The first dose was given 30 min prior to infection with 8B virus. A total of six doses were given, at 24-h intervals. Mice were sacrificed at 7 days postinfection.

Viral titer determination. Injected hind limbs and whole hearts were placed in 1 ml of gel saline and immediately frozen at −70°C. After three freeze (−70°C)-thaw (37°C) cycles, the tissues were sonicated approximately 15 to 30 s by using a microtip probe (Heat Systems model XL2020) until a homogenous solution was obtained. The virus suspensions were serially diluted in 10-fold steps in gel saline and placed in duplicate on L-cell monolayers for plaque assay, as previously described (13). Virus titers were expressed as $\log_{10}$ PFU per milliliter.

Serum CPK. Following decapitation of mice, whole blood was collected from individual mice into plasma separator tubes with lithium heparin to prevent coagulation (Microtainer; Becton Dickinson). Samples were collected from 8B-infected mice treated with CX295 (n = 20), 8B-infected mice treated with the inactive diluent (n = 20), and uninfected age-matched controls (n = 9). Serum creatine phosphokinase (CPK) measurements were performed by the University of Colorado Health Sciences Center Clinical Laboratory and were expressed as units per liter.

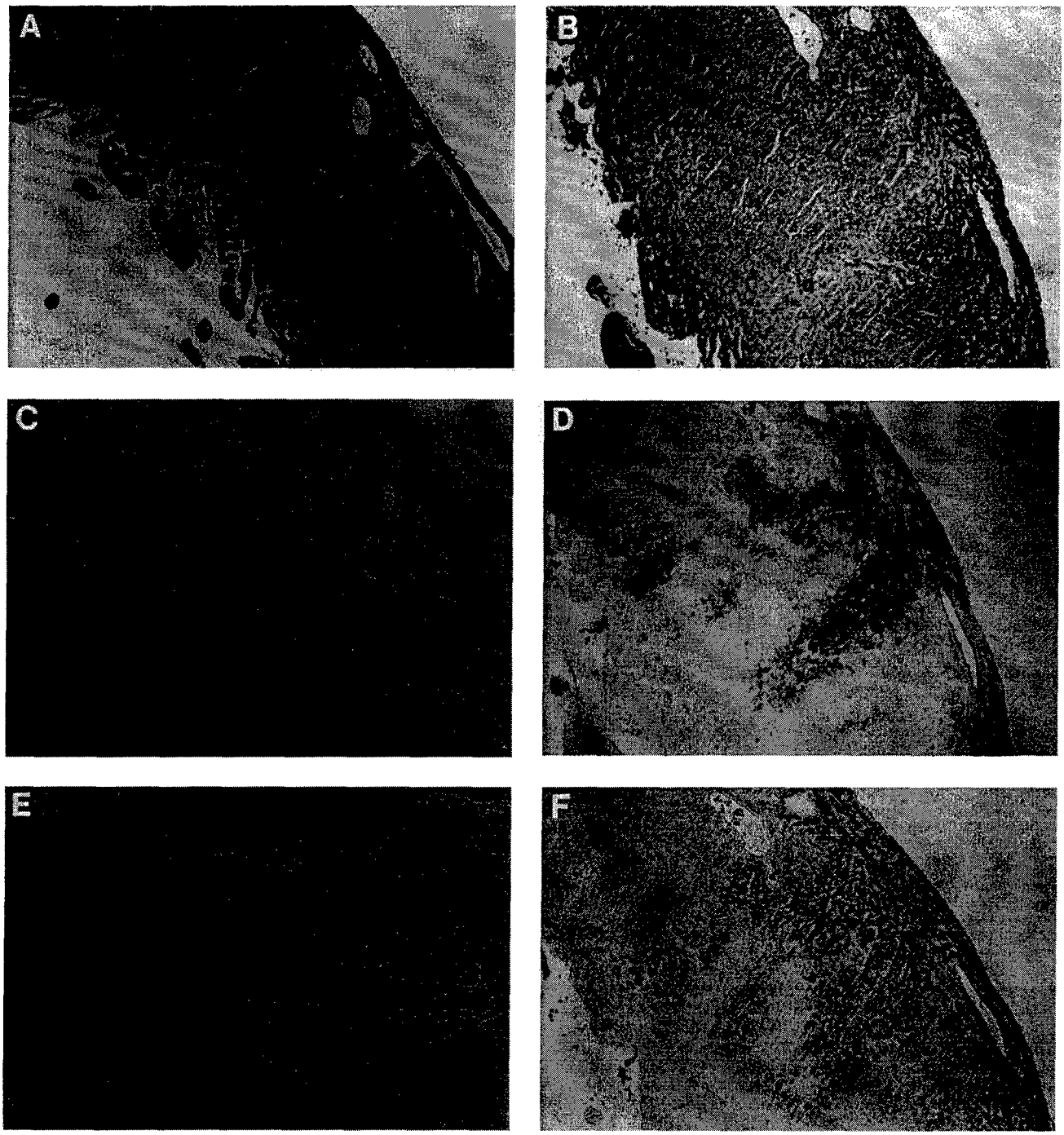

FIG. 1. Consecutive cardiac midsections from mock-infected (A, C, and E) and reovirus 8B-infected (B, D, and F) neonatal mice 7 days after left hind limb inoculation with 1,000 PFU of strain 8B reovirus or mock inoculation. Hematoxylin- and eosin-stained tissue reveals marked disruption of myocardial architecture in the 8B-infected heart (B) compared to that in the mock-infected heart (A). Despite the degree of injury, there is minimal inflammatory cell infiltrate. The degree of cellularity seen in both mock-infected and infected hearts is normal for neonatal mice. In situ detection of DNA nick ends by TUNEL revealed positively staining nuclei in the same region of an injured 8B-infected heart (D), which are absent in a mock-infected animal (C). Immunohistochemistry with anti-type 3 Dearing reovirus antibody reveals the presence of viral antigen in the areas of myocardial injury in the 8B-infected mouse (F), absent in the mock-infected animal (E). Original magnification, ×25.

Growth. Mice were infected with 10 PFU of 8B reovirus. Infected drug-treated ($n = 15$) and infected control ($n = 15$) mice were weighed daily on days 0 to 14 postinfection. Additional experiments using a higher dose of virus (1,000 PFU) were also completed, with daily weighing on days 0 to 7 postinfection. In these experiments, weights were also compared to those of normal age-matched uninfected mice.

Statistics. The results of all experiments are reported as means ± standard errors of the means. Means were compared using parametric two-tailed *t* tests

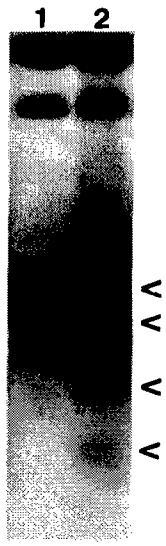

FIG. 2. DNA laddering in 8B-infected-neonatal-mouse hearts. DNA was extracted from reovirus 8B-infected and mock-infected hearts and detected by end-labeling analysis. DNA from the heart of a representative 8B-infected mouse (lane 2) is fragmented into oligonucleosomal-length pieces. These fragments result from internucleosomal DNA cleavage, a hallmark of apoptosis. (Arrowheads indicate DNA fragments, ranging in length from 200 to 1,000 bp). Fragmentation is absent in the mock-infected animal (lane 1).

(Graph Pad; Prism), and differences were considered significant if P values were <0.05.

RESULTS

(i) Reovirus 8B induces myocardial injury by apoptosis. Mice were inoculated intramuscularly into the hind limb with either 1,000 PFU of strain 8B reovirus or gel saline (mock infection). At 7 days postinfection, mice were sacrificed and transverse cardiac sections were prepared for histologic evaluation. In the 8B-infected hearts, there was marked myocardial disruption and diffuse edema (Fig. 1B). Numerous pyknotic nuclei and apoptotic bodies were present (Fig. 1B; see also Fig. 5E). Despite the degree of myocardial injury, only rare mononuclear cells (predominantly macrophages) and neutrophils were present. Myocardial disruption and edema were not seen in mock-infected hearts (Fig. 1A). Extensive areas of apoptotic TUNEL-positive nuclei were noted in the 8B-infected hearts (Fig. 1D), which correlated with the areas of histologic abnormality described above. Mock-infected hearts were TUNEL negative (Fig. 1C). Large regions of reovirus antigen-positive tissue were noted in the 8B-infected hearts (Fig. 1F) and occurred in the same distribution as the areas of histologic injury and TUNEL-positive cells.

In order to provide further confirmation that the morphological changes seen in virus-infected hearts were indeed due to apoptosis, DNAs were extracted from 8B-infected and mock-infected hearts, end labeled, and analyzed by agarose gel electrophoreses. DNAs from infected hearts, but not mock-infected controls, showed fragmentation into oligonucleosomal-length ladders, characteristic of apoptosis (Fig. 2). Taken together, these findings indicate that reovirus-induced myocardial injury is due to apoptosis.

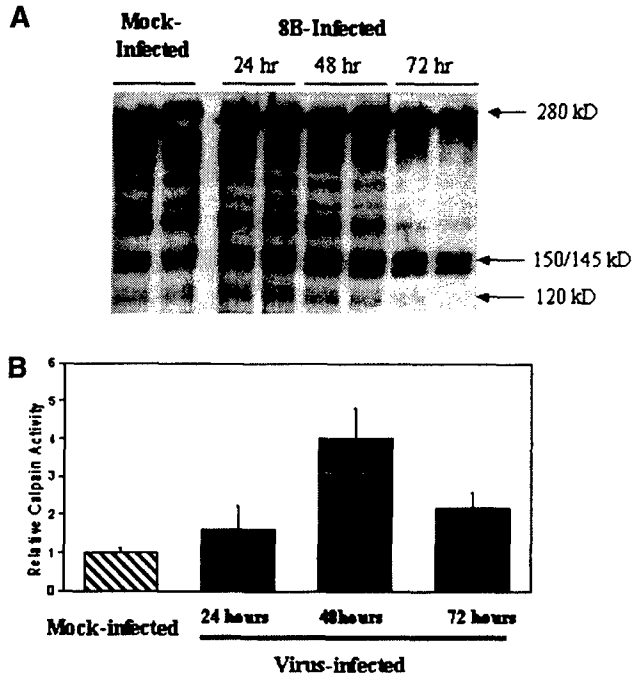

FIG. 3. Calpain activity in a reovirus-infected primary cardiac myocyte culture. (A) Activity was measured by monitoring proteolysis of spectrin (280 kDa), a preferred calpain substrate, to its calpain-specific breakdown products (150- to 145-kDa doublet) by immunoblot assay. Lysates of 8B-infected cardiomyocytes (MOI, 20) were prepared at 24, 48, and 72 h postinfection and compared to lysates of mock-infected cells at 48 h postinfection (experiments with all conditions were performed in duplicate). Compared to that of mock-infected mice, 8B-infected mice had increased calpain activity (150- to 145-kDa doublet) beginning at 24 h postinfection, which was markedly increased at 48 h postinfection and still present, but decreasing, at 72 h postinfection. No change was detectable in the intact (280-kDa) spectrin band following infection. (B) Densitometric analysis of calpain-specific spectrin breakdown products (150- to 145-kDa doublet) reveals a peak fourfold increase in calpain activity following infection with 8B reovirus.

(ii) Calpain is activated in 8B-infected murine cardiac myocytes. We have previously shown that reovirus infection in L929 cells results in increased calpain activity, which precedes apoptosis (13). We wished to determine whether calpain activity was also increased in myocardial cells following reovirus infection. Proteolysis of spectrin (fodrin), a preferred calpain substrate, was examined as an indication of calpain activation. Intact spectrin (280 kDa) is degraded by calpain, resulting in a characteristic spectrin breakdown product doublet seen at 150 and 145 kDa. Mouse primary cardiac myocyte cultures were infected with reovirus strain 8B (MOI, 20) or mock infected. Lysates were prepared after harvesting of cells at 24, 48, and 72 h postinfection. Western blot analysis of these cytoplasmic fractions revealed increased calpain activity following 8B infection compared to that of mock-infected cytoplasmic fractions. This increase was first detectable at 24 h, reached maximal intensity by 48 h, and was still present at 72 h postinfection (Fig. 3A). Densitometric analysis of calpain-specific breakdown products revealed a peak fourfold increase in calpain activity following virus infection (Fig. 3B). Caspase degradation of spectrin results in breakdown products at 120 kDa,

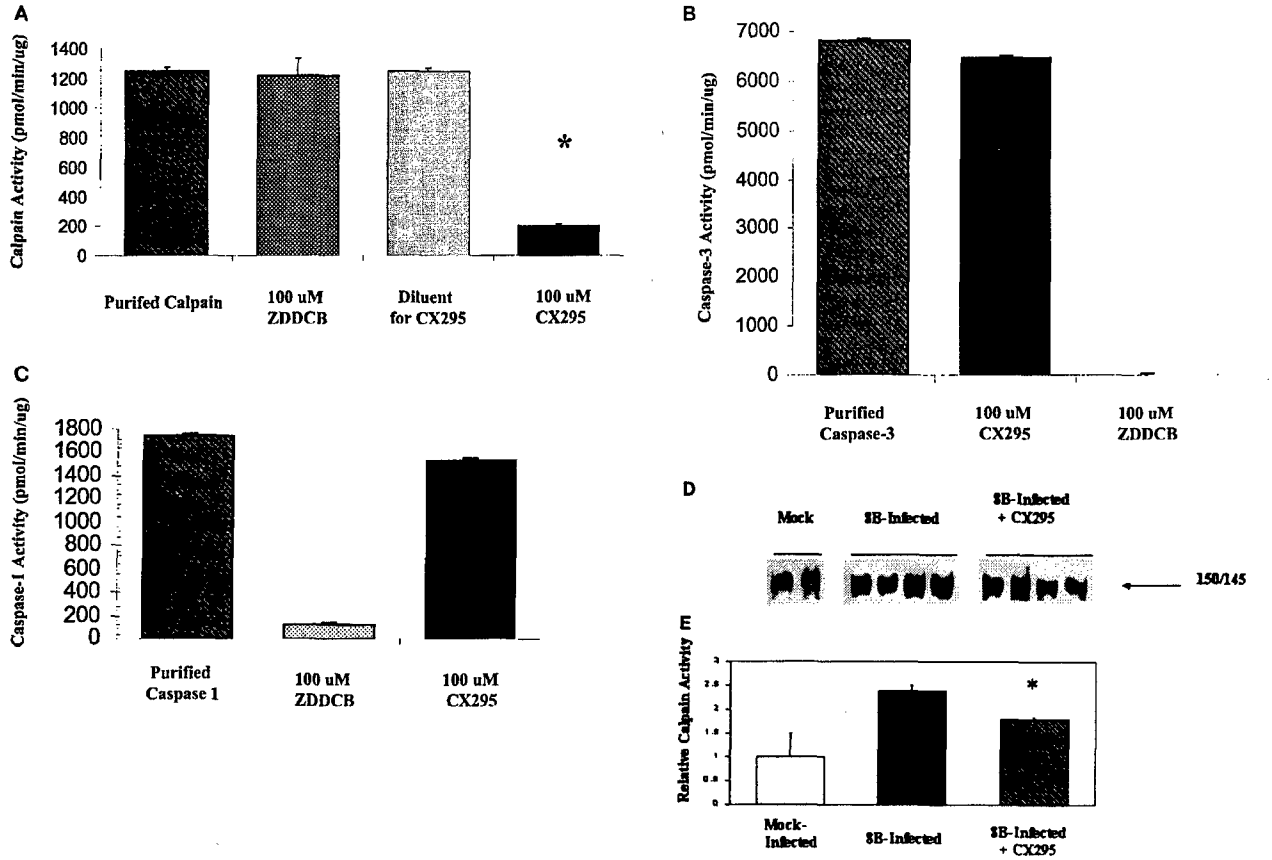

FIG. 4. Efficacy and specificity of the calpain inhibitor CX295. The effects of the calpain inhibitor CX295 on purified calpain (A), caspase 3 (B), and caspase 1 (C) activity were evaluated using a fluorogenic substrate assay, in which SLY-AMC, DEVD-AMC, and YVAD-AMC, respectively, served as substrates. Activities are expressed as purified calpain or caspase activity per minute, per micromole or picomole of substrate. One hundred micro-molar CX295 significantly inhibited calpain activity (the asterisk indicates a P of <0.0001) (A) but had minimal effect on caspase 3 or caspase 1 activity. Z-D-DCB, a pan-caspase inhibitor, was used as a control. Z-D-DCB had no effect on calpain activity but nearly completely inhibited caspase 3 and 1 activities (B and C). CX295 also effectively inhibited calpain activity in 8B-infected cardiomyocytes in vitro (D). Calpain activity (measured by densitometric analysis of the 150- to 145-kDa calpain-specific fodrin degradation product) increased by 2.4-fold in 8B-infected cardiomyocytes compared to that in mock-infected cardiomyocytes. Calpain activity was significantly reduced in CX295-treated, 8B-infected cells compared to that in infected, untreated cells ($P = 0.04$). (The 150- to 145-kDa doublet appears as a single large band due to the gel conditions.)

which were not observed in this experiment. These data demonstrate that an increase in calpain activity occurs following infection of myocardiocytes with reovirus strain 8B, in a time course that parallels the onset of apoptosis.

(iii) CX295 is an effective calpain inhibitor and does not appreciably inhibit caspases. Based on our findings that (i) 8B-induced myocarditis is due to apoptosis, (ii) calpain is activated in 8B-infected myocardiocytes, and (iii) inhibition of calpain activation inhibits reovirus-induced apoptosis in vitro, we wished to determine if calpain inhibition could prevent 8B-induced myocardial injury in vivo. CX295 is a dipeptide alpha-ketoamide compound that inhibits calpain at the active site and is nontoxic and effective in vivo (4, 48). To confirm the specificity of the compound, the activity of purified calpain was monitored in the presence and absence of CX295. The inactive diluent of CX295 and the pan-caspase inhibitor Z-D-DCB were used as controls. Purified calpain activity (measured as cleavage of SLY-AMC) was markedly reduced by CX295 (Fig. 4A). Calpain activity was decreased from 1,255 ± 22 to 206 ± 4 pmol/min/μg in the presence of CX295 ($P < 0.0001$). Neither the diluent nor Z-D-DCB controls had appreciable effect on calpain activity.

To further confirm that CX295 is a specific calpain inhibitor and does not inhibit caspases, the activities of purified caspase 1 and caspase 3 were monitored in the presence and absence of CX295, as well as in the presence of the known pan-caspase inhibitor Z-D-DCB (positive control). CX295 had a minimal inhibitory effect on either caspase 1 or caspase 3 activity (measured as cleavage of YVAD-AMC and DEVD-AMC, respectively), whereas Z-D-DCB inhibited both caspases nearly completely (Fig. 4B and C). Purified caspase 1 activity decreased from 6,829 ± 39 to 6,496 ± 36 pmol/min/ng in the presence of CX295, compared to 0 pmol/min/ng in the presence of Z-D-DCB. Purified caspase 3 activity decreased from 1,752 ± 6 to 1,533 ± 9 pmol/min/ng in the presence of CX95, compared to 118 ± 4 pmol/min/ng in the presence of Z-D-DCB.

CX295 also effectively inhibited calpain activity in primary cardiomyocyte culture. Calpain activity was quantified by im-

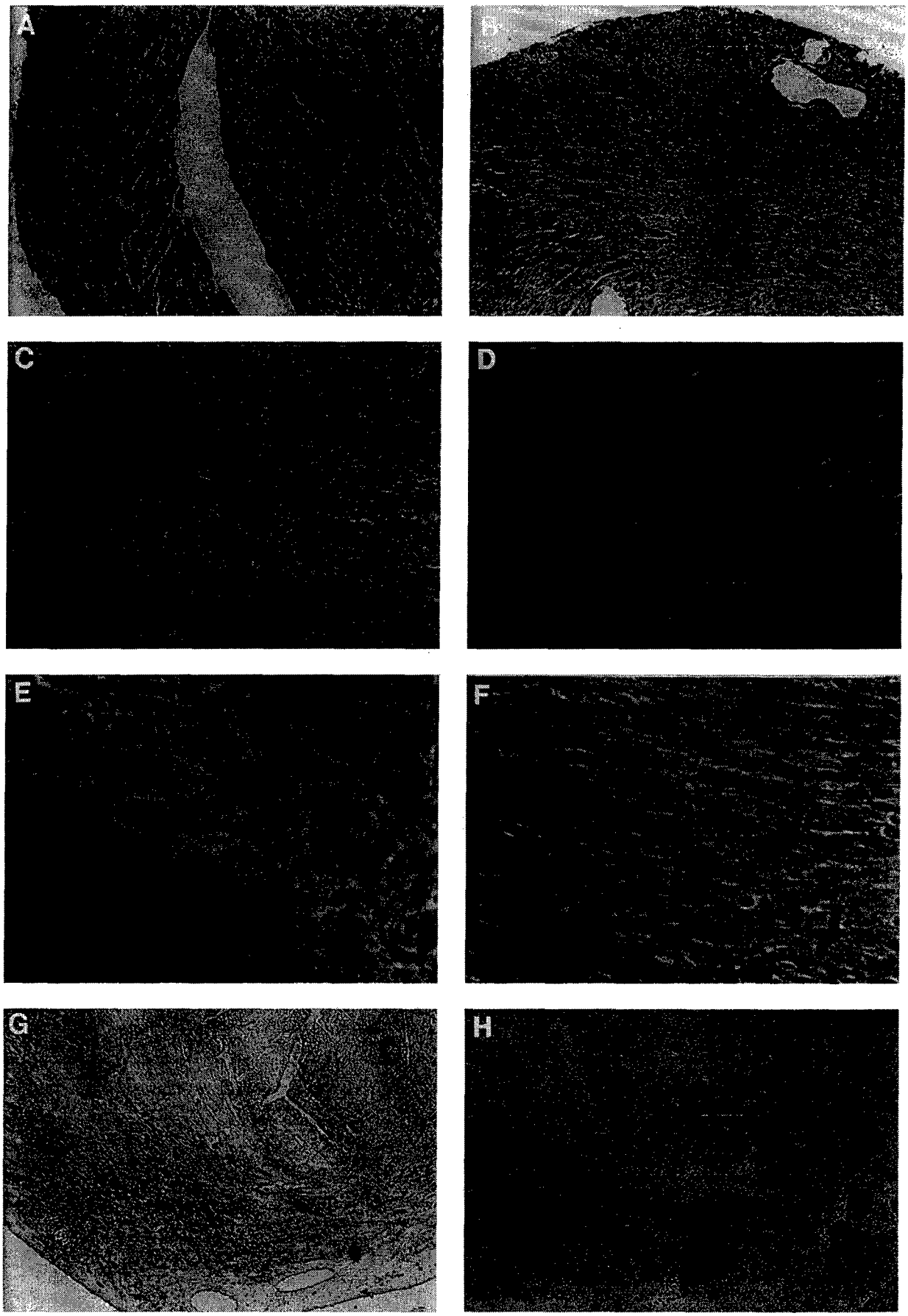
A
B
C
D
E
F
G
H

munoblotting in reovirus-infected myocytes, in the presence and absence of CX295. Calpain activity (measured by densitometric analysis of the 150- and 145-kDa calpain-specific fodrin breakdown product) increased by 2.4-fold in 8B-infected cardiomyocytes compared to that in mock-infected cardiomyocytes. Calpain activity was significantly reduced in CX295-treated, 8B-infected cells compared to that in infected, untreated cells ($P = 0.04$) (Fig. 4D and E).

These experiments confirm that CX295 is both an effective and a specific calpain inhibitor.

(iv) Calpain inhibitor CX295 inhibits 8B-induced myocardial injury. Two-day-old Swiss-Webster mice were infected with 1,000 PFU of 8B virus and received six daily intraperitoneal injections of either active CX295 (70 mg/kg) or its inactive saline diluent as a control (see Materials and Methods). Mice were sacrificed on day 7 postinfection, and myocardial sections were prepared.

Transverse cardiac sections from 8B-infected mice treated with CX295 or its inactive diluent (control) were stained with hematoxylin and eosin and viewed by light microscopy (Fig. 5A to F). Cardiac tissue from control mice (Fig. 5A) showed extensive focal areas of myocardial damage, which were absent in the CX295-treated animals, despite identical viral infection (Fig. 5B). Marked disruption of the normal myocardial architecture was evident in hearts of control mice (Fig. 5C), compared to that of drug-treated animals (Fig. 5D). Nuclei with apoptotic morphology were easily seen within these areas in the control mice (Fig. 5E), including in cells with condensed and pyknotic nuclei, as well as apoptotic bodies. These characteristics were absent in the drug-treated animals (Fig. 5F). Staining by TUNEL of comparable sections from drug-treated and diluent-treated (control) infected mice was examined. Nuclei that stained positive by TUNEL were virtually absent in the drug-treated mice (Fig. 5H), unlike with control infected animals (Fig. 5G).

For quantification of the degree of myocardial injury, hematoxylin- and eosin-stained midcardiac sections (at least six sections per heart) were scored using a previously validated scoring system (58). Twenty infected, CX295-treated animals and 23 control (infected, diluent-treated) mice were evaluated. There was a highly significant reduction in the myocardial injury scores of animals treated with CX295. The mean score for control animals was 3.0 ± 0.1 (range, 2 to 4), compared to 0.6 ± 0.1 (range 0 to 1.5) for CX295-treated animals ($P < 0.0001$) (Fig. 6).

CPK is an intracellular enzyme present in cardiac and skeletal muscle that is released upon tissue injury. It can be measured in the serum and used as a quantitative marker of skeletal and cardiac muscle damage (2). Blood was collected from infected mice treated with CX295 and inactive diluent-treated

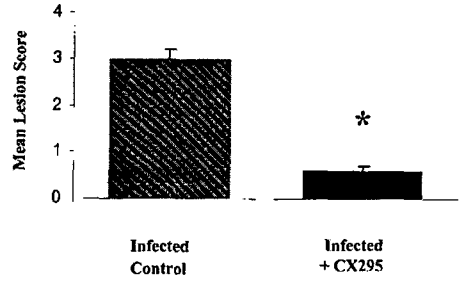

Heart Lesion Scoring
0 = no lesions
1 = one or a few small
2 = many small or a few large
3 = multiple small and large
4 = massive

FIG. 6. Reduction in myocardial injury score. Myocardial injury of 8B-infected animals was quantified by blindly scoring hematoxylin- and eosin-stained midcardiac sections of drug-treated and control (inactive-diluent-treated) animals upon light microscopy. At least six sections per heart were scored from 20 to 23 animals in each group. A highly significant reduction in myocardial injury score was noted for drug-treated animals. The mean lesion score was 3.0 ± 0.1 (range 2 to 4) for controls, compared to 0.6 ± 0.1 (range 0 to 1.5) for CX295-treated animals. *, $P < 0.0001$. See Materials and Methods for explanations of mean lesion scores.

controls at 7 days postinfection, as well as uninfected age-matched mice. Serum CPK levels were significantly elevated in 8B-inoculated mice compared to those in uninfected mice, indicative of 8B-induced muscle injury. There was a statistically significant reduction in serum CPK level toward a normal level in CX295-treated mice compared to the level in control mice (Fig. 7). Uninfected age-matched mice had a mean CPK level of 4,521 ± 431 U/liter. 8B-infected mice had a mean CPK level of 5,658 ± 359 U/liter, representing an increase of 1,137 U/liter above normal. Treatment of infected animals with CX295 reduced the mean CPK value to 4,634 ± 350 U/liter, not significantly elevated compared to normal levels but significantly reduced compared to levels in infected, nontreated animals ($P < 0.05$).

To determine if reductions in myocardial injury were also associated with reduction in viral titer at primary (hind limb) and secondary (heart) sites of replication, the titers of virus in tissues were determined by plaque assay of tissue homogenates. There was a 0.5-$\log_{10}$-PFU/ml reduction in viral titers in the hind limbs of CX295-treated animals compared to those for controls (7.2 ± 0.1 to 6.7 ± 0.2 $\log_{10}$ PFU/ml; $P = 0.003$). Hearts of CX295-treated animals had a 0.7-$\log_{10}$-PFU/ml reduction in viral titer (6.1 ± 0.2 to 5.4 ± 0.2 $\log_{10}$ PFU/ml; $P < 0.01$) (Fig. 8). Although these decrements were statistically

FIG. 5. Cardiac midsections from reovirus 8B-infected neonatal mice treated with the calpain inhibitor CX295 (B, D, F, and H) compared to those from inactive diluent control mice (A, C, E, and G) 7 days following intramuscular inoculation with 1,000 PFU of reovirus 8B. Hematoxylin- and eosin-stained sections at an original magnification of ×25 reveal extensive focal areas of myocardial injury (arrows) in the control animal (A), which is absent in the CX295-treated animal (B), despite identical viral infections. Views at an original magnification of ×50 demonstrate minimal inflammatory cell infiltrate in the affected area (C), but myocardial architecture is dramatically disrupted, compared to that of a CX295-treated mouse (D). At an original magnification of ×100, nuclei with apoptotic morphology are easily seen in the control animal (E), as are cells with condensed and pyknotic nuclei (long arrow) as well as apoptotic bodies (shorter arrows). These characteristics are absent in the drug-treated mouse (F). TUNEL analysis of the control animal reveals extensive areas of positively staining cells in the same regions of injury (G) but no TUNEL-positive areas in the drug-treated mouse (H).

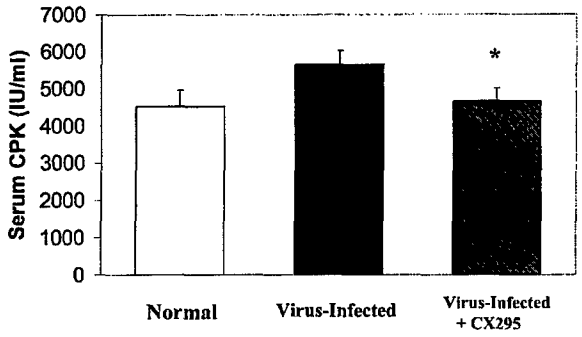

FIG. 7. Reduction in serum CPK. CPK was measured as a marker of myocardial damage in 8B-infected animals treated with CX295, and levels were compared to those for control (inactive-diluent-treated) infected animals, as well as age-matched uninfected controls. There was a significant reduction in serum CPK toward normal levels in CX295-treated infected mice compared to levels in infected control animals ($P < 0.05$).

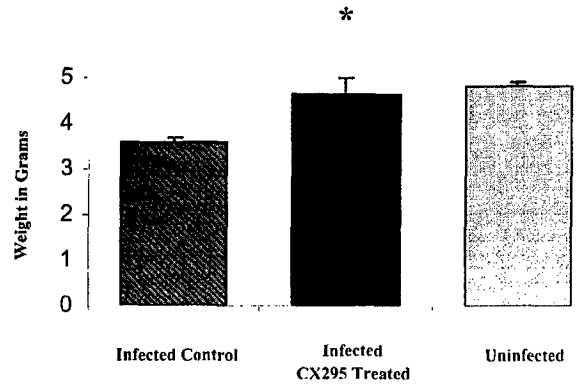

FIG. 9. Growth of infected mice. Growth, as measured by weight gain, was assessed in 8B-infected mice treated with CX295 and inactive diluent (control). Improved growth was noted for infected, CX295-treated animals at 7 days postinfection compared to the growth of infected controls (*, $P = 0.008$). Weights of infected, treated animals were not significantly different from those of uninfected, age-matched controls.

significant, they were modest in degree, and substantial viral replication occurred in both the drug-treated and the control animals (1,000- to 10,000-fold).

We wished to determine whether the reduction in myocardial damage caused by CX295 treatment reduced morbidity in mice. We therefore measured growth (weight gain) in infected, drug-treated mice and compared to that in infected, untreated controls. CX295-treated mice had improved growth compared to that of control mice (4.6 ± 0.4 versus 3.6 ± 0.1 g at 7 days postinfection; $P = 0.008$), and growth was not significantly different from that of uninfected age-matched animals (4.6 ± 0.4 versus 4.8 ± 0.1 g; $P = 0.6$, not significant) (Fig. 9).

DISCUSSION

Viral myocarditis remains a serious disease without reliable or effective treatment. The events following viral attachment and replication in myocardial tissue that lead to myocarditis are not clearly understood. A variety of mechanisms from various models have been suggested, including direct viral injury and persistence (9, 24), autoimmune phenomena (17, 45, 51), cytokine fluxes (18, 33, 52, 59), inflammation (29, 53), and apoptosis (12, 77, 78). A clearer understanding of pathogenic mechanisms is crucial for the development of effective therapeutic strategies, since currently employed antiviral agents have not made a significant impact on outcomes from this clinical syndrome. Reoviral myocarditis is an ideal model with which to study these events, since myocardial injury is a direct effect of virus infection and does not involve immune-mediated effects.

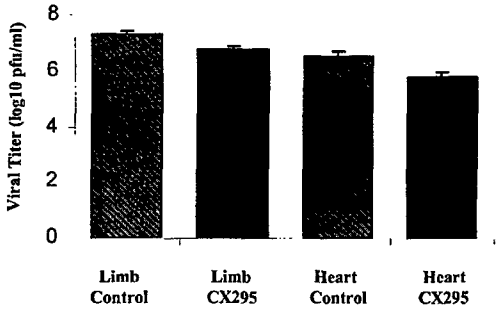

FIG. 8. Tissue-specific viral titers. Titers were measured by plaque assay at 7 days postinfection from homogenates of limbs (site of primary replication) and hearts (site of secondary replication) of 8B-infected mice. A slight reduction in peak viral titers was seen in the CX295-treated group. Both CX295-treated and control animals showed a >3-$\log_{10}$-unit increase in virus over the input inoculum (10^3 PFU/mouse).

Reovirus 8B induces myocarditis by apoptosis. Reovirus 8B induces myocarditis in mice by direct viral injury to myocytes, and we now show that this occurs by induction of apoptosis. This conclusion is supported by the presence of distinctive morphologic criteria upon microscopic examination of infected heart tissues; TUNEL-positive nuclei were found exclusively in regions of viral infection and myocardial injury. The presence of apoptosis was confirmed by the presence of the characteristic intranucleosomal cleavage pattern of extracted DNA. It has been shown previously that multiple viral genes (M1, L1 and L2, and S1) encoding core and attachment proteins are determinants of reovirus-induced acute myocarditis (56). Interactions between these proteins determine myocarditic potential. Several of these genes have been associated with reovirus RNA synthesis and reovirus induction of and sensitivity to beta interferon in cardiac myocyte cultures, which are determinants of reovirus myocarditic potential. In addition, the S1 gene, which codes for the viral attachment protein σ1, is the primary determinant of apoptotic potential among strains of reovirus (69). It is likely, therefore, that the extent of reovirus-induced myocardial injury is determined by a combination of host responses, encompassing both the interferon and the apoptosis pathways. Indeed, just as inhibition of the interferon pathway was sufficient to enhance reovirus-induced myocarditis (59), we show here that inhibition of the apoptotic pathway is sufficient to abrogate reovirus-induced myocarditis. Thus, apoptosis is an integral component of reovirus-induced myocardial injury.

Calpain activity is increased in reovirus-infected myocardiocytes, and calpain inhibition is protective against reovirus-induced myocarditis. Calpain is a calcium-activated cysteine protease that has proven importance with regard to the initiation of apoptosis in the reoviral model, as well as several other unrelated models of apoptosis (see the introduction). We first demonstrated that calpain activity is increased in cardiac myocytes in vitro following 8B infection, in a time course paralleling induction of apoptosis. We then demonstrated that calpain inhibition resulted in a reduction of calpain activity in infected cells and dramatic reductions in reovirus-induced injury, as well as apoptosis. Clinically significant reduction in myocardial injury was documented by reduced serum CPK levels and improved growth in treated mice.

It is likely that CX295 acted primarily by interfering with crucial signal transduction cascades involving calpain, required for induction of apoptotic cell death. Additionally, it is possible that CX295 provided some portion of its effect by inhibiting viral growth at either the primary (hind limb) or secondary (heart) site of replication, since viral titers were slightly lower in drug-treated animals than in controls. Slight reductions in viral titer do not seem a likely explanation for the majority of drug effect, since in prior experiments involving reovirus-induced myocarditis, yields of virus at early and late times postinfection did not correlate with the degree of myocardial injury (57). In addition, efficiently myocarditic and poorly myocarditic reovirus strains replicate to similar titers in the heart; thus, differences in myocarditic potential do not simply reflect viral growth in the heart (56).

One must be cautious in attributing a role for calpain in disease pathogenesis based solely on data derived from calpain inhibition. Currently available calpain inhibitors suitable for in vivo use have weak, but measurable, inhibitory activities against other cysteine proteases. However, the inhibitor employed in our experiments, CX295, is 500- to 900-fold more active against calpains than cathepsins (the K_i for calpain is 0.027 − 0.042 μM, versus a K_i for cathepsin B of 24 μM) and failed to inhibit caspase activity in vitro, as described in this paper. We believe that inhibition of calpain, rather than of other cysteine proteases, is the essential element of CX295's protective effect against 8B-induced myocardial apoptosis and injury.

It is not clear what constitutes the upstream and downstream components of a signaling cascade within which calpain might fit, either during reovirus infection or in other systems where calpain is involved. The mechanisms by which reovirus triggers increased cellular calpain activity are not known but may include initiation of calcium fluxes following viral attachment, as demonstrated with rotavirus, a closely related virus (15); upregulation of growth factors which facilitate calpain activation (37, 66); or upregulation of endogenous calpain activator proteins which have been characterized for several cell types (49). Calpain may play a physiologic role in the regulation of a variety of cellular transcription factors and cell cycle-regulating factors implicated in apoptosis, including Jun, Fos, p53, cyclin D, and NF-κB (3, 7, 73). We have recently shown that activation of NF-κB is required for reovirus-induced apoptosis (J. L. Connolly, S. E. Rodgers, B. Pike, P. Clarke, K. L. Tyler, and T. S. Dermody, Abstr. 17th Ann. Meet. Am. Soc. Virology, abstr. 17-2, 1998), suggesting the possibility that calpain inhibition acts to modulate NF-κB-induced signal transduction. Calpains may also modulate cell death by cleaving Bax, a proapoptotic protein located in the cytosol (75). In addition, the caspase and calpain proteolytic cascades may interact. Caspases may play a role in the regulation of calpain by cleavage of calpastatin, the endogenous inhibitor of calpain (43, 71, 76). Reflexively, calpain may be involved in the proteolytic activation of some caspases (47).

Potential therapeutic efficacy of calpain inhibitors. In conclusion, our data suggest that reovirus-induced myocarditis occurs by direct viral induction of apoptotic cell death and that injury can be markedly reduced with the use of a calpain inhibitor. To our knowledge, this is the first successful demonstration of the use of calpain inhibition in vivo to ameliorate myocarditis in particular and virus-induced disease in general. However, future experiments are needed to determine whether calpain inhibition remains effective when it is administered after the onset of viral infection. Our results demonstrate the utility of apoptosis inhibition as a strategy for protection against viral infection.

ACKNOWLEDGMENTS

We thank Gary Rogers of Cortex Pharmaceutical for providing the calpain inhibitor CX295 and its inactive diluent. The University of Colorado Cancer Center provided core tissue culture and medium facilities.

This work was supported by Public Health Service grant 1RO1AG14071 from the National Institute of Aging, Merit and REAP grants from the Department of Veterans Affairs, a U.S. Army Medical Research and Material Command grant (USAMRMC 98293015) (K.L.T.), a Young Investigator Award from the National Kidney Foundation (C.L.E.), Public Health Service grant 1RO1HL57161, and North Carolina State University College of Veterinary Medicine grant 204743 (B.S.).

REFERENCES

1. **Aubert, M., and J. A. Blaho.** 1999. The herpes simplex virus type 1 regulatory protein ICP27 is required for the prevention of apoptosis in human cells. J. Virol. **73**:2803–2813.
2. **Bachmeir, K., J. Mair, F. Offner, C. Pummerer, and N. Neu.** 1995. Serum cardiac troponin T and creatine kinase-MB elevations in murine autoimmune myocarditis. Circulation **92**:1927–1932.
3. **Baghdiguian, S., M. Martin, I. Richard, F. Pons, C. Astier, N. Bourg, R. T. Hay, R. Chemaly, G. Haleby, J. Loiselet, L. V. Anderson, A. Lopez de Muvigin, M. Fardeu, P. Mangeat, J. S. Beckmann, and G. Lefranc.** 1999. Calpain 3 deficiency is associated with myonuclear apoptosis and profound perturbation of the IκBα/NF-KB pathway in limb-girdle muscular dystrophy type 2A. Nat. Med. **5**:503–511.
4. **Bartus, R. T., K. L. Baker, A. D. Heiser, S. D. Sawyer, R. L. Dean, P. J. Elliott, and J. A. Straub.** 1994. Postischemic administration of AK275, a calpain inhibitor, provides substantial protection against focal ischemic brain damage. J. Cerebr. Blood Flow Metab. **14**:537–544.
5. **Baty, C. J., and B. Sherry.** 1993. Cytopathogenic effect in cardiac myocytes but not in cardiac fibroblasts is correlated with reovirus-induced myocarditis. J. Virol. **67**:6295–6298.
6. **Bowles, N. E., and J. A. Towbin.** 1998. Molecular aspects of myocarditis. Curr. Opin. Cardiol. **13**:179–184.
7. **Chen, F., Y. Lu, D. C. Kuhn, M. Maki, X. Shi, and L. M. Demers.** 1997. Calpain contributes to silica-induced IKB-degradation and nuclear factor κB activation. Arch. Biochem. Biophys. **34**:383–388.
8. **Chen, S. J., M. E. Bradley, and T. C. Lee.** 1998. Chemical hypoxia triggers apoptosis of cultured neonatal rat cardiac myocytes: modulation by calcium-regulated proteases and protein kinases. Mol. Cell. Biochem. **178**:141–149.
9. **Chow, L. H., K. W. Beisel, and B. M. McManus.** 1992. Enteroviral infection of mice with severe combined immunodeficiency. Evidence for direct viral pathogenesis of myocardial injury. Lab. Investig. **66**:24–31.
10. **Cohen, G. M.** 1997. Caspases: the executioners of apoptosis. Biochem. J. **326**:1–16.
11. **Colamussi, M. L., M. R. White, E. Crouch, and K. L. Hartshorn.** 1999. Influenza A virus accelerates neutrophil apoptosis and markedly potentiates apoptotic effects of bacteria. Blood **93**:2395–2403.

12. **Colston, J. T., B. Chandrasakar, and G. L. Freeman.** 1998. Expression of apoptosis-related proteins in experimental coxsackie myocarditis. Cardovasc. Res. **38**:158–168.
13. **DeBiasi, R. L., M. K. T. Squier, B. Pike, M. Wynes, T. S. Dermody, and K. L. Tyler.** 1999. Reovirus-induced apoptosis is preceded by increased cellular calpain activity and is blocked by calpain inhibitors. J. Virol. **73**:695–701.
14. **Dockrell, D. H., A. D. Badley, J. S. Villacian, C. J. Heppelman, A. Algeciras, S. Ziesvnar, H. Yagita, D. H. Lynch, P. C. Roche, P. J. Leibson, and C. V. Paya.** 1998. The expression of Fas ligand by macrophages and its upregulation by human immunodeficiency virus infection. J. Clin. Investig. **101**:2394–2405.
15. **Dong, Y., C. Q. Zeng, J. M. Ball, M. K. Estes, and A. P. Morris.** 1997. The rotavirus enterotoxin NSP4 mobilizes calcium in human intestinal cells by stimulating phospholipase C-mediated inositol 1,4,5-triphosphate production. Proc. Natl. Acad. Sci. USA **94**:3960–3965.
16. **Edelstein, C. L., H. Ling, P. E. Gengaro, R. A. Nemenoff, B. A. Bahr, and R. W. Schrier.** 1997. Effect of glycine on prelethal and postlethal increases in calpain activity in rat renal proximal tubules. Kidney Int. **52**:1271–1278.
17. **Fairweather, D., C. M. Lawson, A. J. Chapman, C. M. Brown, T. W. Booth, J. M. Papadimitriou, and G. R. Snellam.** 1998. Wild isolates of murine cytomegalovirus induce myocarditis and antibodies that cross-react with virus and cardiac myosin. Immunology **94**:263–270.
18. **Freeman, G. L., J. T. Colston, M. Zabalgoitia, and B. Chandrasekar.** 1998. Contractile depression and expression of proinflammatory cytokines and iNOS in viral myocarditis. Am. J. Physiol. **274**:H249–H258.
19. **Galvan, V., R. Brandimarti, and B. Roizman.** 1999. Herpes simplex virus 1 blocks caspase-3-independent and caspase-dependent pathways to cell death. J. Virol. **73**:3219–3226.
20. **Gauntt, C. J.** 1997. Roles of the humoral response in coxsackievirus B-induced disease. Curr. Top. Microbiol. Immunol. **223**:259–282.
21. **Girard, S., T. Couderc, J. D. Destombes, J. Thiesson, F. Delpeyroux, and B. Blondel.** 1999. Poliovirus induces apoptosis in the mouse central nervous system. J. Virol. **73**:6066–6072.
22. **Ichimi, R., T. Jin-o, and M. Ito.** 1999. Induction of apoptosis in cord blood lymphocytes by HHV-6. J. Med. Virol. **58**:63–68.
23. **Jaworski, A., and S. M. Crowe.** 1999. Does HIV cause depletion of CD4+ T cells in vivo by the induction of apoptosis? Immunol. Cell Biol. **77**:90–98.
24. **Kanda, T., H. Koike, M. Arai, J. E. Wilson, C. M. Carthy, D. Yang, B. M. McManus, R. Nagai, and I. Kobayashi.** 1999. Increased severity of viral myocarditis in mice lacking lymphocyte maturation. Int. J. Cardiol. **68**:13–22.
25. **Kawai, C.** 1999. From myocarditis to cardiomyopathy: mechanisms of inflammation and cell death: learning from the past for the future. Circulation **99**:1091–1100.
26. **Kerr, J. F. R., A. H. Wylie, and A. R. Currie.** 1972. Apoptosis: a basic biological phenomenon with wide-ranging implications in tissue kinetics. Br. J. Cancer **26**:239–257.
27. **Kohli, V., J. F. Madden, R. C. Bentley, and P. A. Clavien.** 1999. Calpain mediates ischemic injury of the liver through modulation of apoptosis and necrosis. Gastroenterology **116**:168–178.
28. **Krammer, P. H., I. Behrmann, P. Daniel, J. Dhein, and K. M. Debatin.** 1994. Regulation of apoptosis in the immune system. Curr. Opin. Immunol. **6**:276–289.
29. **Lee, J. K., S. H. Zaidi, P. Liu, F. Dawood, A. Y. Cheah, W. H. Wen, Y. Saiki, and M. Rabinovitch.** 1998. A serine elastase inhibitor reduces inflammation and fibrosis and preserves cardiac function after experimentally-induced murine myocarditis. Nat. Med. **4**:1383–1391.
30. **Liu, P., T. Martino, M. A. Opavsky, and J. Penninger.** 1996. Viral myocarditis: balance between viral infection and immune response. Can. J. Cardiol. **12**:935–943.
31. **Marshall, W. L., C. Yim, E. Gustafson, T. Graf, D. R. Sage, K. Hanify, L. Williams, J. Fingeroth, and R. W. Finberg.** 1999. Epstein-Barr virus encodes a novel homolog of the bcl-2 oncogene that inhibits apoptosis and associates with Bax and Bak. J. Virol. **73**:5181–5185.
32. **Martin, S. J., and D. R. Green.** 1995. Protease activation during apoptosis: death by a thousand cuts? Cell **82**:349–352.
33. **Matsumori, A.** 1996. Cytokines in myocarditis and cardiomyopathies. Curr. Opin. Cardiol. **11**:302–309.
34. **Megyeri, K., K. Berencsi, T. D. Halazonetis, G. C. Prendergast, G. Gri, S. A. Plotkin, G. Rovera, and E. Gonczol.** 1999. Involvement of a p53-dependent pathway in rubella virus-induced apoptosis. Virology **259**:74–84.
35. **Murachi, T.** 1983. Calpain and calpastatin. Trends Biochem. Sci. **8**:167–169.
36. **Nath, R., K. J. Raser, D. Stafford, I. Hajimohammadreza, A. Posner, H. Allen, R. V. Talanian, P. Yuen, R. B. Gilbertsen, and K. K. Wang.** 1996. Non-erythroid α-spectrin breakdown by calpain and interleukin 1 B-converting-enzyme-like protease(s) in apoptotic cells: contributory roles of both protease families in neuronal apoptosis. Biochem. J. **319**:686–690.
37. **Neuberger, T., A. K. Chakrabarti, T. Russell, G. H. DeVreis, E. L. Hogan, and N. L. Banik.** 1997. Immunolocalization of cytoplamic and myelin mCalpain in transfected Schwann cells. I. Effect of treatment with growth factors. J. Neurosci. Res. **47**:521–530.
38. **Oberhaus, S. M., R. L. Smith, G. H. Clayton, T. S. Dermody, and K. L. Tyler.** 1997. Reovirus infection and tissue injury in the mouse central nervous system are associated with apoptosis. J. Virol. **71**:2100–2106.
39. **Oberhaus, S. M., T. S. Dermody, and K. L. Tyler.** 1998. Apoptosis and the cytopathic effects of reovirus. Curr. Top. Microbiol. Immunol. **233**:23–49.
40. **O'Brien, V.** 1998. Viruses and apoptosis. J. Gen. Virol. **79**:1833–1834.
41. **Patel, T., G. J. Gores, and S. H. Kaufmann.** 1996. The role of proteases during apoptosis. FASEB J. **10**:587–597.
42. **Pignata, C., M. Fiore, S. deFilippo, M. Cavalcanti, L. Gaetaniello, and I. Scotese.** 1998. Apoptosis as a mechanism of peripheral blood mononuclear cell death after measles and varicella-zoster virus infections in children. Pediatr. Res. **43**:77–83.
43. **Porn-Ares, M. I., A. Samali, and S. Orenius.** 1998. Cleavage of the calpain inhibitor, calpastatin, during apoptosis. Cell Death Differ. **5**:1028–1033.
44. **Rodgers, S. E., E. S. Barton, S. M. Oberhaus, B. Pike, C. A. Gibson, K. L. Tyler, and T. S. Dermody.** 1997. Reovirus-induced apoptosis of MDCK cells is not linked to viral yield and is blocked by Bcl-2. J. Virol. **71**:2540–2546.
45. **Rose, N. R., A. Herskowitz, and D. A. Neumann.** 1993. Autoimmunity in myocarditis: models and mechanisms. Clin. Immunol. Immunopathol. **68**: 95–99.
46. **Rose, N. R., and S. L. Hill.** 1996. The pathogenesis of postinfectious myocarditis. Clin. Immunol. Immunopathol. **80**:S92–S99.
47. **Ruiz-Vela, A., G. Gonzalez de Buitrago, and A.-C. Martinez.** 1999. Implication of calpain in caspase activation during B cell clonal deletion. EMBO J. **18**:4988–4998.
48. **Saatman, K. E., H. Murai, R. T. Bartus, D. H. Smith, N. J. Hayward, B. R. Perri, and T. K. McIntosh.** 1996. Calpain inhibitor AK295 attenuates motor and cognitive deficits following experimental brain injury in the rat. Proc. Natl. Acad. Sci. USA **93**:3428–3433.
49. **Salamino, F., R. DeTullio, P. Mengotti, P. L. Viotti, E. Melloni, and S. Pontremoli.** 1993. Site-directed activation of calpain is promoted by a membrane-associated natural activator protein. Biochem. J. **290**:191–197.
50. **Schultz-Cherry, S., and V. S. Hinshaw.** 1996. Influenza virus neuraminidase activates latent transforming growth factor beta. J. Virol. **70**:8624–8629.
51. **Schwimmbeck, P. L., S. A. Huber, and H. P. Schultheiss.** 1997. Roles of T cells in coxsackie-B induced disease. Curr. Top. Microbiol. Immunol. **223**: 283–303.
52. **Seko, Y., N. Takahashi, H. Yagita, K. Okumura, and Y. Yazaki.** 1997. Expression of cytokine mRNA's in murine hearts with acute myocarditis caused by coxsackievirus b3. J. Pathol. **183**:105–108.
53. **Seko, Y., N. Takahashi, M. Azuma, H. Yagita, K. Okumura, and Y. Yazaki.** 1998. Expression of costimulatory molecule CD40 in murine heart with acute myocarditis and reduction of inflammation by treatment with anti-CD40L/B7-1 monoclonal antibodies. Circ. Res. **83**:463–469.
54. **Shen, Y., and T. E. Shenk.** 1995. Viruses and apoptosis. Curr. Opin. Genet. Dev. **5**:105–111.
55. **Sherry, B.** 1998. Pathogenesis of reovirus myocarditis, p. 51–66. *In* K. L. Tyler and M. B. A. Oldstone (ed.), Reoviruses II: cytopathogenicity and pathogenesis. Springer-Verlag, Berlin, Germany.
56. **Sherry, B., and M. A. Blum.** 1994. Multiple viral core proteins are determinants of reovirus-induced acute myocarditis. J. Virol. **63**:8461–8465.
57. **Sherry, B., C. J. Baty, and M. A. Blum.** 1996. Reovirus-induced acute myocarditis in mice correlates with viral RNA synthesis rather than generation of infectious virus in cardiac myocytes. J. Virol. **70**:6709–6715.
58. **Sherry, B., F. J. Schoen, E. Wenske, and B. N. Fields.** 1989. Derivation and characterization of an efficiently myocarditic reovirus variant. J. Virol. **63**: 4840–4849.
59. **Sherry, B., J. Torres, and M. A. Blum.** 1998. Reovirus induction of and sensitivity to beta interferon in cardiac myocyte cultures correlate with induction of myocarditis and are determined by viral core proteins. J. Virol. **72**:1314–1323.
60. **Sherry, B., X.-Y. Li, K. L. Tyler, J. M. Cullen, and H. W. Virgin.** 1993. Lymphocytes protect against and are not required for reovirus-induced myocarditis. J. Virol. **67**:6119–6124.
61. **Sindram, D., V. Kohli, J. F. Madden, and P. A. Clavien.** 1999. Calpain inhibition prevents sinusoidal endothelial cell apoptosis in the cold ischemic rat liver. Transplantation **68**:136–140.
62. **Solary, E., B. Eymin, N. Droin, and M. Haugg.** 1998. Proteases, proteolysis, and apoptosis. Cell Biol. Toxicol. **14**:11–32.
63. **Sorimachi, H., S. Ishiura, and K. Suzuki.** 1997. Structure and physiological function of calpains. Biochem. J. **328**:721–732.
64. **Squier, M. K., A. J. Sehnert, K. S. Sellins, A. M. Malkinson, E. Takanoand, and J. J. Cohen.** 1999. Calpain and calpastatin regulate neutrophil apoptosis. J. Cell. Physiol. **178**:311–319.
65. **Squier, M. K. T., and J. J. Cohen.** 1997. Calpain, an upstream regulator of thymocyte apoptosis. J. Immunol. **158**:3690–3697.
66. **Strong, J. E., D. Tang, and P. W. K. Lee.** 1993. Evidence that the epidermal growth factor receptor on host cells confers reovirus infection efficiency. Virology **197**:405–411.
67. **Teodoro, J. G., and P. E. Branton.** 1997. Regulation of apoptosis by viral gene products. J. Virol. **71**:1739–1746.
68. **Thomas, M., and L. Banks.** 1999. Human papillomavirus (HPV) E6 interactions with Bak are conserved amongst E6 proteins from high and low risk HPV types. J. Gen. Virol. **80**:1513–1517.

69. **Tyler, K. L., M. K. T. Squier, S. E. Rodgers, B. E. Schneider, S. M. Oberhaus, T. A. Grdina, J. J. Cohen, and T. S. Dermody.** 1995. Differences in the capacity of reovirus strains to induce apoptosis are determined by viral attachment protein σ1. J. Virol. **69**:6972–6979.
70. **Valentin, H., O. Azocar, B. Horvat, R. Willeims, R. Garrone, A. Evlasher, M. L. Toribio, and C. Rabourdin-Combe.** 1999. Measles virus infection induces terminal differentiation of human thymic epithelial cells. J. Virol. **73**:2212–2221.
71. **Wang, K. K., R. Postmantur, R. Nadimpalli, R. Nath, P. Mohan, R. A. Nixon, R. V. Talanian, M. Keegan, L. Herzog, and H. Allen.** 1998. Caspase-mediated fragmentation of calpain inhibitor protein calpastatin during apoptosis. Arch. Biochem. Biophys. **356**:187–196.
72. **Wang, K. K. W., and P. Yuen.** 1994. Calpain inhibition: an overview of its therapeutic potential. Trends Pharmacol. Sci. **15**:412–419.
73. **Watt, F., and P. L. Molloy.** 1993. Specific cleavage of transcription factors by the thiol protease, m-calpain. Nucleic Acids Res. **21**:5092–5100.
74. **Weller, M., J. B. Schulz, U. Wullner, P. A. Loschmann, T. Klockgether, and J. Dichgans.** 1997. Developmental and genetic regulation of programmed neuronal death. J. Neural Transm. **50**:115–123.
75. **Wood, D. E., A. Thomas, L. A. Devi, Y. Berman, R. C. Beavis, J. C. Reed, and E. W. Newcomb.** 1998. Bax cleavage is mediated by calpain during drug-induced apoptosis. Oncogene **17**:1069–1078.
76. **Wood, D. E., and E. W. Newcomb.** 1999. Caspase-dependent activation of calpain during drug-induced apoptosis. J. Biol. Chem. **274**:8309–8315.
77. **Yang, D., J. Yu, Z. Luo, C. M. Carthy, J. E. Wilson, Z. Liu, and B. M. McManus.** 1999. Viral myocarditis: identification of five differentially expressed genes in coxsackievirus B3-infected mouse heart. Circ. Res. **84**:704–712.
78. **Yeh, E. T.** 1997. Life and death in the cardiovascular system. Circulation **95**:782–786.
79. **Zhivotovsky, B., D. H. Burgess, D. M. Vanags, and S. Orrenius.** 1997. Involvement of cellular proteolytic machinery in apoptosis. Biochem. Biophys. Res. Commun. **230**:481–488.

Reoviruses and the host cell

Kenneth L. Tyler, Penny Clarke, Roberta L. DeBiasi, Douglas Kominsky and George J. Poggioli

Reovirus infection of target cells can perturb cell cycle regulation and induce apoptosis. Differences in the capacity of reovirus strains to induce cell cycle arrest at G1 and G2/M have been mapped to the viral S1 genome segment, which also determines differences in the ability of reovirus strains to induce apoptosis and to activate specific mitogen-activated protein kinase (MAPK) cascades selectively. Reovirus-induced apoptosis involves members of the tumor necrosis factor (TNF) superfamily of death receptors and is associated with activation of both death receptor- and mitochondrial-associated caspases. Reovirus infection is also associated with the activation of a variety of transcription factors, including nuclear factor (NF)-κB. Junctional adhesion molecule (JAM) has recently been identified as a novel reovirus receptor. Reovirus binding to JAM appears to be required for induction of apoptosis and activation of NF-κB, although the precise cellular pathways involved have not yet been identified.

Kenneth L. Tyler*
Depts of Neurology, Medicine, Microbiology & Immunology and Pediatrics,
Penny Clarke
Dept of Neurology,
Douglas Kominsky
Dept of Neurology,
Roberta L. DeBiasi
Dept of Pediatrics,
George J. Poggioli
Dept of Microbiology,
University of Colorado Health Sciences Center, Campus Box B-182, 4200 E, 9th Avenue, Denver, CO 80262, USA.
*e-mail: Ken.Tyler@UCHSC.edu

Reovirus infection has long been a classical experimental system for studying the role played by individual viral genes and the proteins they encode during distinct stages of viral pathogenesis *in vivo* (reviewed in Ref. 1). Recent studies have dramatically enhanced our understanding of reovirus–host interactions at the cellular level and have shed light on how these viruses activate cellular signaling pathways, perturb cell cycle regulation and induce apoptotic cell death (Fig. 1).

Virus–receptor interaction

The reovirus cell-attachment protein σ1 is an oligomer located at the icosahedral vertices in the outer capsid of the virion. σ1 has a globular head domain and a long fibrous tail. Most serotype three reoviruses (T3) contain a receptor-binding domain (RBD) within the fibrous tail of σ1 encompassing amino acids 198–205, which binds α-linked sialic acid (SA) residues[2,3]. A second RBD, common to both serotype 1 (T1) and T3 reoviruses, is located within the globular head of σ1; the head RBD plays a key role in determining the neurotropism of T3 reoviruses, both *in vitro* and *in vivo*[1].

Several T3 reovirus strains that fail to bind SA (T3SA–) have been identified (e.g. clones T3C43, T3C44 and T3C84), and these strains provide an opportunity to investigate cell attachment mediated by the σ1 head RBD in the absence of tail RBD-mediated binding to SA. Recent studies have provided compelling evidence that the σ1 head RBD binds to junctional adhesion molecule (JAM), and that JAM is a host cell receptor for reoviruses[4]. JAM was identified as a putative reovirus receptor by transfecting COS-7 cells, a reovirus-resistant cell line, with a cDNA library derived from reovirus-susceptible human neuronal precursor (NT2) cells. The transfected cells were selectively enriched for their ability to bind fluoresceinated T3SA– virions. Four clones were identified that each encoded human JAM (hJAM). The ability of JAM to function as a reovirus receptor was confirmed by showing that: (1) anti-hJAM monoclonal antibodies blocked binding of T3SA– virus to a variety of target cells including NT2, HeLa and Caco-2; and (2) murine erythroleukemia (MEL) cells, which are resistant to infection with T3SA–, and chick embryo fibroblasts (CEF), which are resistant to reovirus infection by both SA+ and SA– reovirus strains, both became permissive following transient transfection with either hJAM (MELs and CEFs) or murine JAM (CEFs). Surface plasmon resonance was used to show that a fusion protein comprising the extracellular domain of hJAM coupled to rabbit immunoglobulin Fc (Fc-hJAM) could bind to purified T3 σ1 protein and to the proteolytically derived head domain of σ1. A monoclonal antibody specific for a conformational epitope within the σ1 head domain blocked binding of T3 virions to Fc-hJAM, an effect that was not seen with a competitive inhibitor of reovirus binding to SA (α-sialyllactose, SLL). This suggests that reovirus binding to JAM occurs via the virion head RBD and does not require SAs. Reovirus–JAM binding is of high affinity, with a calculated K_d of 6×10^{-8} M.

Junctional adhesion molecule

JAM is a member of the immunoglobulin superfamily that contains two extracellular immunoglobulin-like domains and a short cytoplasmic tail[5,6]. It is a type 1 transmembrane protein that is located predominantly at the subapical region of inter-epithelial cell tight junctions. Although the evidence that JAM is a reovirus receptor is compelling, some aspects of its biology suggest that it might not be the exclusive target of reovirus head RBDs, and other candidate receptors have previously been identified. It is important to recognize that both SA and JAM can serve independently as reovirus receptors, and it is likely that additional virus–receptor interactions also occur. The predominant localization of JAM to subapical regions of tight junctions would seem to limit its accessibility for virus binding. Studies establishing JAM as a reovirus receptor were performed in cultured cells under conditions in which tight junctions could not form. It remains to be seen

http://tim.trends.com 0966-842X/01/$ – see front matter Published by Elsevier Science Ltd. PII: S0966-842X(01)02103-5

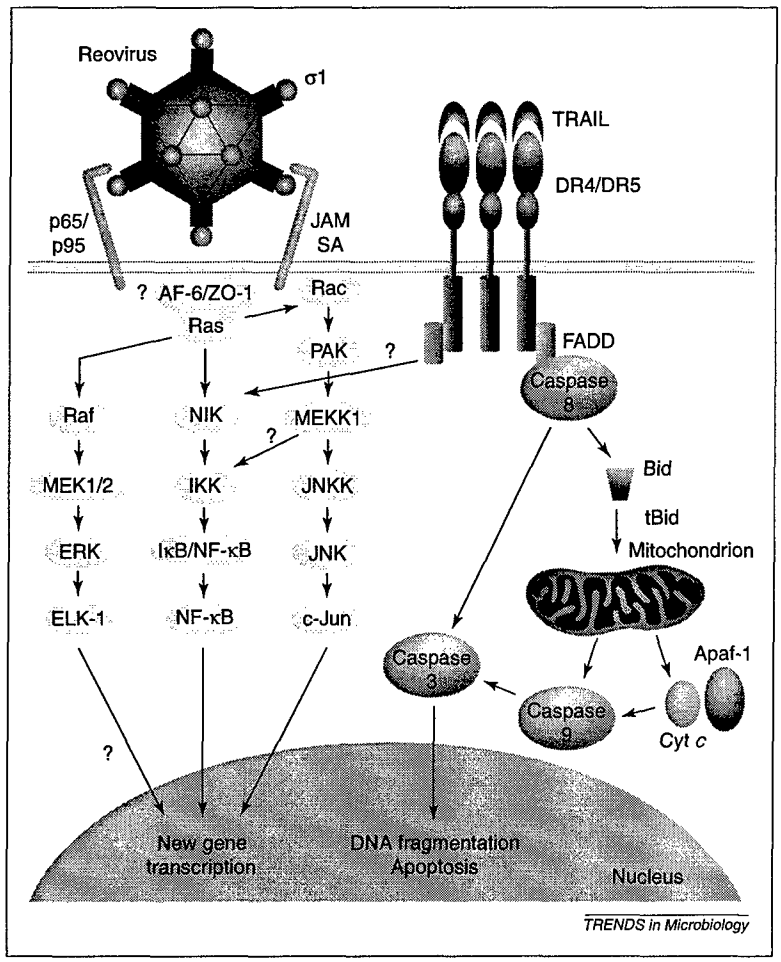

Fig. 1. Reovirus-induced changes in cellular signaling pathways. Reovirus infection is associated with changes in kinase pathways involved in the regulation of NF-κB, and MAPK cascades involving both JNK and ERK. Infection results in new gene transcription and upregulation of apoptotic pathways including the TRAIL/DR4/DR5 death receptor and mitochondrial pathways. Mitochondrial-mediated cell death involves the activation of an initiator caspase, caspase 9, and an effector caspase, caspase 3. Reovirus receptors including JAM, SA and an uncharacterized heterodimeric 'p65/p95' receptor have all been implicated in reovirus-induced changes in cell signaling pathways. The mechanisms by which receptor engagement leads to changes in intracellular signaling and the exact receptor(s) involved in activating specific pathways remain to be defined. See text for details regarding individual pathways. Abbreviations: Apaf-1, apoptotic protease activating factor 1; Cyt *c*, cytochrome *c*; DR, death receptor; ELK-1, Ets-like kinase 1; ERK, extracellular signal response kinase; FADD, Fas-associated death domain; IκB, inhibitor of κB; IKK, IκB kinase complex; JAM, junctional adhesion molecule; JNK, c-Jun amino-terminal kinase; JNKK, JNK kinase; MAPK, mitogen-activated protein kinase; MEK, MAPK kinase; NF-κB, nuclear factor-κB; NIK, NF-κB-inducing kinase; PAK, p21-activated kinase; SA, sialic acid; TRAIL, tumor necrosis factor-related apoptosis-inducing ligand.

whether JAM is in fact accessible for viral attachment in target tissues *in vivo*. Although JAM is highly conserved among mammalian species and is expressed on many cell types that are susceptible to reovirus infection, it is unclear whether the tissue- and cell type-specific distributions of JAM correspond with the known cell and tissue tropisms of reovirus. However, the recent identification of proteins with homology to JAM (e.g. JAM-2)[7,8], which vary in their cell and tissue localization, raises the intriguing possibility that these could also be functional reovirus receptors.

Several recent studies suggest that JAM is associated with a complex of tight junction proteins that can interact with membrane-associated guanylate kinase homologs including the Ras- and Rap1A-interacting proteins AF-6 and ZO-1 (Refs 9,10). These membrane-associated guanylate kinases can in turn activate mitogen-activated protein kinase (MAPK) kinase (MEK) signaling cascades. Thus, although JAM is not conventionally considered a signal transduction protein, it will be intriguing to see what role, if any, it plays in mediating reovirus-induced changes in cellular signal transduction pathways. Nonetheless, reovirus interaction with JAM is unlikely to provide a complete explanation for reovirus-induced activation of cellular transcription factors, MAPK cascades and perturbation in cell cycle regulation. For example, reovirus binding to a heterodimeric p65/p95 cell surface receptor found on certain proliferating cells, including R1.1 thymoma cells and activated T cells, has been associated with reovirus-induced G1 cell cycle arrest and inhibition of Ras-related signaling pathways[11,12].

Reovirus-induced activation of nuclear transcription factors

One of the earliest events following T3 infection is activation of the nuclear factor (NF)-κB family of transcription factors, and this activation appears to be required for the subsequent initiation of reovirus-induced apoptosis[13]. Using electrophoretic mobility-shift assays (EMSA), NF-κB complexes that include p50 and p65 (RelA) can be detected in the nucleus of infected HeLa cells within 4 hrs of infection and reovirus-induced expression of an NF-κB-dependent luciferase reporter gene can be detected within 12 hrs. Inhibition of NF-κB activation by stable expression of a super-repressor form of inhibitor of κB (IκB), by inhibition of the proteosomal degradation of IκB or by using immortalized mouse embryo fibroblasts (MEFs) lacking the p50 or p65 (RelA) components of the NF-κB complex inhibits reovirus-induced apoptosis[13].

The upstream events leading to reovirus-induced NF-κB activation are just beginning to be elucidated. Monoclonal antibodies to hJAM inhibit NF-κB activation and the subsequent apoptosis in HeLa cells despite the fact that these cells remain susceptible to SA-mediated reovirus binding and infection[4]. However, removal of surface SA by neuraminidase treatment blocks both NF-κB activation and apoptosis[14], suggesting that engagement of both JAM and SA might be required for their optimal induction. It remains to be established whether these events are the result of activation of a signal transduction cascade initiated through JAM and/or SA binding, or whether these interactions are merely required to initiate appropriate early steps in reovirus cell entry and replication. However, as replication-incompetent UV-inactivated virus can induce both NF-κB activation[13] and apoptosis[15], this suggests that JAM

and/or SA binding is likely to play a greater role than simply facilitating viral entry into target cells.

JAM has not been linked to canonical NF-κB activation pathways. Under normal circumstances, inactive NF-κB is retained in the cytoplasm complexed to its repressor, IκB. Phosphorylation of IκB by the IκB kinase complex (IKK) leads to the ubiquitination and proteosomal degradation of IκB. IKK is itself activated by proteins that function as IKK kinases, including MEK kinase 1 (MEKK1), NF-κB-inducing kinase (NIK) and the interferon (IFN)-induced double-stranded RNA-activated protein kinase (PKR)[16,17]. Cells expressing dominant-negative (DN) forms of NIK fail to activate NF-κB in response to reovirus infection. Embryonal stromal (ES) cells derived from mice with targeted disruptions in the gene encoding MEKK1 show normal levels of reovirus-induced NF-κB activation[18], suggesting that NIK rather than MEKK1 might be the significant IKK kinase activated following reovirus infection. Perhaps surprisingly, given the ease with which reovirus infection induces IFN (see Refs 19,20), PKR does not appear to play a role in reovirus-induced apoptosis or NF-κB activation. Cells transiently expressing DN-PKR and MEFs lacking PKR have normal levels of reovirus-induced NF-κB activation and apoptosis [P. Clarke *et al.* (2000) MEKK1 and NIK contribute to the activation of NF-κB in reovirus-infected cells via IKK. Abstracts of the 19th Annual Meeting of the American Society for Virology, Fort Collins, CO, USA. Abstract W20-9]. It is important to recognize that there are alternative pathways for NF-κB activation other than kinase-activated degradation of IκB. For example, calpain-mediated proteolysis of IκB can also lead to NF-κB activation. Calpains are activated in response to reovirus infection in a variety of target cells including fibroblasts and myocardiocytes *in vitro*, and in reovirus-infected tissue such as the heart *in vivo*[21,22].

Reovirus activation of MAPK cascades

In addition to the activation of NF-κB, reovirus infection leads to the selective activation of MAPK cascades. Activation of MAPK cascades usually begins with a small G protein and then proceeds through sequential kinase cascades leading from MAP kinase kinase kinase kinases (MAP4Ks) to MAP3Ks, MAP2Ks and MAPKs. MAPKs in turn phosphorylate and activate transcription factors. T3 reovirus infection is associated with activation of c-Jun amino-terminal kinase (JNK) and its substrate, the transcription factor c-Jun. JNK activation can be detected within 8–10 hrs of infection and persists for at least 24 hrs[18,23]. The capacity to activate JNK is reovirus strain-specific, with the prototype T3 strains Abney (T3A) and Dearing (T3D) being significantly more potent inducers than T1L. This difference is determined by the same viral genes (*S1* and *M2*) that determine strain-specific differences in apoptosis induction[15,24] and correlates with apoptosis induction[23]. Reovirus infection of ES cells lacking the MAP3K MEKK1 results in a marked reduction in JNK activation[18], indicating that activation of MEKK1 plays a crucial role in this process.

Ras signaling

Reovirus infection of R1.1 thymoma cells decreases Raf-1 phosphorylation and extracellular signal response kinase (ERK) activity[12]. Raf-1 is part of a MAPK cascade that begins with conversion of Ras-GDP to Ras-GTP and leads sequentially to phosphorylation and activation of Raf-1, MEK 1/2 and ERK. Paradoxically, cells overexpressing constitutively active Ras signaling pathway molecules including Sos and Ras, which have increased levels of ERK 1/2 activity, show enhanced efficiency of reovirus infection[25]. It has been suggested that increases in Ras signaling might play a role, through as-yet-undefined mechanisms, in preventing reovirus-induced PKR activation and thereby augmenting viral protein synthesis[25,26].

Cellular pathways involved in reovirus-induced apoptosis

Reovirus-induced apoptosis involves JAM and/or SA binding, and the activation of transcription factors including NF-κB and possibly c-Jun. This suggests that new gene expression is an essential component of reovirus-induced cell death. Identification of the specific genes involved is likely to provide important insights into the mechanism of reovirus-induced apoptosis, and studies are currently under way to identify virus-associated changes in gene transcription using high-density oligonucleotide microarrays (GeneChip; Affymetrix, CA, USA). Preliminary studies suggest that reovirus infection leads to altered expression of a limited subset of host genes that can be functionally categorized as encoding proteins involved in IFN responses, apoptotic signaling, DNA damage and repair processes, and cell cycle regulation [R.L. Debiasi *et al.* (2001) Reovirus infection results in altered transcription of genes related to cell cycle, apoptosis and DNA repair including BRCA-1, GADD45 and regulators of BCL-2. Abstracts of the 20th Annual Meeting of the American Society for Virology, Madison, WI, USA. Abstract W12-3].

Cell surface death receptors

Ribonuclease protection assays suggest that members of the tumor necrosis factor (TNF) superfamily of cell-surface death receptors, specifically death receptors 4 (DR4) and 5 (DR5) and their ligand (TNF-related apoptosis-inducing ligand, TRAIL), are involved in reovirus-induced apoptosis. Antibodies against TRAIL and soluble forms of DR4 and DR5 inhibit reovirus-induced apoptosis[27,28]. A similar effect is seen in cells stably overexpressing DcR2 (Ref. 28), a decoy receptor that binds TRAIL

Questions for future research

- What are the cellular pathways linking reovirus engagement of JAM and/or other host cell surface receptors and activation of MAPK pathways and transcription factors?
- What are the specific genes essential for reovirus-induced apoptosis and cell cycle dysregulation and which transcription factors control their expression?
- What is the role of apoptosis in reovirus-induced tissue injury in different organs *in vivo*, and what are the effects on viral pathogenesis of inhibiting apoptosis?
- What role do reovirus-induced alterations in cell cycle regulation play in viral replication *in vitro* and pathogenesis *in vivo*?
- What is the relationship between reovirus receptors identified *in vitro*, and the cell and tissue tropism of the virus *in vivo*? Do differences in patterns of receptor utilization or expression explain age-related and/or strain-specific differences in patterns of viral infection?

but fails to activate apoptotic signaling pathways. Reovirus-induced apoptosis results in activation of the death-receptor-associated initiator caspase, caspase 8 and subsequent activation of the downstream effector caspases, caspases 3 and 7 [Ref. 28; D. Kominsky (2001) Reovirus infection contributes both extrinsic death receptor- and intrinsic mitochondrial-mediated pathways of apoptosis. Abstracts of the 20th Annual Meeting of the American Society for Virology, Madison, WI, USA. Abstract W2-7]. Reovirus infection also induces activation of the mitochondrial apoptotic pathway with release of cytochrome *c* and activation of the mitochondrion-associated initiator caspase, caspase 9. Both caspase 8 and caspase 9 are capable of activating the effector caspase, caspase 3. The death receptor and mitochondrial apoptotic pathways are linked by Bid, a Bcl-2 family protein. Reovirus infection results in caspase-8-dependent cleavage of Bid, which can then translocate to the mitochondrion and trigger release of cytochrome *c* [D. Kominsky (2001) Reovirus infection contributes both extrinsic death receptor- and intrinsic mitochondrial-mediated pathways of apoptosis. Abstracts of the 20th Annual Meeting of the American Society for Virology, Madison, WI, USA. Abstract W2-7]. Reovirus-induced apoptosis is significantly inhibited by cell-permeable tetrapeptide inhibitors of caspase 8 and by stable overexpression of DN Fas-associated death domain (FADD)[27]. Bid cleavage and cytochrome *c* release are also both inhibited in reovirus-infected cells stably expressing DN-FADD [D. Kominsky (2001) Reovirus infection contributes both extrinsic death receptor- and intrinsic mitochondrial-mediated pathways of apoptosis. Abstracts of the 20th Annual Meeting of the American Society for Virology, Madison, WI, USA. Abstract W2-7], suggesting that activation of the mitochondrial apoptosis pathway is initiated by death-receptor activation and uses Bid-mediated crosstalk. The mitochondrial pathway provides a crucial amplification step in reovirus apoptosis, as inhibition of mitochondrial release of cytochrome *c* by stable overexpression of Bcl-2 inhibits reovirus-induced apoptosis[29] [D. Kominsky (2001) Reovirus infection contributes both extrinsic death receptor- and intrinsic mitochondrial-mediated pathways of apoptosis. Abstracts of the 20th Annual Meeting of the American Society for Virology, Madison, WI, USA. Abstract W2-7].

Reovirus-induced perturbation of cell cycle regulation

Reovirus infection is associated with inhibition of DNA synthesis and inhibition of cellular proliferation[24]. Depending on the cells investigated and the experimental methods employed, reovirus has been reported to induce cell cycle arrest in both the G1 (Ref. 12) and G2/M phase[30,31]. Differences in the capacity of reovirus strains to induce cell cycle arrest are determined by the viral S1 genome segment[24], which is bicistronic. Cell cycle arrest in G1 has been associated with the S1-encoded σ1 protein[12], whereas G2/M arrest requires the S1-encoded non-structural protein, σ1s (Ref. 30). T3 virions lacking σ1s fail to induce G2/M arrest and induced expression of σ1s causes an accumulation of cells in G2/M (Ref. 30). Reovirus-induced arrest in G2/M is associated with hyper-phosphorylation and inhibition of the key G2-to-M transition kinase, $p34^{cdc2}$ (Ref. 31). $p34^{cdc2}$ hyper-phosphorylation can be induced by σ1s expression, and fails to occur in cells infected with a T3 σ1s-deficient virus. Reovirus-induced G1 arrest in R1.1 thymoma cells is associated with Ras inhibition and can be reversed by constitutive expression of *v*-Ha-*ras* (Ref. 12).

Reovirus and the host

Reovirus-induced perturbations of cell signaling pathways including those involved in apoptosis regulation, cell cycle perturbation and MAPK cascades were all initially identified *in vitro*, and their potential significance to pathogenesis *in vivo* is only beginning to be understood. Following intracerebral inoculation of neonatal mice, T3D induces a lethal encephalitis. Within the central nervous system (CNS), there is an excellent correlation between the areas of viral infection as identified by antigen staining, the presence of apoptotic neurons identified by terminal deoxynucleotidyl transferase-mediated dUTP nick end labeling (TUNEL), the morphological characteristics of apoptosis and neuropathological injury[32]. A similar correlation has been seen in the heart following intramuscular inoculation of neonatal mice with the myocarditic reovirus 8B strain (Ref. 22). DNA isolated from either infected brains or hearts shows the inter-nucleosomal fragmentation pattern characteristic of apoptosis ('laddering'). In the CNS, double-labeling of cells for the presence of viral antigen and for apoptosis by TUNEL indicates that both infected cells and

non-infected (bystander) cells in proximity to infected cells can undergo apoptosis[32]. In cultured fibroblasts and myocardiocytes, and in the heart, reovirus infection is associated with activation of calpain, a calcium-dependent cysteine protease[21,22]. Inhibition of calpain activation *in vitro* inhibits reovirus-induced apoptosis[21]. Administration of calpain inhibitors *in vivo* prevents myocardial apoptosis and dramatically inhibits reovirus-induced myocardial injury[22]. These studies strongly suggest that apoptosis is an important feature of reovirus infection *in vivo*, and a major contributory factor to virus-induced tissue injury.

Unlike apoptosis, the significance of reovirus-induced perturbations in cell cycle regulation and MAPK signaling in pathogenesis remains largely unknown. It has not yet been established whether reovirus infection alters cellular proliferation or cell cycle regulation following infection *in vivo*. The importance of reovirus-induced perturbations in Ras signaling or in JNK and ERK MAPK cascades for pathogenesis *in vivo* also remains to be established. One glimpse into this area comes from studies of the capacity of reovirus to kill homo- or xenografted tumor cells[26,33]. Intratumoral injection of virus has been shown to cause regression of U87 glioblastoma and transformed fibroblast-derived tumors established in mice[33]. It has been suggested that the susceptibility of transformed cells to reovirus infection both *in vitro* and in homo- and xenografts *in vivo* reflects the presence of an activated Ras signaling pathway[26,33]. However, it remains unknown whether the basal state or reovirus-induced changes in MAPK signaling pathways also influence the susceptibility of non-transformed cells to reovirus infection during natural infection in the host.

Conclusion

Reoviruses have long served as a model system for studying viral pathogenesis *in vivo*. Recent studies have dramatically advanced our understanding of reovirus–host interactions at the cellular level, and have provided new insights into viral host cell receptors, the mechanisms of virus-induced cell death, and the effects of viral infection on cellular signaling pathways and cell cycle regulation. A better understanding of the inter-relationships of these various events and their consequences for viral pathogenesis, are the key goals for future research.

Acknowledgements
Research support has been provided by the Dept of Veterans Affairs (MERIT and REAP Awards), the US Army (Medical Research Grant DAMD17-98-1-8614), and the National Institute on Aging (1R01 AG14071).

References

1 Tyler, K.L. (2001) Mammalian reoviruses. In *Fields Virology* (4th edn) (Knipe, D.M. *et al.*, eds), pp. 1729–1745, Lippincott–William & Wilkins
2 Chappell, J.D. *et al.* (1997) Mutations in type 3 reovirus that determine binding to sialic acid are contained in the fibrous tail domain of viral attachment protein σ1. *J. Virol.* 71, 1834–1841
3 Chappell, J.D. *et al.* (2000) Identification of carbohydrate-binding domains in the attachment proteins of type 1 and type 3 reoviruses. *J. Virol.* 74, 8472–8479
4 Barton, E.S. *et al.* (2001) Junctional adhesion molecule is a receptor for reovirus. *Cell* 104, 441–451
5 Liu, Y. *et al.* (2000) Human junction adhesion molecule regulates tight junction resealing in epithelia. *J. Cell Sci.* 113, 1–11
6 Martin-Padura, I. *et al.* (1998) Junctional adhesion molecule, a novel member of the immunoglobulin superfamily that distributes at intercellular junctions and mediates monocyte transmigration. *J. Cell Biol.* 142, 117–127
7 Cunningham, S.A. *et al.* (2000) A novel protein with homology to the junctional adhesion molecule. *J. Biol. Chem.* 275, 34750–34756
8 Aurrand-Lions, M. *et al.* (2001) JAM-2, a novel immunoglobulin superfamily molecule, expressed by endothelial and lymphatic cells. *J. Biol. Chem.* 276, 2733–2741
9 Ebnet, K. *et al.* (2000) Junctional adhesion molecule interacts with the PDZ-domain-containing proteins AF-6 and ZO-1. *J. Biol. Chem.* 275, 27979–27988
10 Boettner, B. *et al.* (2000) The junctional multidomain protein AF-6 is a binding partner of the Rap1A GTPase and associated with the actin cytoskeletal regulator profilin. *Proc. Natl. Acad. Sci. U. S. A.* 97, 9064–9069
11 Roux, E. *et al.* (1998) A cell cycle regulating receptor is localized on cell surface and in nuclei of mitotically and meiotically dividing cells. *DNA Cell Biol.* 17, 239–247
12 Saragovi, H.U. *et al.* (1999) A G_1 cell cycle arrest induced by ligands of the reovirus type 3 receptor is secondary to inactivation of $p21^{ras}$ and mitogen-activated protein kinase. *DNA Cell Biol.* 18, 763–770
13 Connolly, J.L. *et al.* (2000) Reovirus-induced apoptosis requires activation of transcription factor NF-κB. *J. Virol.* 74, 2981–2989
14 Connolly, J.L. *et al.* (2001) Reovirus binding to cell surface sialic acid potentiates virus-induced apoptosis. *J. Virol.* 75, 4029–4039
15 Tyler, K.L. *et al.* (1995) Differences in the capacity of reovirus strains to induce apoptosis are determined by the viral attachment protein σ1. *J. Virol.* 69, 6972–6979
16 Barkett, M. and Gilmore, T.D. (1999) Control of apoptosis by Rel/NF-κB transcription factors. *Oncogene* 18, 6910–6924
17 Hiscott, J. *et al.* (2001) Hostile takeovers: viral appropriation of the NF-κB pathway. *J. Clin. Invest.* 107, 143–151
18 Yujiri, T. *et al.* (2000) MEK kinase 1 gene disruption alters cell migration and c-Jun NH_2-terminal kinase regulation but does not cause a measurable defect in NF-κB activation. *Proc. Natl. Acad. Sci. U. S. A.* 97, 7272–7277
19 Sherry, B. *et al.* (1998) Reovirus induction of and sensitivity to β interferon in cardiac myocyte cultures correlate with induction of myocarditis and are determined by viral core proteins. *J. Virol.* 72, 1314–1323
20 Samuel, C.E. *et al.* (1998) Reoviruses II. Cytopathicity and pathogenesis. *Curr. Topics Microbiol. Immunol.* 233, 125–146
21 Debiasi, R.L. *et al.* (1998) Reovirus-induced apoptosis is preceded by increased cellular calpain activity and is blocked by calpain inhibitors. *J. Virol.* 73, 695–701
22 Debiasi, R.L. *et al.* (2001) Calpain inhibition protects against virus-induced apoptotic myocardial injury. *J. Virol.* 75, 351–361
23 Clarke, P. *et al.* Reovirus infection activates JNK-dependent transcription factor c-Jun. *J. Virol.* (in press)
24 Tyler, K.L. *et al.* (1996) Linkage between reovirus-induced apoptosis and inhibition of cellular DNA synthesis: role of the S1 and M2 genes. *J. Virol.* 70, 7984–7991
25 Strong, J.E. *et al.* (1998) The molecular basis of oncolysis: usurpation of the Ras signaling pathway by reovirus. *EMBO J.* 17, 3351–3362
26 Norman, K.L. and Lee, P.W.K. (2000) Reovirus as a novel oncolytic agent. *J. Clin. Invest.* 105, 1035–1038
27 Clarke, P. *et al.* (2000) Reovirus-induced apoptosis is mediated by TRAIL. *J. Virol.* 74, 8135–8139
28 Clarke, P. *et al.* Caspase-8 dependent sensitization of cancer cells to TRAIL–induced apoptosis following reovirus infection. *Oncogene* (in press)
29 Rodgers, S.E. *et al.* (1997) Reovirus-induced apoptosis of MDCK cells is not linked to viral yield and is inhibited by bcl-2. *J. Virol.* 71, 2540–2546
30 Poggioli, G.J. *et al.* (2000) Reovirus-induced G_2/M cell cycle arrest requires σ1s and occurs in the absence of apoptosis. *J. Virol.* 74, 9562–9570
31 Poggioli, G.J. *et al.* (2001) Reovirus-induced σ1s-dependent G_2/M cell cycle arrest is associated with inhibition of $p34^{cdc2}$. *J. Virol.* 75, 7429–7434
32 Oberhaus, S.M. *et al.* (1997) Reovirus infection and tissue injury in the mouse central nervous system are associated with apoptosis. *J. Virol.* 71, 2100–2106
33 Coffey, M.C. *et al.* (1998) Reovirus therapy of tumors with activated Ras pathway. *Science* 282, 1332–1334

JOURNAL OF VIROLOGY, Oct. 2000, p. 9562–9570 Vol. 74, No. 20
0022-538X/00/$04.00+0

Reovirus-Induced G_2/M Cell Cycle Arrest Requires σ1s and Occurs in the Absence of Apoptosis

GEORGE J. POGGIOLI,[1] CHRISTOPHER KEEFER,[2] JODI L. CONNOLLY,[3,4] TERENCE S. DERMODY,[2,3,4] AND KENNETH L. TYLER[1,5,6,7,8]*

Departments of Neurology,[5] Medicine,[6] Microbiology,[1] and Immunology,[7] University of Colorado Health Sciences Center, and Neurology Service, Denver Veterans Affairs Medical Center,[8] Denver, Colorado 80220, and Departments of Pediatrics[2] and Microbiology and Immunology[3] and Elizabeth B. Lamb Center for Pediatric Research,[4] Vanderbilt University School of Medicine, Nashville, Tennessee 37232

Received 1 May 2000/Accepted 18 July 2000

Serotype-specific differences in the capacity of reovirus strains to inhibit proliferation of murine L929 cells correlate with the capacity to induce apoptosis. The prototype serotype 3 reovirus strains Abney (T3A) and Dearing (T3D) inhibit cellular proliferation and induce apoptosis to a greater extent than the prototype serotype 1 reovirus strain Lang (T1L). We now show that reovirus-induced inhibition of cellular proliferation results from a G_2/M cell cycle arrest. Using T1L × T3D reassortant viruses, we found that strain-specific differences in the capacity to induce G_2/M arrest, like the differences in the capacity to induce apoptosis, are determined by the viral S1 gene. The S1 gene is bicistronic, encoding the viral attachment protein σ1 and the nonstructural protein σ1s. A σ1s-deficient reovirus strain, T3C84-MA, fails to induce G_2/M arrest, yet retains the capacity to induce apoptosis, indicating that σ1s is required for reovirus-induced G_2/M arrest. Expression of σ1s in C127 cells increases the percentage of cells in the G_2/M phase of the cell cycle, supporting a role for this protein in reovirus-induced G_2/M arrest. Inhibition of reovirus-induced apoptosis failed to prevent virus-induced G_2/M arrest, indicating that G_2/M arrest is not the result of apoptosis related DNA damage and suggests that these two processes occur through distinct pathways.

Reovirus infection of cultured cells results in inhibition of cellular proliferation (10, 17–19, 21, 24–27, 38, 40, 41, 44). Serotype 3 prototype strains type 3 Abney (T3A) and type 3 Dearing (T3D) inhibit cellular DNA synthesis to a greater extent than the serotype 1 prototype strain type 1 Lang (T1L) (40, 44). Studies using T1L × T3A and T1L × T3D reassortant viruses indicate that the S1 gene is the primary determinant of DNA synthesis inhibition (40, 44). Earlier studies suggested that reovirus-induced inhibition of cellular proliferation results from inhibition of the initiation of DNA synthesis, consistent with a G_1-S transition block (10, 19, 26, 27, 38).

Reovirus infection also results in apoptosis (11, 36, 37, 44, 45). Reovirus strains T3A and T3D induce apoptosis to substantially greater extent than T1L (44, 45). A significant correlation exists between the capacities of both T1L × T3A (r = 0.937) and T1L × T3D (r = 0.772) reassortant viruses and reovirus field isolate strains (r = 0.851) to inhibit cellular proliferation and induce apoptosis (44). Like strain-specific differences in DNA synthesis inhibition, strain-specific differences in apoptosis induction also segregate with the S1 gene (36, 44, 45).

The viral S1 gene segment is bicistronic, encoding the viral attachment protein, σ1, and a non-virion-associated protein with no known function, σ1s, from overlapping reading frames (20, 30, 39). Using a σ1s-deficient virus strain, it was shown that σ1s is not required for reovirus growth in cell culture and is dispensable for the induction of apoptosis (37). These observations in conjunction with the genetic mapping studies suggest that σ1 is the primary determinant of strain-specific differences in apoptosis induction. The S1 gene product associated with reovirus-induced inhibition of cellular DNA synthesis has not been identified.

We conducted experiments to further investigate the relationship between reovirus-induced cellular DNA synthesis inhibition and apoptosis. We found that inhibition of cellular proliferation in response to reovirus infection is caused by an arrest in the G_2/M phase of the cell cycle. Reovirus strains differ in the capacity to induce G_2/M arrest, and we used reassortant viruses to demonstrate that these differences segregate with the S1 gene. A reovirus σ1s mutant fails to induce G_2/M arrest but retains the capacity to induce apoptosis. Inducible expression of σ1s results in the accumulation of cells in G_2/M phase. Inhibition of reovirus-induced apoptosis does not affect reovirus-induced G_2/M arrest. These results indicate that the σ1s protein is required for reovirus-induced G_2/M arrest and suggest that reovirus-induced inhibition of cellular proliferation and induction of apoptosis involve independent pathways.

MATERIALS AND METHODS

Cells and viruses. Spinner-adapted mouse L929 cells (ATCC CCL1) were grown in Joklik's modified Eagle's minimal essential medium (JMEM) supplemented to contain 5% heat-inactivated fetal bovine serum (Gibco BRL, Gaithersburg, Md.) and 2 mM L-glutamine (Gibco). Human embryonic kidney (HEK293) cells (ATCC CRL1573), Madin-Darby canine kidney (MDCK) cells (ATCC CCL34), C127 cells (ATCC CRL1616), and HeLa cells (ATCC CCL2) were grown in Dulbecco's modified Eagle's medium (DMEM) supplemented to contain 10% heat-inactivated fetal bovine serum (HEK293, MDCK, and C127) or 10% non-heat-inactivated fetal bovine serum (HeLa), 2 mM L-glutamine, and 100 U of penicillin and 100 μg of streptomycin per ml (Gibco). IκB-ΔN2 cells are HEK293 cells expressing a strong dominant-negative IκB mutant lacking the phosphorylation sites that regulate signal-dependent activation of NF-κB (7).

Reovirus strains T1L, T3A, and T3D are laboratory stocks. T1L × T3D reassortant viruses were grown from stocks originally isolated by Kevin Coombs, Bernard Fields, and Max Nibert (4, 9). The reovirus field-isolate strain type 3 clone 84 (T3C84) was isolated from a human host, and T3C84-MA was isolated

* Corresponding author. Mailing address: Department of Neurology (B-182), University of Colorado Health Sciences Center, 4200 E. 9th Ave., Denver, CO 80262. Phone: (303) 393-2874. Fax: (303) 393-4686. E-mail: Ken.Tyler@UCHSC.edu.

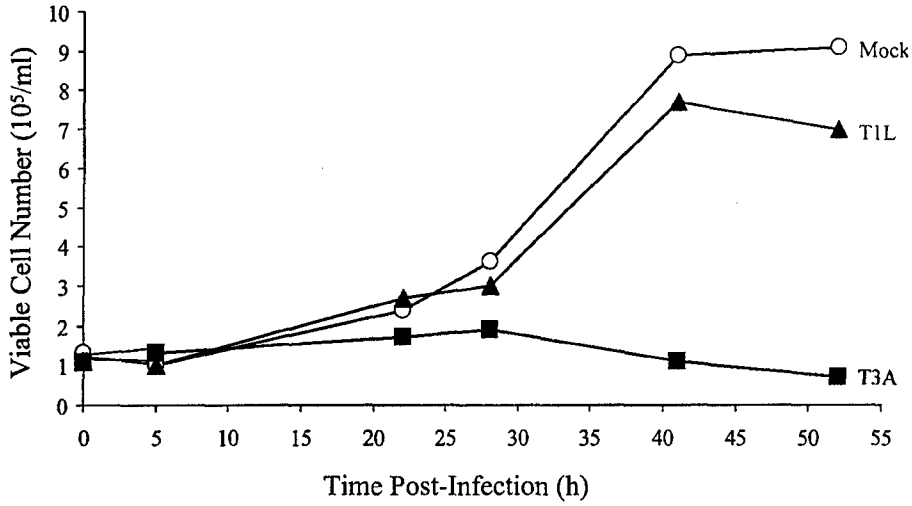

FIG. 1. Reovirus inhibits cellular proliferation. Asynchronous, subconfluent monolayers of L929 cells were either mock infected (circles) or infected with T1L (triangles) or T3A (squares) at an MOI of 100 PFU per cell. Cells were harvested at the indicated times postinfection and counted. Cells that excluded trypan blue were scored as viable. Results are presented as the number of viable cells $\times 10^5$ per ml. The results from a representative experiment of three independent experiments are shown.

as previously described (6, 12). Viral strains were plaque purified and passaged two to three times in L929 cells to generate working stocks as previously described (43).

Isolation and characterization of T3C84-MA/σ1s+. T3C84-MA/σ1s+ was isolated following serial passage of T3C84 in MEL cells as previously described (6). To isolate a sialic acid binding MEL cell-adapted variant derived from T3C84 that retains the capacity to express σ1s, virus isolates from a fifth-passage murine erythroleukemia (MEL) cell lysate stock were plaque purified twice on L929 cell monolayers. Plaques were amplified twice in L929 cell cultures and used to infect L929 cells (10^7) at a multiplicity of infection (MOI) of 10 PFU per cell. Cytoplasmic extracts were prepared 24 h following infection as previously described (8). Protein (100 μg) was electrophoresed in a 14% sodium dodecyl sulfate-polyacrylamide gel and transferred to a nitrocellulose membrane. An immunoblot for σ1s was performed as previously described (37). The S1 gene of a fifth-passage isolate that expresses σ1s, termed T3C84-MA/σ1s+, was sequenced as previously described (6). T3C84-MA/σ1s+ contains the mutation at nucleotide 616 that results in a tryptophan-to-arginine substitution at residue 202 of the σ1 protein, which is also present in the S1 gene of T3C84-MA and confers the capacity to bind sialic acid but does not contain the mutation that results in the introduction of a stop codon following amino acid six in the σ1s protein.

Cellular proliferation. L929 cells were seeded in six-well plates (Costar, Cambridge, Mass.) at 10^5 cells per well in a volume of 2.5 ml in JMEM supplemented to contain nonessential amino acids, 5% fetal bovine serum, 2 mM L-glutamine, 100 U of penicillin per ml, and 100 μg of streptomycin per ml. After 24 h of incubation, when cells were 10 to 20% confluent, the medium was removed, and cells were infected with viral strains at an MOI of 100 PFU per cell in a volume of 100 μl at 37°C for 1 h. After viral infection, 2.5 ml of fresh medium was added to each well. At various times postinfection, cells were harvested, resuspended in 2 ml of phosphate-buffered saline (PBS), and counted using a hemacytometer. Cell viability was determined by trypan blue exclusion. Results are presented as the viable cell numbers per milliliter.

Flow cytometry. L929, HEK293, MDCK, and HeLa cells were seeded in either 12-well plates (Costar) at 10^5 cells per well in a volume of 1 ml per well or 24-well plates (Costar) at 3.7×10^4 cells per well in a volume of 0.5 ml per well and then infected with reovirus as described above. Cells were harvested, washed once with PBS, and stained at 4°C overnight with Krishan's stain containing 3.8 mM trisodium citrate (Sigma Chemical Co., St. Louis, Mo.), 70 μM propidium iodide (Sigma), 0.01% Nonidet P-40 (Sigma), and 0.01 mg of RNase A (Boehringer Mannheim Co., Indianapolis, Ind.) per ml (33). Cell cycle analysis was performed using a Coulter Epics XL flow cytometer (Beckman-Coulter, Hialeah, Fla.). Alignment of the instrument was verified daily using DNA check beads (Coulter). Peak versus integral gating was used to exclude doublet events from the analysis. Data were collected for 10,000 events. The Modfit LT program (Verity Software House, Topsham, Maine) was used for cell cycle modeling.

Cell synchronization. L929 cells were seeded in 24-well plates at 3.7×10^4 cells per well in a volume of 0.5 ml per well. After 24 h, cells were treated with 1 μM amethopterin (methotrexate) (Sigma) and 50 μM adenosine (Sigma) for 16 h. Cells were washed twice with PBS, infected with reovirus, and incubated with fresh JMEM supplemented to contain 5% heat-inactivated fetal bovine serum, 2 mM L-glutamine, and 2 mg of thymidine (Sigma) per ml. At various times after infection, cells were harvested, washed once with PBS, and stained at 4°C overnight with Krishan's stain as described above.

Quantitation of apoptosis by acridine orange staining. L929, HEK293, MDCK, and HeLa cells were seeded and infected with reovirus as described above. The percentage of apoptotic cells was determined at 48 h postinfection as previously described (16, 45). Cells were harvested, washed once with PBS, resuspended in 25 μl of cell culture medium, and stained with 1 μl of a dye solution containing 100 μg of acridine orange (Sigma) per ml and 100 μg of ethidium bromide (Sigma) per ml. Cells were examined by epifluorescence microscopy (Nikon Labophot-2; B-2A filter; excitation, 450 to 490 nm; barrier, 520 nm; dichroic mirror, 505 nm) and scored as apoptotic if their nuclei contained uniformly stained condensed or fragmented chromatin (16, 45).

Apoptosis inhibitors. L929 cells were seeded in 24-well plates at 3.7×10^4 cells per well in a volume of 0.5 ml per well. After 24 h of incubation, cells were incubated with the calpain inhibitor PD150606 (Parke-Davis Pharmaceutical Research, Ann Arbor, Mich.) (50 μM, L929 cell), the caspase 3 inhibitor DEVD-CHO (Clontech, Palo Alto, Calif.) (100 μM, HEK293), or anti-TRAIL antibody (Affinity Bioreagents, Golden, Colo.) (30 μM, HEK293) for 1 h. Cells were then infected with T3A at an MOI of 100 PFU per cell at 37°C for 1 h. Following infection, media containing the apoptosis inhibitor was added. Cells were harvested and analyzed for either apoptosis or cell cycle arrest at 48 h postinfection.

Inducible expression of σ1s. C127 stable transformants expressing T3D σ1s (BPX-6) from the mouse metallothionein promoter and vector control (BPV-12) were provided by Aaron Shatkin (21). BPX-6 and BPV-12 cells were seeded in 24-well plates at 3.0×10^4 cells per well in a volume of 0.5 ml per well. After 24 h of incubation, cells were incubated with 1 μM $CdCl_2$ to induce σ1s expression (22) and harvested at various times postinduction for cell cycle analysis.

RESULTS

Reovirus strains T1L and T3A differ in the capacity to inhibit cellular proliferation. We have previously shown that T1 and T3 reovirus strains differ in the capacity to inhibit cellular DNA synthesis as measured by [^{3}H]thymidine incorporation (40, 44). To determine whether reovirus-induced DNA synthesis inhibition is associated with inhibition of cellular proliferation, we infected L929 cells with either T1L or T3A at an MOI of 100 PFU per cell. At various intervals after infection, viable cells were counted (Fig. 1). Infection with T3A resulted in complete inhibition of cellular proliferation. A modest reduction in proliferation was observed for cells infected with T1L compared to mock-infected controls. Therefore, strain-specific differences in inhibition of cellular proliferation parallel those previously reported for DNA synthesis inhibition.

T3 reoviruses induce G_2/M arrest. To identify the phase in the cell cycle that T3 reoviruses inhibit cellular proliferation,

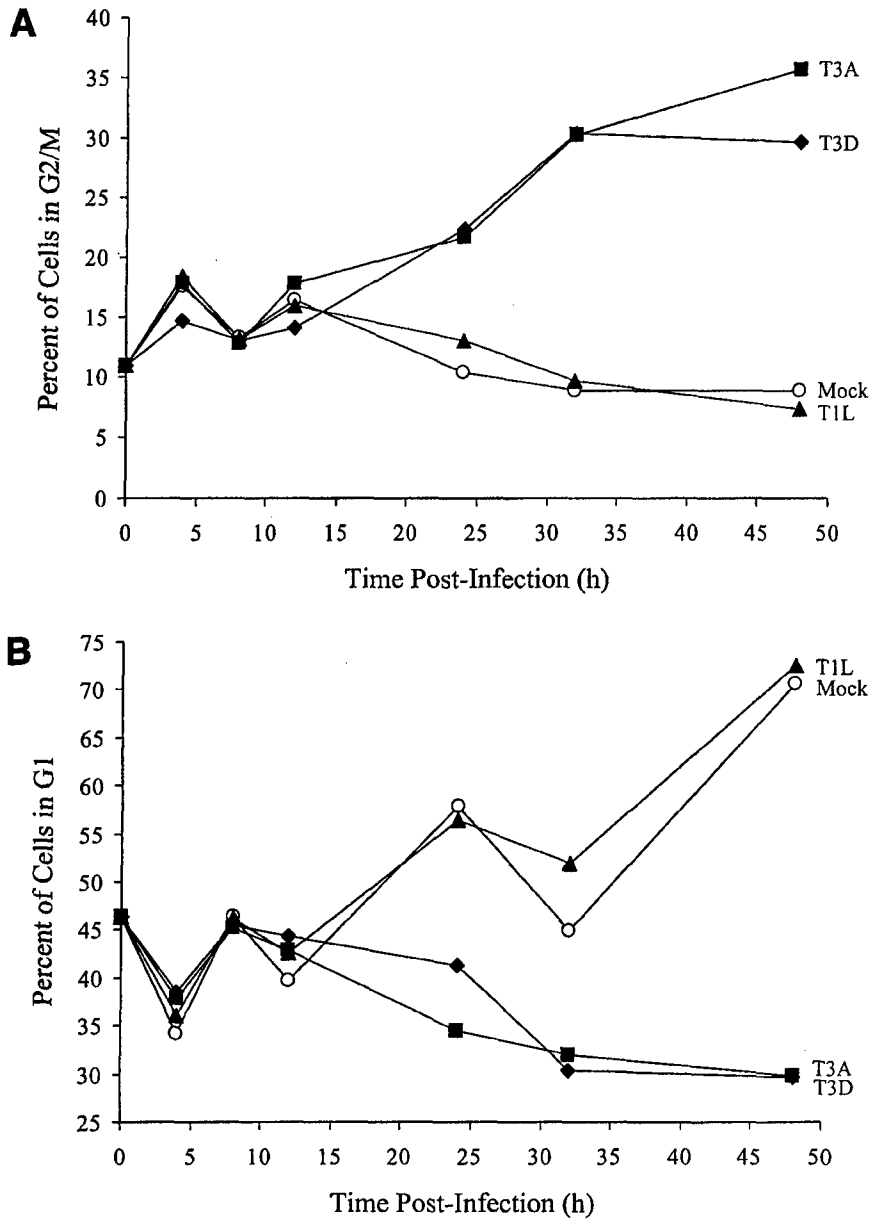

FIG. 2. T3 reovirus induces an increase in the percentage of cells in the G_2/M phase of the cell cycle. Asynchronous, subconfluent monolayers of L929 cells were either mock infected (circles) or infected with T1L (triangles), T3A (squares), or T3D (diamonds) at an MOI of 100 PFU per cell. Cells were harvested at the indicated times postinfection, stained with Krishan's stain, and analyzed for DNA content using flow cytometry. Results are presented as the percentage of cells in G_2/M phase (A) or G_1 phase (B) of the cell cycle. Results of a representative experiment of three independent experiments are shown. (C) L929 cells were synchronized with 1 μM methotrexate and 50 μM adenosine for 16 h. Cells were released using fresh media containing 2 mg of thymidine per ml and either mock infected or infected with T1L or T3A at an MOI of 100 PFU per cell. Cells were harvested at the indicated times postinfection, stained with Krishan's stain, and analyzed for DNA content using flow cytometry. Results are presented as the cell cycle distribution following either mock, T1L, or T3A infection at the indicated times postinfection.

we analyzed reovirus-infected cells using flow cytometry. L929 cells were infected with T1L, T3A, or T3D at an MOI of 100 PFU per cell and stained with Krishan's stain (33) containing propidium iodide to determine cellular DNA content at various intervals postinfection. The results were converted to the percentage of cells in G_2/M phase of the cell cycle using Modfit LT software (Fig. 2). Infection with either T3A or T3D resulted in a substantial increase in the percentage of cells in the G_2/M phase of the cell cycle compared to T1L-infected or mock-infected cells by 24 h postinfection (Fig. 2A). There also was a corresponding decrease in the percentage of cells in G_1 phase following infection with either T3A or T3D compared to T1L-infected or mock-infected cells (Fig. 2B). To confirm these results, L929 cells were synchronized with methotrexate prior to reovirus infection and assessed for cell cycle progression (Fig. 2C). Similar to findings with unsynchronized cells, T3A induced a significant increase in the proportion of cells in the G_2/M phase of the cell cycle compared to T1L or mock infection. The increase in the proportion of cells in G_2/M was first seen at 12 h postinfection and was maintained throughout the observation period (48 h). These findings indicate that the inhibition of proliferation induced by T3 reoviruses is caused by a block in the G_2/M phase of the cell cycle. Following T1L or mock infection, cells traverse the cell cycle, proliferate, and

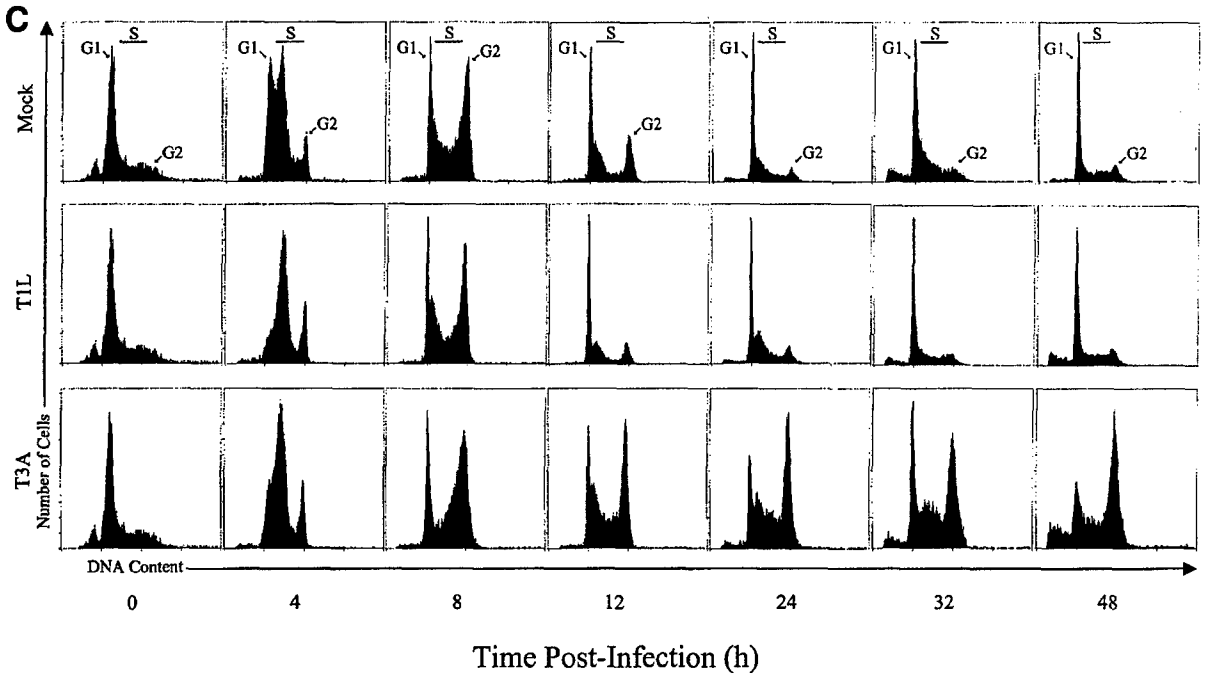

FIG. 2—*Continued.*

reenter the cell cycle. Conversely, T3-infected cells enter the cell cycle, stall in G_2/M phase, and do not proliferate.

T3 reovirus-induced G_2/M arrest is dose dependent. To investigate the relationship between MOI and the induction of G_2/M arrest, we infected L929 cells with T3A at MOIs of 1, 10, and 100 PFU per cell. Cells were harvested at 48 h postinfection, stained with Krishan's stain (33), and analyzed for DNA content by flow cytometry (Fig. 3). T3A infection induced a greater percentage of cells in G_2/M than mock infection at each MOI tested, and the effect was dose dependent.

G_2/M arrest occurs in a variety of cell lines following T3 reovirus infection. To determine whether the capacity of reovirus to block cell cycle progression is cell type dependent, L929, MDCK, C127, HEK293, and HeLa cells were either mock infected or infected with T1L or T3A at an MOI of 100 PFU per cell. Cells were harvested at 48 h postinfection, stained with Krishan's stain (33), and analyzed for DNA content by flow cytometry (Fig. 4). T3A infection induced a greater percentage of cells in G_2/M than either T1L or mock infection in all cell lines tested. However, the magnitude of the strain-specific difference was greatest in L929 (Fig. 4A), MDCK (Fig. 4B), and C127 (Fig. 4C) cells. Therefore, reovirus-induced G_2/M arrest is not cell type specific and likely requires non-cell-type-specific factors to mediate G_2/M arrest.

T3 reovirus G_2/M arrest phenotype is dominant. To determine whether G_2/M arrest resulting from T3 reovirus infection could be overcome by T1 reovirus infection, we coinfected L929 cells with equivalent MOIs of T1L and T3A and measured the percentage of cells in G_2/M by flow cytometry at 48 h postinfection. The percentage of cells in G_2/M after coinfection with T1L and T3A was identical to that of T3A alone and significantly greater than that of T1L alone (Fig. 5). These results indicate that the G_2/M arrest phenotype of T3 reovirus is dominant.

G_2/M arrest by T1L × T3D reassortant viruses. To identify viral genes associated with differences in the capacity of T1L and T3D to induce G_2/M arrest, we tested 12 T1L × T3D reassortant viruses for the capacity to induce G_2/M arrest in unsynchronized and synchronized L929 cells (Table 1). The results demonstrate a significant association between the capacity of reassortant viruses to induce G_2/M arrest in unsynchronized L929 cells and the S1 gene segment (Student t test, $P = 0.004$; Mann-Whitney, $P = 0.007$). No other viral genes were significantly associated with G_2/M arrest in this analysis (t test and Mann-Whitney, all $P > 0.05$). However, when L929 cells were synchronized prior to infection, the results demonstrate a significant association between the capacity of reassortant viruses to induce G_2/M arrest and the derivation of the S1 gene segment (Student t test, $P = 0.007$; Mann-Whitney, $P = 0.016$) and the M2 gene segment (Student t test, $P = 0.007$; Mann-Whitney, $P = 0.016$). We used parametric stepwise linear regression analysis to determine whether the S1 and M2

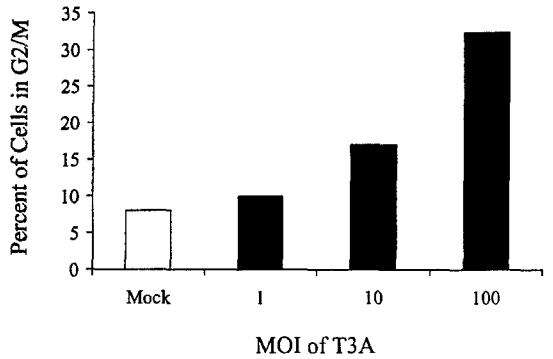

FIG. 3. G_2/M arrest induced by T3 reovirus is dose dependent. Asynchronous, subconfluent monolayers of L929 cells were either mock infected or infected with T3A at MOIs of 1, 10, and 100 PFU per cell. Cells were harvested at 48 h postinfection, stained with Krishan's stain, and analyzed for DNA content using flow cytometry. Results are presented as the percentage of cells in G_2/M phase.

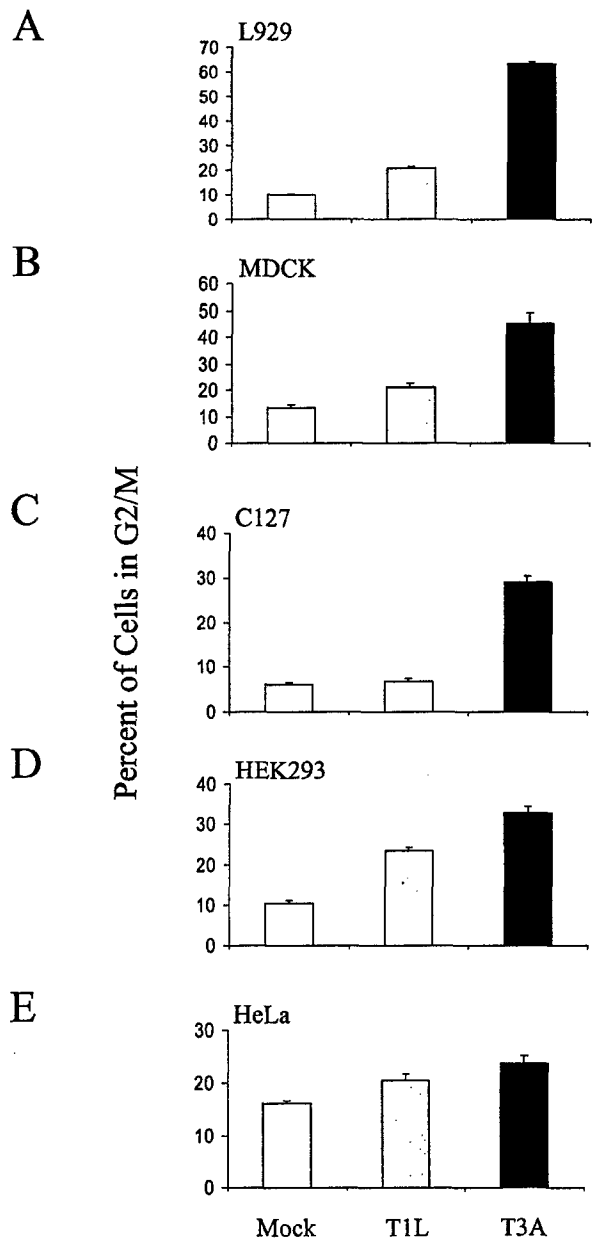

FIG. 4. T3 reovirus induces G_2/M arrest in murine, canine, and human cells. Asynchronous, subconfluent monolayers of L929 (A), MDCK (B), C127 (C), HEK293 (D), and HeLa (E) cells were either mock infected (white) or infected with T1L (gray) or T3A (black) at an MOI of 100 PFU per cell. Cells were harvested at 48 h postinfection, stained with Krishan's stain, and analyzed for DNA content using flow cytometry. Results are presented as the mean percentage of cells in G_2/M phase for three independent experiments. The error bars indicate the standard errors of the mean. A significantly greater percentage of T3A-infected cells were in G_2/M than mock-infected cells in all cell lines tested ($P < 0.01$ to 0.001). A significantly greater percentage of T3A-infected cells were in G_2/M than T1L-infected cells in all cell lines tested ($P < 0.01$ to 0.001) except HeLa. A significantly greater percentage of T1L-infected cells were in G_2/M than mock-infected cells in L929 and HEK293 cells ($P < 0.001$).

genes contributed independently to the capacity of T1L × T3D reassortant viruses to induce G_2/M arrest. We obtained R^2 values of 91.3 and 96.7% for the regression equation using all 10 reovirus genes for unsynchronized and synchronized L929 cells, respectively: 52.2% ($P = 0.004$) for S1 in unsynchronized L929 cells and 84.9% ($P < 0.001$) for S1 and M2 and 53.5% ($P = 0.007$) for the S1 gene alone in synchronized L929 cells. These results indicate that the S1 gene segment is the primary determinant of strain-specific differences in reovirus-induced G_2/M arrest.

G_2/M arrest induced by T3 reovirus. The S1 gene segment encodes two proteins, the viral attachment protein σ1 and the nonstructural protein σ1s (20, 30, 39). To determine whether σ1s is required for G_2/M arrest, we infected L929 cells with reovirus strain T3C84-MA, which does not express σ1s (37) (Fig. 6). The percentage of cells in G_2/M following infection with T3C84-MA was significantly less than the percentage of cells in G_2/M following infection with the σ1s-expressing parental virus, T3C84. T3C84-MA failed to induce G_2/M arrest, even at an MOI 10-fold greater than T3C84. T3C84-MA/σ1s+, a MEL-cell-adapted strain that does not contain the point mutation in S1 that results in an early stop codon in σ1s but contains the tryptophan-to-arginine substitution at position 202 in σ1, induced a level of G_2/M arrest that was significantly greater than T3C84-MA at an MOI of 100 in L929 cells ($P = 0.002$; percentage of cells in G_2/M following T3C84-MA/σ1s+ infection, 23.02 ± 1.1%). These findings indicate that functional σ1s is required for reovirus-induced G_2/M arrest.

Expression of T3 σ1s induces an increase in the percentage of cells in G_2/M phase. To determine whether σ1s alone is sufficient to induce the accumulation of cells in G_2/M phase, we analyzed the DNA content of C127 cells engineered to express the T3D σ1s protein. Expression of σ1s from the mouse metallothionein promoter was induced by 1 μM $CdCl_2$ (21) however, levels of σ1s were substantially less than levels found following natural virus infection (data not shown). The percentage of cells in G_2/M following induction was significantly greater in cells expressing σ1s than in vector control cells at 45 and 55 h postinduction ($P = 0.03$ and $P = 0.005$, respectively) (Fig. 7). These results provide additional evidence that σ1s expression is involved in the accumulation of cells in the G_2/M phase of the cell cycle.

Reovirus-induced apoptosis can be dissociated from reovirus-induced G_2/M arrest. Previous studies indicate that the capacity of reovirus to inhibit DNA synthesis correlates with the capacity to induce apoptosis (44). Like strain-specific differences in reovirus-induced G_2/M arrest, differences in the capacity of reovirus strains to inhibit DNA synthesis and induce apoptosis are determined by the S1 gene (40, 44). To determine whether apoptosis-associated disruption of cellular DNA is required for reovirus-induced inhibition of cellular proliferation, L929 cells or HEK293 cells were either mock infected or infected with T3A in the presence or absence of inhibitors of reovirus-induced apoptosis (7, 8, 11). Treatment of cells with the calpain inhibitor PD150606 (11), the caspase inhibitor DEVD-CHO (D. J. Kominsky, personal communication), or anti-TRAIL antibody (7) blocks reovirus-induced apoptosis, as does expression of an IκB mutant that blocks NF-κB activation (7, 8). G_2/M arrest was evaluated by flow cytometry at 48 h postinfection (Fig. 8). Treatment with the calpain inhibitor PD150606 (Fig. 8A), the caspase 3 inhibitor DEVD-CHO (Fig. 8B), or anti-TRAIL antibody (Fig. 8C) using conditions that inhibit reovirus-induced apoptosis, had no effect on T3A-induced G_2/M arrest, nor did inhibition of NF-κB by expression of a dominant-negative IκB (7, 8) (Fig. 8D). Therefore, inhibitors of reovirus-induced apoptosis do not inhibit reovirus-induced G_2/M arrest. These findings indicate that apoptosis induced DNA damage is not required for reovirus-induced G_2/M arrest.

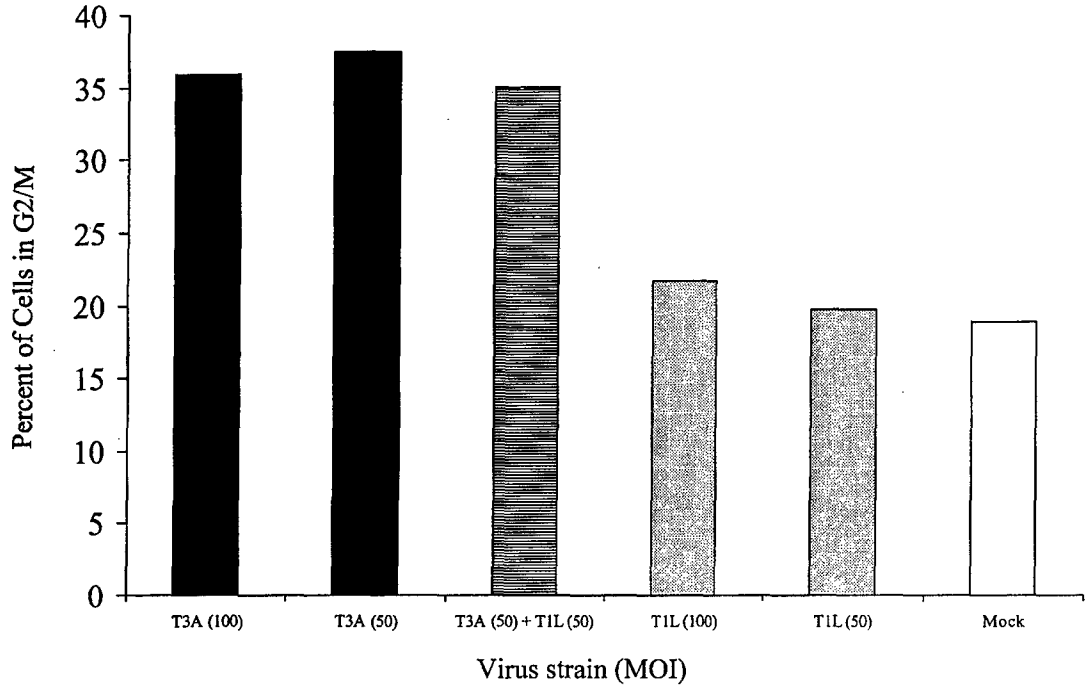

FIG. 5. T3A-induced G_2/M arrest phenotype is dominant. L929 cells were either mock infected (white), coinfected with equivalent MOIs of T1L and T3A (the MOI of each virus was 50 PFU per cell) (hatched), or infected with T1L (shaded) or T3A (solid) alone at MOIs of 50 or 100 PFU per cell. L929 cells were harvested at 48 h postinfection and analyzed using flow cytometry. The results are presented as the percentage of cells in the G_2/M phase of the cell cycle.

DISCUSSION

T3 reovirus strains inhibit host cell proliferation, as measured by cellular DNA synthesis inhibition, to a substantially greater extent than T1 reovirus strains (40, 44). It had been suggested, based on extrapolation of results obtained using [^{3}H]thymidine incorporation, that T3 reoviruses induce cell cycle arrest at the G_1-to-S transition. We now show, using flow cytometry to directly analyze cell cycle progression in reovirus-infected cells, that reovirus-induced inhibition of cellular pro-

TABLE 1. Capacities of T1L × T3D reassortant viruses to induce G_2/M arrest

Virus strain	Genome segment[a]										% Cells in G_2/M[b]	
	L1	L2	L3	M1	M2	M3	S1	S2	S3	S4	Unsynchronized	Synchronized
EB138	3D	1L	1L	3D	3D	1L	3D	3D	1L	1L	ND	24.56
EB28	3D	3D	1L	3D	3D	3D	3D	1L	3D	3D	38.13	28.59
KC150	3D	1L	1L	1L	3D	1L	3D	3D	1L	3D	33.91	36.47
EB97	3D	3D	1L	3D	3D	3D	3D	3D	3D	1L	30.30	28.35
G2	1L	3D	1L	1L	1L	1L	3D	1L	1L	1L	29.09	13.92
H41	3D	3D	1L	1L	1L	3D	1L	1L	3D	1L	26.56	ND
T3D	3D	3D	3D	3D	3D	3D	3D	3D	3D	3D	25.71	38.51
H15	1L	3D	3D	1L	3D	3D	3D	3D	3D	1L	24.95	31.63
EB127	3D	3D	1L	1L	3D	1L	1L	3D	3D	1L	23.54	ND
H9	3D	3D	1L	3D	1L	1L	3D	3D	3D	3D	23.11	17.17
EB85	1L	1L	1L	1L	1L	3D	1L	3D	1L	1L	21.88	ND
T1L	1L	1L	1L	1L	1L	1L	1L	1L	1L	1L	19.23	5.56
EB145	3D	3D	3D	3D	3D	1L	1L	3D	3D	3D	15.72	14.72
EB121	3D	3D	1L	3D	1L	3D	1L	3D	3D	3D	14.98	9.45
EB1	1L	3D	1L	1L	3D	1L	1L	1L	3D	1L	11.89	16.19
Significance (P)[c]												
Unsynchronized L cells												
t test	0.30	0.84	0.60	0.85	0.46	0.36	**0.004**	0.78	0.58	0.66		
MW	0.30	1	0.77	0.95	0.41	0.38	**0.007**	0.80	0.73	0.85		
Synchronized L cells												
t test	0.25	1	0.27	0.73	**0.007**	0.16	**0.007**	0.18	0.67	0.53		
MW	0.28	1	0.28	0.76	**0.016**	0.2	**0.016**	0.21	0.57	0.48		

[a] The parental origin of each genome segment in the reassortants strains: 1L, genome segment derived from T1L; 3D, genome segment derived from T3D.
[b] Unsynchronized or synchronized L cells were infected with viral strains at an MOI of 100 PFU per cell and analyzed by flow cytometry at 48 h postinfection. ND, not determined.
[c] As determined by two-sample parametric Student *t* test (*t* test) and Mann-Whitney nonparametric analysis (MW). Values in boldface are statistically significant.

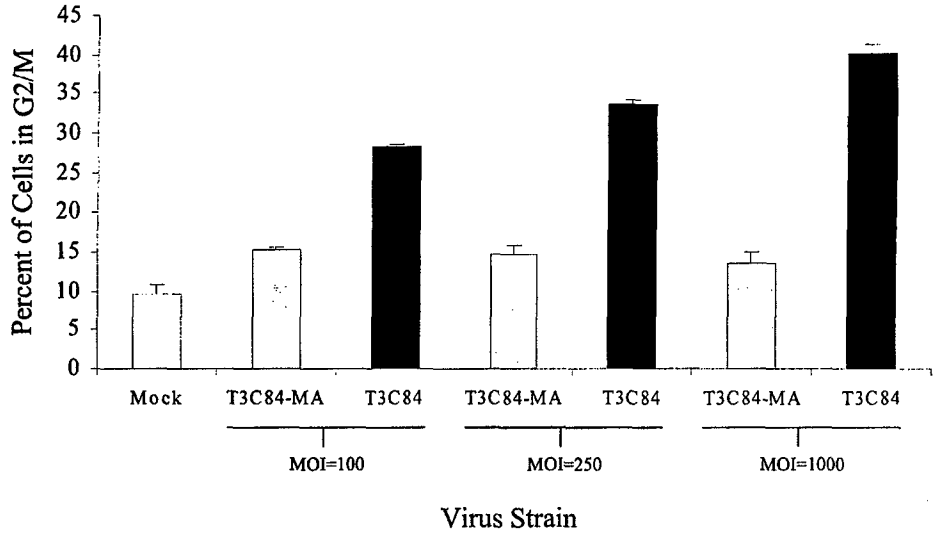

FIG. 6. Reovirus-induced G_2/M arrest requires σ1s. L929 cells were either mock infected (white) or infected with wild-type T3C84 (black) or σ1s-null mutant T3C84-MA (gray) at MOIs of 100, 250, or 1,000 PFU per cell. Cells were harvested 48 h postinfection, stained with Krishan's stain, and analyzed using flow cytometry. The results are presented as the mean percentage of cells in G_2/M phase of the cell cycle for six independent experiments at an MOI of 100 and three independent experiments at MOIs of 250 and 1,000. The error bars indicate the standard errors of the mean. A significantly greater percentage of T3C84-infected cells were in G_2/M than T3C84-MA-infected cells at each MOI tested ($P < 0.001$).

liferation results from G_2/M arrest. This effect is not cell type specific and is dominant in strains that block cell cycle progression.

Differences in the capacity of reovirus strains to inhibit cellular proliferation are determined by the viral S1 gene (40, 44). Our results indicate that the same is true for G_2/M arrest. The reovirus S1 gene is bicistronic, encoding the structural protein σ1 and the nonstructural protein σ1s using overlapping, alternative reading frames (20, 30, 39). As a result of this coding strategy, there is no sequence similarity between the σ1 and σ1s proteins (12). To determine which of the two S1-encoded proteins are required for G_2/M arrest, we examined the capacity of the σ1s null mutant T3C84-MA to induce G_2/M arrest. T3C84-MA and its σ1s expressing parent, T3C84, produce equivalent yields of viral progeny in L929 cells, and both viruses are equally effective in inducing apoptosis (37). However, T3C84-MA fails to induce G_2/M arrest. This finding suggests that σ1s is required for blockade of cell cycle progression following T3 reovirus infection. It is also possible that differences in the capacity of T3C84 and T3C84-MA to induce cell cycle arrest are influenced by other sequence differences. The mutation in the S1 gene that introduces a termination codon in the σ1s open reading frame also results in a lysine-to-isoleucine substitution at residue 26 in the deduced amino acid sequence of σ1. The T3C84-MA S1 gene also contains an additional mutation that results in a tryptophan-to-arginine substitution at residue 202 in σ1, which determines the capacity of this strain to bind sialic acid. To exclude the possibility that sialic acid binding influences cell cycle arrest, we isolated and characterized an additional T3C84-MA variant, T3C84-MA/σ1s+, that binds to sialic acid and expresses σ1s. In contrast to T3C84-MA, which binds sialic acid but does not express σ1s, T3C84-MA/σ1s+ induces G_2/M arrest. Therefore, it is unlikely that the capacity to bind sialic acid influences the efficiency of cell cycle arrest induced by T3 reoviruses.

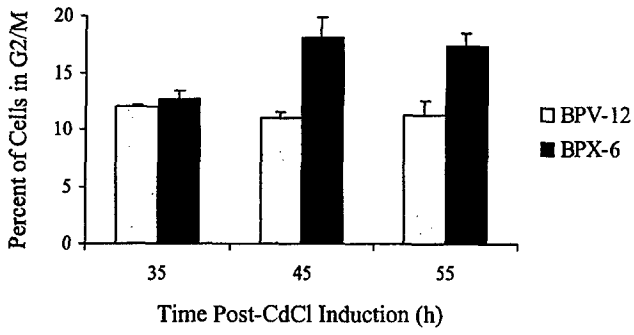

FIG. 7. σ1s expression induces an increase in the percentage of cells in G_2/M phase. C127 cells stably transfected with σ1s (BPX-6) or vector control (BPV-12) under the control of the mouse metallothionein promoter were induced with $CdCl_2$, harvested at the indicated times postinduction, and analyzed for DNA content by flow cytometry. The results are presented as the mean percentage of cells in the G_2/M phase of the cell cycle for three to six independent experiments. The error bars indicate the standard errors of the mean. The percentage of cells in G_2/M was significantly greater in the σ1s-expressing cells than in the vector-control cells at 45 h ($P = 0.03$, $n = 4$) and 55 h ($P = 0.005$, $n = 6$) postinduction.

To corroborate findings made using viruses that vary in σ1s expression, we also tested the capacity of cells engineered to express σ1s under the control of an inducible promoter to undergo cell cycle arrest. Following induction of σ1s expression, we observed an increase in the percentage of cells in the G_2/M phase of the cell cycle, which suggests that σ1s is capable of mediating cell cycle blockade at the G_2/M checkpoint. This observation suggests that the reovirus σ1s protein is similar to the human immunodeficiency virus (HIV) Vpr protein (2, 28, 31, 35) or the human papillomavirus (HPV) E2 protein (23), which similarly block cell cycle progression at the G_2/M boundary. Thus, our findings indicate that reovirus-induced G_2/M arrest requires σ1s and provide the first evidence of a functional role for this nonstructural protein.

We have previously shown that the capacity of reovirus to induce apoptosis correlates with the capacity to inhibit cellular proliferation and that both properties are determined by the viral S1 gene (44). Our results clearly show that G_2/M arrest can occur in cells treated with potent inhibitors of reovirus-

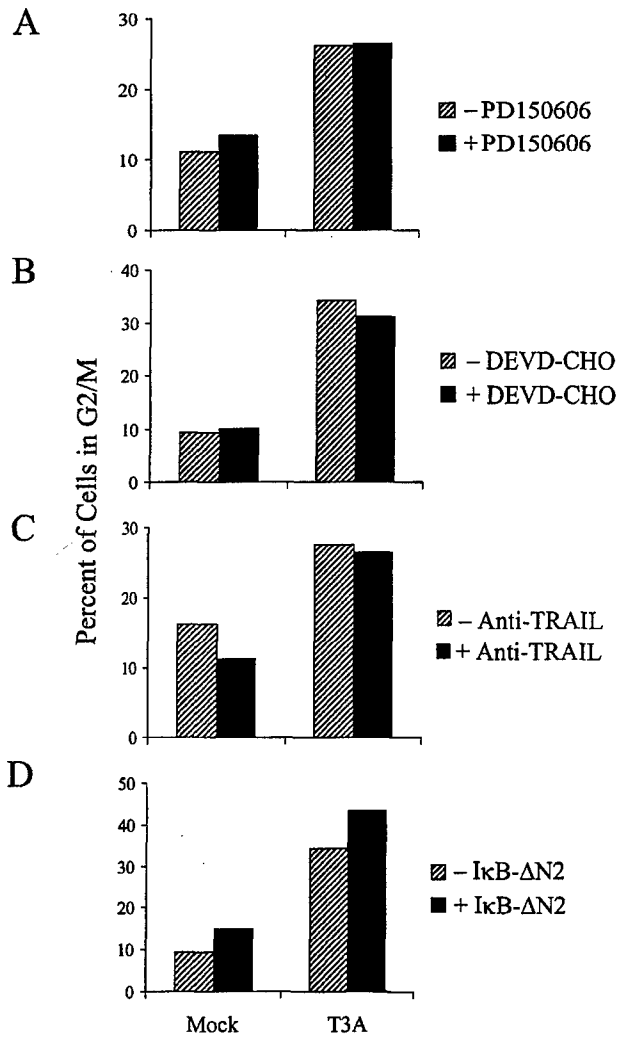

FIG. 8. Inhibitors of reovirus-induced apoptosis do not inhibit reovirus-induced G_2/M arrest. (A) Effect of calpain inhibitor PD150606 on T3A-induced G_2/M arrest. L929 cells were treated with either 25 μM calpain inhibitor PD150606 or an ethanol control and then either mock infected or infected with T3A at an MOI of 100 PFU per cell. (B) Effect of caspase 3 inhibitor DEVD-CHO on T3A-induced G_2/M arrest. HEK293 cells were treated with either 100 μM caspase 3 inhibitor DEVD-CHO or a dimethyl sulfoxide control and then either mock infected or infected with T3A at an MOI of 100 PFU per cell. (C) Effect of anti-TRAIL antibodies on T3A-induced G_2/M arrest. HEK293 cells were treated with either 30 μg of an anti-TRAIL antibody per ml or mock treated as a control and then either mock infected or infected with T3A at an MOI of 100 PFU per cell. (D) Effect of NF-κB inhibition on T3A-induced G_2/M arrest. HEK293 cells expressing a dominant-negative form of IκB (IκB-ΔN2) to inhibit NF-κB activation or untransfected HEK293 cells were either mock infected or infected with T3A at an MOI of 100 PFU per cell. In all cases, G_2/M arrest was assessed 48 h postinfection.

induced apoptosis. These findings indicate that the induction of G_2/M arrest and apoptosis by reovirus are functionally independent at some stage following infection. Moreover, although strain-specific differences in reovirus-induced G_2/M arrest and apoptosis induction segregate with the viral S1 gene, each property is determined by a different S1 gene product. Strain-specific differences in reovirus-induced G_2/M arrest are determined by σ1s, whereas differences in reovirus-induced apoptosis are determined by σ1 (36, 45). The induction of G_2/M arrest by HIV Vpr is apparently required for Vpr-induced apoptosis (42), whereas reovirus-induced apoptosis can occur in the absence of G_2/M arrest (37). These findings suggest that viruses may utilize different mechanisms to induce G_2/M arrest and apoptosis.

The G_2/M transition is regulated by the kinase cdc2/cdk1 (13–15, 32, 34). Expression of HIV Vpr (28, 35) or HPV E2 protein (23) results in inhibition or delayed activation of cdc2 kinase activity resulting in an accumulation of cells in the G_2/M phase of the cell cycle. In contrast, the baculovirus *Autographa californica* nuclear polyhydrosis virus (AcNPV) (3) and herpes simplex virus (HSV) (1, 29) induce G_2/M arrest by a mechanism that is cdc2 independent, since cells infected with either of these viruses maintain high levels of cdc2 kinase activity. HIV, HPV, AcNPV, and HSV require a nuclear phase to replicate, whereas reovirus replicates in the cytoplasm. T3 σ1s has been detected in the nucleus as well as in the cytoplasm following reovirus infection (5, 37), and it is possible that this nuclear localization is required for reovirus-induced G_2/M arrest. Future studies will be aimed at identifying which cell cycle regulatory proteins are involved in reovirus-induced cell cycle perturbation, the role of cellular localization of σ1s in this process, and the significance of cell cycle arrest in reovirus-induced cytopathology and pathogenesis.

ACKNOWLEDGMENTS

This work was supported by Public Health Service grant 1RO1AG14071 from the National Institute of Aging, Merit and REAP grants from the Department of Veterans Affairs, and a U.S. Army Medical Research and Material Command grant (USAMRMC 98293015) (K.L.T.). This work also was supported by Public Health Service grant AI38296 from the National Institute of Allergy and Infectious Diseases and the Elizabeth B. Lamb Center for Pediatric Research (T.S.D.).

The University of Colorado Cancer Center provided core flow cytometry facilities.

REFERENCES

1. **Advani, S. J., R. Brandimarti, R. R. Weichselbaum, and B. Roizman.** 2000. The disappearance of cyclins A and B and the increase in activity of the G(2)/M-phase cellular kinase cdc2 in herpes simplex virus 1-infected cells require expression of the alpha22/U(S)1.5 and U(L)13 viral genes. J. Virol. **74**:8–15.
2. **Bartz, S. R., M. E. Rogel, and M. Emerman.** 1996. Human immunodeficiency virus type 1 cell cycle control: Vpr is cytostatic and mediates G_2 accumulation by a mechanism which differs from DNA damage checkpoint control. J. Virol. **70**:2324–2331.
3. **Braunagel, S. C., R. Parr, M. Belyavskyi, and M. D. Summers.** 1998. *Autographa californica* nucleopolyhedrovirus infection results in Sf9 cell cycle arrest at G2/M phase. Virology **244**:195–211.
4. **Brown, E. G., M. L. Nibert, and B. N. Fields.** 1983. The L2 gene of reovirus serotype 3 controls the capacity to interfere, accumulate deletions and establish persistent infection, p. 275–287. *In* R. W. Compans and D. H. L. Bishop (ed.), Double-stranded RNA viruses. Elsevier, New York, N.Y.
5. **Ceruzzi, M., and A. J. Shatkin.** 1986. Expression of reovirus p14 in bacteria and identification in the cytoplasm of infected mouse L cells. Virology **153**:35–45.
6. **Chappell, J. D., V. L. Gunn, J. D. Wetzel, G. S. Baer, and T. S. Dermody.** 1997. Mutations in type 3 reovirus that determine binding to sialic acid are contained in the fibrous tail domain of viral attachment protein sigma1. J. Virol. **71**:1834–1841.
7. **Clarke, P., S. M. Meintzer, G. Spencer, C. Widmann, T. P. Garrington, G. L. Johnson, and K. L. Tyler.** 2000. Reovirus-induced apoptosis is mediated by TRAIL. J. Virol. **74**:8135–8139.
8. **Connolly, J. L., S. E. Rodgers, P. Clarke, D. W. Ballard, L. D. Kerr, K. L. Tyler, and T. S. Dermody.** 2000. Reovirus-induced apoptosis requires activation of transcription factor NF-κB. J. Virol. **74**:2981–2989.
9. **Coombs, K. M., B. N. Fields, and S. C. Harrison.** 1990. Crystallization of the reovirus type 3 Dearing core. Crystal packing is determined by the lambda 2 protein. J. Mol. Biol. **215**:1–5.
10. **Cox, D. C., and J. E. Shaw.** 1974. Inhibition of the initiation of cellular DNA synthesis after reovirus infection. J. Virol. **13**:760–761.
11. **Debiasi, R. L., M. K. Squier, B. Pike, M. Wynes, T. S. Dermody, J. J. Cohen, and K. L. Tyler.** 1999. Reovirus-induced apoptosis is preceded by increased cellular calpain activity and is blocked by calpain inhibitors. J. Virol. **73**:695–701.

12. **Dermody, T. S., M. L. Nibert, R. Bassel-Duby, and B. N. Fields.** 1990. Sequence diversity in S1 genes and S1 translation products of 11 serotype 3 reovirus strains. J. Virol. **64**:4842–4850.
13. **Draetta, G., and D. Beach.** 1988. Activation of cdc2 protein kinase during mitosis in human cells: cell cycle-dependent phosphorylation and subunit rearrangement. Cell **54**:17–26.
14. **Draetta, G., and J. Eckstein.** 1997. Cdc25 protein phosphatases in cell proliferation. Biochim. Biophys. Acta **1332**:M53–M63.
15. **Draetta, G., H. Piwnica-Worms, D. Morrison, B. Druker, T. Roberts, and D. Beach.** 1988. Human cdc2 protein kinase is a major cell-cycle regulated tyrosine kinase substrate. Nature **336**:738–744.
16. **Duke, R. C., and J. J. Cohen.** 1992. Morphological and biochemical assays of apoptosis, p. 3.17.1–3.17.16. *In* J. E. Coligan (ed.), Current protocols in immunology. Wiley, New York, N.Y.
17. **Duncan, M. R., S. M. Stanish, and D. C. Cox.** 1978. Differential sensitivity of normal and transformed human cells to reovirus infection. J. Virol. **28**:444–449.
18. **Ensminger, W. D., and I. Tamm.** 1969. Cellular DNA and protein synthesis in reovirus-infected L cells. Virology **39**:357–360.
19. **Ensminger, W. D., and I. Tamm.** 1969. The step in cellular DNA synthesis blocked by reovirus infection. Virology **39**:935–938.
20. **Ernst, H., and A. J. Shatkin.** 1985. Reovirus hemagglutinin mRNA codes for two polypeptides in overlapping reading frames. Proc. Natl. Acad. Sci. USA **82**:48–52.
21. **Fajardo, E., and A. J. Shatkin.** 1990. Expression of the two reovirus S1 gene products in transfected mammalian cells. Virology **178**:223–231.
22. **Fajardo, J. E., and A. J. Shatkin.** 1990. Translation of bicistronic viral mRNA in transfected cells: regulation at the level of elongation. Proc. Natl. Acad. Sci. USA **87**:328–332.
23. **Fournier, N., K. Raj, P. Saudan, S. Utzig, R. Sahli, V. Simanis, and P. Beard.** 1999. Expression of human papillomavirus 16 E2 protein in *Schizosaccharomyces pombe* delays the initiation of mitosis. Oncogene **18**:4015–4021.
24. **Gaulton, G. N., and M. I. Greene.** 1989. Inhibition of cellular DNA synthesis by reovirus occurs through a receptor-linked signaling pathway that is mimicked by antiidiotypic, antireceptor antibody. J. Exp. Med. **169**:197–211.
25. **Gomatos, P., and I. Tamm.** 1963. Macromolecular synthesis in reovirus-infected L cells. Biochim. Biophys. Acta **72**:651–653.
26. **Hand, R., W. D. Ensminger, and I. Tamm.** 1971. Cellular DNA replication in infections with cytocidal RNA viruses. Virology **44**:527–536.
27. **Hand, R., and I. Tamm.** 1974. Initiation of DNA replication in mammalian cells and its inhibition by reovirus infection. J. Mol. Biol. **82**:175–183.
28. **He, J., S. Choe, R. Walker, P. Di Marzio, D. O. Morgan, and N. R. Landau.** 1995. Human immunodeficiency virus type 1 viral protein R (Vpr) arrests cells in the G_2 phase of the cell cycle by inhibiting p34cdc2 activity. J. Virol. **69**:6705–6711.
29. **Hobbs, W. E., and N. A. DeLuca.** 1999. Perturbation of cell cycle progression and cellular gene expression as a function of herpes simplex virus ICP0. J. Virol. **73**:8245–8255.
30. **Jacobs, B. L., and C. E. Samuel.** 1985. Biosynthesis of reovirus-specified polypeptides: the reovirus s1 mRNA encodes two primary translation products. Virology **143**:63–74.
31. **Jowett, J. B., V. Planelles, B. Poon, N. P. Shah, M. L. Chen, and I. S. Chen.** 1995. The human immunodeficiency virus type 1 vpr gene arrests infected T cells in the G_2 + M phase of the cell cycle. J. Virol. **69**:6304–6313.
32. **King, R. W., P. K. Jackson, and M. W. Kirschner.** 1994. Mitosis in transition. Cell **79**:563–571.
33. **Krishan, A.** 1975. Rapid flow cytofluorometric analysis of mammalian cell cycle by propidium iodide staining. J. Cell Biol. **66**:188–193.
34. **Morla, A. O., G. Draetta, D. Beach, and J. Y. Wang.** 1989. Reversible tyrosine phosphorylation of cdc2: dephosphorylation accompanies activation during entry into mitosis. Cell **58**:193–203.
35. **Re, F., D. Braaten, E. K. Franke, and J. Luban.** 1995. Human immunodeficiency virus type 1 Vpr arrests the cell cycle in G_2 by inhibiting the activation of p34cdc2-cyclin B. J. Virol. **69**:6859–6864.
36. **Rodgers, S. E., E. S. Barton, S. M. Oberhaus, B. Pike, C. A. Gibson, K. L. Tyler, and T. S. Dermody.** 1997. Reovirus-induced apoptosis of MDCK cells is not linked to viral yield and is blocked by Bcl-2. J. Virol. **71**:2540–2546.
37. **Rodgers, S. E., J. L. Connolly, J. D. Chappell, and T. S. Dermody.** 1998. Reovirus growth in cell culture does not require the full complement of viral proteins: identification of a σ1s-null mutant. J. Virol. **72**:8597–8604.
38. **Roner, M. R., and D. C. Cox.** 1985. Cellular integrity is required for inhibition of initiation of cellular DNA synthesis by reovirus type 3. J. Virol. **53**:350–359.
39. **Sarkar, G., J. Pelletier, R. Bassel-Duby, A. Jayasuriya, B. N. Fields, and N. Sonenberg.** 1985. Identification of a new polypeptide coded by reovirus gene S1. J. Virol. **54**:720–725.
40. **Sharpe, A. H., and B. N. Fields.** 1981. Reovirus inhibition of cellular DNA synthesis: role of the S1 gene. J. Virol. **38**:389–392.
41. **Shaw, J. E., and D. C. Cox.** 1973. Early inhibition of cellular DNA synthesis by high multiplicities of infectious and UV-inactivated reovirus. J. Virol. **12**:704–710.
42. **Stewart, S. A., B. Poon, J. B. Jowett, and I. S. Chen.** 1997. Human immunodeficiency virus type 1 Vpr induces apoptosis following cell cycle arrest. J. Virol. **71**:5579–5592.
43. **Tyler, K. L., R. T. Bronson, K. B. Byers, and B. Fields.** 1985. Molecular basis of viral neurotropism: experimental reovirus infection. Neurology **35**:88–92.
44. **Tyler, K. L., M. K. Squier, A. L. Brown, B. Pike, D. Willis, S. M. Oberhaus, T. S. Dermody, and J. J. Cohen.** 1996. Linkage between reovirus-induced apoptosis and inhibition of cellular DNA synthesis: role of the S1 and M2 genes. J. Virol. **70**:7984–7991.
45. **Tyler, K. L., M. K. Squier, S. E. Rodgers, B. E. Schneider, S. M. Oberhaus, T. A. Grdina, J. J. Cohen, and T. S. Dermody.** 1995. Differences in the capacity of reovirus strains to induce apoptosis are determined by the viral attachment protein sigma 1. J. Virol. **69**:6972–6979.

Brain Pathology 11: 452-464(2001)

SYMPOSIUM: Herpesvirus Infections of the Nervous System

Polymerase Chain Reaction as a Diagnostic Adjunct in Herpesvirus Infections of the Nervous System

B. K. Kleinschmidt-DeMasters, M.D.[1,2], Roberta L. DeBiasi, M.D.[2,3], Kenneth L. Tyler, M.D.[2,4,5]

Departments of [1]Pathology, [2]Neurology, [3]Pediatrics, [4]Microbiology, and [5]Immunology and Medicine, University of Colorado Health Sciences Center and The Denver Veterans Administration Hospital, Denver, Colorado, USA

Polymerase chain reaction (PCR) is a powerful technique that allows detection of minute quantities of DNA or RNA in cerebrospinal fluid (CSF), vesicle and endoneurial fluids, blood, fresh-frozen, and even formalin-fixed tissues. Various infectious agents can be detected with high specificity and sensitivity, including bacteria, parasites, rickettsia and viruses. PCR analysis of CSF has revolutionized the diagnosis of nervous system viral infections, particularly those caused by human herpesviruses (HHV), and has now replaced brain biopsy as the gold standard for diagnosis of herpes simplex virus (HSV) encephalitis. PCR analysis of both CSF and nervous system tissues has also broadened our understanding of the spectrum of disease caused by HSV-1 and -2, cytomegalovirus (CMV), Epstein-Barr virus (EBV), varicella zoster virus (VZV), and HHV-6. Nonetheless, positive tissue PCR results must be interpreted cautiously, especially in cases that lack corroborating clinical and neuropathologic evidence of infection. Moreover, positive PCR results from tissues do not distinguish latent from productive (lytic) viral infections. In several neurological diseases, negative PCR results have provided strong evidence against a role for herpesviruses as the causative agents. This review focuses on the use of PCR tests to diagnose HSV and VZV infections of the nervous system.

Introduction

Polymerase chain reaction (PCR) can be applied to the diagnosis of any disease in which nucleic acids (*e.g.* DNA, RNA) or their expression as messenger RNA (mRNA) play a role. PCR is useful to study congenital diseases, malignancies, autoimmune disorders, and infections (23); PCR aids in diagnosis, therapy, disease classification, epidemiology, and basic research. In infectious disorders, PCR is ideally suited for identifying fastidious organisms that may be difficult, or impossible, to culture (24). The technique can be performed rapidly and inexpensively, and test results are typically available faster than with standard culture or serological methods. Nucleic acids of bacteria, mycobacteria, rickettsia, parasites, treponemes, and viruses can be identified by PCR analysis of any body secretion, fluid, or tissue. The widespread availability of an in-house test in most hospitals, or ready access to a reference laboratory, has led to the incorporation of PCR testing on CSF and body fluids into medical practice in the United States and other developed countries. Unfortunately, the rapid proliferation of testing has led to substantial variation among laboratories in terms of quality control, techniques and procedures.

Despite the wide application of PCR to CSF and other body fluids, such as vesicle or endoneurial fluids, PCR analysis of central (CNS) and peripheral (PNS) nervous system tissues remains primarily a research tool and is not available at all institutions. PCR on tissues and CSF, sometimes in conjunction with immunohistochemistry or *in situ* hybridization techniques, have furthered our understanding of the role of herpesvirus in cases of encephalitis, meningitis, meningoencephalitis, myelitis, ventriculoencephalitis, polymyeloradiculitis, and brainstem infections. PCR of cerebral arteries has established a direct role for VZV in cases of waxing and waning vasculitis (36), and PCR of temporal arteries has negated a role for VZV in giant cell arteritis (66).

Interpretation of positive PCR amplification of herpesvirus genome in brain tissues from patients with neurological disorders of uncertain etiology can be problematic. Since amplification of viral nucleic acid does

Corresponding author:
B.K. Kleinschmidt-DeMasters, Department of Pathology B216, University of Colorado Health Sciences Center, 4200 East Ninth Avenue, Denver, CO 80262; Tel.: (303) 315-7298; Fax (303) 315-6721; E-mail: BK.DeMasters@UCHSC.edu

not distinguish between genomic fragments, latent infection, low-grade persistent infection, or active (lytic) infection. The interpretation of a positive result may depend on the precise gene or genes being amplified, and whether the methods used are designed to detect genomic DNA, RNA, or mRNA. Herpesviruses are generally classified as either neurotropic (HSV, VZV) or lymphotropic (EBV, HHV-6, HHV-7, HHV-8) based on their tissue location during latency; defined as "the persistence of the virus in a host in the absence of clinically apparent infection," with the capacity to reactivate (31). Considerable information is available about the physical state, viral nucleic acids and proteins during latency of neurotropic herpesviruses (see companion article by Cohrs *et al.*) Numerous studies have also documented latency of herpesviruses in cells other than those of the nervous system, including peripheral blood mononuclear cells (78), B-lymphocytes, and T-lymphocytes.

In the CNS, nucleic acid hybridization first detected HSV viral genome in human brains in 1979 (73) and again in 1981 (32). PCR on human brain revealed HSV DNA in brainstem, olfactory bulbs and limbic areas (7). Since HSV has never been isolated from normal human brain tissue, the presence of the viral genome does not definitively signal latent viral infection or the capacity for reactivation, and instead might represent random viral sequences or fragments of virus. Although the viral transcripts associated with latency (LATS) have been identified in a mouse model of HSV infection (27), their presence has not been definitively demonstrated in human brain tissue (see accompanying article by Cohrs *et al.*). Several laboratories have also reported detection of viral genomic material of HHV-6, HHV-7, and HHV-8 in normal autopsy human brain (15, 21). It remains to be proven whether these viruses establish latency within brain. In contrast, VZV DNA has not been detected in normal human brain in most studies, and its presence on tissue PCR usually indicates productive infection of CNS.

This review summarizes the principles of PCR testing and the role of CSF PCR in the diagnosis and therapeutic management of herpesvirus infections of the nervous system, particularly HSV and VZV. Problems inherent in interpretation of positive tissue PCR for viruses that may become latent in the nervous system are also discussed.

Principles of PCR testing

PCR techniques allow the *in vitro* synthesis of millions of copies of a specific gene segment, and in turn,

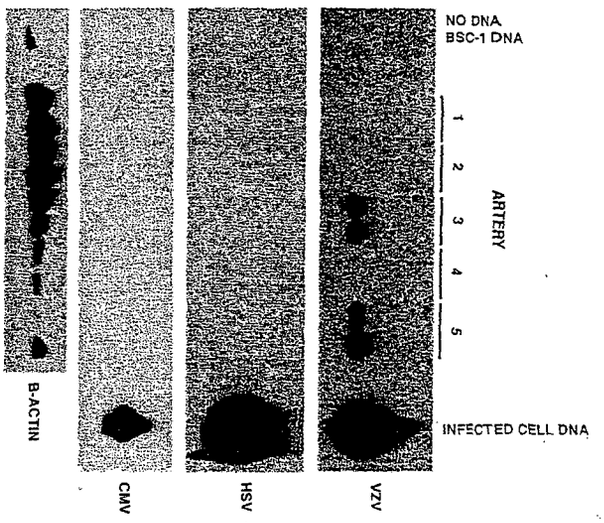

Figure 1. *PCR gel.* PCR detection of VZV DNA in cerebral artery sections from a patient with waxing/waning vasculitis (see ref 36). Total DNA was extracted from: BSC-1 cells; sections of multiple cerebral arteries; VZV- or HSV-1-infected BSC-1 cells; and CMV-infected human WI38 cells. Template DNA was omitted from one of the reaction tubes (no DNA). One ng of DNA from uninfected and virus-infected cells, and 10 μl of duplicate samples of DNA from sections of right middle cerebral artery (1), anterior cerebral artery (2), basilar artery (3), right vertebral artery (4), and right posterior cerebral artery (5) were PCR-amplified, using primers specific for VZV gene 29, HSV-1 gene UL30, genes corresponding to the CMV major immediate early genes, or human β-actin. Figure reproduced with permission; American Academy of Neurology.

the rapid detection of even a few copies of the target nucleic acid (see refs. 23 and 24 for reviews). DNA is often the target nucleic acid, although RNA can also be detected by reverse transcription (RT-PCR).

PCR uses the heat-stable DNA-synthesizing enzyme, DNA polymerase, to extend synthetic DNA fragments onto oligonucleotide primers designed to bind to target DNA segments. Oligonucleotide primers have sequences complementary to each strand of DNA to be amplified and are (usually) 20 to (rarely) 40 bases in length. Primer design is crucial for efficient and accurate PCR analysis. In the past, primer sequences were generated manually. Currently, software programs that facilitate optimal primer design are available *(http://www.genome.wi.mit.edu/cgi-bin/primer/primer3.cgi)* to address issues such as guanine-cytosine content, melting points that match for both primer sequences, and the reduction of unwanted primer-primer formation.

The first step in PCR is the denaturation of the double-stranded target DNA by heating the sample to 95°C. During heating, the DNA polymerase remains intact.

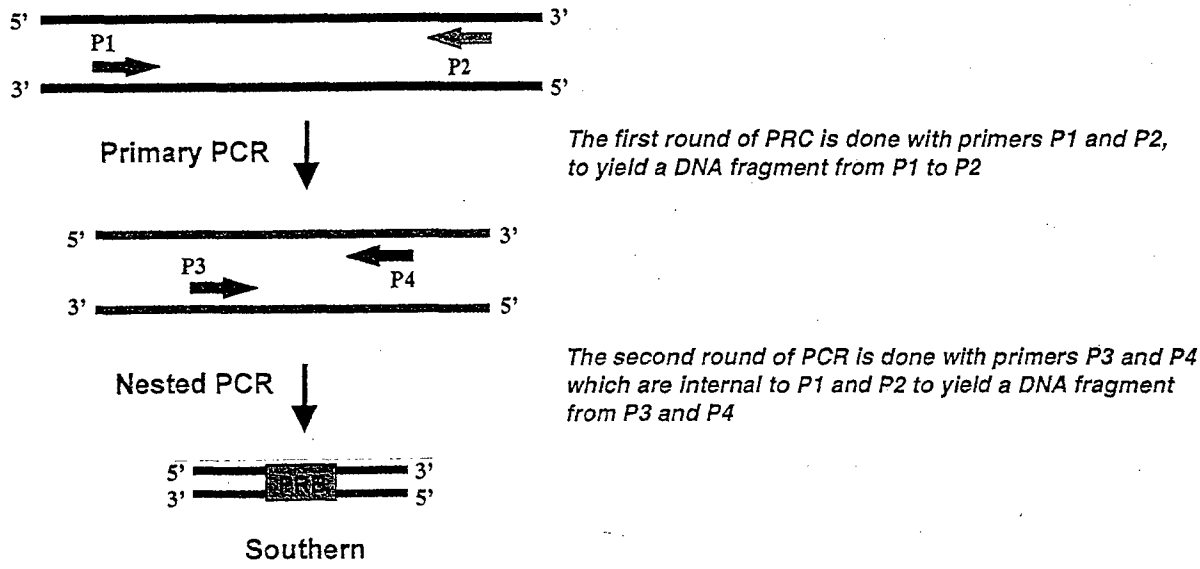

Figure 2. *Schematic of Nested PCR.*

Oligonucleotide primers are supplied in considerable excess to ensure that more primers rather than the original (*de novo*) complementary strand of DNA are available for binding. As the sample containing the denatured DNA, primers, and DNA polymerase is cooled to 55-70°C, the primers anneal (bind) to their respective complementary template strands. The nucleotide building blocks adenine, guanine, thymidine, and cytosine are also supplied in molar excess. Using these nucleotides, the DNA polymerase (usually *Taq*) "reads" the target DNA strand in a 5′ to 3′ direction and forms a new, complementary DNA sequence downstream from the primer. This results in two complete double-stranded DNA pairs concluding the first cycle of PCR testing. Multiple cycles (30-40) of denaturing, annealing of new primers and strand elongation amplify DNA into 10^6-10^9 copies over 2-3 hours.

The resulting PCR product is visualized and identified based on its migration in an electrophoretic agarose gel containing ethidium bromide. The generation of a PCR product (amplicon) of the appropriate size, as predicted from the target gene and primer set used is the first indication of a positive reaction. However, Southern blotting is usually performed to ensure that the products generated are specific. The amplified fragment is transferred from the gel and analyzed using a radioactively or fluorescently labeled probe that is complementary to the expected target gene (Figure 1). Failure of the probe to bind to the amplicon indicates a false-positive PCR product due to mispriming or other technical issues, whereas confirmation of the specificity of amplified PCR products by Southern blot ensures that the product is derived from the target gene. Direct sequencing of the amplified product is also used for PCR product confirmation; however, this approach is limited primarily to the research setting since it is too labor-intensive for routine use.

Nested PCR is a modification that increases the specificity and especially the sensitivity of PCR. Nested PCR involves a second round of PCR in which an additional set of new primers internal to the original primers is utilized (Figure 2). A fragment smaller than the original target fragment becomes the second target. While nested PCR can increase the sensitivity of PCR, it also increases the likelihood of false-positive reactions. Results from studies using nested PCR may vary considerably from those that utilize non-nested PCR.

Quantitative PCR (using Taqman) is increasingly being applied to CSF, and occasionally to tissues. The technique involves the use of internal oligonucleotides — labeled at one end with a fluorescent dye and at the other end with a quencher dye — along with the PCR primers during amplification. Fluorescence emitted during PCR is measured and directly correlated to the number of copies of the target.

The ability of PCR to generate and amplify a high number of DNA strand copies from the original sample, which may contain as few as 1 to 10 copies of the target DNA, is both its greatest virtue and greatest limitation. The exquisite sensitivity of the test can easily lead to false-positive results from amplification of minute amounts of contaminating DNA. This problem is well-recognized by experienced laboratories, and rigorous controls are run simultaneously with the clinical samples, using all reagents except the unknown specimen to insure that the reagents do not harbor contaminants. Dedicated work areas and separate reagents used exclusively for PCR testing, frequent glove changes, and testing in laminar flow hoods alleviate false-positives. False-negative test results due to deterioration of the original sample specimen, incorrect heating of the sample, or use of incorrect proportions of the various mixture reagents are more easily rectified.

PCR works very well on biopsy or autopsy tissues frozen soon after removal from the body; DNA can be amplified by PCR even when tissues are stored for several years at -80°C. Although one of the greatest assets of PCR is that it can also be used on archival, formalin-fixed, paraffin-embedded tissue samples, yields of extracted DNA are usually less from fixed than from fresh tissues. Extraction of target DNA involves removal of the wax with several rounds of xylene immersion and centrifugation, and the procedure itself may slightly diminish the DNA yield from fixed tissues. The DNA yield from fixed tissues may also be reduced due to cross-linking after prolonged fixation (several years), or in association with use of osmic acid or other fixatives. Both fresh-frozen and fixed tissues must be digested with proteinase K prior to performing the PCR techniques described above. The protocol for extraction of DNA is described in the commercial kit literature (DNeasy Tissue Kit Handbook, Qiagen, 28159 Avenue Stanford, Valencia, CA, 91355, USA).

PCR of CSF

One of the most successful applications of CSF PCR is in the diagnosis of viral nervous system infections (8, 67, 88). PCR is preferable to serological testing, which usually requires 2-4 weeks after acute infection to reveal an antibody response. In contrast, CSF PCR yields positive results during acute infections, when the amount of replicating virus is maximal. Unlike traditional culture methods that may show negative results after the patient receives even small doses of antimicrobial drugs, CSF PCR retains its sensitivity after short courses of antiviral therapy (24). This allows the rapid start of empiric therapy when the patient initially presents with suspected meningitis or encephalitis, without potentially compromising the definitive diagnostic test. CSF PCR is also ideal for patients in whom brain biopsy is contraindicated clinically, such as patients with advanced acquired immunodeficiency syndrome (AIDS) (22).

Positive CSF PCR testing indicates the presence of viral DNA and is a marker of recent or ongoing active viral infection. Despite the high prevalence of seropositivity to HSV in the population and the fact that the virus becomes latent in multiple ganglia of most humans, HSV DNA is not detected in CSF of HSV-seropositive individuals without neurological disease or with other types of inflammatory non-HSV CNS infections (82). In general, a positive CSF PCR for viral DNA indicates a CNS infection by that particular pathogen, especially in an immunocompetent individual (82). A possible exception might arise from a breakdown of the blood-brain barrier (e.g., in severe bacterial meningitis), or contamination of the CSF with blood, resulting in a positive CSF PCR in the absence of viral infection (82). However, in one very recent study that addressed this problem, false-positive CSF PCR results for herpesviruses were not seen in any of 10 control patients with bacterial meningitis, despite high CSF white cell counts (75).

Replicating virus and viral DNA do not persist indefinitely, so that the CSF PCR test becomes negative over time, especially in immunocompetent patients. While most CSF testing in the clinical setting of suspected meningitis or meningoencephalomyelitis is performed within 1-2 days following onset of neurological symptoms, positive test results at least 2 and up to 4 weeks after onset of clinical disease have been recorded (88). False-negative tests can occur if PCR inhibitors are present in the CSF, such as hemoglobin products resulting from breakdown of red blood cells. However, modest xanthochromia does not negatively impact CSF PCR testing, nor does high CSF protein level or white blood cell count (24).

CSF PCR testing is optimally performed on fresh samples. However, DNA is more stable than RNA, and usually refrigeration for a few hours or even days does

not appear to significantly reduce the yield of the test although this has not been rigorously studied (24). In order to avoid cell lysis that liberates viral DNA into the supernatant and effectively dilutes the sample, CSF and body fluids for PCR should not be frozen prior to shipping. Optimally, samples are shipped overnight at room temperature, centrifuged, and the pellet examined for virus-specific DNA. The exquisite sensitivity of the technique implies the need for only small volumes of CSF for analysis (*i.e.* 30 μl) although laboratories generally request at least 0.5 ml.

Occasional immunocompetent or immunocompromised patients reveal more than one herpesvirus on CSF PCR, and EBV has been the most frequent agent associated with a dual positive result (75). In a large series of 662 patients, mostly immunocompetent, detection of HHV-6 and EBV by CSF PCR did not correlate clinically in several individuals with the presence of a CNS infection known to be caused by that virus (75). In contrast, detection of HSV-1, HSV-2, CMV, and VZV DNA correlated strongly with specific clinical syndromes of encephalitis/myelitis and meningitis (75). Similarly, in a large study of HIV-infected individuals, conducted to assess the diagnostic reliability of CSF PCR by comparison with biopsy or autopsy diagnoses, the most frequent false-positive herpesvirus detected was HHV-6 (19). In this study, seven of the 219 patients with corresponding tissue samples lacked histological evidence of a CNS disease that could be attributed to their HHV-6 DNA detected by CSF PCR (19). Additional large studies are necessary to determine the extent of false-positive PCR results for herpesviruses, especially HHV-6 and EBV.

Occasional false-negative and false-positive CSF PCR results for CMV have been seen in AIDS patients. In AIDS patients, CSF PCR detected HSV-1 or HSV-2 in all six cases (100%) of histologically confirmed HSV encephalitis, compared to 37 of 45 cases (82%) with CMV infections of CNS (19). An earlier study had suggested that a CSF PCR positive for CMV DNA correlated strongly with systemic CMV infections but not with CMV brain infections in AIDS patients at autopsy (1). Recent studies employing quantitative CSF PCR for CMV have indicated that AIDS patients with autopsy-confirmed CMV encephalitis harbor significantly higher levels of viral genome than do those with symptoms unrelated to CMV (91). These studies suggest the usefulness of quantitation in clarifying the clinical relevance of a positive CSF PCR result for CMV in AIDS patients (6). Despite these difficulties, CSF PCR for CMV has been used to monitor the efficacy of antimicrobial therapies and clearance of CMV viral burden in AIDS patients (16). Overall, CSF PCR testing has been crucial in diagnosing herpesviruses nervous system infections in AIDS patients and a positive CSF PCR result for herpesvirus in the majority of patients corresponds to CNS infection by that pathogen, just as it does in immunocompetent patients. CSF PCR has the potential to identify infections in AIDS patients who may not mount a classical serological response to viral infection or demonstrate protracted clinical manifestations (37).

CSF PCR testing has played a critical role in establishing the frequency and distribution of herpesvirus infections in immunocompetent populations. In the study by Studahl *et al.*, 87% of patients with herpesvirus DNA detected in CSF were immunocompetent, with HSV-1 identified in 18 patients, EBV in 16, HSV-2 in 9, CMV in 7, HHV-6 in 6, and VZV in 6 of 69 positive patients (75).

The sensitivity and specificity of CSF PCR exceeds 95% for HSV encephalitis (55, 88). For HSV-1, the existing standards to which CSF PCR results are compared, such as brain biopsy, are actually *less* sensitive than PCR (55). Hence, CSF PCR has dramatically reduced the need for brain biopsy as a diagnostic test. CSF PCR has also led to the identification of mild or atypical forms of HSV encephalitis that were formerly attributed to other viruses, often in the absence of brain biopsy (26, 30), and that may account for 17% of total cases of HSV encephalitis (30). CSF PCR has established the diagnosis and role of HSV-1 in brainstem encephalitis (84), myelitis (75), multifocal or diffuse encephalitis without temporal lobe involvement in children (71), and neonatal encephalitis (75). HSV encephalitis in children may relapse after therapy, and CSF PCR has been used to identify the subset of children in which HSV viral DNA reappears (43, 49). Quantitative CSF PCR may also provide valuable information in cases of pediatric HSV encephalitis in monitoring response to antiviral drugs (4)

CSF PCR has helped clinicians to recognize that HSV-2 can cause aseptic meningitis even in the absence of genital herpetic lesions (72), and has established HSV-2 as the most common cause of benign recurrent lymphocytic meningitis, including many cases previously diagnosed as Mollaret's meningitis (79). Even when CSF viral cultures are negative, CSF PCR is positive in patients with recurrent episodes of meningitis following an initial episode of herpes simplex meningitis (79). CSF PCR has illustrated that immunocompetent adults may manifest HSV-2-induced meningoencephalitis as well as meningitis (75). CSF PCR has identified

rare cases of HSV-2 brainstem encephalitis and recurrent thoracic myelitis (65).

CSF PCR testing has been found to be nearly 100% specific and sensitive as a tumor marker for EBV-related CNS lymphoma (18, 19, 22, 87), and has changed the way in which clinicians diagnose CNS lymphoma in immunocompromised individuals. In one study of AIDS patients with CNS mass lesions, a positive EBV CSF PCR correctly identified all 17 CNS lymphoma cases and was positive in only 1 of 68 AIDS patients with non-CNS lymphoma mass lesions (18). CSF PCR for EBV is also positive during the acute phase of the illness in children with infectious mononucleosis and neurological complications such as transverse myelitis, meningoencephalitis, and aseptic meningitis (88).

A sensitivity of 82% and specificity of 99% of CSF PCR for detecting CMV CNS infections has been reported in AIDS patients (16). A sensitivity of 60% for CSF PCR is cited for congenital CMV infections, and positive results may correlate with poorer neurologic outcome in affected infants (81). CMV viral load has also been monitored in peripheral blood leukocytes as a method to predict which immunosuppressed patients might develop a systemic (and CNS) infection (9, 29).

CSF PCR testing has corroborated the role of HHV-6 in febrile seizures, meningitis, encephalitis, and encephalopathy in immunocompetent and immunocompromised individuals (48, 92). HHV-6 genome has been demonstrated in CSF from up to 57% of children younger than one year of age who have febrile seizures ,and has also been seen in children with recurrent febrile convulsions (92). The role of HHV-7 in neurological disease is unclear, although detection of HHV-7 DNA in CSF and serum of children with exanthem subitum and encephalopathy has been reported (80, 85). Encephalitis in immunocompromised individuals associated with HHV-8 has been described (68), but this awaits additional confirmation. HHV-8 DNA has been detected in primary CNS lymphomas in some studies (20) but not others (5). In the study in which HHV-8 was detected, the virus was surmised to play an indirect role in the development of primary CNS lymphoma, and was thought to be present in the adjacent non-neoplastic lymphocytes but not the lymphoma cells (20).

CSF PCR for VZV has considerably broadened the understanding of the neurologic complications due to this virus (3, 8). VZV, along with EBV, displays the most protean manifestations of nervous system infection of any of the herpesviruses (35, 50, 51). Serological techniques and CSF PCR for VZV have been particularly helpful in identifying cases of VZV CNS infections without associated rash (*sine herpete*) (8, 11). Since the virus can rarely be cultured from CSF, diagnosis of meningitis or meningoencephalitis previously depended on the presence of a characteristic vesicular erythematous rash before, during, or after CNS infection, and VZV-mediated neurologic diseases were under-recognized. CSF PCR for VZV has shown that aseptic meningitis and brainstem encephalitis due to this virus can occur in immunocompetent hosts (75). In a study of 514 consecutive HIV-positive patients, CSF PCR for VZV became negative in patients whose clinical conditions improved following antiviral therapy and remained positive despite appropriate therapy in several patients who subsequently died (17). Hence, CSF PCR for VZV DNA may have utility in monitoring therapeutic response and in predicting outcomes. In the same study, several patients with positive CSF PCR for VZV DNA, but without clinically recognizable VZV meningoencephalitis, were considered to have subclinical reactivation of VZV, treated with antiviral agents and survived. In those cases, positive CSF PCR was considered to antedate clinical disease and allowed effective use of prophylactic therapy (17).

CSF PCR testing for VZV has established a role for the virus in cases of stroke (granulomatous arteritis), multifocal infarcts, myelitis, and neuritis. CSF PCR has served as the diagnostic test for large vessel encephalitis (also called granulomatous arteritis, herpes zoster ophthalmicus with contralateral hemiplegia, or simply stroke with VZV) (62), small vessel vasculopathy (leukoencephalitis) (3), myelitis (34), and zoster *sine herpete* (39). Some of these complications had been previously linked to VZV but received full confirmation from PCR testing.

PCR testing of body fluids other than CSF

PCR testing of skin vesicle fluid from patients with varicella (chickenpox) and zoster (shingles) has identified VZV in 97% of patients; in traditional viral culture methods, virus was isolated in only 23% of these same patients (25). PCR for VZV DNA was positive for vesicles up to 14 days after the onset of the rash, even from crusted cutaneous lesions, compared to culture specimens that were positive only when taken within 5 days of rash onset (25).

PCR analysis of peripheral blood mononuclear cells and CSF has furthered our understanding of the pathogenic mechanism in postherpetic neuralgia, the most common complication of VZV reactivation from latency in the elderly. Postherpetic neuralgia is characterized by pain that persists for more than the 4-6 weeks asso-

ciated with zoster (shingles) (35). The cause of the persistent pain is unknown. Using PCR, VZV DNA was detected in blood mononuclear cells from 11 of 51 postherpetic neuralgia patients, but not in any of 19 zoster patients without the persistent pain syndrome or in any of 11 elderly control individuals without zoster (58). While it is not possible to examine dorsal root ganglia — the site of VZV latency (56) — during the life of these patients, it seems likely that the PCR results reflect the greater level of VZV present in these ganglia during pain episodes than during periods of latency. Blood mononuclear cells may traffic through ganglia during periods of putative ganglionitis and acquire viral DNA. Thus, PCR analysis of blood mononuclear cells provides a window to indirectly assess levels of VZV replication in deep ganglionic tissues of patients with postherpetic neuralgia.

PCR on both CSF and fluid from auricular vesicles has confirmed that VZV causes Ramsey-Hunt syndrome, the second most common cause of 7th nerve facial paralysis after Bell palsy (64). Ramsey-Hunt syndrome can be difficult to recognize since the rash is hidden in the ear or mouth, and rash may be delayed, particularly in pediatric patients (41). PCR on endoneurial fluids and posterior auricular muscle samples collected during decompressive facial nerve surgery for Bell palsy identified HSV-1 DNA in 79% of patients and suggested that neither EBV or VZV is an important cause of idiopathic Bell palsy (63). A subsequent study using PCR identified a subset of patients with acute peripheral facial palsy that have zoster *sine herpete* (33). Acute facial palsy due to VZV constituted a significant percentage of the overall patient population (29%) in that study, and an even higher incidence of VZV reactivation (88%) was responsible for the palsy in the patients who were HSV-seronegative (33). Hence, PCR has verified a role for herpesviruses in both of the common causes of facial nerve paralysis and distinguishes which virus is causative in clinically confusing cases.

PCR testing on blood mononuclear cells has also impacted patient care for transplant recipients, AIDS patients, and other populations at-risk for CMV infections or EBV-related lymphoproliferative disorders. Monitoring of CMV viral loads by PCR in blood has led to prophylactic therapy with antiviral agents in AIDS and transplant patients to prevent systemic (and CNS) viral infections (29).

Confirmation of herpesvirus etiology in nervous system infections by tissue PCR

PCR testing on fresh, frozen, or archival fixed and paraffin-embedded tissues has allowed assessment of viral presence, even from small or imperfectly preserved specimens. Tissue PCR of cerebral arteries has established a direct role for VZV in cases of large vessel (62) and small vessel vasculopathy. In a patient with waxing and waning VZV vasculitis, detection of VZV DNA by PCR led to the discovery that VZV antigen was also present, indicating a productive infection in blood vessels as the cause of disease (36). Brain tissues may be positive for VZV DNA by PCR even when virus is no longer detectable by other methods, such as light microscopy for viral inclusions, immunohistochemistry, or *in situ* hybridization (52).

VZV latency in human sensory ganglia was originally demonstrated with Southern blotting by Gilden *et al.* (38) and was later confirmed by PCR (59). More recently, PCR techniques have been used on dorsal root ganglionic tissues to address the important question of whether neurons, satellite cells, or both harbor latent virus. PCR combined with *in situ* hybridization on sorted neuronal and non-neuronal cells fractions showed that latent VZV resides primarily, if not exclusively, in neurons at a level of two to five viral copies per latently infected neuron (54).

Our laboratory has used PCR to address the role of subclinical reactivation of VZV. Understanding the extent of viral burden in transplant recipients may help in monitoring their response to the doses of prophylactic antiviral agents currently being utilized. Quantitative PCR applied to autopsy trigeminal ganglia to assess VZV DNA burden in transplant recipients at risk for reactivation demonstrated an average of 119 copies of VZV DNA/μg of total ganglionic DNA, compared to an average of 71 copies in controls (B.K. Kleinschmidt-DeMasters, R. Mahalingam, unpublished data). These results suggest an increased viral burden in transplant recipients despite "optimal" antiviral prophylactic therapies. Future studies are needed to determine the clinical and statistical significance of the increased viral load in a larger number of transplant recipients, as well as the extent of host inflammatory response and viral antigen production, if any.

Exclusion of herpesvirus etiology in nervous system disease by tissue PCR

Given the protean manifestations of herpesvirus-mediated infections of the central and peripheral nervous system, efforts have been made to detect these viruses by PCR on tissues from several disease entities characterized by arteritis and/or inflammation. PCR

testing of various tissue specimens has suggested that VZV is not the cause of giant cell arteritis (66) and has shown no role for VZV, CMV, EBV, or HSV in childhood multifocal encephalomalacia (89). PCR also suggests that HSV is not the cause of Meniere's disease (90). A survey of a variety of normal and disease peripheral nerve conditions, including inflammatory peripheral neuropathies, revealed no HSV DNA by PCR in peripheral nerves (76), thus excluding a role for this herpesvirus in several disorders with a plausible viral etiology.

Questionable herpesvirus etiology in nervous system disease despite positive tissue PCR

Positive PCR on tissues from patients without definite clinicopathologic evidence of infection is difficult to interpret. For example, the HSV genome is present in brain tissues from both controls and patients with a variety of neurologic diseases (7), so that assignment of a role for this herpesvirus in a disease condition is especially problematic. Positive PCR results on tissues have been most challenging to interpret in patients who might not manifest classic clinical features of infection, but who exhibit tissue inflammation, such as putative chronic herpes simplex encephalitis in children (47), Rasmussen encephalitis (46, 86), and multiple sclerosis (MS) (69). Also problematic are positive PCR results in tissues from certain other non-inflammatory seizure disorders (28, 70), Alzheimer's disease (44, 45, 60), and brain tumors (14, 21).

Jay *et al.* identified HSV DNA in surgical resection tissues of pediatric patients with remote, antecedent clinical histories of HSV-1 encephalitis, subsequent intractable seizure disorders, and chronic encephalitis (47). That study described 3 pediatric patients whose brains revealed microglial nodules, lymphocytic infiltrates, and gliosis, but negative immunohistochemistry and electron microscopy for virus (47), suggesting that the HSV genome was present but that infectious virus was not being produced or produced only at extremely low levels. It remains unclear whether the chronic inflammation was a result of persistent low-grade viral replication or an immune response to prior infection. HSV DNA detection might reflect either the presence of latent virus no longer responsible for the encephalitis or the presence of herpesviruses that "simply accumulate in CNS with the passage of time," a possible explanation for some positive tissue PCR results offered by Vinters *et al.* (86). Clinicopathologic features in encephalitic cases such as these do not help clarify the interpretation of positive PCR results.

Identification of viral genomes in patients with Rasmussen encephalitis has been similarly problematic. Jay *et al.* detected CMV and HSV genomic sequences in 10 patients with intractable seizures and chronic encephalitis, and several controls (46). In another study, PCR revealed small amounts of CMV and EBV DNA in 6 patients with Rasmussen encephalitis (86). Comparison of the PCR signal strength for the CMV and EBV DNA found in the Rasmussen encephalitis cases to that in controls (AIDS patients with documented CMV encephalitis or EBV-driven CNS lymphomas, respectively) revealed considerably lower amounts of viral nucleic acid in Rasmussen encephalitis patients than those in patients with diseases known to be caused by these viruses (86). The authors suggested that EBV and CMV did not directly cause Rasmussen encephalitis, but could not rule out an indirect role for these herpesviruses. The issue of viral etiology versus autoimmunity in Rasmussen encephalitis has recently been reviewed (40). Greenlee and Rose note that virus has never been cultured from brain tissues of Rasmussen encephalitis patients and conclude that "at the present time, there is no convincing evidence for a viral etiology" for the disease (40).

PCR has also identified HSV DNA in brain samples from other non-inflammatory types of epilepsy patients (70), but methodology and selection of controls in that study have been questioned (83). An additional report of HSV, CMV, and HHV-6 DNA in brain tissues from young seizure patients (28) awaits corroboration. A higher than expected prevalence of HSV genomic material in brain tissue from patients with Alzheimer's disease has been reported by some investigators (44, 45), but could not be confirmed by others (60).

Unlike the situation for HSV DNA, PCR studies have not demonstrated VZV DNA in autopsy brain tissues. Liedtke *et al.* detected VZV in only 1% of olfactory bulbs (56). VZV DNA was not detected by PCR of temporal lobe cortex from any of 8 schizophrenic patients, 8 non-schizophrenic suicide victims, or 8 normal control subjects (2). In a study using frozen brain tissue from 31 schizophrenic and 23 control subjects, no CMV, EBV, HSV-1, VZV, or HHV-6 was detected (77). No VZV DNA was found in brain from either Alzheimer's disease patients or normal age-matched controls (57). Only one group has reported detection of VZV DNA, as well as many other herpesviruses (HSV, EBV, CMV, HHV-6), in a significant percentage of both multiple sclerosis and control brains (69). Others have not reproduced these results.

Whereas PCR reveals an abundance of CMV and EBV DNA in brain from patients with CMV encephalitis and EBV-associated CNS lymphoma, the significance of low levels of these lymphotropic herpesviruses in brain tissues remains unclear, especially in AIDS patients. One quantitative PCR study of CMV genome in brains of AIDS patients with and without neuropathologic evidence of CMV encephalitis found significantly higher viral copy numbers in brains of patients with clinicopathologic evidence of productive viral infection than in non-encephalitic AIDS brains (53). Like quantitative CSF PCR, quantitative tissue PCR for CMV may identify which positive cases are due to productive lytic infection by the virus.

Viral DNA sequences of lymphotropic herpesviruses have been recently identified by PCR in normal brain tissue, including HHV-6 (21), HHV-7, and HHV-8 (15). HHV-6 genomic material was also detected in neoplastic brain tissues in 37% of 118 biopsies from primary (115) and metastatic (3) tumors, compared to 32% of normal controls (21). The presence of viral genome in brain tumors was considered to represent "reactivation from latency in immunocompromised patients," based on the detection of HHV-6 immediate early protein p41 by immunohistochemistry (21). Interestingly, peripheral blood lymphocytes from 7 of the HHV-6-positive tumor patients contained the same HHV-6 variant (A or B) as did their respective brain tumor sample. Chan *et al.* also demonstrated HHV-6 and HHV-7 sequences by PCR on tissues in 8.2% and 14.3%, respectively, of primary brain tumors (14). HHV-6 has been identified in oligodendrocytes in patients with progressive multifocal leukoencephalopathy, but genome has also been found in normal, AIDS, and other control brains, especially with increasing patient age (10). In cases of HHV-6 meningoencephalitis, lymphocytes, microglia, and some neurons are infected (42). However, latent virus need not reside in the same cells as those involved in productive, lytic infections. VZV, for example, can infect glia, neurons, and blood vessels in the CNS in cases of encephalitis (50), but has never been shown to become latent in these CNS sites. Further studies are needed to firmly establish which cells in the CNS, if any, harbor latent HHV-6, HHV-7, and HHV-8.

PCR for HHV-6 has been intensively applied to the study of multiple sclerosis (MS). In one of the best-known studies, HHV-6 DNA was identified in >70% of MS brains and controls by PCR (13). In contrast to tissue PCR, analysis of CSF with this technique has not always revealed HHV-6 in MS patients (61). HHV-6 antigens have been identified by immunohistochemistry in oligodendrocytes in MS brains, but not in normal controls (13), suggesting the presence of viral activation, especially within the demyelinative plaques. However, as noted by the authors themselves, the PCR (and immunohistochemical) data were insufficient to establish a causal link between HHV-6 and MS (13). The role of this virus in MS is a complex topic and is discussed in a recent review of controversies in neurologic infectious diseases (40). As noted by these authors, MS may not have a singular causation and even if an infectious organism such as HHV-6 is found, it may only be related to the disease in a subset of patients (40). Positive tissue PCR could be detecting an agent of no etiological importance, a commensal organism, or a virus that causes an infection that non-specifically precipitates a clinical relapse, but is not the direct cause of MS (40).

One possible explanation for some positive tissue PCR results for the blood-borne herpesviruses may be that lymphocytes and mononuclear cells harboring these viruses are entrapped within the lesional tissue. A recent study of a large number of arthritis patients has also raised the possibility that PCR on fluids and tissues might detect viruses in peripheral white blood cells that are migrating into inflamed tissues (74). In that study, PCR demonstrated CMV in 25, EBV in 12, and HSV DNA in 16 of 73 samples of synovial fluid or tissue (74). Based on analysis of several viruses from a large number of patients with a spectrum of arthritides and arthropathies, those investigators argued rather convincingly that inflammatory cells harboring viral DNA(s) migrate into damaged tissues but are not directly causative of arthritis. It remains uncertain whether similar mechanisms occur in some CNS disorders involving large numbers of lymphocytes or mononuclear cells and can explain some positive tissue PCR results.

In summary, tissue PCR is a valuable tool for specific diagnosis of VZV CNS infections, since the overwhelming majority of PCR studies on human brain do not reveal VZV genomic material in normal controls. When VZV is detected by PCR in tissues or CSF, the patient is likely to harbor a nervous system infection caused by VZV. Positive CSF PCR results for HSV-1 or HSV-2 in patients also usually correspond to clinical syndromes of meningitis, encephalitis, or myelitis. In contrast, HSV viral genomic material is present in a large percentage of brains from individuals without neurologic diseases, and positive PCR results on tissues do not equate with productive HSV infection. CSF PCR for EBV DNA is an excellent diagnostic adjunct for detection of CNS lymphomas in immunosuppressed patients.

The presence of low copy numbers of CMV and EBV in immunosuppressed patients and in patients with Rasmussen encephalitis suggests that quantitation of viral load in tissues or CSF may further assist in identifying disorders directly caused by productive infection by these viruses. Finally, the very recent identification by tissue PCR of HHV-6, HHV-7, and HHV-8 genomic sequences in normal and neoplastic brain awaits further studies to establish whether these lymphotropic viruses are latent in cells of the CNS.

Acknowledgements

The authors thank Ravi Mahalingam and Mary Wellish for helpful comments regarding technical aspects of the PCR methodology; Ravi Mahalingam and Tiffany White for assistance with Figure 2; Marina Hoffman for editorial review, and Virginia McCullough and Nancy Hart for typing.

Supported in part by grants from the Department of Veteran's Affairs (KLT, RBD), U.S. Army DAMD17-98-1-8614 (KLT, BKD), and NIH AI38296 (KLT).

References

1. Achim CL, Nagra RM, Wang R, Nelson JA, Wiley CA (1994) Detection of cytomegalovirus in cerebrospinal fluid autopsy specimens form AIDS patients. *J Infect Dis* 169: 623-627
2. Alexander RC, Cabirac G, Lowenkopf T, Casanova M, Kleinman J, Wyatt RJ, Kirch DG (1992) Search for evidence of herpes simplex virus, type 1, or varicella-zoster virus infection in postmortem brain tissue from schizophrenic patients. *Acta Psychiatr Scand* 86: 418-420
3. Amlie-Lefond C, Kleinschmidt-DeMasters BK, Mahalingam R, Davis LE, Gilden DH (1995) The vasculopathy of varicella-zoster virus encephalitis. *Ann Neurol* 37: 784-790
4. Ando Y, Kimura H, Miwata H, Kudo T, Shibata M, Morishima T (1993) Quantitative analysis of herpes simplex virus DNA in cerebrospinal fluid of children with herpes simplex encephalitis. *J Med Virol* 41: 170-173
5. Antinori A, Larocca LM, Fassone L, Cattani P, Capello D, Cingolani A, Saglio G, Fadda G, Gaidano G, Ortona L (1999) HHV-8/KSHV is not associated with AIDS-related primary central nervous system lymphoma. *Brain Pathol* 9: 199-208
6. Arribas JR, Clifford DB, Fichtenbaum CJ, Commins DL, Powderly WG, Storch GA (1995) Level of cytomegalovirus (CMV) DNA in cerebrospinal fluid of subjects with AIDS and CMV infections of the central nervous system. *J Infect Dis* 172: 527-531
7. Baringer JR, Pisani P (1994) Herpes simplex virus genomes in human nervous system tissue analyzed by polymerase chain reaction. *Ann Neurol* 36: 823-829
8. Bergström T (1996) Polymerase chain reaction for diagnosis of varicella zoster virus central nervous system infections without skin manifestations. *Scan J Dis Suppl* 100: 41-45
9. Bitsch A, Kirchner H, Dupke R, Bein G (1993) Cytomegalovirus transcripts in peripheral blood leukocytes of actively infected transplant patients detected by reverse transcription-polymerase chain reaction. *J Infect Dis* 167: 740-743
10. Blumberg BM, Mock DJ, Powers JM, Ito M, Assouline JG, Baker JV, Chen B, Goodman AD (2000) The HHV6 paradox: ubiquitous commensal or insidious pathogen? A two-step in situ PCR approach. *J Clin Virol* 16: 159-78
11. Burke DG, Kalayjian RC, Vann VR, Madreperla SA, Shick HE, Leonard DGB (1997) Polymerase chain reaction detection and clinical significance of varicella-zoster virus in cerebrospinal fluid from human immunodeficiency virus-infected patients. *J Infect Dis* 176: 1080-1084
12. Cantin EM, Lange W, Openshaw H. (1991) Application of polymerase chain reaction assays to studies of herpes simplex virus latency. *Intervirology* 32: 93-100
13. Challoner PB, Smith KT, Parker JD, MacLeod DL, Coulter SN, Rose TM, Schultz ER, Bennett JL, Garber RL, Chang M, Schad PA, Stewart PM, Nowinski RC, Brown JP, Burmer GC (1995) Plaque-associated expression of human herpesvirus 6 in multiple sclerosis. *Proc Natl Acad Sci USA* 92: 7440-7444
14. Chan PK, Ng HK, Cheung AF (1999) Detection of human herpesviruses 6 and 7 genomic sequences in brain tumours. *J Clin Path* 52: 620-623
15. Chan PK, Ng HK, Hui M, Ip M,Cheung JL, Cheng AF (1999) Presence of human herpesviruses 6, 7, and 8 DNA sequences in normal brain tissue. *J Med Virol* 59: 491-495
16. Cinque P, Baldanti F, Vago L, Terreni MR, Lillo F, Furione M, Castagna A, Monforte AD, Lazzarin A, Linde A (1995) Ganciclovir therapy for cytomegalovirus (CMV) infection of the central nervous system in AIDS patients: monitoring by CMV DNA detection in cerebrospinal fluid. *J Infect Dis* 171: 1603-1606
17. Cinque P, Bossolasco S, Vago L, Fornara C, Lipari S, Racca S, Lazzarin A, Linde A (1997) Varicella-zoster virus (VZV) DNA in cerebrospinal fluid of patients infected with human immunodeficiency virus: VZV disease of the central nervous system or subclinical reactivation of VZV infection? *Clin Infect Dis* 25: 634-639
18. Cinque P, Brytting M, Vago L, Castagna A, Parravicini C, Zanchetta N, D'Arminio Monforte A, Wahren B, Lazzarin A, Linde A (1993) Epstein-Barr virus DNA in cerebrospinal fluid from patients with AIDS-related primary lymphoma of the central nervous system. *Lancet* 342: 398-401
19. Cinque P, Vago L, Dahl H, Brytting M, Terreni MR, Fornara C, Racca S, Castagna A, Monforte AD, Wahren B, Lazzarin A, Linde A (1996) Polymerase chain reaction on cerebrospinal fluid for diagnosis of virus-associated opportunistic diseases of the central nervous system in HIV-infected patients. *AIDS* 10: 951-958
20. Corboy JR, Garl PJ, Kleinschmidt-DeMasters BK (1998) Human herpesvirus 8 DNA in CNS lymphomas from patients with and without AIDS. *Neurology* 50: 335-340
21. Cuomo L, Trivedi P, Cardillo MR, Gagliardi FM, Vecchione A, Caruso R, Calogero A, Frati L, Faggioni A, Ragona G (2001) Human herpesvirus 6 infection in neoplastic and normal brain tissue. *J Med Virol* 63: 45-51

22. d'Arminio Monforte A, Cinque P, Vago L, Rocca A, Castagna A, Gervasoni C, Terreni MR, Novati R, Gori A, Lazzarin A, Moroni M (1997) A comparison of brain biopsy and CSF-PCR in the diagnosis of CNS lesions in AIDS patients. *J Neurol* 244: 35-39
23. Darnell RB (1993) The polymerase chain reaction: Application to nervous system disease. *Ann Neurol* 34: 513-523
24. DeBiasi RL, Tyler KL (1999) Polymerase chain reaction in the diagnosis and management of central nervous system infections. *Arch Neurol* 56: 1215-1219
25. Dlugosch D, Eis-Hübinger AM, Kleim J-P, Kaiser R, Bierhoff E, Schneweis KR (1991) Diagnosis of acute and latent varicella-zoster virus infections using the polymerase chain reaction. *J Med Virol* 35: 136-141
26. Domingues RB, Tsanaclis AMC, Pannuti CS, Mayo MS, Lakeman FD (1997) Evaluation of the range of clinical presentations of herpes simplex encephalitis by using polymerase chain reaction assay of cerebrospinal fluid samples. *Clin Infect Dis* 25: 86-91
27. Drummond CW, Eglin RP, Esiri MM (1994) Herpes simplex virus encephalitis in a mouse model: PCR evidence for CNS latency following acute infection. *J Neurol Sci* 127: 159-163
28. Eeg-Olofsson O, Bergstrom T, Osterland CK, Andermann F, Oliver A (1995) Epilepsy etiology with special emphasis on immune dysfunction and neurovirology. *Brain Dev* 17: 58-60
29. Ehrnst A (1996) The clinical relevance of different laboratory tests in CMV diagnosis. *Scand J Infect Dis Suppl* 100: 64-71
30. Fodor PA, Levin MJ, Weinberg A, Sandberg E, Sylman J, Tyler KL (1998) Atypical herpes simplex virus encephalitis diagnosed by PCR amplification of viral DNA from CSF. *Neurology* 51: 554-559
31. Fraser NW, Block TM, Spivack JG (1992) The latency-associated transcripts of herpes simplex virus: RNA in search of function. *Virology* 191: 1-8.
32. Fraser NW, Lawrence WC, Wroblewska Z, Gilden DH, Koprowski H (1981) Herpes simplex type 1 DNA in human brain tissue. *Proc Natl Acad Sci USA* 78: 6461-6465
33. Furuta Y, Ohtani F, Kawabata H, Fukuda S, Bergstrom T (2000) High prevalence of varicella-zoster virus reactivation in herpes simplex virus-seronegative patients with acute peripheral facial palsy. *Clin Infect Dis* 30: 529-533
34. Gilden DH, Beinlich BR, Rubinstein EM, Stommel E, Swenson R, Rubinstein D, Mahalingam R (1994) Varicella-zoster virus myelitis: An expanding spectrum. *Neurology* 44: 1818-1823
35. Gilden DH, Kleinschmidt-DeMasters BK, LaGuardia JJ, Mahalingam R, Cohrs RJ (2000) Neurologic complications of varicella zoster virus reactivation. *N Engl J Med* 342: 635-646
36. Gilden DH, Kleinschmidt-DeMasters BK, Wellish M, Hedley-Whyte ET, Rentier B, Mahalingam R (1996) Varicella zoster virus, a cause of waxing and waning vasculitis: The New England Journal of Medicine case 5-1995 revisited. *Neurology* 47: 1441-1446
37. Gilden DH, Murray RS, Wellish M, Kleinschmidt-DeMasters BK, Vafai A (1988) Chronic progressive varicella-zoster virus encephalitis in an AIDS patient. *Neurology* 38: 1150-1153
38. Gilden DH, Vafai A, Shtram Y, Becker Y, Devlin M, Wellish M (1983) Varicella-zoster virus DNA in human sensory ganglia. *Nature* 306: 478-480
39. Gilden DH, Wright RR, Schneck SA, Gwaltney JM, Mahalingam R (1994) Zoster sine herpete, a clinical variant. *Ann Neurol* 35: 530-533
40. Greenlee JE, Rose JW (2000) Controversies in neurological infectious diseases. *Semin Neurol* 20: 375-386
41. Hato N, Kisaki H, Honda N, Gyo K, Murakami S, Yanagihara N (2000) Ramsay Hunt syndrome in children. *Ann Neurol* 48: 254-256
42. Ito M, Baker JV, Mock DJ, Goodman AD, Blumberg BM, Shrier DA, Powers JM (2000) Human herpesvirus 6-meningoencephalitis in an HIV patient with progressive multifocal leukoencephalopathy. *Acta Neuropathol* 100: 337-41
43. Ito Y, Kimura H, Yabuta Y, Ando Y, Murakami T, Shiomi M, Morishima T (2000) Exacerbation of herpes simplex encephalitis after successful treatment with acyclovir. *Clin Inf Dis* 30: 185-187
44. Itzhaki RF, Lin WR, Shang D, Wilcock GK, Faragher B, Jamisson GA (1997) Herpes simplex virus type 1 in brain and risk of Alzheimer's disease. *Lancet* 349: 241-244.
45. Jamieson GA, Maitland NJ, Wilcock GK, Craske J, Itzhaki RF (1991) Latent herpes simplex virus type I in normal and Alzheimer's disease brains. *J Med Virol* 33: 224-227
46. Jay V, Becker LE, Otsubo H, Cortez M, Hwang P, Hoffman HJ, Zielenska M (1995) Chronic encephalitis and epilepsy (Rasmussen's encephalitis): detection of cytomegalovirus and herpes simplex virus 1 by the polymerase chain reaction and *in situ* hybridization. *Neurology* 45: 108-117
47. Jay V, Hwang P, Hoffman HJ, Becker LE, Zielenska M (1998) Intractable seizure disorder associated with chronic herpes infection. HSV1 detection in tissue by the polymerase chain reaction. *Child Nerv Syst* 14: 15-20
48. Kimberlin DW, Whitley RJ (1998) Human herpesvirus-6: neurologic implications of a newly-described viral pathogen. *J Neurovirol* 4: 474-485
49. Kimura H, Aso K, Kuzushima K, Hanada N, Shibata M, Morishima T (1992) Relapse of herpes simplex encephalitis in children. *Pediatrics* 89: 891-894
50. Kleinschmidt-DeMasters BK, Amlie-Lefond C, Gilden DH (1996) The patterns of varicella zoster virus encephalitis. *Hum Pathol* 27: 927-938
51. Kleinschmidt-DeMasters BK, Gilden DH (2001) Varicella zoster virus infections of the nervous system—clinical and pathological correlates. *Arch Path Lab Med* 125: 770-780
52. Kleinschmidt-DeMasters BK, Mahalingam R, Shimek C, Marcoux HL, Wellish M, Tyler KL, Gilden DH (1998) Profound cerebrospinal fluid pleocytosis and Froin's syndrome secondary to widespread necrotizing vasculitis in an HIV-positive patient with varicella zoster virus encephalomyelitis. *J Neurol Sci* 159: 213-218

80. Torigoe S, Koide W, Yamada M, Miyashiro E, Tanaka-Taya K, Yamanishi K (1996) Human herpesvirus 7 infection associated with central nervous system manifestations. *J Ped* 129: 301-305

81. Troendle-Atkins J, Demmler GJ, Williamson WD, McDonald JM, Istas AS, Buffone GJ (1994) Polymerase chain reaction to detect cytomegalovirus DNA in the cerebrospinal fluid of neonates with congenital infection. *J Infect Dis* 169: 1334-1337

82. Tyler KL (1994) Polymerase chain reaction and the diagnosis of viral central nervous system disease. *Ann Neurol* 36: 809-811

83. Tyler KL (1998) Serious methodological failures concerning presence of HSV DNA in surgical tissue from human epileptic seizure foci detected by PCR. *Arch Neurol* 55: 1031-1032

84. Tyler KL, Tedder DG, Yamamoto LJ, Klapper JA, Ashley R, Lichtenstein KA, Levin MJ (1995) Recurrent brainstem encephalitis associated with herpes simplex virus type 1 DNA in cerebrospinal fluid. *Neurology* 45: 2246-2250

85. Van den Berg JS, van Zeijl JH, Rotteveel JJ, Melchers WJ, Gabreels FJ, Galama JM (1999) Neuroinvasion by human herpesvirus type 7 in a case of exanthem subitum with severe neurologic manifestations. *Neurology* 52: 1077-1079

86. Vinters HV, Wang R, Wiley CA (1993) Herpesviruses in chronic encephalitis associated with intractable childhood epilepsy. *Hum Pathol* 24: 871-879

87. Weber T (1999) Cerebrospinal fluid analysis for the diagnosis of human immunodeficiency virus-related neurologic diseases. *Semin Neurol* 19: 223-233

88. Weber T, Frye S, Bodemer M, Otto M, Luke W (1996) Clinical implications of nucleic acid amplification methods for the diagnosis of viral infections of the nervous system. *J Neurovirol* 2: 175-190

89. Weidenheim KM, Bodhireddy SR, Nuovo GJ, Nelson SJ, Dickson DW (1995) Multicystic encephalopathy: Review of eight cases with etiologic considerations. *J Neuropathol Exp Neurol* 54: 268-275

90. Welling DB, Miles BA, Western L, Prior TW (1997) Detection of viral DNA in vestibular ganglia tissue from patients with Meniere's disease. *Am J Otol* 18: 734-737

91. Wildemann B, Haas J, Lynen N, Stingele K, Storch-Hagenlocher B (1998) Diagnosis of cytomegalovirus encephalitis in patients with AIDS by quantitation of cytomegalovirus genomes in cells of cerebrospinal fluid. *Neurology* 50: 693-697

92. Yoshikawa T, Asano Y (2000) Central nervous system complications in human herpesvirus-6 infection. *Brain Develop* 22: 307-314

JOURNAL OF VIROLOGY, Dec. 2001, p. 11275–11283 Vol. 75, No. 23
0022-538X/01/$04.00+0 DOI: 10.1128/JVI.75.23.11275–11283.2001

Reovirus Infection Activates JNK and the JNK-Dependent Transcription Factor c-Jun

PENNY CLARKE,[1] SUZANNE M. MEINTZER,[1] CHRISTIAN WIDMANN,[2]† GARY L. JOHNSON,[2] AND KENNETH L. TYLER[1,3,4,5]*

Departments of Neurology,[1] Pharmacology,[2] Medicine,[3] and Microbiology and Immunology,[4] University of Colorado Health Science Center, Denver, Colorado 80262, and Denver Veterans Affairs Medical Center, Denver, Colorado 80220[5]

Received 6 April 2001/Accepted 22 August 2001

Viral infection often perturbs host cell signaling pathways including those involving mitogen-activated protein kinases (MAPKs). We now show that reovirus infection results in the selective activation of c-Jun N-terminal kinase (JNK). Reovirus-induced JNK activation is associated with an increase in the phosphorylation of the JNK-dependent transcription factor c-Jun. Reovirus serotype 3 prototype strains Abney (T3A) and Dearing (T3D) induce significantly more JNK activation and c-Jun phosphorylation than does the serotype 1 prototypic strain Lang (T1L). T3D and T3A also induce more apoptosis in infected cells than T1L, and there was a significant correlation between the ability of these viruses to phosphorylate c-Jun and induce apoptosis. However, reovirus-induced apoptosis, but not reovirus-induced c-Jun phosphorylation, is inhibited by blocking TRAIL/receptor binding, suggesting that apoptosis and c-Jun phosphorylation involve parallel rather than identical pathways. Strain-specific differences in JNK activation are determined by the reovirus S1 and M2 gene segments, which encode viral outer capsid proteins (σ1 and μ1c) involved in receptor binding and host cell membrane penetration. These same gene segments also determine differences in the capacity of reovirus strains to induce apoptosis, and again a significant correlation between the capacity of T1L × T3D reassortant reoviruses to both activate JNK and phosphorylate c-Jun and to induce apoptosis was shown. The extracellular signal-related kinase (ERK) is also activated in a strain-specific manner following reovirus infection. Unlike JNK activation, ERK activation could not be mapped to specific reovirus gene segments, suggesting that ERK activation and JNK activation are triggered by different events during virus-host cell interaction.

Mitogen-activated protein kinases (MAPKs) play a critical role in the transduction of a wide variety of extracellular signals (22). MAPKs include the extracellular signal-related kinases (ERKs), which are activated by growth factors and many other mitogenic stimuli (11) and are generally thought to have antiapoptotic properties, and the c-Jun N-terminal kinases (JNKs, also called stress-activated protein kinases, SAPKs) (16, 39) and p38 MAPKs (23, 40, 53), which are activated by stress stimuli and function to communicate growth-inhibitory and apoptotic signals within cells. It is thought that the commitment to apoptosis and determination of cell fate may involve the balance between the activity of the JNK and p38 kinases and that of ERK (7). For example, the inhibition of ERK activity and the coordinate activation of JNK and p38 kinase correlate with the induction of apoptosis in nerve growth factor-deprived PC12 pheochromocytoma cells (61), Fas-treated Jurkatt cells (37, 60), and UV-irradiated mouse fibroblasts (3).

Infection with a wide variety of viruses can result in perturbation of host cell signaling pathways including MAPK cascades. Some viruses show a dependence on the ERK signaling cascades for replication, and viral proteins that induce ERK activation have been identified (34, 36, 38, 43, 57). Virus-induced MAPK activation, including JNK and p38, has also been described (19, 31, 32, 42, 44, 49, 54, 63), as has the activation of MAPK-associated transcription factors (33, 42, 54, 63). However, the reason for their activation following infection remains largely unclear.

Reovirus is a double-stranded RNA virus that induces apoptosis in cultured cells in vitro (46, 50, 58) and in target tissues in vivo including the central nervous system and heart (14, 46, 47). Reovirus-induced apoptosis correlates with pathology in vivo and is a critical mechanism by which disease is triggered in the host (14, 47). Strain-specific differences in the capacity of reoviruses to induce apoptosis are determined by the viral S1 and M2 gene segments (58, 59). Reovirus-induced apoptosis requires viral binding to cell surface receptors, including junctional adhesion molecule (2), but not completion of the full viral replication cycle (50, 58). Reovirus induces apoptosis by a p53-independent mechanism that involves cellular proteases including calpains (15) and caspases (10), is dependent on reovirus-induced NF-κB activation (2, 12), and is inhibited by overexpression of Bcl-2 (50).

We have previously shown that reovirus-induced apoptosis is mediated by tumor necrosis factor (TNF) related apoptosis-inducing ligand (TRAIL) (10), which is released from infected cells, and can be inhibited by antibodies against TRAIL or by treatment of infected cells with soluble forms of TRAIL receptors. TRAIL interacts with several members of the TNF receptor superfamily including the apoptosis-associated receptors DR4 (TRAIL-R1) and DR5 (TRAIL-R2/TRICK2/KILL-

* Corresponding author. Mailing address: Department of Neurology (127), Denver VA Medical Center, 1055 Clermont St., Denver, CO 80220. Phone: (303) 393-2874. Fax: (303) 393-4686. E-mail: Ken.Tyler@uchsc.edu.

† Present address: Institute de Biologie Cellulaire et de Morphologie, Lausanne, Switzerland.

ER). These receptors contain an intracellular 80-amino-acid "death domain" (reviewed in reference 1), which is indispensable for apoptosis since it interacts with death domains found in cytoplasmic adapter proteins such as TNF-R1-associated death domain protein (29) and Fas-associated protein with death domain (5, 8). Adapter proteins have additional domains that enable interaction with the prodomains of apoptotic caspases (4, 17, 45) and with members of the TNF receptor-associated factor family (27, 28) of molecules involved in the activation of NF-κB and JNK (52, 56). In addition to activating apoptotic caspases, TRAIL-receptor activation in reovirus-infected cells is thus also likely to result in the activation of NF-κB (35) and JNK (30).

The capacity of reovirus to induce apoptosis through a TRAIL-dependent pathway in infected cells suggests that pro-apoptotic MAPKs, including JNK, might be activated in reovirus-infected cells. Reovirus infection also disrupts cell cycle regulation by inducing a G_2/M arrest (48), suggesting that ERK, which promotes cell cycle progression, might also be inhibited following reovirus infection. This study investigated the activation of MAPKs in reovirus-infected cells. We showed that reovirus infection causes the selective activation of both the JNK and ERK MAPK cascades. Strain-specific differences in JNK, but not ERK, activation are determined by the viral S1 and M2 gene segments, suggesting that different mechanisms are involved in the activation of these kinases in reovirus-infected cells. The viral S1 and M2 gene segments also determine differences in the capacity of reoviruses to induce apoptosis, and we now show that there is a significant correlation between the capacity of reassortant reoviruses to activate JNK and to induce apoptosis. Blocking TRAIL-receptor interaction does not prevent the early activation of c-Jun by reovirus, indicating that death receptor-independent signaling pathways are required for reovirus-induced JNK activation.

MATERIALS AND METHODS

Cells and virus. Mouse L929 cells (ATCC CCL1) were grown in Joklik's modified Eagle's medium supplemented to contain 5% fetal bovine serum and 2 mM L-glutamine (Gibco BRL). Reovirus strains Type 3 Abney (T3A), Type 3 Dearing (T3D), and Type 1 Lang (T1L) are laboratory stocks, which have been plaque purified and passaged (twice) in L929 (ATCC CCL1) cells to generate working stocks (59). T1L × T3D reassortant viruses were grown from stocks originally isolated by Kevin Coombs, Max Nibert, and Bernard Fields (6, 13). Virus infections were performed at a multiplicity of infection (MOI) of 100 to ensure that 100% of susceptible cells were infected and to maximize the synchrony of virus replication.

Western Blot analysis and antibodies. Following infection with reovirus, cells were pelleted by centrifugation, washed twice with ice-cold phosphate-buffered saline, and lysed by sonication in 200 μl of a buffer containing 15 mM Tris (pH 7.5), 2 mM EDTA, 10 mM EGTA, 20% glycerol, 0.1% NP-40, 50 mM β-mercaptoethanol, 100 μg of leupeptin per ml, 2 μg of aprotinin per ml, 40 μM Z-Asp-2,6-dichlorobenzoyloxime, and 1 mM phenylmethylsulfonyl fluoride. The lysates were then cleared by centrifugation at 16,000 × *g* for 5 min, normalized for protein amount, mixed 1:1 with SDS sample buffer (100 mM Tris [pH 6.8], 2% sodium dodecyl sulfate [SDS], 300 mM β-mercaptoethanol, 30% glycerol, 5% pyronine Y), boiled for 5 min and stored at −70°C. Proteins were subjected to SDS-polyacrylamide gel electrophoresis (PAGE) (10% polyacrylamide gels) and probed with antibodies directed against phospho-ERK, phospo c-Jun, and total c-Jun (New England Biolabs, Beverly, Mass.). All lysates were standardized for protein concentration with antibodies directed against actin (no. CP01; Oncogene, Cambridge, Mass.). Autoradiographs were quantitated by densitometric analysis using a Fluor-S MultiImager (Bio-Rad Laboratories, Hercules, Calif.).

In vitro kinase assays. L929 cells were solubilized in TX-100 lysis buffer (70 mM β-glycerophosphate, 1 mM EGTA, 100 μM Na_3VO_4, 1 mM dithiothreitol, 2 mM $MgCl_2$, 0.5% Triton X-100, 20 μg of aprotinin per ml). Cellular debris was removed by centrifugation at 8,000 × *g* for 5 min. The protein concentration was determined by a Bradford assay using bovine serum albumin as a standard. JNK activity was measured using a solid-phase kinase assay in which glutathione *S*-transferase–c-Jun bound to glutathione-Sepharose 4B beads was used to affinity purify JNK from cell lysates as described previously (20, 25). The phosphorylation of glutathione *S*-transferase–c-Jun was quantitated with a PhosphorImager instrument (Molecular Dynamics). ERK activation was measured by first incubating the lysate with 2 μg of an anti-ERK2 antibody (Santa Cruz Biotechnology, Inc.) per ml for 1 hr at 4°C with agitation followed by the addition of 15 μl of a slurry of protein A-Sepharose beads (no. P-3391; Sigma) and a further 20-min incubation at 4°C. The beads were washed twice with 1 ml of lysis buffer and twice with 1 ml of lysis buffer without Triton X-100. A 35-μl volume of the last wash was left in the tube, mixed with 20 μl of ERK reaction mix (50 mM β-glycerophosphate, 100 μM Na_3VO_4, 20 mM $MgCl_2$, 200 μM ATP, 0.5 μCi of [γ-^{32}P]ATP per μl 400 μM epidermal growth factor receptor peptide 662–681, 100 μg of IP-20 per μl, 2 mM EGTA), and incubated for 20 min at 20°C. The reaction was stopped with 10 μl of 25% trichloroacetic acid, and the reaction product was spotted on P81 Whatman paper. The samples were washed three times for 5 min each in 75 mM phosphoric acid and once for 2 min in acetone. They were then air dried, and their radioactivity was measured in a β-counter. The activity of p38 was measured as described by Gerwins et al. (21).

Apoptosis assays and reagents. At 48 h after infection with reovirus, the cells were harvested and stained with acridine orange, for determination of nuclear morphology and ethidium bromide in order to distinguish cell viability, at a final concentration of 1 μg/ml (18). Following staining, the cells were examined by epifluorescence microscopy (Nikon Labophot-2; B-2A filter; excitation, 450 to 490 nm; barrier, 520 nm; dichroic mirror, 505 nm). The percentage of cells containing condensed nuclei and/or marginated chromatin in a population of 100 cells was recorded. The specificity of this assay has been previously established in reovirus-infected cells by using DNA-laddering techniques and electron microscopy (10, 58). Soluble death receptors (Fc:DR5 and Fc:DR4) were obtained from Alexis Corp. (Pittsburgh, Pa.).

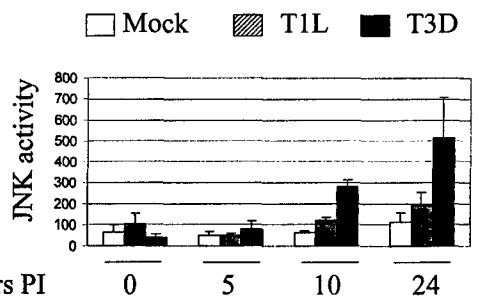

FIG. 1. Reovirus activates JNK infected cells. L929 cells were infected with two different serotypes of reovirus, T1L and T3D (MOI, 100) or were mock infected. At various times p.i., lysates were prepared and JNK activity was determined by in vitro kinase assays. The graph shows the mean JNK activity, as measured by c-Jun phosphorylation (arbitrary imager units), of three independent experiments. Error bars represent standard errors of the mean.

RESULTS

Reovirus activates JNK in infected cells. We first investigated whether JNK was activated in reovirus-infected cells. L929 cells were infected (MOI, 100) with two prototype strains of reovirus, T3D and T1L. At 0, 5, 10 and 24 h postinfection (p.i.), the cells were harvested and the presence of JNK activity was detected by in vitro kinase assays (Fig. 1). In three independent experiments, JNK activity was significantly increased ($P < 0.01$) at 24 h p.i. in T3D-infected cells compared to mock-infected cells. However, JNK activity was not significantly increased ($P > 0.05$) at 24 h p.i. in T1L-infected cells compared to mock-infected cells. An increase in JNK activity was apparent in T3D-infected cells at 10 h p.i. Although sta-

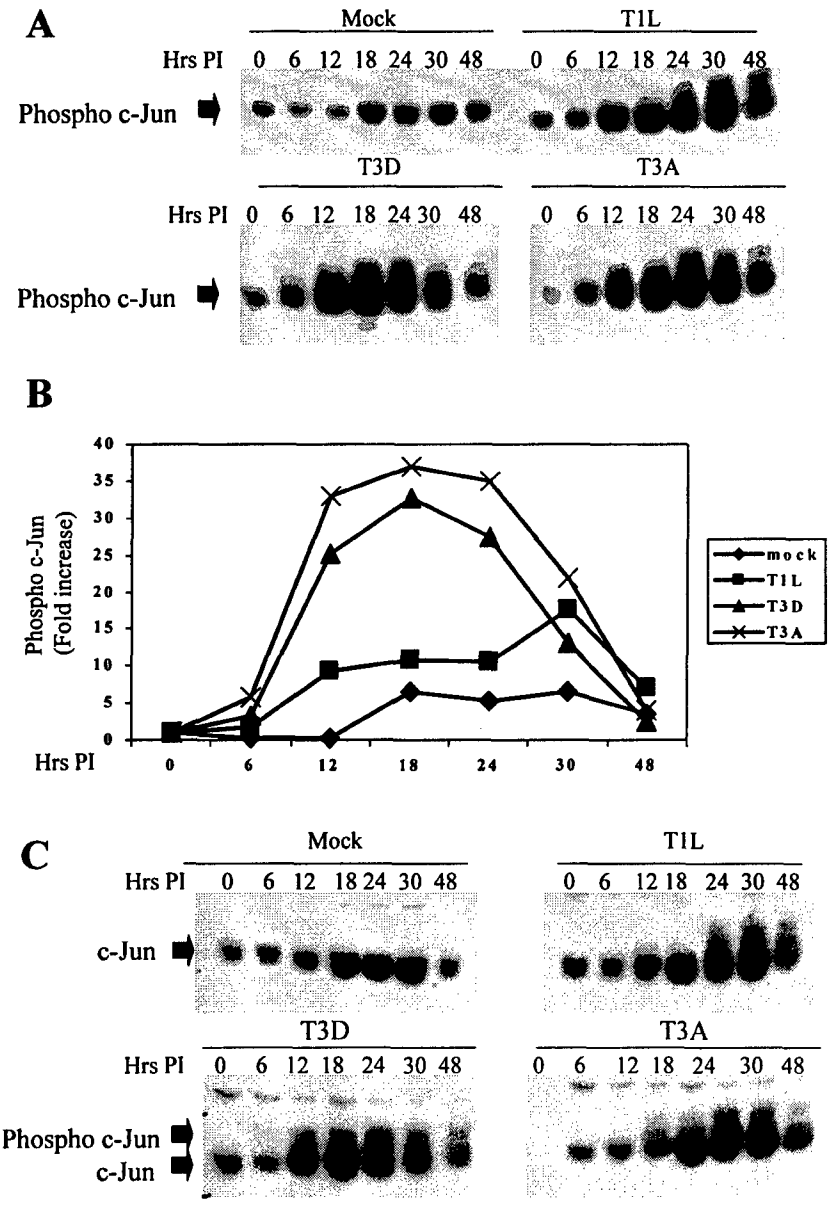

FIG. 2. c-Jun is activated following infection with reovirus. Cells were infected with different strains of reovirus (MOI, 100) and were harvested at various times p.i. (A and C) Extracts were standardized for protein concentration, using an anti-actin antibody, and equal amounts of protein were separated by SDS-PAGE and probed with antibodies directed against phosphorylated (A) or total (C) c-Jun. Bands corresponding to phosphorylated and unphosphorylated c-Jun are shown. The gels are representative of at least two independent experiments. (B) Graphical representation of the Western blot shown in panel A, showing the fold increase in the levels of phophorylated c-Jun over time.

tistically significant, variability in JNK activity was greater in the T3D-infected cells at 24 h p.i. than for other times and conditions, reflecting the increase in the mean value.

Levels of phosphorylated c-Jun are increased in reovirus-infected cells. The activation of JNK results in the phosphorylation and activation of the transcription factor c-Jun, which in turn regulates the transcription of a multitude of cellular genes. Having shown that JNK was activated in reovirus-infected cells, we wished to determine whether the JNK-dependent transcription factor c-Jun was also activated following reovirus infection. Cells were infected with three different strains of reovirus, T1L, T3D, and T3A, the second prototypic T3 strain. The cells were then harvested at various times p.i., and the activation state of c-Jun was determined by Western blot analysis using an antibody directed against the phosphorylated, activated form of c-Jun. Levels of phosphorylated c-Jun were increased in cells infected with the T1L, T3D, and T3A strains compared to those in mock-infected cells (Fig. 2). Increased levels of activated c-Jun were present 12 h p.i., which closely parallels the activation of JNK (Fig. 1). There were

TABLE 1. Reovirus-induced JNK activation is determined by the S1 and M2 gene segments

Virus strain[a]	JNK activity (imager units)	Reovirus gene segment									
		L1	L2	L3	M1	M2	M3	S1	S2	S3	S4
EB97	189,000	T3D	T3D	T1L	T3D	T3D	T3D	T3D	T3D	T3D	T1L
T3D	108,000	T3D	T3D	T3D	T3D	T3D	T3D	T3D	T3D	T3D	T3D
EB13	108,000	T3D	T3D	T3D	T3D	T3D	T3D	T3D	T3D	T3D	T1L
H15	102,000	T1L	T3D	T3D	T1L	T3D	T3D	T3D	T3D	T3D	T1L
KC150	84,000	T3D	T1L	T1L	T1L	T3D	T1L	T3D	T3D	T1L	T3D
EB121	81,000	T3D	T3D	T1L	T3D	T1L	T3D	T1L	T3D	T3D	T3D
EB1	78,000	T1L	T3D	T1L	T1L	T3D	T1L	T1L	T1L	T3D	T1L
EB85	75,000	T1L	T1L	T1L	T1L	T1L	T3D	T1L	T3D	T1L	T1L
EB31	63,000	T1L	T1L	T1L	T3D	T1L	T1L	T1L	T3D	T3D	T1L
T1L	54,000	T1L	T1L	T1L	T1L	T1L	T1L	T1L	T1L	T1L	T1L
H41	24,000	T3D	T3D	T1L	T1L	T1L	T3D	T1L	T3D	T3D	T1L
None (mock)	20,000										
t test		0.33	0.18	0.19	0.15	**0.026**	0.20	**0.04**	0.24	0.19	0.83
M-W test		0.17	0.16	0.08	0.12	**0.014**	0.22	**0.008**	0.29	0.24	0.41

[a] *t* test and M-W values are *P* values, with significant values in bold type.

serotype-specific differences in the ability of reovirus to phosphorylate c-Jun with T3 strains (T3D and T3A), inducing higher levels of phosphorylated c-Jun at earlier times p.i., and T1L strains. For example, at 12 h p.i., the levels of phosphorylated c-Jun were increased 8-fold in T1L-infected cells compared to those seen in mock-infected cells whereas the levels of phosphorylated c-Jun were increased 24-fold in T3D-infected cells and 33-fold in T3A-infected cells. Some increase in c-Jun phosphorylation was observed in mock-infected cells, which may be due to increasing cell confluence. We probed the same lysates with an antibody that detects total c-Jun (both phosphorylated and unphosphorylated forms [Fig. 2C]). These blots show that there was also an increase in the levels of total c-Jun in both mock and reovirus-infected cells. Also visible on these blots are bands corresponding to the phosphorylated form of c-Jun (Fig. 2C). Once again, serotype-specific differences in the ability of reovirus to phosphorylate c-Jun were observed, with T3D and T3A inducing higher levels of phosphorylated c-Jun than T1L did.

In support of the association between JNK activation and c-Jun phosphorylation, there was a high correlation between the ability of reovirus to induce JNK activation and to phosphorylate c-Jun (Pearson parametric correlation $R^2 = 0.99$, $P = 0.0217$).

Reovirus-induced JNK activation is determined by the S1 and M2 gene segments. Having shown that T3D activates JNK to a greater extent than T1L does, we wished to identify whether specific viral genes determined these differences. L929 cells were infected with a panel of T1L × T3D reassortant reoviruses (MOI, 100). At 24 h p.i., the cells were harvested and the JNK activity was determined by the in vitro kinase assay. JNK activation following infection with different reassortant viruses, as well as with parental strains, and the derivation of the various genome segments of each virus are shown in Table 1. The results were analyzed using both parametric (*t* test) and nonparametric (Mann-Whitney [M-W] test) methods. The reovirus S1 (*t* test, $P = 0.04$; M-W test, $P = 0.008$) and M2 (*t* test, $P = 0.026$; M-W test, $P = 0.014$) gene segments were both significantly associated with strain-specific differences in virus-induced apoptosis. Using linear-regression analysis, we obtained R^2 values of 48.6% ($P = 0.017$) for the S1 gene segment and 42.5% ($P = 0.03$) for the M2 gene segment. These results indicate that both the S1 and M2 gene segments contribute to strain-specific differences in the capacity of reovirus to activate JNK in infected cells. The nature of the reassortant pool tested, in which eight of nine viruses were concordant for the parental origin of their S1 and M2 segments, prevented us from more accurately defining the relative contributions of these two segments to JNK activation.

It is important to note that although statistical analysis identifies the S1 and M2 gene segments as important determining factors in the ability of reoviruses to induce JNK activation, some viruses with differing genotypes (e.g., KC150 and EB121) have closely related JNK activity levels. This suggests that nongenetic factors also contribute to reovirus-induced JNK activation.

Reovirus-induced c-Jun phosphorylation and reovirus-induced apoptosis are correlated. Reovirus prototypic strains T3D and T3A induce more apoptosis in infected cells than T1L (58, 59). Since our results indicate that Type 3 reoviruses also induce higher levels of phosphorylated c-Jun and JNK activity, we compared the ability of the prototypic strains of reovirus to phosphorylate c-Jun at 12 and 18 h p.i. (Fig. 2) with their ability to induce apoptosis (Fig. 3A and B). Apoptosis was measured at 48 h p.i., and the apoptosis experiments were set up in parallel to the c-Jun experiments to ensure that the experimental conditions were as similar as possible. A significant association between the capacity of reoviruses to induce apoptosis and phosphorylate c-Jun was found (Pearson parametric correlation $R^2 = 0.964$ using c-Jun values obtained at 12 h p.i. and $R^2 = 0.9330$ using c-Jun values obtained at 18 h p.i.). We also investigated whether there was a correlation between the capacity of T1L × T3D reassortants to phosphorylate c-Jun (Fig. 3C) or activate JNK (Fig. 3D) and to induce apoptosis. Significant associations between the capacity of reovirus reassortants to induce apoptosis and both activate JNK (Pearson parametric correlation $R^2 = 0.6077$, $P = 0.0028$) and phosphorylate c-Jun (Pearson parametric correlation $R^2 = 0.30$, $P = 0.0354$) were found. The larger pool of viruses used to generate the

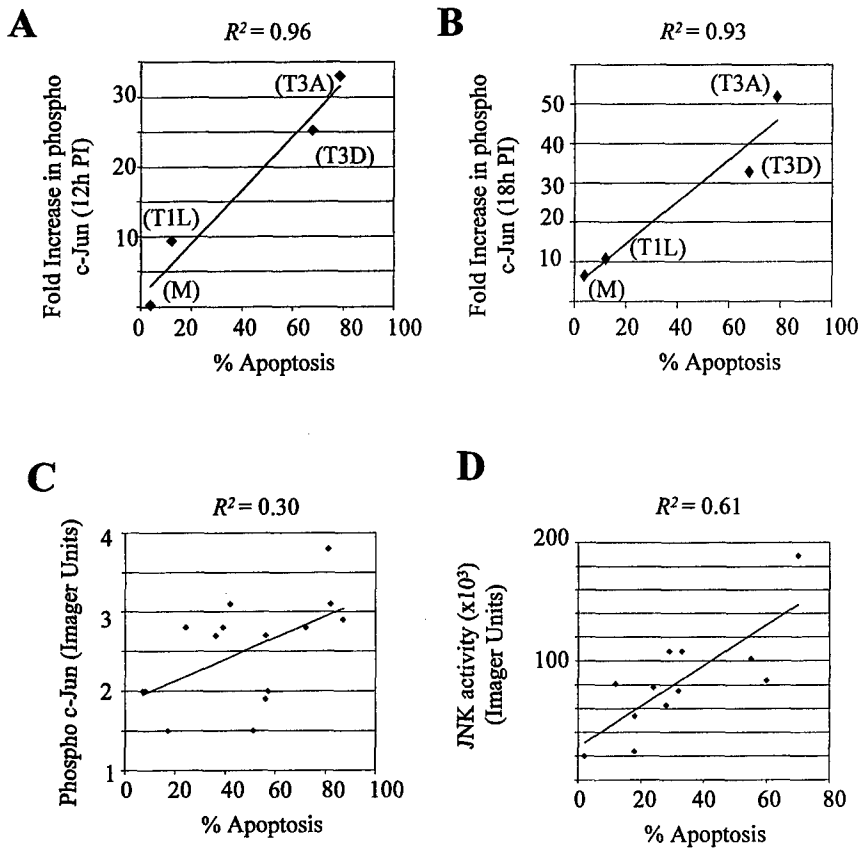

FIG. 3. There is a correlation between the capacities of different prototype strains of reovirus to phosphorylate c-Jun and induce apoptosis and between the capacities of T1L × T3D reassortant viruses to induce JNK activation or c-Jun phosphorylation and apoptosis. The abilities of different strains of reovirus (T3A, T3D, and T1L) and mock (M) infection to induce increased levels of phosphorylated c-Jun, at 12 h (A) and 18 h (B) p.i. (values taken from Fig. 2) and apoptosis are shown. Experiments to determine c-Jun phosphorylation and apoptosis were set up in parallel. (C) The capacity of reovirus reassortants (MOI, 100) to induce phosphorylated c-Jun and apoptosis was plotted. Each point represents a single reassortant virus. Lysates were harvested at 18 h p.i., standardized for protein concentration, and analyzed by Western blotting using an antibody directed against phospho c-Jun. Apoptosis values were obtained in a parallel experiment and represent the mean value from three separate wells (24-well tissue culture plate) of the same experiment. (D) The capacities of reovirus reassortants (MOI, 100) to induce JNK activity and apoptosis were plotted. Each point represents a single reassortant virus. JNK activity values were taken from Table 1. Apoptosis values were obtained in a parallel experiment and represent the mean value from three separate wells (24-well tissue culture plate) of the same experiment.

reassortant data enabled us to derive *P* values for these correlations.

Soluble TRAIL receptors block reovirus-induced apoptosis but not reovirus-induced c-Jun activation. TRAIL receptor ligation results in the activation of JNK (30). We have previously shown that reovirus-induced apoptosis requires TRAIL receptor ligation (10). We next investigated whether TRAIL receptor activation was required for the activation of c-Jun in reovirus-infected cells. A combination of the soluble TRAIL receptors Fc:DR5 and Fc:DR4 was used to inhibit the binding of TRAIL to its functional cellular receptors. L929 cells were infected with T3D (MOI, 50) in the presence or absence of Fc:DR5 and Fc:DR4 (final concentration, 100 ng/ml each) and were harvested after 18 h. Lysates were then analyzed by Western blot analysis using an anti-phospho-c-Jun antibody. In parallel, cells were infected with reovirus in the presence of a combination of Fc:DR5 and Fc:DR4 and were assayed for reovirus-induced apoptosis after 48 h (Fig. 4). The presence of soluble TRAIL receptors did not inhibit c-Jun activation in T3D-infected cells (Fig. 4A and B). In fact, there seemed to be an increase in levels of phosphorylated c-Jun when cells were infected with reovirus in the presence of soluble TRAIL receptors compared to levels seen in untreated, infected cells. Conversely, the presence of soluble TRAIL receptors markedly reduced the ability of T3D to induce apoptosis (Fig. 4C), indicating that inhibition of TRAIL receptor ligation inhibits apoptosis but fails to reduce the activation of c-Jun in reovirus-infected cells. This suggests that pathways other than those initiated by TRAIL contribute to reovirus-induced JNK activation.

ERK, but not p38 MAPK, is activated following reovirus infection. Having shown that JNK is activated in reovirus-infected cells we wished to determine whether other MAPK pathways are also activated following reovirus infection. The activities of p38 and ERK were thus investigated in reovirus-infected L929 cells (MOI, 100) at 24 and 48 h p.i. by in vitro kinase assays. T3D, but not T1L, infection resulted in the activation of ERK. ERK activation peaked at 24 h p.i., with a

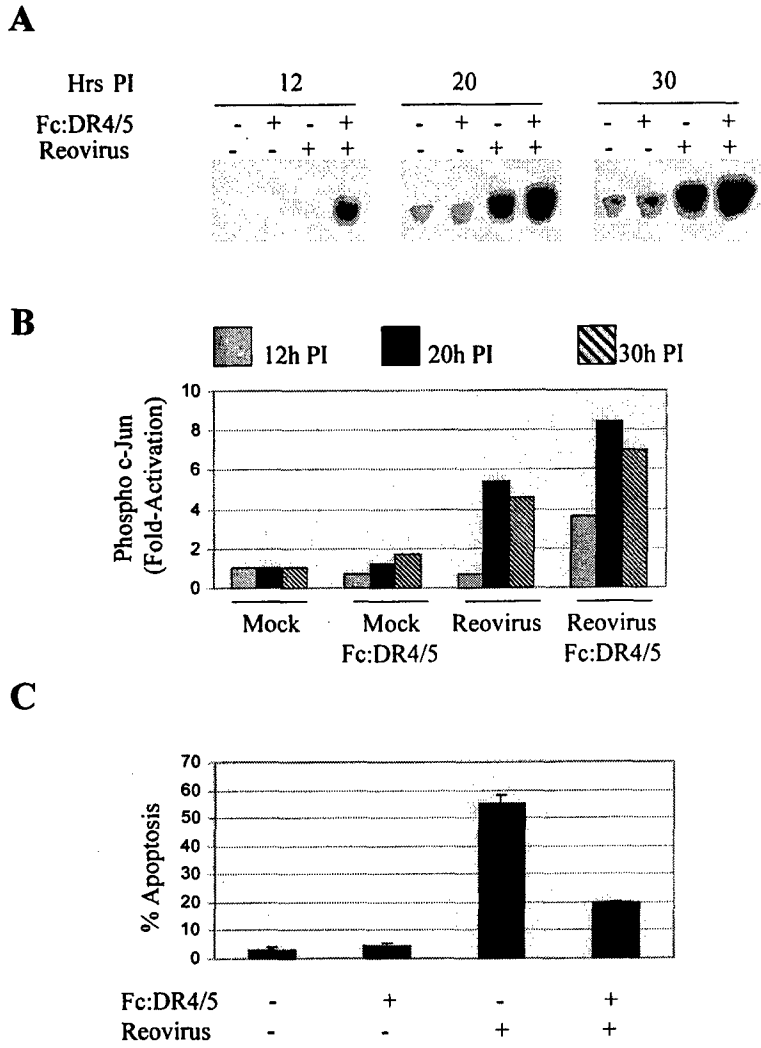

FIG. 4. Apoptosis but not c-Jun phosphorylation is inhibited in T3D-infected cells in the presence of the soluble TRAIL receptors Fc:DR5 and Fc:DR4. In parallel experiments, cells were infected with T3D (MOI, 50) and were assayed for c-Jun activation at various times p.i. and for apoptosis after 48 h. (A) Representative autoradiograph showing levels of phosphorylated c-Jun following infection with reovirus (T3D), in the presence or absence of Fc:DR5 and Fc:DR4 (final concentrations, 100 ng/ml each). Equal amounts of protein, as determined by actin concentration (data not shown), were loaded. (B) Graphical analysis of the results shown in panel A showing the fold increase in c-Jun phosphorylation compared to that in mock-infected, untreated cells, at 12 h, 20 h, and 30 h p.i. (C) Graph showing the percentage of cells with apoptotic nuclear morphology in reovirus (T3D)- or mock-infected cells in the presence or absence of soluble TRAIL receptors (final concentration, 100 ng/ml each). Error bars represent standard errors of the mean from three separate wells (24-well tissue culture plate) of the same experiment.

four fold increase in the levels of ERK activation compared to those in mock-infected cells (Fig. 5A). There was a slight decrease in p38 activity following infection with the T1L and T3D strains of reovirus (Fig. 5B).

Since MAPKs can be activated rapidly in some systems, we also looked at MAPK activation at very early times (less than 2 h) after reovirus infection. Using antibodies directed against the phosphorylated, active form of ERK, we were able to show that ERK had an additional activation peak at around 20 min p.i. (Fig. 5C). This activation peak was also strain specific, with T3D and T3A inducing more activity than T1L did. JNK and p38 were not activated within 2 h of infection (results not shown). Taken together with our above-described data, these results indicate that reovirus preferentially and selectively activates the JNK and ERK MAPK pathways.

Although we were able to show strain-specific differences in the activation of ERK in infected cells, we have been unable to map this phenomenon to a specific reovirus gene segment (results not shown), suggesting that ERK and JNK activation involve different types of virus-host cell interactions. The activation of ERK is generally associated with antiapoptotic effects. Conversely, the inhibition of ERK activity often correlates with the activation of JNK and p38 kinase and the resultant induction of apoptosis. We therefore wished to investigate whether reovirus-induced apoptosis would be enhanced by treatment with PD 98059, a chemical inhibitor of

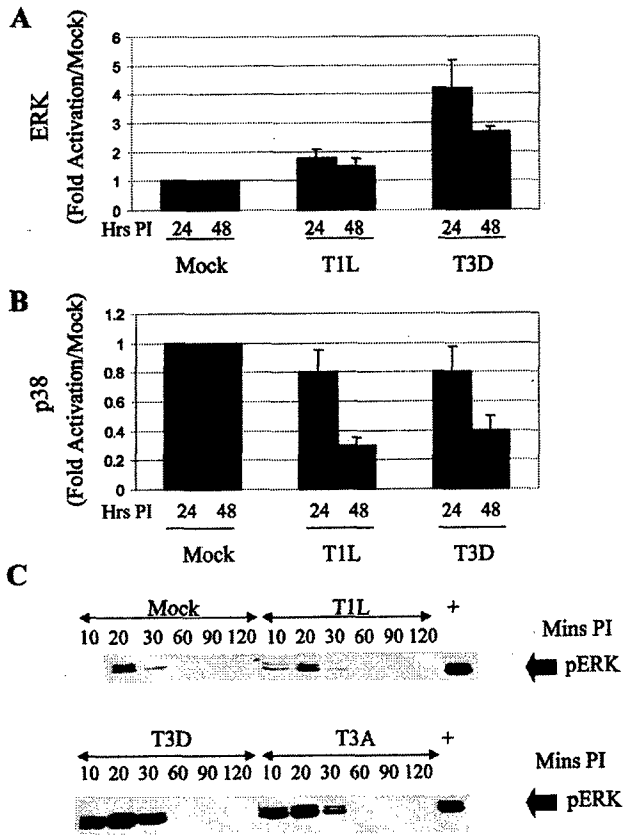

FIG. 5. Reovirus activates ERK but not p38 in infected cells. (A and B) The activities of ERK (A) and p38 (B) were investigated in reovirus-infected L929 cells (MOI, 100) at 24 and 48 h p.i. by in vitro kinase assays. The graphs show fold activation compared to that in mock-infected cells. Error bars represent standard errors of the mean from three independent experiments. (C) ERK is activated at early times after reovirus infection. L929 cells were infected with reovirus (MOI, 100) and harvested at various times p.i. Proteins were separated by SDS-PAGE and subjected to Western blot analysis using antibodies directed against phospho-ERK. Actin was used to standardize for protein loading (data not shown).

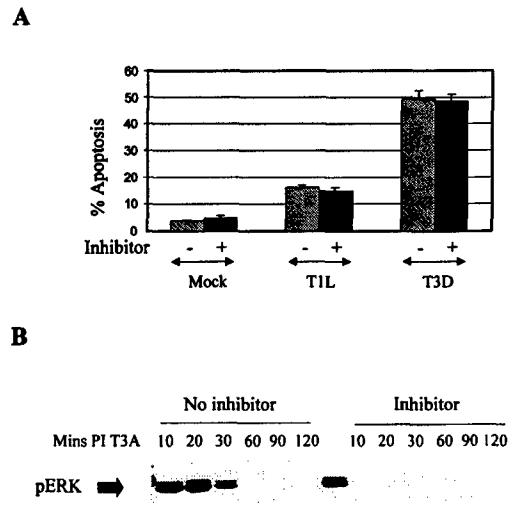

FIG. 6. Inhibition of ERK activation does not affect reovirus-induced apoptosis. (A) Reovirus-induced apoptosis (MOI, 100) was measured in the presence of a chemical inhibitor of ERK activation (PD 98059). L929 cells were pretreated with inhibitor (10 μM) for 2 h prior to infection with reovirus and were maintained in medium in the presence of inhibitor for 48 h following reovirus infection. They were then harvested and assayed for apoptosis. The graph shows percent apoptosis. Error bars represent standard errors of the mean. (B) Activation-phosphorylation of ERK following reovirus (T3D) infection (MOI, 100) in the presence of PD 98059 (10 μM) as determined by Western blot analysis using antibodies directed against phospho-ERK.

ERK activation. Cells were pretreated with 10 μM PD 98059 for 2 h prior to infection with reovirus and were maintained in medium in the presence of inhibitor for 48 h following infection. There was no change in reovirus-induced apoptosis in cells treated with PD 98059 (Fig. 6A), even though ERK activation following reovirus infection was blocked (Fig. 6B). The activity of MAPK p38 is decreased in reovirus-infected cells, and, as expected, chemical inhibitors of p38 (PD 169316 and SB 202190) did not affect reovirus-induced apoptosis (results not shown).

DISCUSSION

Our results indicate that reovirus infection selectively induces MAPK activation in infected cells. JNK is activated following reovirus infection in a strain-specific manner, with the type 3 prototype reovirus strain (T3D) inducing more JNK activation than the type 1 prototype reovirus strain (T1L) does. Reovirus-induced JNK activation is associated with phosphorylation, and hence activation, of the JNK-dependent transcription factor c-Jun. The phosphorylation of c-Jun is also a strain-specific event, with the prototype 3 strains (T3D and T3A) inducing more JNK activation than T1L does.

Strain-specific differences in JNK activation are determined by the S1 and M2 reovirus gene segments, which both encode reovirus capsid proteins. The reovirus S1 gene is bicistronic, encoding both the viral attachment protein σ1 and a nonvirion-associated protein, σ1s, that is required for reovirus-induced G_2/M cell cycle arrest (48) but is not required for reovirus growth in cell culture or for the induction of apoptosis (51, 59). Reovirus-induced c-Jun activation is not blocked following infection by a σ1s-deficient virus strain (results not shown), indicating that σ1s is not required for c-Jun activation in reovirus-infected cells. The M2 segment encodes the main reovirus outer capsid protein μ1c, which plays a key role in membrane penetration and in the transmembrane transport of virions (24, 26, 41).

The S1 and M2 gene segments also determine the ability of reovirus to induce apoptosis (59), and there is a correlation between the ability of different prototype reovirus strains, and T3D × T1L reassortant reoviruses to induce apoptosis and to activate JNK and/or phosphorylate c-Jun. This suggests that JNK activation and c-Jun phosphorylation and apoptosis either are components of the same pathway that induces apoptosis following reovirus infection or are components of distinct, parallel pathways induced by the same viral factors.

Reovirus-induced apoptosis is mediated by TRAIL-induced activation of death receptors and is associated with the release of TRAIL from infected cells (10). TRAIL receptor activation can also result in the activation of JNK (30), suggesting that

this may be the mechanism by which reovirus induces JNK activation. However, reovirus-induced TRAIL release and TRAIL receptor activation do not occur until 24 to 48 h p.i. (10), suggesting that death receptor-independent signaling pathways are responsible for the earlier (10-h p.i.) activation of JNK and c-Jun that occurs following reovirus infection. The fact that reovirus-induced apoptosis can be inhibited by soluble TRAIL receptors, without affecting reovirus-induced c-Jun phosphorylation, indicates that pathways leading to apoptosis and JNK activity can be disassociated and also suggests that these pathways are distinct rather than identical. Both these observations are consistent with our previous studies showing that reovirus-induced JNK activity (62), but not apoptosis (results not shown), is inhibited in MEKK1$^{-/-}$ embryonic stem cells. However, until we can find methods to completely block apoptosis or JNK activity, we cannot rule out the possibility of a common pathway.

Reovirus-induced JNK activation is a specific event. For example, p38 MAPK is not activated following reovirus infection. In addition, although ERK is activated in a serotype-specific manner in infected cells, our inability to map this activation to a specific reovirus gene segment indicates that ERK is activated by a different mechanism from that used for JNK activation. The kinetics of ERK and JNK activation also differ, with ERK showing an early phase of activation that is not seen with JNK, again suggesting that ERK and JNK are activated by different mechanisms. The specificity of reovirus-induced JNK activation suggests that it is important for some aspect of the reovirus life cycle. The role of virus-induced JNK activation is not yet known; however, reovirus growth is not inhibited in MEKK1$^{-/-}$ cells (results not shown) despite a marked reduction in reovirus-induced JNK activation (62). This suggests that JNK activation is not essential for viral replication. Reovirus-induced JNK activation is associated with activation of the JNK-dependent transcription factor c-Jun. We have previously shown (12) that reovirus infection is also associated with activation of the transcription factor NF-κB, suggesting that virus-induced perturbation of gene expression plays a critical role in viral pathogenesis and cytopathicity. This is confirmed by our recent studies showing that reovirus infection is associated with alterations in the expression of a number of host cell genes involved in the regulation of cell cycle, apoptosis, and DNA repair (R. DeBiasi, personal communication). In addition, one of the largest functional groups of genes whose expression is altered following reovirus infection is the group associated with interferon activation, consistent with the known role of c-Jun in the optimal induction of alpha-1 and beta interferon transcription (9) and onset of the antiviral response (55).

ACKNOWLEDGMENTS

This work was supported by Public Health Service grants 1RO1AG14071 and GM30324 from the National Institutes of Health, merit and REAP grants from the Department of Veterans Affairs, and a U.S. Army Medical Research and Material Command grant (DAMD17-98-1-8614).

The University of Colorado Cancer Center provided core tissue culture and medium facilities.

REFERENCES

1. **Ashkenazi, A., and V. M. Dixit.** 1998. Death receptors: signaling and modulation. Science **281**:1305–1308.
2. **Barton, E. S., J. C. Forrest, J. L. Connolly, J. D. Chappell, Y. Liu, F. J. Schnell, A. Nusrat, C. A. Parkos, and T. S. Dermody.** 2001. Junction Adhesion Molecule is a receptor for reovirus. Cell **104**:441–451.
3. **Berra, E., M. M. Municio, L. Sanz, S. Frutos, M. T. Diaz-Meco, and J. Moscat.** 1997. Positioning atypical protein kinase C isoforms in the UV-induced apoptotic signaling cascade. Mol. Cell. Biol. **17**:4346–4354.
4. **Boldin, M. P., T. M. Goncharov, Y. V. Goltsev, and D. Wallach.** 1996. Involvement of MACH, a novel MORT1/FADD-interacting protease, in Fas/APO-1- and TNF receptor-induced cell death. Cell **85**:803–815.
5. **Boldin, M. P., E. E. Varfolomeev, Z. Pancer, I. L. Mett, J. H. Camonis, and D. Wallach.** 1995. A novel protein that interacts with the death domain of Fas/APO1 contains a sequence motif related to the death domain. J. Biol. Chem. **270**:7795–7798.
6. **Brown, E. G., M. L. Nibert, and B. N. Fields.** 1983. The L2 gene of reovirus serotype 3 controls the capacity to interfere, accumulate deletions and establish persistent infection, p. 275–287. *In* R. W. Compans and D. H. L. Bishop (ed.), Double-stranded RNA-viruses. Elsevier, New York, N.Y.
7. **Canman, C. E., and M. B. Kastan.** 1996. Signal transduction. Three paths to stress relief. Nature **384**:213–214.
8. **Chinnaiyan, A. M., K. O'Rourke, M. Tewari, and V. M. Dixit.** 1995. FADD, a novel death domain containing protein, interacts with the death domain of Fas and initiates apoptosis. Cell **81**:505–512.
9. **Chu, W.-M., D. Ostertag, Z-W. Li, L. Chang, Y. Chen, Y. Hu, B. Williams, J. Perrault, and M. Karin.** 1999. JNK2 and IKKβ are required for activating the inate response to viral infection. Immunity **11**:721–731.
10. **Clarke, P., S. M. Meintzer, S. Gibson, C. Widmann, T. Garrington, G. L. Johnson, and K. L. Tyler.** 2000. Reovirus-induced apoptosis is mediated by TRAIL. J. Virol. **74**:8135–8139.
11. **Cobb, M. H., T. G. Boulton, and D. J. Robbins.** 1991. Extracellular signal-related kinases: ERKs in progress. Cell Regul. **2**:965–978.
12. **Connolly, J. L., S. E. Rodgers, P. Clarke, D. W. Ballard, L. D. Kerr, K. L. Tyler, and T. S. Dermody.** 2000. Reovirus-induced apoptosis requires activation of transcription factor NF-κB. J. Virol. **74**:2981–2989.
13. **Coombs, K. M., B. N. Fields, and S. C. Harrison.** 1990. Crystallization of the reovirus type 3 Dearing core. Crystal packing is determined by the lambda 2 protein. J. Mol. Biol. **215**:1–5.
14. **DeBiasi, R. L., C. L. Edelstein, B. Sherry, and K. L. Tyler.** 2001. Calpain inhibition protects against virus-induced apoptotic myocardial injury. J. Virol. **75**:351–361.
15. **DeBiasi, R. L., M. K. T. Squier, B. Pike, M. Wynes, T. S. Dermody, J. J. Cohen, and K. L. Tyler.** 1999. Reovirus-induced apoptosis is preceded by increased cellular calpain activity and is blocked by calpain inhibitors. J. Virol. **73**:695–701.
16. **Derijard, B., M. Hibi, I. H. Wu, T. Barrett, B. Su, T. Deng, M. Karin, and R. J. Davis.** 1994. JNK1: a protein kinase stimulated by UV light and Ha-Ras that binds and phosphorylates the c-Jun activation domain. Cell **76**:1025–1037.
17. **Duan, H., and V. M. Dixit.** 1997. RAIDD is a new death adaptor molecule. Nature **385**:86–89.
18. **Duke, R. C., and J. J. Cohen.** 1992. Morphological and biochemical assays of apoptosis, p. 3.17.1–3.17.6. *In* J. E. Coligan, (ed), Current protocols in immunology, John Wiley & Sons, Inc., New York, N.Y.
19. **Eliopoulos, A. G., and L. S. Young.** 1988. Activation of c-Jun N-terminal kinase (JNK) by the Epstein-Barr virus-encoded latent membrane protein 1 (LMP-1). Oncogene **16**:1731–1742.
20. **Gardner, A. M., and G. L. Johnson.** 1996. Fibroblast growth factor 2 suppression of tumor nerosis factor alpha-mediated apoptosis requires Ras and the activation of mitogen-activated protein kinase. J. Biol. Chem. **271**:14560–14566.
21. **Gerwins, P., J. L. Blank, and G. L. Johnson.** 1997. Cloning of a novel mitogen-activated protein kinase kinase kinase, MEKK4, that selectively regulates the c-Jun amino terminal kinase pathway. J. Biol. Chem. **272**:8288–8295.
22. **Graves, J. D., J. S. Campbell, and E. G. Krebs.** 1995. Protein serine/threonine kinases of the MAPK cascade. Ann. N. Y. Acad. Sci. **766**:320–343.
23. **Han, J., J. D. Lee, L. Bibbs, and R. J. Ulevitch.** 1994. A MAP kinase targeted by endotoxin and hyperosmolarity in mammalian cells. Science **265**:808–811.
24. **Hazelton, P. R., and K. M. Coombs.** 1995. The reovirus mutant tsA279 has temperature sensitive lesions in the M2 and L2 genes: the M2 gene is associated with decreased viral protein production and blockade in transmembrane transport. Virology **207**:46–58.
25. **Hibi, M., A. Lin, T. Smeal, A. Minden, and M. Karin.** 1993. Identification of an oncoprotein- and UV-responsive protein kinase that binds and potentiates the c-Jun activation domain. Genes Dev. **7**:2135–2148.
26. **Hooper, J. W., and B. N. Fields.** 1996. Role of the μ1 protein in reovirus stability and capacity to cause chromium release from host cells. J. Virol. **70**:459–467.
27. **Hsu, H., J. N. Huang, H. B. Shu, V. Baichwal, and D. V. Goeddel.** 1996. TNF-dependent recruitment of the protein kinase RIP to the TNF receptor-1 signaling complex. Immunity **4**:387–396.
28. **Hsu, H., H. B. Shu, M. G. Pan, and D. V. Goeddel.** 1996. TRADD-TRAF2 and TRADD-FADD interactions define two distinct TNF receptor 1 signal

transduction pathways. Cell **84**:299–308.
29. **Hsu, H., J. Xiong, and D. V. Goeddel.** 1995. The TNF receptor 1-associated protein TRADD signals cell death and NF-kappa B activation. Cell **81**:495–504.
30. **Hu, W. H., H. Johnson, and H. B. Shu.** 1999. Tumor necrosis factor-related apoptosis-inducing ligand receptors signals NF-kappaB and JNK activation and apoptosis through distinct pathways. J. Biol. Chem. **274**:30603–30610.
31. **Huttunen, P., T. Hyypia, P. Vihinen, L. Nissinen, and J. Heino.** 1998. Echovirus 1 infection induces both the stress- and growth-activated mitogen-activated protein kinase pathways and regulates the transcription of cellular immediate-early genes. Virology **250**:85–93.
32. **Iordanov, M. S., J. M. Paranjape, A. Zhou, J. Wong, B. R. G. Williams, E. F. Meurs, R. H. Silverman, and B. E. Magun.** 2000. Activation of p38 mitogen-activated protein kinase and c-Jun NH_2-terminal kinase by double-stranded RNA and encephalomyocarditis virus: involvement of RNase L, protein kinase R and alternative pathways. Mol. Cell. Biol. **20**:617–627.
33. **Iwai, K., N. Mori, M. Oie, N. Yamamoto, and M. Fujii.** 2001. Human T-cell leukemia virus type 1 Tax protein activates transcription through AP-1 site by inducing DNA binding activity in T cells. Virology **279**:38–46.
34. **Jacque, J. M., A. Mann, H. Enslen, N. Sharuva, B. Brichacek, R. J. Davis, and M. Stevenson.** 1998. Modulation of HIV-1 infectivity by MAPK, a virion associated kinase. EMBO J. **17**:2607–2618.
35. **Jeremias, I., and K. M. Debatin.** 1998. TRAIL induces apoptosis and activation of NFkappaB. Eur. Cytokine Netw. **9**:687–688.
36. **Jung, J. U., and R. C. Desrosiers.** 1995. Association of viral oncoprotein, STP-C488, with cellular ras. Mol. Cell. Biol. **15**:6506–6512.
37. **Juo, P., C. J. Kuo, S. E. Reynold, R. F. Konz, J. Raingeaud, R. J. Davis, H.-P. Biemann, and J. Blenis.** 1997. Fas activation of the p38 mitogen-activated protein kinase signaling pathway requires ICE/CED-3 family proteases. Mol. Cell. Biol. **17**:24–35.
38. **King, C. S., J. V. Cooper, B. Moss, and D. R. Twardzik.** 1986. Vaccinia virus growth factor stimulates tyrosine protein kinase activity of A431 cell epidermal growth factor receptors. Mol. Cell. Biol. **6**:332–336.
39. **Kyriakis, J. M., P. Banerjee, E. Nikolakaki, T. Dai, E. A. Rubie, M. F. Ahmad, J. Avruch, and J. R. Woodgett.** 1994. The stress-activated protein kinase subfamily of c-Jun kinases. Nature (London) **369**:156–160.
40. **Lee, J. C., J. T. Laydon, P. C. McDonnell, T. F. Gallagher, S. Kumar, D. Green, D., McNulty, M. J. Blumenthal, J. R. Heys, S. W. Landvatter, J. E. Strickler, M. M. McLaughlin, I. R. Siemens, S. M. Fisher, G. P. Livi, J. R. White, J. L. Adams, and P. R. Young.** 1994. A protein kinase involved in the regulation of inflammatory cytokine biosynthesis. Nature (London) **372**:739–746.
41. **Lucia-Jandris, P., J. W. Hooper, and B. W. Fields.** 1993. Reovirus M2 gene is associated with chromatin release from mouse L cells. J. Virol. **67**:5339–5345.
42. **Ludwig, S., C. Ehrhardt, E. R. Neumeier, M. Kracht, U. R. Rapp, and S. Pleschka.** 2001. Influenza virus-induced AP-1 dependent gene expression requires activation of the Jun-N-terminal kinase (JNK) signaling pathway. J. Biol. Chem. **276**:10990–10998.
43. **Martin, P., W. C. Vass, J. T. Schiller, D. R. Lowry, and T. J. Velu.** 1989. The bovine papilloma virus E5 transforming protein can stimulate the transforming activity of EGF and CSF-1 receptors. Cell **59**:21–32.
44. **McLean, T. I., and S. L. Bachenheimer.** 1999. Activation of cJun N-terminal kinase by herpes simplex virus type 1 enhances viral replication. J. Virol. **73**:8415–8426.
45. **Muzio, M., A. M. Chinnaiyan, F. C. Kischkel, K. O'Rourke, A. Shevchenko, J. Ni, C. Scaffidi, J. D. Bretz, M. Zhang, R. Gentz, M. Mann, P. H. Krammer, M. E. Peter, and V. M. Dixit.** 1996. FLICE, a novel FADD-homologous ICE/CED-3-like protease, is recruited to the CD95 (Fas/APO-1) death-inducing signaling complex. Cell **85**:817–827.
46. **Oberhaus, S. M., T. S. Dermody, and K. L. Tyler.** 1998. Apoptosis and the cytopathic effects of reovirus. Curr. Top. Microbiol. Immunol. **233**:23–49.
47. **Oberhaus, S. M., R. L. Smith, G. H. Clayton, T. S. Dermody, and K. L. Tyler.** 1997. Reovirus infection and tissue injury in mouse central nervous system are associated with apoptosis. J. Virol. **71**:2100–2106.
48. **Poggioli, G. J., C. Keefer, J. L. Connolly, T. S. Dermody, and K. L. Tyler.** 2000. Reovirus-induced G_2/M cell cycle arrest requires σ1s and occurs in the absence of apoptosis. J. Virol. **74**:9562–9570.
49. **Popik, W., and P. M. Pitha.** 1998. Early activation of mitogen-activated protein kinase kinase, extracellular signal-regulated kinase, p38 mitogen-activated protein kinase, and c-Jun N-terminal kinase in response to binding of simian immunodeficiency virus to Jurkat TT cells expressing CCR5 receptor. Virology **252**:210–217.
50. **Rodgers, S. E., E. S. Barton, S. M. Oberhaus, B. Pike, C. A. Gibson, K. L. Tyler, and T. S. Dermody.** 1997. Reovirus-induced apoptosis of MDCK cells is not linked to viral yield and is blocked by Bcl-2. J. Virol. **71**:2540–2546.
51. **Rodgers, S. E., J. L. Connolly, J. D. Chappell, and T. S. Dermody.** 1998. Reovirus growth in cell culture does not require a full complement of viral proteins: identification of a σ1s-null mutant. J. Virol. **72**:8597–8604.
52. **Rothe, M., V. Sarma, V. M. Dixit, and D. V. Goeddel.** 1995. TRAF2-mediated activation of NF-kappa B by TNF receptor 2 and CD40. Science **269**:1424–1427.
53. **Rouse, J., P. Cohen, S. Trigon, M. Morange, A. Alonso Llamazares, D. Zamanillo, T. Hunt, and A. R. Nebreda.** 1994. A novel kinase cascade triggered by stress and heat shock that stimulates MAPKAP kinase-2 and phosphorylation of the small heat shock proteins. Cell **78**:1027–1037.
54. **See, B. H., and Y. Shi.** 1998. Adenovirus E1B 19,000-molecular weight protein activates c-Jun N-terminal kinase and c-Jun-mediated transcription. Mol. Cell. Biol. **18**:4012–4022.
55. **Sen, G. C., and P. Lengyel.** 1992. The interferon system. A birds eye view of its biochemistry. J. Biol. Chem. **267**:5017–5020.
56. **Song, H. Y., C. H. Regnier, C. J. Kirschning, D. V. Goeddel, and M. Rothe.** 1997. Tumor necrosis factor (TNF)-mediated kinase cascades: bifurcation of nuclear factor-kappa B and c-jun N-terminal kinase (JNK/SAPK) pathways at TNF receptor-associated factor. Proc. Natl. Acad. Sci. USA **94**:9792–9796.
57. **Sontag, E., S. Fedorov, C. Kamibayashi, D. Robbins, M. Cobb, and M. Mumby.** 1993. The interaction of SV40 small tumor antigen with protein phosphatase 2A stimulates the MAP kinase pathway and induces cell proliferation. Cell **75**:887–897.
58. **Tyler, K. L., M. K. T. Squier, S. E. Rodgers, B. E. Schneider, S. M. Oberhaus, T. A. Grdina, J. J. Cohen, and T. S. Dermody.** 1995. Differences in the capacity of reovirus strains to induce apoptosis are determined by the viral attachment protein sigma 1. J. Virol. **69**:6972–6979.
59. **Tyler K. L., M. K. T. Squier, A. L. Brown, B. Pike, D. Willis, S. M. Oberhaus, T. S. Dermody, and J. J. Cohen.** 1996. Linkage between reovirus-induced apoptosis and inhibition of cellular DNA synthesis: role of the S1 and M2 genes. J. Virol. **70**:7984–7991.
60. **Wilson, D. J., K. A. Fortner, D. H. Lynch, R. R. Mattingly, I. G. Macara, J. A. Posada, and R. C. Budd.** 1996. JNK, but not MAPK, activation is associated with Fas-mediated apoptosis in human T cells. Eur. J. Immunol. **26**:989–999.
61. **Xia, Z., M. Dickens, J. Raingeaud, R. J., Davis, and M. E. Greenberg.** 1995. Opposing effects of ERK and JNK-p38 MAP kinases on apoptosis. Science **270**:1326–1331.
62. **Yujuri, T., M. Ware, C. Widmann, R. Oyer, D. Russell, E. Chan, Y. Zaitsu, P. Clarke, K. L. Tyler, Y. Oka, G. R. Fanger, P. Henson, and G. L. Johnson.** 2000. Cell migration and c-jun NH2-terminal kinase but not NF-κB are regulated by MEK kinase 1. Proc. Natl. Acad. Sci. USA **97**:7272–7277.
63. **Zachos, G., B. Clements, and J. Conner.** 1999. Herpes simplex virus type 1 infection stimulates p38/c-Jun N-terminal mitogen-activated protein kinase pathways and activates transcription factor AP-1. J. Biol. Chem. **274**:5097–5103.

Oncogene (2001) 20, 6910–6919

www.nature.com/onc

Caspase 8-dependent sensitization of cancer cells to TRAIL-induced apoptosis following reovirus-infection

Penny Clarke[1], Suzanne M Meintzer[1], Aaron C Spalding[2], Gary L Johnson[2] and Kenneth L Tyler*[,1,3,4]

[1]*Department of Neurology, University of Colorado Health Sciences, Denver, Colorado, CO 80262, USA;* [2]*Department of Pharmacology, University of Colorado Health Sciences, Denver, Colorado, CO 80262, USA;* [3]*Department of Medicine, Microbiology and Immunology, University of Colorado Health Sciences, Denver, Colorado, CO 80262, USA;* [4]*Denver Veteran's Affairs Medical Center, Denver, Colorado, CO 80220, USA*

TRAIL (TNF-related apoptosis-inducing ligand) induces apoptosis in susceptible cells by binding to death receptors 4 (DR4) and 5 (DR5). TRAIL preferentially induces apoptosis in transformed cells and the identification of mechanisms by which TRAIL-induced apoptosis can be enhanced may lead to novel cancer chemotherapeutic strategies. Here we show that reovirus infection induces apoptosis in cancer cell lines derived from human breast, lung and cervical cancers. Reovirus-induced apoptosis is mediated by TRAIL and is associated with the release of TRAIL from infected cells. Reovirus infection synergistically and specifically sensitizes cancer cell lines to killing by exogenous TRAIL. This sensitization both enhances the susceptibility of previously resistant cell lines to TRAIL-induced apoptosis and reduces the amount of TRAIL needed to kill already sensitive lines. Sensitization is not associated with a detectable change in the expression of TRAIL receptors in reovirus-infected cells. Sensitization is associated with an increase in the activity of the death receptor-associated initiator caspase, caspase 8, and is inhibited by the peptide IETD-fmk, suggesting that reovirus sensitizes cancer cells to TRAIL-induced apoptosis in a caspase 8-dependent manner. Reovirus-induced sensitization of cells to TRAIL is also associated with increased cleavage of PARP, a substrate of the effector caspases 3 and 7. *Oncogene* (2001) **20,** 6910–6919.

Keywords: apoptosis; TRAIL; reovirus; caspase 8; chemotherapy

Introduction

TNF-related apoptosis-inducing ligand (TRAIL, also called Apo2L) belongs to a family of structurally related molecules, which also includes TNF, Fas ligand (FasL), and APO3 ligand. These ligands are expressed as type II membrane proteins that are cleaved into soluble, active forms and which bind to members of the TNF receptor super-family. Ligand-mediated receptor activation triggers a cascade of events that begins with death receptor (DR) oligomerization and the close association of their cytoplasmic death domains (DDs). This is followed by DD-associated interaction with adapter molecules and cellular proteases critical to DR-induced apoptosis, including the initiator caspase, caspase 8 and its associated effector caspases, caspases 3 and 7 (reviewed in Ashkenazi and Dixit, 1998). In addition to activating caspase 8, TRAIL-induced apoptosis is also associated with the cleavage of Bid and the loss of mitochondrial potential (Belka *et al.*, 2001). TRAIL induces apoptosis by binding to the TNF receptor super-family members DR4 (also called TRAIL-R1) and DR5 (also called Apo2, TRAIL-R2, TRACK2 or KILLER). TRAIL can also bind to the receptors DcR-1 (for Decoy Receptor 1) and DcR-2 that do not transmit apoptotic signals and can prevent the induction of apoptosis in TRAIL-treated cells.

Many cancer chemotherapeutic drugs in clinical use induce apoptosis in sensitive cells suggesting that death-receptor ligands might prove useful as cancer therapeutic agents. Unfortunately, the apoptosis-inducing ligands FasL and TNF are also toxic to non-transformed cells (Nagata, 1997). TRAIL induces apoptosis in a variety of transformed cells (Wiley *et al.*, 1995; Pitti *et al.*, 1996), including cells derived from lung, breast, colon, kidney, brain and skin cancers (Ashkenazi *et al.*, 1999) and is effective at reducing mammary adenocarcinoma growth in mice (Walczak *et al.*, 1999). Although normal cultured hepatocytes do show some sensitivity to TRAIL-induced killing (Jo *et al.*, 2000), this toxicity can be overcome by simultaneous exposure to the caspase inhibitor, Z-LEHD-fmk (Ozoren *et al.*, 2000).

TRAIL kills cancer cells derived from a variety of human cancers of diverse type. However, cancer cells of all types appear to differ in their sensitivity to TRAIL-induced apoptosis (Keane *et al.*, 1999; Zhang *et al.*, 1999). Understanding the basis of TRAIL sensitivity is thus crucial in designing TRAIL-based cancer therapeutic strategies. TRAIL induced apopto-

*Correspondence: KL Tyler, Department of Neurology (B 182), University of Colorado Health Sciences Center, 4200 East 9th Avenue, Denver, Colorado 80262, USA; E-mail: Ken.Tyler@uchsc.edu
Received 2 June 2001; revised 16 July 2001; accepted 16 July 2001

sis is dependent, in part, on the surface expression of its receptors (Zhang *et al.*, 1999) and agents which increase the cell surface expression of DR4 and DR5 enhance TRAIL-induced killing in some epithelial-derived tumor cells (Gibson *et al.*, 2000). Alteration in receptor expression, however, does not fully explain TRAIL sensitivity (Keane *et al.*, 1999; Zhang *et al.*, 1999; Cuello *et al.*, 2001).

Reovirus infection induces apoptosis in cultured cells *in vitro* (Tyler *et al.*, 1985, 1995, 1996). Apoptosis occurs through a p53-independent mechanism that involves cellular proteases including caspases and calpains (DeBiasi *et al.*, 1999). Reovirus-induced apoptosis in HEK293 cells is mediated by TRAIL and is inhibited by anti-TRAIL antibodies or by soluble forms of DR4 and DR5 (Clarke *et al.*, 2000). Reovirus infection results in the release of TRAIL from infected HEK293 cells and reovirus sensitizes these cells to TRAIL-induced killing (Clarke *et al.*, 2000). In neonatal mice, reovirus also induces apoptosis in infected tissues *in vivo* (Oberhaus *et al.*, 1997, 1998; DeBiasi *et al.*, 2001). However, reovirus infection is not associated with significant disease in adult mice or in humans. Reovirus infection may therefore provide a useful model system for investigations of TRAIL-induced apoptosis in cancer cells. A better understanding of how reovirus infection sensitizes cancer cells to TRAIL-induced cell death may suggest novel mechanisms for increasing the efficacy of TRAIL as a cancer therapeutic agent.

Reovirus has previously been shown to induce killing of human glioblastoma cells *in vitro* as well as inducing regression of transplanted tumors in mice, although the mechanism for reovirus-induced 'oncolysis' has not been fully identified (Coffey *et al.*, 1998; Strong *et al.*, 1998). We now show that reovirus kills cancer cells by apoptosis and that this apoptosis is both mediated by TRAIL and is associated with the release of TRAIL from infected cells. We further show that reovirus specifically sensitizes cancer cell lines to TRAIL-induced apoptosis and that this sensitization requires the activation of caspase 8 and is associated with increased activity of effector caspases.

Results

Reovirus and TRAIL induce similar amounts of apoptosis in human cancer cells

It has been reported that reovirus can infect and kill cancer cells (Coffey *et al.*, 1998; Strong *et al.*, 1998). Our previous work in tissue culture has shown that reovirus-induced killing of many types of non-cancerous cells (Tyler *et al.*, 1985, 1995, 1996) and of cells derived from a human cervical carcinoma (HeLa cells) is due to apoptosis. We therefore wished to determine whether reovirus induced killing of other cancer cell lines was due to apoptosis. Cell lines derived from two different human lung (A157 and H549) and breast cancers (MDA231 and ZR75-1) were infected with reovirus (multiplicity of infection, MOI 100) and were harvested and assayed for apoptosis at 48 h post infection. We first assayed apoptosis by determination of the percentage of cells with apoptotic nuclear morphology (Figure 1A). The specificity of this assay for the detection of apoptotic nuclear morphology in reovirus-infected cells has been previously established by our laboratory using DNA laddering techniques and electron microscopy (Tyler *et al.*, 1995). HeLa cells, which have previously been shown to be susceptible to both reovirus-infection and reovirus-induced apoptosis (Connolly *et al.*, 2000), were used as positive controls. Reovirus induced significant ($P<0.05$) apoptosis in all of the cancer cell lines tested, but with different degrees of efficiency. HeLa, A549 and MDA231 cells were the

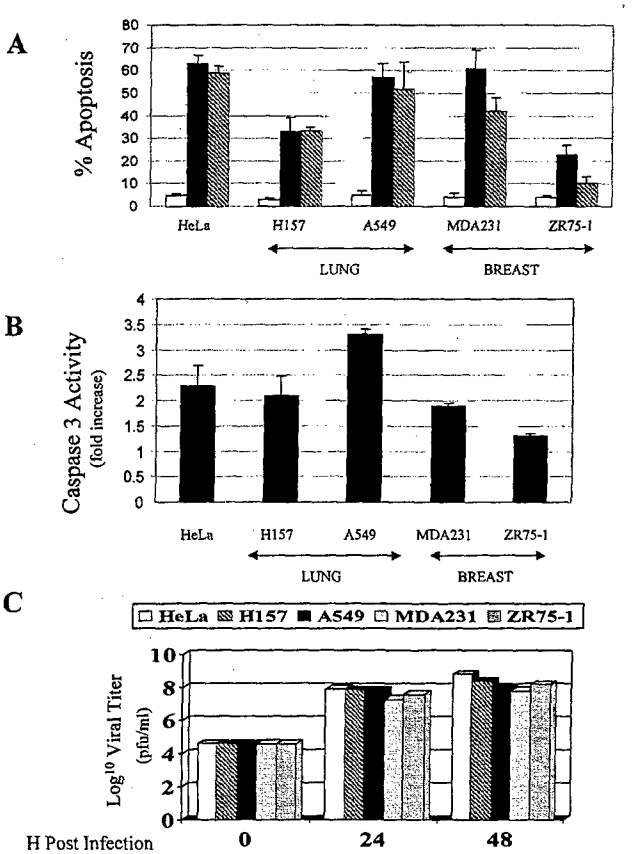

Figure 1 Reovirus induces apoptosis in human tumor cell lines. (**A**) Cell lines derived from human cervical (HeLa), lung (H157 and A549) and breast (MDA231 and ZR75-1) cancers were infected with reovirus (MOI 100) and were harvested and assayed for apoptosis at 48 h post infection. In a parallel experiment cells were treated with TRAIL (200 ng/ml). The graph shows the mean per cent apoptosis in reovirus (black bars), mock-infected (clear bars) and TRAIL-treated (shaded bars) cancer cells from at least three separate experiments. Error bars represent standard errors of the mean. (**B**) Caspase 3 activation in reovirus (MOI 100) compared to mock-infected cancer cell lines, at 24 h post infection, as determined by fluorogenic substrate assay. The graph shows the mean fold-increase in fluorescence from at least three separate experiments. Error bars represent standard errors of the mean. (**C**) One step growth curves of reovirus in human cancer cell lines used. Cells were infected with reovirus and were harvested and assayed for growth at 24 and 48 h post infection. The graph shows Log_{10} virus yield over time

most susceptible to reovirus-induced apoptosis whereas H157 and ZR75-1 cells showed the least susceptibility. These differences were not caused by differences in viral growth since one-step growth curves indicated that reovirus grows efficiently and equivalently in all the cell lines (Figure 1C).

The sensitivity of cells to reovirus-induced apoptosis was compared to their sensitivity to TRAIL-induced apoptosis. Cells were treated with 200 ng/ml TRAIL and assayed for apoptosis after 24 h. All but one (ZR75-1) of the cell lines tested demonstrated significant sensitivity ($P<0.05$) to TRAIL induced apoptosis (Figure 1A). A significant correlation was shown between the sensitivity of these cancer lines to reovirus-induced and TRAIL-induced apoptosis (Pearson linear correlation test: correlation coefficient (R) = 0.9154, coefficient of determination (R sq.) = 0.8380, P value (2-tailed) 0.0291).

To confirm that reovirus-induced killing of cancer cells was due to apoptosis we investigated the activity of the apoptosis-specific effector caspase, caspase 3, in reovirus-infected cells. Reovirus infection induced a twofold or more activation of caspase 3 in all of the cell lines tested except for ZR75-1 cells. The smaller increase in caspase 3-activation (1.3-fold), seen in ZR75-1 cells corresponds to the low level of apoptosis induced in these cells following reovirus infection (Figure 1B).

Reovirus induced apoptosis is mediated by TRAIL

Reovirus induced apoptosis of HEK293 and L929 cells requires the binding of TRAIL to the apoptosis-inducing cell surface receptors DR4 and DR5 (Clarke *et al.*, 2000). Soluble TRAIL receptors (Fc:DR4 and Fc:DR5), but not soluble TNF receptor (Fc:TNFR), specifically inhibit TRAIL-induced apoptosis by binding TRAIL and preventing its interaction with functional cell surface DR4 and DR5 (Clarke *et al.*, 2000). We wished to determine whether reovirus-induced apoptosis of cancer cell lines was also mediated by TRAIL. Human lung, breast and cervical cancer cell lines were infected with reovirus (MOI 50), in the presence or absence of soluble TRAIL receptor (Fc:DR5) or a soluble control receptor (Fc:TNFR), and assayed for apoptosis 48 h following infection with reovirus. Reovirus-induced apoptosis in all of the cancer cell lines, except ZR75-1, was significantly inhibited ($P<0.05$), by treatment with Fc:DR5, but not by Fc:TNFR, indicating that apoptosis in these cells is mediated by TRAIL (Figure 2A). In the case of ZR75-1 cells, the low basal level of reovirus-induced apoptosis may have precluded the determination of a significant level of inhibition.

To further demonstrate the involvement of TRAIL in reovirus-induced apoptosis we next showed that reovirus-induced apoptosis could be inhibited in a cell line that stably over-expresses the anti-apoptotic TRAIL receptor, DcR-1. MDA-231 cells were transfected with a vector expressing DcR-1 and enhanced cell surface expression of DcR-1 was determined by flow cytometry (data not shown). These cells were then infected with reovirus (MOI 100) and assayed for apoptosis after 48 h (Figure 2B). Over-expression of DcR-1 significantly ($P<0.01$) inhibited reovirus-induced apoptosis in MDA-231 cells, when compared to MDA-231 control cells transfected with empty vector, again indicating that TRAIL plays a key role in reovirus-induced apoptosis.

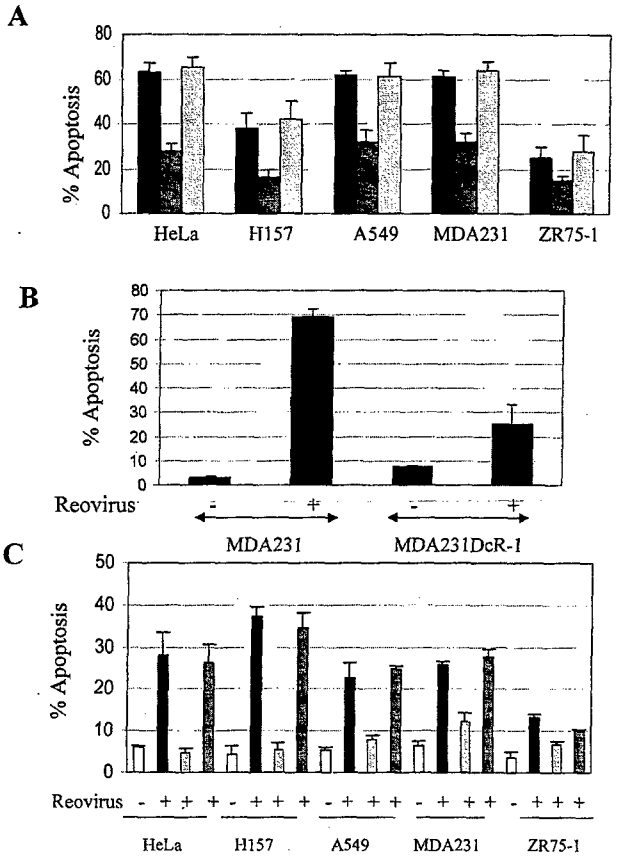

Figure 2 Reovirus induced apoptosis of cancer cells is inhibited by soluble TRAIL receptor (Fc:DR5) or the over-expression of DcR-1 and is associated with the release of TRAIL from infected cells. (**A**) Human cancer cell lines were infected with reovirus (MOI 50), in the absence (black bars) or presence of soluble TRAIL receptor (Fc:DR5, shaded bars) or a soluble control receptor (Fc:TNFR, grey bars) and were assayed for apoptosis 48 h following infection with reovirus. (**B**) MDA231 cells over-expressing DcR-1 (MDA231DcR-1) and MDA231 cells expressing vector control were infected with reovirus. Forty-eight hours following infection cells were harvested and assayed for the presence of apoptotic nuclear morphology. (**C**) Twenty-four hours following infection of cells with reovirus (MOI 100) the supernatant was collected and transferred onto a TRAIL-sensitive indicator cell line (HeLa). After a further 24 h the indicator cells were assayed for apoptosis. Empty bars represent supernatants from mock infected cells, black bars represent supernatants from reovirus infected cells, grey bars represent supernatants from reovirus infected cells that were treated with Fc:DR5 to determine that the apoptosis seen in the indicator cell line was TRAIL-specific and shaded bars represent supernatants from reovirus infected cells that were treated with anti-reovirus antibody to ensure that apoptosis in the indicator cell line was not due to any reovirus present in the transferred supernatant. The graphs (**A**, **B** and **C**) show per cent apoptosis from three separate experiments. Error bars represent standard errors of the mean

TRAIL is released from reovirus infected cancer cells

TRAIL is normally expressed as a type II membrane protein that is cleaved into a soluble form. We have previously shown that TRAIL is released from reovirus-infected HEK293 cells (Clarke *et al.*, 2000). We next investigated whether TRAIL was released from reovirus-infected cancer cells into the supernatant. Twenty-four hours following infection of cancer cells with reovirus the supernatant was collected and transferred onto a TRAIL-sensitive indicator cell line (HeLa). After a further 24 h the indicator cells were assayed for apoptosis. Significant apoptosis ($P<0.05$) was induced in the indicator cell line following treatment with supernatant collected from reovirus-infected, but not from mock-infected Hela, H157, A549 and MDA231 cells (Figure 2C). This apoptosis was blocked by soluble DR5 (Fc:DR5) indicating that the apoptosis seen in the indicator cells following supernatant transfer from reovirus-infected cancer cells was specific to TRAIL. Supernatant from reovirus-infected ZR75-1 cells did not induce significant apoptosis in the indicator cell line. A neutralizing polyclonal anti-reovirus antisera, that we have previously shown inhibits virus attachment, neutralizes infectivity and blocks apoptosis induced by infectious virus (Tyler *et al.*, 1996), did not block apoptosis induced in the indicator cells by supernatant transfer from reovirus-infected cancer cells. This antibody did inhibit viral growth and virus-induced apoptosis in reovirus-infected cancer cells (data not shown) indicating that the apoptotic effects of infected cancer cell supernatants are not due to the presence of infectious virus.

Reovirus synergistically augments TRAIL-mediated apoptosis in infected cancer cells

Reovirus infection sensitizes HEK293 cells to TRAIL-induced apoptosis. We next wished to determine whether reovirus infection also sensitized cancer cells to TRAIL-induced apoptosis, and if so, whether this sensitization was specific for TRAIL-induced apoptosis or whether it also occurred with other death-receptor associated ligands. ZR75-1 and H157 cells, which were the cancer cell lines that showed the least susceptibility to TRAIL (200 ng/ml)-induced apoptosis (Figure 1A), were infected with reovirus (MOI 10). After 24 h infected cells were treated with a low dose of TRAIL (20 ng/ml) and apoptosis assays were performed after a further 24 h. In H157 and ZR75-1 cells neither low doses of TRAIL (20 ng/ml) or reovirus (MOI 10) alone induce significant apoptosis compared to untreated cells (Figure 3A). However, when cells were infected with reovirus and were then treated with TRAIL the number of apoptotic cells was significantly increased ($P<0.05$) when compared to uninfected cells, or to cells treated with either TRAIL or reovirus alone. The increase in apoptosis induced by a combination of reovirus-infection and TRAIL treatment was synergistic rather than additive, compared to that seen with either agent alone, and the amount of apoptosis seen with TRAIL and reovirus together was significantly different from the sum of reo- and TRAIL-induced apoptosis when each was administered separately. To confirm that cell death resulting from a combination of reovirus-infection and TRAIL treatment was due to apoptosis we also showed that a combination of reovirus and TRAIL, but not the same doses of reovirus or TRAIL alone, produced oligosomal DNA fragmentation, also known as 'DNA laddering' (Figure 3B).

Reovirus infection also significantly ($P<0.05$) augmented apoptosis induced in ZR75-1 and H157 cells by an activating Fas antibody (0.025 μg/ml) compared to cells treated with either the antibody or reovirus alone (Figure 3C). This augmentation was additive rather

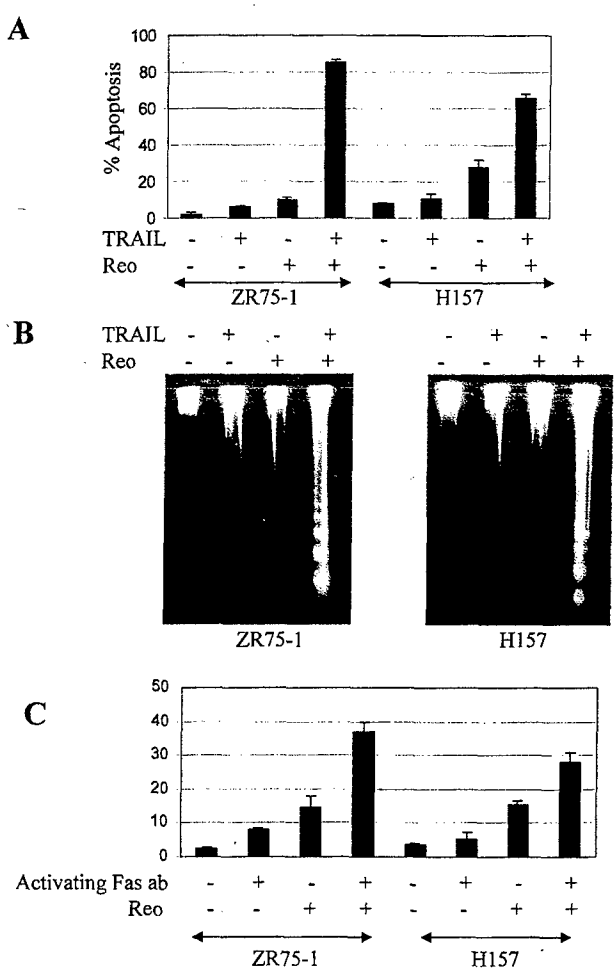

Figure 3 Reovirus infection synergistically sensitizes cancer cells to TRAIL-induced apoptosis but not to an activating Fas antibody. (**A**) H157 and ZR75-1 cells were either mock-infected or infected with reovirus (MOI 10). After 24 h cells were treated with TRAIL (20 ng/ml), an activating Fas antibody (0.025 μg/ml), or were left untreated. The graphs (**A** and **C**) show the mean per cent of apoptotic nuclei in cells from three separate experiments (error bars represent standard errors of the mean) in reovirus-infected TRAIL/Fas antibody treated cells. The gels (**B**) show the presence of fragmented DNA in the reovirus-infected, TRAIL-treated cells

than synergistic and the amount of apoptosis seen with a combination of antibody and reovirus was not significantly different from the sum of reo- and antibody-induced apoptosis when each was administered separately. This indicates that the synergistic sensitization of reovirus-infected cells to TRAIL is a specific event.

Reovirus does not augment doxorubicin-induced apoptosis

Doxorubicin is a cancer therapeutic agent that augments TRAIL induced apoptosis. Doxorubicin induces apoptosis in treated cells, as demonstrated by caspase 3 activation (Keane *et al.*, 1999) but this apoptosis does not occur through cellular death receptors. We wondered whether reovirus infection might enhance doxorubicin-induced, as well as TRAIL-induced, apoptosis. ZR75-1 cells, which are sensitized to TRAIL-induced apoptosis following reovirus infection, were treated with different concentrations of doxorubicin 24 h following reovirus or mock-infection and were assayed for the presence of apoptotic nuclear morphology after a further 24 h. Figure 4A shows that doxorubicin concentrations of below 0.5 μM did not induce apoptosis in either infected or uninfected ZR75-1 cells, concentrations of 1–2 μM induced around 60–80% apoptosis in either infected or uninfected cells and doxorubicin concentrations of 3 μM killed 100% of treated cells. There was no significant difference in doxorubicin-induced apoptosis in reovirus-infected, compared to uninfected cells, at any of the doxorubicin concentrations tested. We selected concentrations of 0.25 and 0.5 μM doxorubicin to further investigate the effect of reovirus-infection on doxorubicin-induced apoptosis. We also investigated the effect of TRAIL (20 ng/ml) on doxorubicin-induced apoptosis. Cells were infected with reovirus (MOI 10), or were mock-infected. Twenty-four hours later cells were treated with doxorubicin (0.25 and 0.5 μM) and/or TRAIL (20 ng/ml) and were assayed for apoptosis after a further 24 h. Figure 4B shows that reovirus-infection does not significantly augment 0.25 μM doxorubicin-induced apoptosis in ZR75-1 cells, compared to cells treated with 0.25 μM doxorubicin alone (similar results were obtained with 0.5 μM doxorubicin, results not shown). As shown above ZR75-1 cells were sensitized to TRAIL-induced apoptosis following reovirus infection. Doxorubicin also augmented TRAIL-induced apoptosis in ZR75-1 cells. Similar results were obtained in H157 cells (data not shown). These results suggest that reovirus infection does not sensitize cells to doxorubicin-induced apoptosis and supports our finding that the sensitization of reovirus-infected cells to TRAIL is a specific event.

Reovirus infection does not alter the expression of TRAIL receptors in cancer cell lines

Having shown that reovirus specifically augments TRAIL-induced apoptosis we wished to determine the mechanism by which this occurs. The sensitivity of cells

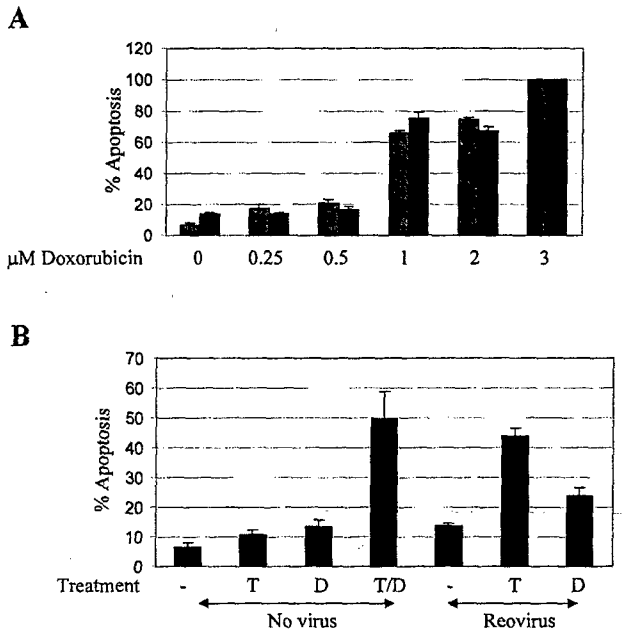

Figure 4 Reovirus infection does not sensitize cells to doxorubicin-induced apoptosis. (**A**) ZR75-1 cells were infected with reovirus (MOI 10, black bars) or were mock-infected (shaded bars). After 24 h cells were treated with increasing concentrations of doxorubicin and were assayed for apoptosis after a further 24 h. (**B**) ZR75-1 cells were infected with reovirus (MOI 10) or were mock-infected. After 24 h cells were treated with TRAIL (T), doxorubicin (D) or a combination of TRAIL and doxorubicin (T/D). The graphs show the mean numbers of cells with apoptotic nuclear morphology from three separate experiments. Error bars represent standard errors of the mean

to TRAIL-induced apoptosis is dependent, in part on the expression of the apoptosis-inducing receptors DR4 and DR5. We therefore assayed TRAIL receptor expression in reovirus-infected cancer cells to determine whether reovirus sensitizes cells to TRAIL-induced apoptosis by altering TRAIL receptor expression in infected cells. Gene expression was analysed in mock- and reovirus-infected lung and cervical cancer cells by semi-quantitative RTPCR, 12 and 24 h post infection (Figure 5A) and by FACS analysis of cell surface receptor expression in breast cancer cells, 24 h post infection (Figure 5B). DR5 mRNA was expressed in all the cell lines tested and did not alter following infection with reovirus. DR5 cell surface expression was also unaltered following infection with reovirus and FACS analysis of DR5 staining in mock-infected and reovirus-infected cells produced identical traces (Figure 5B). The expression of DR4 mRNA is dependent on cell type. HeLa and H157 cells express DR4 mRNA whereas A549 cells express very little DR4 mRNA. However, there is no change in the expression of either DR4 mRNA (Figure 5A), or of cell surface DR4 (Figure 5B), in cells following reovirus infection. The expression of neither DcR-1 nor DcR-2 mRNA was altered by reovirus infection (data not shown).

Taken together these results indicate that reovirus infection does not alter TRAIL-receptor expression and that changes in receptor expression do not

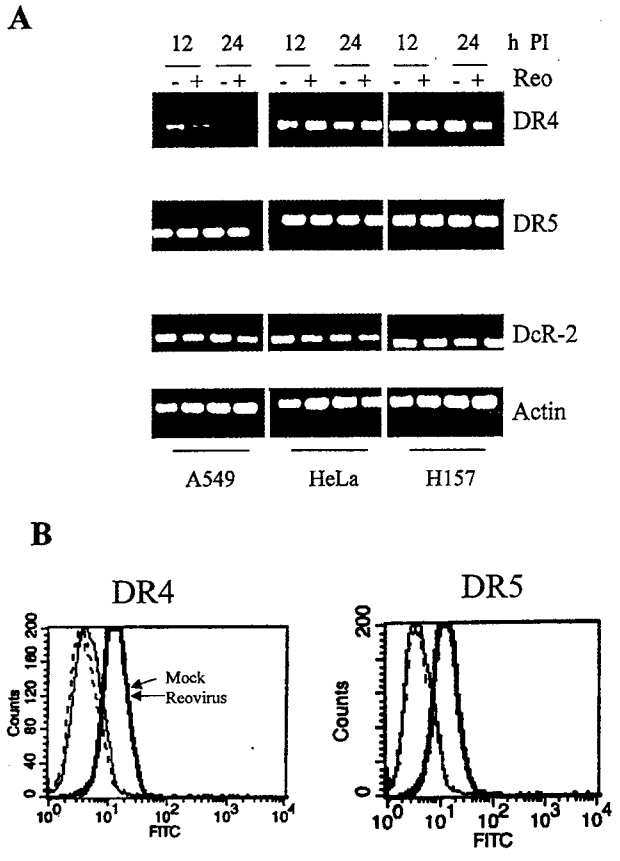

Figure 5 Expression of TRAIL receptors following reovirus infection in cancer cell lines. (**A**) Expression of TRAIL receptor mRNA does not change in reovirus infected cells. Lung (A549 and H157) and cervical (HeLa) cancer cells were infected with reovirus (MOI 100). After 12 and 24 h cells were harvested and semi-quantitative RTPCR was performed using primers specific for DR4, DR5, DcR-2 and actin. (**B**) Flow cytometric analysis of TRAIL receptor expression in breast cancer cells following infection with reovirus. MDA231 cells were infected with reovirus (MOI 100). Twenty-four hours post infection cells were harvested, stained and analysed for surface expression of TRAIL receptors DR4 and DR5. The unlabeled traces correspond to mock and reovirus-infected cells stained with an anti FITC antibody in the absence of antibody to DR4 or DR5

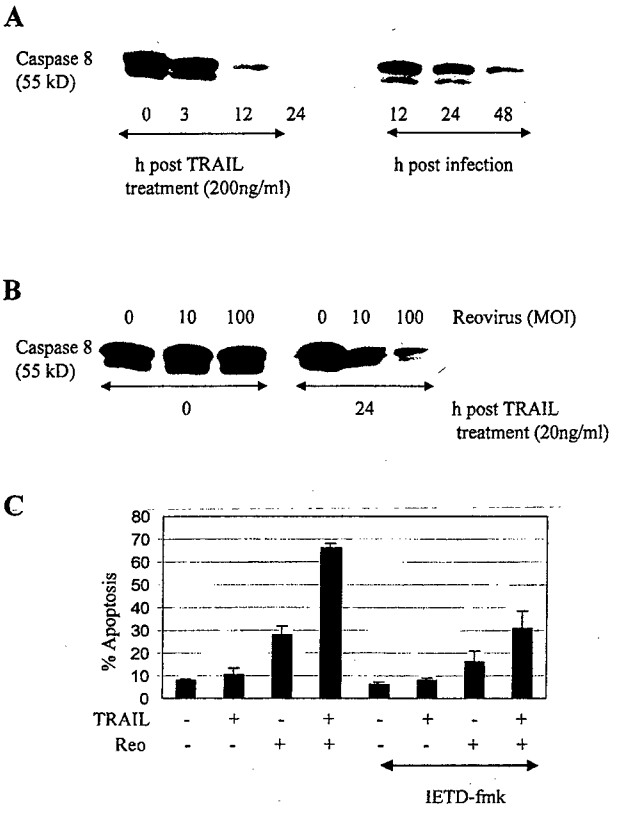

Figure 6 Reovirus infection increases the activation of caspase 8 in TRAIL treated cells and reovirus-induced sensitization of cells to TRAIL is blocked by an inhibitor of caspase 8 activity. (**A**) High doses of TRAIL (200 ng/ml) alone and reovirus (MOI 100) alone both induce the cleavage of procaspase 8 in H157 cells. (**B**) H157 cells were infected with reovirus (MOI 0, 10, 100). Twelve hours following infection cells were treated with low dose TRAIL (20 ng/ml) and were harvested at various times post treatment. For the detection of caspase 8 activation extracts were run on tricine gels and were probed with antibody directed against pro-caspase 8. All samples were standardized for protein concentration using actin (not shown). (**C**) ZR75-1 cells were either mock-infected or infected with reovirus (MOI 10). After 24 h cells were treated with TRAIL (20 ng/ml), or were left untreated, in the presence or absence of IETD-fmk (50 μM). The graph shows the mean per cent of apoptotic nuclei in cells from three separate experiments. Error bars represent standard errors of the mean

contribute to the capacity of reovirus infection to sensitize cancer cells to TRAIL-induced killing.

Reovirus-induced sensitization to TRAIL is associated with an increase in the activity of caspase 8

Since both TRAIL (Muhlenbeck *et al.*, 1998) and reovirus-induced (Kominsky *et al.*, submitted) apoptosis are associated with the activation of caspase 8 we wished to determine whether caspase 8 was involved in reovirus-induced sensitization of cells to TRAIL. As expected high doses of TRAIL alone (200 ng/ml) and of reovirus alone (MOI 100) activated caspase 8 in H157 cells, as determined by the cleavage of pro-caspase 8 (Figure 6A). We next looked to see if the activity of caspase 8 was increased in reovirus-infected, TRAIL-treated cells compared to cells treated with TRAIL alone. We tested the ability of increasing doses of reovirus (MOI 0, 10, 100) to augment TRAIL-induced caspase 8 activation in cells treated with low levels of TRAIL (20 ng/ml), that are insufficient to activate caspase 8 by themselves. H157 cells were infected with reovirus and 12 h following infection were treated with TRAIL (20 ng/ml). Cells were harvested 0 and 24 h later and extracts were run on tricine gels and were probed with antibody directed against pro-caspase 8 (Figure 6B). Pro-caspase 8 was not cleaved in the presence of low doses (20 ng/ml) of TRAIL alone but was cleaved in the presence of TRAIL (20 ng/ml) and reovirus, in a MOI-dependent manner (Figure 6B). These results indicate that reovirus augments caspase 8 activation in TRAIL treated cells.

Having shown that reovirus-induced sensitization to TRAIL is associated with an increase in the activation of caspase 8 we next wanted to see if reovirus-induced sensitization of cells was blocked using IETD-fmk, a

peptide capable of inhibiting caspase 8 activity. The presence of IETD-fmk (50 μM) significantly ($P<0.05$) reduced the ability of reovirus to sensitize cells to TRAIL in both H157 (data not shown) and ZR75-1 cells (Figure 6C), providing further evidence that reovirus-induced sensitization of cells to TRAIL involves a caspase 8-dependent pathway.

Reovirus-induced sensitization to TRAIL is associated with an increase in the activity of effector caspases

Having shown that reovirus-induced sensitization to TRAIL is associated with an increase in the activation of caspase 8 we next looked to see whether there was an increase in the activation of downstream, effector, caspases in reovirus-infected, TRAIL-treated cells compared to cells treated with TRAIL alone. The effector caspases that have been shown to operate downstream of caspase 8 are caspases 3 and 7. We thus examined the cleavage of the caspase 3 and 7 substrate PARP, as a monitor of activation of effector caspases. Cells were infected with reovirus (MOI 0, 10, 100) and were treated with TRAIL (20 ng/ml) 12 h following infection. After a further 3 h cells were harvested and probed with an antibody directed against PARP. Figure 7 shows the disappearance of PARP (corresponding to its cleavage) in the cell lysates, following treatment with TRAIL. This was enhanced when the cells were first infected with reovirus, indicating that reovirus infection increases the amount of effector caspase activation in TRAIL-treated cells.

Discussion

Our results demonstrate that reovirus induces apoptosis in a variety of cell lines derived from human cancers. Apoptosis was determined by the presence of apoptotic nuclear morphology and the increase in the activity of caspase 3 in reovirus-infected cells. Although the 2–3-fold increase in the activity of caspase 3 that we obtained following reovirus infection is fairly modest it is typical of results obtained in other cell lines (Dr D Kominski, personal communication). It is unclear to us why reovirus produces such a low level of caspase 3 activity in infected cells. Possibly, a low level of activation over a long period of time is sufficient for reovirus-induced apoptosis. Alternatively reovirus may induce increased levels of additional effector caspases, which contribute to apoptosis in reovirus-infected cells. Certainly, the cancer cell lines that we have used show a much higher caspase 3 activity (20+fold) following TRAIL treatment (results not shown).

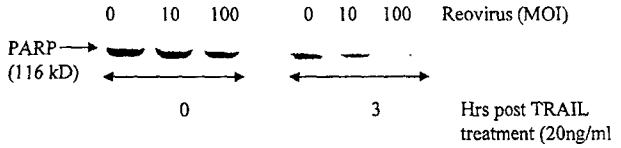

Figure 7 Reovirus infection increases the activation of caspase 3 in TRAIL treated cells. H157 cells were infected with reovirus (MOI 0, 10, 100). Twelve hours following infection cells were treated with low dose TRAIL (20 ng/ml) and were harvested at various times post treatment. Extracts were probed with antibody directed against the caspase 3 substrate, PARP. Samples were standardized for protein concentration using actin (not shown)

Similar to a recent report that showed that cells that were resistant to chemotherapy were also resistant to TRAIL (Cuello *et al.*, 2001), there is a significant correlation between the sensitivity of the cancer cell lines to apoptosis induced by reovirus and TRAIL. Further, reovirus-induced apoptosis is blocked both by the presence of soluble TRAIL receptor Fc:DR5 and by the over-expression of DcR-1. These results indicate that reovirus-induced apoptosis in cancer cells is mediated by TRAIL. Similar to our results in HEK293 cells (Clarke *et al.*, 2000) we now show that TRAIL is released from all but one of the cancer cell lines tested following infection with reovirus.

Reovirus-induced oncolysis has been previously described (Coffey *et al.*, 1998). Our current results indicate that oncolysis results from apoptosis and that TRAIL plays an essential role in this process. Other viruses may also utilize the TRAIL apoptotic pathway. For example, HIV infection increases the expression of TRAIL and sensitizes T-cells to TRAIL-mediated apoptosis (Jeremias *et al.*, 1998). Modulation of TRAIL and TRAIL receptor expression also occurs following infection with human cytomegalovirus (Sedger *et al.*, 1999) and Theiler's murine encephalomyelitis virus has been shown to induce apoptosis through a mechanism involving TRAIL (Jelachich and Lipton, 2001). Previous studies have suggested that other members of the TNFR death receptor superfamily may also be involved in virus-induced apoptosis. Alteration of the cell surface expression of Fas may be involved in virus-induced, or viral regulation of, apoptosis in cells infected with influenza virus (Takizawa *et al.*, 1993, 1995), herpes simplex virus type 2 (Sieg *et al.*, 1996), bovine herpesvirus 4 (BHV 4) (Wang *et al.*, 1997), adenovirus (Tollefson *et al.*, 1998) and human immunodeficiency virus type 1 (HIV 1) (Conaldi *et al.*, 1998; Kaplan and Sieg, 1998). Similarly, apoptosis induced by Hepatitis B (Su and Schneider, 1997), HIV-1 (Herbein *et al.*, 1998), BHV 4 (Wang *et al.*, 1997) parvovirus H-1 (Rayet *et al.*, 1998) and Theiler's murine encephalomyelitis virus (Jelachich and Lipton, 2001), may involve the TNFR signaling pathway.

In addition to its capacity to kill cancer cells by apoptosis, we show that reovirus infection also sensitizes cancer cells to TRAIL induced apoptosis in a synergistic manner. H157 and ZR75-1 cells, which are relatively resistant to TRAIL-induced killing, became much more susceptible following infection with reovirus. Reovirus-induced sensitization of cells is specific for TRAIL and reovirus does not synergistically sensitize cells to Fas-mediated apoptosis (another death receptor apoptotic pathway) or to apoptosis

induced by doxorubicin (a non-death receptor apoptotic agent).

We next investigated the mechanism by which reovirus sensitizes cells to TRAIL. The level of TRAIL receptor expression at the cell surface does not change following infection with reovirus indicating that up-regulation of TRAIL receptor is not the mechanism by which reovirus sensitizes cells to TRAIL. The activation of caspase 8 however, is increased in cells following a combination of reovirus-infection and TRAIL-treatment, compared to uninfected cells or to cells treated with TRAIL or reovirus alone. Caspase 8, an initiator caspase, activates the effector caspases 3 and 7 and we show that there is increased cleavage of the effector caspase substrate, PARP, in reovirus-infected, TRAIL-treated cells, compared to cells treated with TRAIL alone. The role of caspase 8 in reovirus-induced sensitization of cells to TRAIL is supported by our demonstration that the peptide IETD-fmk, which inhibits caspase 8 activity and blocks both TRAIL-induced (Yu *et al*., 2000) and reovirus-induced (Clarke *et al*., 2000) apoptosis, blocks reovirus-induced sensitization to TRAIL. The expression of DN-FADD, which blocks the activation of caspase 8, also blocks reovirus-induced sensitization to TRAIL in HEK293 cells (results not shown).

The involvement of caspase 8 in reovirus-induced sensitization of cells to TRAIL suggests that reovirus sensitizes cells to TRAIL-induced apoptosis by augmenting the TRAIL pathway of apoptosis rather than by activating a second apoptotic pathway. This suggests that the mechanism by which reovirus sensitizes cells to TRAIL-induced apoptosis differs from the recently identified mitochondrial-dependent pathway by which sodium nitroprusside (Lee *et al*., 2001) and ionizing radiation (Belka *et al*., 2001) enhance TRAIL-induced apoptosis. The release of TRAIL from reovirus-infected cells may contribute to the increased activation of caspase 8 in reovirus-infected, TRAIL treated cells. However, ZR75-1 cells, which do not release TRAIL following reovirus infection, are sensitized to TRAIL-induced apoptosis following infection with reovirus. This implies that TRAIL release cannot be the only mechanism for the increased levels of caspase 8 activation in reovirus-infected, TRAIL-treated cells.

The cleavage of procaspase 8 to its active counterpart is required for TRAIL-induced apoptosis. The caspase 8 homologue, FLICE inhibitory protein (cFLIP), promotes cell survival by blocking this reaction and its has been shown that inducers of the transcription factor NF-κB can upregulate cFLIP (Kreuz *et al*., 2001). Although reovirus induces the activation of NF-κB (Connolly *et al*., 2000) similar levels of expression of the cellular inhibitor of caspase 8 activation (FLIP) were observed in reovirus-infected, TRAIL-treated cells compared to that in cells treated with TRAIL alone (results not shown) indicating that the increased activation of caspase 8 is not due to a reduction in FLIP-mediated inhibition of caspase 8.

These results show that reovirus-induced oncolysis of cancer cells occurs through TRAIL-mediated apoptosis and suggest that reovirus-infection is a useful model for investigations of TRAIL-induced apoptosis in cancer cells. Similar to the effects of genotoxins (Gibson *et al*., 2000), reovirus sensitizes cells to TRAIL induced apoptosis. Our results show that reovirus-induced sensitization of cells to TRAIL is inhibited by IETD-fmk and is associated with the activation of caspase 8. Further studies of this phenomenon may suggest new strategies to enhance the killing of cancer cells by TRAIL.

Materials and methods

Cells and virus

HEK293 cells (ATCC CRL1573) were grown in Dulbecco's modified Eagle's medium (DMEM) supplemented with 100 U/ml each of penicillin and streptomycin and containing 10% fetal bovine serum. HeLa cells (ATCC CCL2) were grown in Eagle's minimal essential medium (MEM) supplemented with 2.4 mM L-glutamine, non-essential amino acids, 60 U/ml each of penicillin and streptomycin and containing 10% fetal bovine serum (Gibco BRL, Gaithersburg, MD, USA). HeLa cells were used as indicator cells in the supernatant transfer experiments. The lung cancer cell lines (A549 and H157) and breast cancer cell lines (MDA-MB231 and ZR75-1) were obtained from the University of Colorado Cancer Center. Reovirus (Type 3 Abney, T3A) is a laboratory stock, which has been plaque purified and passaged (twice) in L929 (ATCC CCL1) cells to generate working stocks (Tyler *et al*., 1996). Virus growth was determined by plaque assay as previously described (Tyler *et al*., 1985).

Apoptosis assays and reagents

Determination of Apoptotic Nuclear morphology: 48 h after infection with reovirus cells were harvested and stained with acridine orange, for determination of nuclear morphology and ethidium bromide, to distinguish cell viability, at a final concentration of 1 μg/ml each (Duke and Cohen, 1992). Following staining, cells were examined by epifluorescence microscopy (Nikon Labophot-2: B-2A filter, excitation, 450–490 nm; barrier, 520 nm; dichroic mirror, 505 nm). The percentage of cells containing condensed nuclei and/or marginated chromatin in a population of 100 cells was recorded. The specificity of this assay for detecting apoptotic cells has been previously established in reovirus-infected cells using DNA laddering techniques and electron microscopy (Tyler *et al*., 1995). DNA laddering: Cells (5×10^6) were removed from culture flasks and resuspended in 2 ml digestion buffer (0.1 M NaCl, 10 mM Tris pH 8, 25 mM EDTA, 0.5% SDS and 0.3 mg/ml proteinase K). Following overnight incubation at 50°C the suspension was extracted with phenol/chloroform and then chloroform. DNA was then treated with RNase (20 μg/ml) for 1 h at 37°C, followed by further extraction with phenol/chloroform and then chloroform. DNA was then purified by overnight ethanol precipitation (1/2 volumes 7.5 M NH_4-acetate and three volumes cold 100% ethanol) at −20°C. The precipitate was spun down at 9000 r.p.m. for 30 min, washed in ethanol (85%), dried and resuspended in 200 μl TE. DNA was then

run on a 1.5% agarose gel, stained with ethidium bromide and visualized using a Fluor-S MultiImager and Quantity One software (BioRad, Hercules, CA, USA). For the sensitization experiments cells were infected with reovirus at a multiplicity of infection (MOI) of 10. After 24 h cells were treated with 20 ng/ml TRAIL (Upstate Biotechnology, Lake Placid, NY, USA), 0.025 μg/ml of an activating Fas antibody (Upstate Biotechnology) or 0.25/0.5 μM doxorubicin (Sigma, St. Louis, MO, USA) and apoptosis assays were performed after a further 24 h. Soluble death receptors Fc:DR5 and Fc:TNFR were obtained from Alexis Corporation (Pittsburgh, PA, USA). The cell permeable caspase inhibitor IETD-fmk was obtained from Clontech (Palo Alto, CA, USA). Anti-reovirus antibody is a neutralizing polyclonal anti-reovirus antisera, that neutralizes infectivity and blocks apoptosis induced by infectious virus (Tyler *et al*., 1995).

Caspase 3 activation assays

Caspase 3 activation assays were performed using a kit obtained from Clontech. Experiments were performed using 1×10^6 cells/time point. Cells were centrifuged at 200 *g* for 10 min, supernatants were removed and cell pellets were frozen at -70°C until all time points were collected. Assays were performed in 96 well plates and analysed using a fluoresent plate reader (CytoFluor 4000, PerSeptive Biosystems, Farmington, MA, USA). Cleavage of DEVD-AFC, a synthetic caspase-3 substrate, was used to measure caspase 3 activation in reovirus-infected cells. Cleavage after the second Asp residue produces free AFC that can be detected using a fluorescent plate reader. The amount of fluorescence detected is directly proportional to the amount of caspase 3 activity.

Western blot analysis

Following infection with reovirus, cells were pelleted by centrifugation, washed twice with ice-cold phosphate-buffered saline and lysed by sonication in 200 μl of a buffer containing 15 mM Tris, pH 7.5, 2 mM EDTA, 10 mM EGTA, 20% glycerol, 0.1% NP-40, 50 mM mercaptoethanol, 100 μg/ml leupeptin, 2 μg/ml aprotinin, 40 μM Z-D-DCB, and 1 mM PMSF. The lysates were then cleared by centrifugation at 16 000 *g* for 5 min, normalized for protein amount, mixed 1 : 1 with SDS sample buffer (100 mM Tris, pH 6.8, 2% SDS, 300 mM mercaptoethanol, 30% glycerol, and 5% pyronine Y), boiled for 5 min and stored at -70°C. Proteins were electrophoresed by SDS–PAGE (10% gels) and probed with anti-caspase 8 (B9-2, Pharmingen, San Diego, CA, USA) and anti-PARP (9542, Cell Signaling Technologies, CA, USA) antibodies. All lysates were standardized for protein concentration with antibodies directed against actin (CP01, Oncogene, Cambridge, MA, USA).

RTPCR

Cells were seeded (5×10^6) and were infected with reovirus (MOI 100). At 24 h post infection cells were washed in PBS and were harvested directly into RNA lysis buffer. Total cellular RNA was prepared using RNeasy minicolumns (Qiagen, Valencia, CA, USA). Two μg of RNA was used as template for first strand synthesis using a pre-amplification system (Life Technologies, Grand Island, NY, USA). Semi-quantitative RTPCR amplification reactions specific to DR4, DR5, DcR-1 and DcR-2 were performed (Griffith *et al*., 1999). Actin primers were used as controls.

Flow cytometry

Cells were removed from tissue culture flasks by repeat pipetting or gentle tapping and were suspended in PBS (10^5 cells/ml). Cells were pelleted by centrifugation (2000 r.p.m. for 2 min, then maximum pulse for 10 s) and were then resuspended in 500 μl wash buffer 1 (PBS containing 2% fetal calf serum and 0.02% sodium azide). Cells were pelleted as above and resuspended in 500 μl staining solution (PBS containing 5% fetal calf serum and 0.02% sodium azide) for 5 min at room temperature. Cells were then pelleted as before and resuspended in 50 μl staining solution, alone for negative control and with primary antibody (2 μl/ml) for experimental samples. Cells were then incubated at 4°C in the dark for 30 min before being washed twice in wash buffer 1 (centrifuging as described above). After a final centrifugation step cells were resuspended in staining solution and secondary antibody conjugated to fluorophore (anti-mouse IgG1-FITC) and were incubated at 4°C in the dark for 30 min. Cells were then pelleted (as above) twice and resuspended first in wash buffer 1 and then in wash buffer 2 (PBS containing 0.02% sodium azide). Cells were then centrifuged (as above), fixed in 500 μl 1% paraformaldehyde and analysed by flow cytometry.

For these experiments monoclonal antibodies against human DR4 (huTR1-M271) and DR5 (huTRAILR2-M413) were used (Immunex Corporation, Seattle, WA, USA).

Acknowledgments

This work was supported by Public Health Service grant 1RO1AG14071 and GM30324 from the National Institute of Health, Merit and REAP grants from the Department of Veterans Affairs, a US Army Medical Research and Material Command grant (DAMD17-98-1-8614) (KL Tyler). The University of Colorado Cancer Center provided core tissue culture and media facilities.

References

Ashkenazi A and Dixit VM. (1998). *Science*, **281**, 1305–1308.

Ashkenazi A, Pai RC, Fong S, Leung S, Lawrence DA, Marsters SA, Blackie C, Chang L, McMurtrey AE, Hebert A, DeForge L, Koumenis IL, Lewis D, Harris L, Bussiere J, Koeppen H, Shahrokh Z and Schwall RH. (1999). *J. Clin. Invest.*, **10**, 155–162.

Belka C, Schmid B, Marini P, Durand E, Rudner J, Faltin H, Bamberg M, Schulze-Osthoff K and Budach. (2001). *Oncogene*, **20**, 2190–2196.

Clarke P, Meintzer SM, Gibson S, Widmann C, Garrington TP, Johnson GL and Tyler KL. (2000). *J. Virol.*, **74**, 8135–8139.

Coffey MC, Strong JE, Forsyth PA and Lee PWK. (1998). *Science*, **282**, 1332–1334.

Conaldi PG, Biancone L, Bottelli A, Wade-Evans A, Racusen LC, Boccellino M, Orlandi V, Serra C, Camussi G and Toniolo A. (1998). *J. Clin. Invest.*, **102**, 2041–2049.

Connolly JL, Rodgers SE, Clarke P, Ballard DW, Kerr LD, Tyler KL and Dermody TS. (2000). *J. Virol.*, **74,** 2981–2989.

Cuello M, Ettenberg SA, Nau MM and Lipkowitz S. (2001). *Gynecol. Oncol.*, **81,** 380–390.

DeBiasi RL, Edelstein CL, Sherry B and Tyler KL. (2001). *J. Virol.*, **75,** 351–361.

DeBiasi RL, Squier MKT, Pike B, Wynes M, Dermody TS, Cohen JJ and Tyler KL. (1999). *J. Virol.*, **73,** 695–701.

Duke RC and Cohen JJ. (1992). *Current protocols in immunology,* Coligan, J.E. (ed), Wiley: NY, pp. 3.17.1–3.17.16.

Gibson SB, Oyer R, Spalding AC, Anderson SM and Johnson GL. (2000). *Mol. Cell Biol.*, **20,** 205–212.

Griffith TS, Wiley SR, Kubin MZ, Sedger LM, Maliszewski CR, and Fanger NA. (1999). *J. Exp. Med.*, **189,** 1343–1353.

Herbein G, Mahlknecht U, Batliwalla F, Gregerson P, Pappas T, Butler J, O'Brian WA and Verdin E. (1999). *Nature,* **395,** 189–194.

Jelachich ML and Lipton HL. (2001). *J. Virol.*, **75,** 5930–5938.

Jeremias I, Herr I, Boehler T and Debatin K-M. (1998). *Eur. J. Immunol.*, **28,** 143–152.

Jo M, Kim TH, Seol DW, Esplen JE, Dorko K, Billiar TR and Storm SC. (2000). *Nat. Med.*, **6,** 564–567.

Kaplan D and Sieg S. (1998). *J. Virol.*, **72,** 6279–6282.

Keane MM, Ettenburg SA, Nau MM, Russell EK and Lipkowitz S. (1999). *Cancer Res.*, **59,** 734–741.

Kreuz S, Siegmund D, Scheurich P and Wajant H. (2001). *Mol. Cell Biol.*, **12,** 3964–3973.

Lee YJ, Lee KH, Kim HR, Jessup, JM, Seol DW, Kim TH, Billiar TR and Song YK. (2001). *Oncogene,* **20,** 1476–1485.

Muhlenbeck F, Haas E, Schwenzer R, Schubert G, Grell M, Smith C, Scheurich P and Wajant H. (1998). *J. Biol. Chem.*, **273,** 33091–33098.

Nagata S. (1997). *Cell,* **88,** 355–365.

Oberhaus SM, Dermody TS and Tyler KL. (1998). *Retroviruses II: Cytopathicity and pathogenesis [Current Topics in Microbiology and Immunology].* Tyler KL, Oldstone MBA (eds). Springer-Verlag, Berlin, vol. 233.

Oberhaus SM, Smith RL, Clayton GH, Dermody TS and Tyler KL. (1997). *J. Virol.*, **71,** 2100–2106.

Ozoren N, Kim K, Burns TF, Dicker DT, Moscioni AD and El-Deiry. (2000). *Cancer Res.*, **60,** 6259–6265.

Pitti RM, Marsters SA, Ruppert S, Donahue CJ, Moore A and Ashkenazi A. (1996). *J. Biol. Chem.*, **27,** 12687–12690.

Rayet B, Lopez-Guerro JA, Rommelaere J and Dinsart C. (1998). *J. Virol.*, **72,** 8893–8903.

Sedger LM, Hows DM, Blanton RA, Peschon JJ, Goodwin RG, Cosman D and Wiley SR. (1999). *J. Immunol.*, **163,** 920–926.

Sieg S, Yildirim Z, Smith D, Kayagaki N, Yagita H, Huang Y and Kaplan D. (1996). *J. Virol.*, **70,** 8747–8751.

Strong JE, Coffey MC, Tang D, Sabinin P and Lee PWK. (1998). *EMBO J.*, **17,** 3351–3362.

Su F and Schneider RJ. (1997). *Proc. Natl. Acad. Sci. USA,* **94,** 8744–8749.

Takizawa T, Fukuda R, Miyawaki T, Ohashi K and Nakanishi Y. (1995). *Virology,* **209,** 288–296.

Takizawa T, Matsukawa S, Higuchi Y, Nakamura S, Nakanishi Y and Fukuda R. (1993). *J. Gen. Virol.*, **74,** 2347–2355.

Tollefson AE, Hermiston TW, Lichtenstein DL, Colle CF, Tripp RA, Dimitrov T, Toth K, Wells CE, Doherty PC and Wold WS. (1998). *Nature,* **392,** 726–730.

Tyler KL, Bronson RT, Byers KB and Fields BN. (1985). *Neurol.*, **35,** 88–92.

Tyler KL, Squier MKT, Brown AL, Pike B, Willis D, Oberhaus SM, Dermody TS and Cohen JJ. (1996). *J. Virol.*, **70,** 7984–7991.

Tyler KL, Squier MKT, Rodgers SE, Schneider BE, Oberhaus SM, Grdina TA, Cohen JJ and Dermody TS. (1995). *J. Virol.*, **69,** 6972–6979.

Walczak H, Miller RE, Ariail K, Gliniak B, Griffith TS, Kubin M, Chin W, Jones J, Woodward A, Le T, Smith C, Smolak P, Goodwin RG, Rauch CT, Schuh JC and Lynch DH. (1999). *Nat. Med.*, **5,** 157–163.

Wang GH, Bertin J, Wang Y, Martin DA, Wang J, Tomaselli KJ, Armstrong RC and Cohen JI. (1997). *J. Virol.*, **71,** 8928–8932.

Wiley SR, Schooley K, Smolak PJ, Din WS, Huang CP, Nicholl JK, Sutherland GR, Smith TD, Rauch C, Smith CA and Goodwin RG. (1995). *Immunity,* **3,** 673–682.

Yu R, Mandlekar S, Ruben S, Ni J and Kong ANT. (2000). *Cancer Res.*, **60,** 2384–2389.

Zhang XD, Franco A, Myers K, Gray C, Nguyen T and Hersey P. (1999). *Cancer Res.*, **59,** 2747–2753.

Oncogene (2002) 21, 260–271

www.nature.com/onc

TRAIL and inhibitors of apoptosis are opposing determinants for NF-κB-dependent, genotoxin-induced apoptosis of cancer cells

Aaron C Spalding[1,5], Robert M Jotte[1,5], Robert I Scheinman[4], Mark W Geraci[2], Penny Clarke[3], Kenneth L Tyler[3] and Gary L Johnson*,[1]

[1]Department of Pharmacology, University of Colorado Cancer Center, University of Colorado Health Sciences Center, 4200 East Ninth Avenue, Denver, Colorado, CO 80262, USA; [2]Department of Medicine, University of Colorado Cancer Center, University of Colorado Health Sciences Center, 4200 East Ninth Avenue, Denver, Colorado, CO 80262, USA; [3]Department of Neurology, University of Colorado Cancer Center, University of Colorado Health Sciences Center, 4200 East Ninth Avenue, Denver, Colorado, CO 80262, USA; [4]School of Pharmacy, University of Colorado Cancer Center, University of Colorado Health Sciences Center, 4200 East Ninth Avenue, Denver, Colorado, CO 80262, USA

Opposing pro- and anti-apoptotic actions of TRAIL and the inhibitors of apoptosis (IAPs) contribute to the cell's decision to survive or die. We demonstrate that in H157 human lung carcinoma cells, etoposide and doxorubicin induce the NF-κB-dependent expression of both pro- and anti-apoptotic proteins including TRAIL and its death receptor, DR5, and IAPs. Inhibition of NF-κB activation in H157 cells in response to genotoxin resulted in loss of cell surface expression of TRAIL and DR5, aggressive growth and chemotherapy resistance of tumors in nude mice. Similar to the paracrine TRAIL response in H157 cells, the sensitivity of normal lung and breast epithelium and carcinomas to undergo genotoxin-induced apoptosis correlates strongly with cell surface expression of TRAIL. Suppression of TRAIL signaling by expression of the TRAIL decoy receptor, DcR1, confers chemo-resistance to cancer cells. These findings demonstrate that TRAIL signaling via its death receptors is a significant contributor to genotoxin-induced apoptosis in human epithelial carcinomas.
Oncogene (2002) **21**, 260–271. DOI: 10.1038/sj/onc/1205048

Keywords: TRAIL; IAP; NF-κB; apoptosis; chemotherapy

Introduction

Apoptosis is characterized as being initiated either by death receptor activation or mitochondrial changes mediated by Bcl-2 family members (Yang *et al.*, 1997). Oligomerization of death receptors such as Fas or DR4 and DR5 upon binding FasL or TRAIL leads to caspase 8 activation (Muzio *et al.*, 1996). Activation of pro-apoptotic Bcl-2 family proteins (Bad, Bid, Bax, Bak) results in mitochondrial membrane pore formation, loss of membrane potential and the release of cytochrome *c* and other mitochondrial proteins (Jurgensmeier *et al.*, 1998; Li *et al.*, 1998; Luo *et al.*, 1998; Zha *et al.*, 1996). Apaf-1 binding of released cytochrome *c* leads to caspase 9 activation (Zou *et al.*, 1999). Both caspase 8 and caspase 9 can activate caspase 3 whose activation is generally considered the irreversible commitment to apoptosis.

Cytokines such as FasL and TRAIL trigger the apoptosis module using death receptors as their entry point by activating caspase 8 (Chaudhary *et al.*, 1997; Schneider *et al.*, 1997). Toxins such as antimycin A appear to bind to the BH3 domain of Bcl-2 and Bcl-X_L and initiate apoptosis by influencing mitochondrial pore formation and membrane potential (Tzung *et al.*, 2001). In contrast to the selective actions of FasL, TRAIL and antimycin A, other apoptotic stimuli such as genotoxins can activate apoptosis via both death receptors and regulation of Bcl-2 family proteins (Sun *et al.*, 1999). Genotoxins stimulate mitochondrial cytochrome *c* release via regulation of Bcl-2 and induce the expression of both FasL and TRAIL in different cell types (Ashkenazi and Dixit, 1999; Kasibhatla *et al.*, 1998; Kaufmann and Earnshaw, 2000). The relative contribution of Bcl-2 family proteins and death receptors in genotoxin-induced apoptosis appears to vary depending on the tumor origin and genotoxin.

It is apparent that changes in the expression of death receptors, their ligands and the Bcl-2 family proteins can alter the apoptotic potential of cells. Altered expression or mutation of these proteins provide a survival advantage to tumor cells by down-regulating the entry points that control the activation of apoptosis. We have found with lung and breast-derived epithelial cells, there is a strong correlation between the magnitude of genotoxin-stimulated apoptosis and the expression of TRAIL. Expression of TRAIL and its death receptor, DR5, is regulated in an NF-κB dependent mechanism (Gibson *et al.*, 2000; Ravi *et al.*, 2001). The genotoxins etoposide and doxorubicin strongly activate NF-κB. In concert with controlling TRAIL/DR5 expression, NF-κB regulates the expres-

*Correspondence: GL Johnson, Department of Pharmacology, C236, Room 2809, SOM, University of Colorado Health Sciences Center, 4200 East Ninth Avenue, Denver, Colorado 80262, USA; E-mail: Gary.Johnson@uchsc.edu
[5]Both authors contributed equally to this paper
Received 8 August 2001; revised 19 September 2001; accepted 9 October 2001

sion of several anti-apoptotic proteins. This orchestrated response of pro-apoptotic and anti-apoptotic proteins determines the fate of cells to a genotoxic stress. TRAIL is generally able to overcome the anti-apoptotic gene induction in epithelial cells. However, when the TRAIL response system is inhibited, chemoresistance and the NF-κB dependent anti-apoptotic response prevail. Cumulatively, our findings indicate that inhibition of TRAIL signaling is a mechanism for epithelial-derived carcinomas to escape apoptosis in response to genotoxins.

Results

NF-κB activity is necessary for the apoptotic response to etoposide in lung and breast cancer cells

In H157 lung squamous carcinoma the expression of dominant negative IκBα (DNIκBα) inhibits genotoxin-induced apoptosis (Figure 1a). To define the importance of NF-κB in etoposide-induced apoptosis, wild type (WT) H157 cells and DNIκBα H157 cells were treated with etoposide, and apoptosis was quantitated by acridine orange. Basal levels of apoptosis in unstimulated WT H157 cells was approximately $5\pm1.6\%$ and increased to $31\pm2.1\%$ and $42\pm4.7\%$ with 48 h exposure to 30 and 100 μM etoposide, respectively (Figure 1a). Apoptosis in unstimulated DNIκBα H157 cells was comparable to WT H157 at $6\pm2\%$. With 30 μM etoposide, the apoptotic response was suppressed 40% or greater in DNIκBα relative to WT H157 cells (from $31\pm2.1\%$ in WT H157 to $17\pm6.3\%$ for DNIκBα H157 cells seen in Figure 1a, $P<0.005$). Similarly, the $42\pm4.7\%$ apoptotic cells observed with 100 μM etoposide treatment for 24 h in WT H157 cells decreased to $20\pm4.2\%$ in DNIκBα H157 cells ($P<0.005$). These studies demonstrate that NF-κB activity is required for maximal apoptotic response to etoposide insult in H157 carcinoma cells.

We have observed a similar pro-apoptotic function for NF-κB in other carcinomas from breast and lung. As shown in Figure 1a, ZR-75-1 breast adenocarcinoma cells behave similarly to H157 cells in that DNIκBα inhibits doxorubicin-induced apoptosis. The apoptotic index of WT ZR-75-1 cells rose from $4\pm1\%$ to $14\pm3\%$ with 100 nM doxorubicin and $48\pm6\%$ with 1 μM doxorubicin treatment for 48 h. The stable expression of DNIκBα in ZR-75-1 cells did not change basal apoptosis levels of $4\pm1\%$. Forty-eight hour treatment of the DNIκBα ZR-75-1 cells with 100 nM doxorubicin did not induce apoptosis ($4\pm1\%$, $P<0.005$ vs WT) while 1 μM doxorubicin yielded only 20% of apoptosis found in WT cells ($13\pm3\%$, $P<0.005$ vs WT).

These observations in combination with the role of NF-κB in regulating TRAIL expression (Ravi *et al.*, 2001), led us to examine the role of NF-κB signaling and TRAIL in the control of genotoxin-induced apoptosis in human carcinoma cells. The DNIκBα mutant protein we have used in our studies contains serine to alanine conversions at residues 32 and 36 that abolish the ability of IKKα to phosphorylate these sites. This prevents ubiquitination and degradation of mutant IκBα and subsequent dissociation and nuclear translocation of NF-κB. The inhibition of genotoxin-induced apoptosis was observed in H157 cells stably expressing DNIκBα following transfection and drug selection or acutely after infection with adenovirus encoding DNIκBα (not shown). Because similar results were seen for genotoxin resistance when DNIκBα was expressed by stable transfection or acute adenovirus infection we chose to use stably expressing DNIκBα H157 cells for further study *in vitro* and *in vivo*.

To confirm the dominant negative property of the IκBα mutant, we demonstrated H157 cells expressing DNIκBα fail to stimulate NF-κB DNA binding activity relative to wild type H157 cells following treatment with phorbol ester (PMA) (Figure 1b) or etoposide (Figure 1c). Inhibition of NF-κB DNA binding activity in response to PMA by expression of DNIκBα is specific, as AP-1 DNA binding activity remains intact in the same nuclear extracts. For etoposide treatment, both WT and DNIκBα H157 cells were treated with genotoxin for 12 and 24 h (Figure 1b). NF-κB DNA binding activity is induced following treatment of H157 cells for 12 and 24 h with etoposide, while DNIκBα H157 nuclear extracts show no increase in NF-κB DNA binding activity. Etoposide treatment of WT H157 cells also resulted in decreased levels of IκBα protein detected by immunoblotting, reflective of the phosphorylation, ubiquitination, and protein degradation of IκB that allows nuclear translocation and DNA binding of NF-κB (Figure 1d). DNIκBα H157 cells retain stable and consistent cytosolic levels of IκB protein despite treatment with etoposide. These assays confirm that DNIκBα effectively abolishes the stimulation of NF-κB activity, preventing transcriptional activation of NF-κB target genes.

To assess further the biologic implications of NFκB inhibition, WT and DNIκBα H157 cells were examined for tumorigenic potential in nude mouse xenografts. 1×10^6 WT H157 or DNIκBα H157 cells were injected into nude mice, and tumor volumes were followed for 31 days at which time tumor mass necessitated animal sacrifice. WT and DNIκBα H157 mouse xenografts grew comparably until day 17, when separation of tumor growth curves became apparent (Figure 1e). DNIκBα H157 xenografts grew to a larger size (450 ± 60 mm^3, $n=38$) over a shorter time frame compared to WT H157 xenografts (223 ± 20 mm^3, $n=38$) with growth differences reaching statistical significance ($P<0.005$) at day 17 that persisted until the end of the experiment. At day 31, the DNIκBα H157 xenografts reached a size of 2426 ± 658 mm^3 while WT H157 xenografts had grown to 1233 ± 218 mm^3 ($P<0.005$).

The aggressive tumor growth characteristic of DNIκBα H157 xenografts is not simply the result of a faster growth rate compared with WT H157 cells. In fact, *in vitro* growth curves suggest that DNIκBα H157 cells

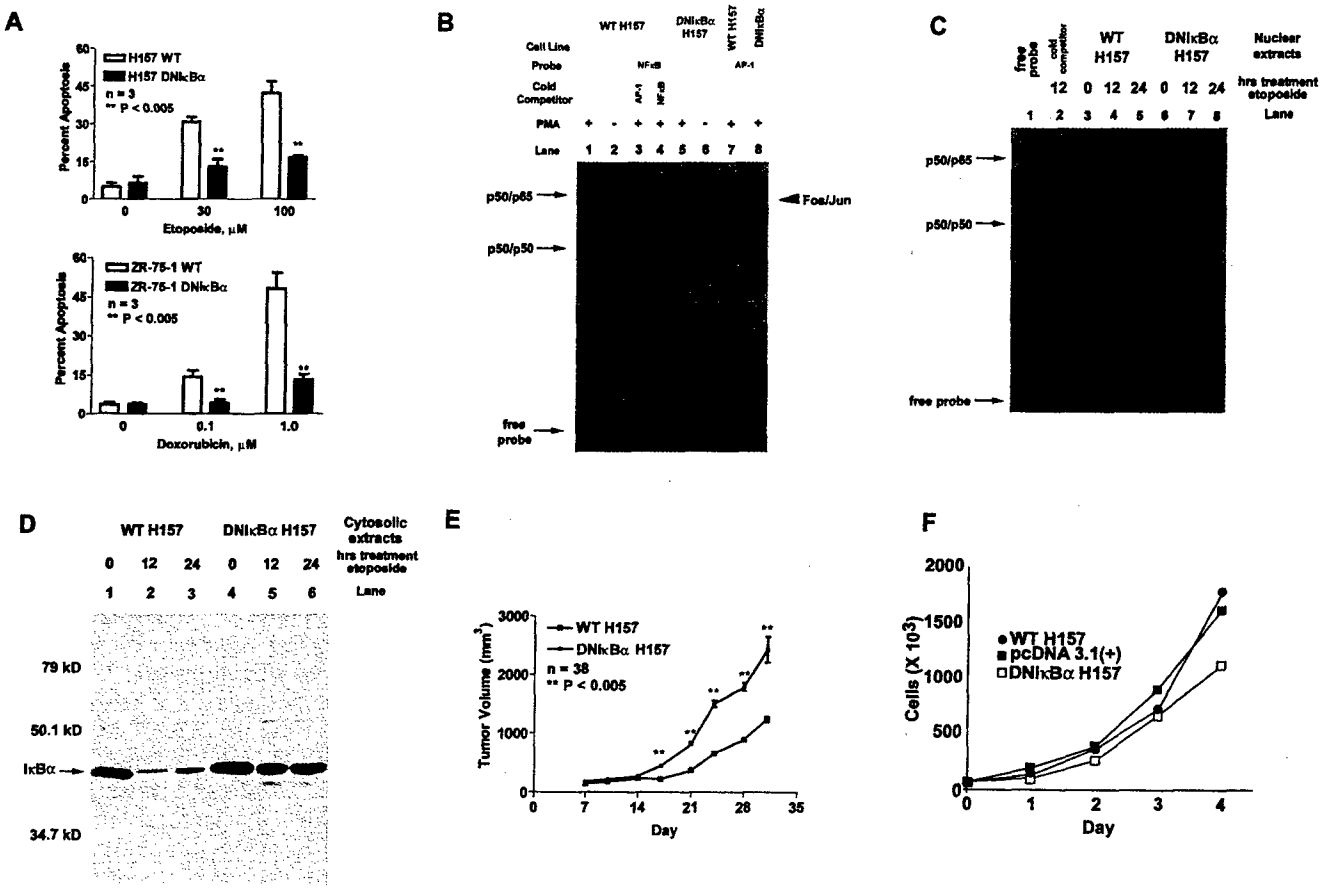

Figure 1 Loss of NF-κB results in chemo-resistance and aggressive tumor growth. (**a**) Loss of NF-κB activity results in a blunted apoptotic response to etoposide and doxorubicin in a dose-dependent manner. We treated WT H157 cells or DNIκBα H157 cells with etoposide for 48 h and then measured apoptosis. WT or DNIκBα ZR-75-1 cells were treated with the indicated doses of doxorubicin for 48 h. Data points represent the means of duplicate samples from three independent experiments while error bars are s.e.m. (**b**) DNIκBα effectively abolishes NF-κB nuclear translocation. Gel shift assays were done on nuclear lysates from WT and DNIκBα H157 in the absence or presence of PMA stimulation. WT H157 cells demonstrate inducible NF-κB DNA binding activity in unstimulated and stimulated cells; no NF-κB DNA binding activity can be demonstrated in DNIκBα nuclear extracts. Binding is specific, as binding is unaffected by AP-1 cold competitor, while NF-κB cold competitor abolishes protein binding to labeled probe (lanes 3,4). Loss of NF-κB DNA binding activity is not the result of a global loss of nuclear protein DNA binding activity, as AP-1 DNA binding activity is conserved in DNIκBα nuclear extracts (lanes 7,8). (**c**) DNIκBα expression attenuates etoposide induced NF-κB translocation to the nucleus. Etoposide induces NF-κB nuclear translocation, which persists to 24 h (lanes 4,5). No NF-κB DNA binding activity can be demonstrated in DNIκBα with etoposide treatment (lanes 7,8). (**d**) Lack of NF-κB DNA binding activity in DNIκBα H157 cells correlates with stable levels of IκBα protein in cytosolic extracts. Western blotting with an IκBα antibody that recognizes both WT and dominant negative IκBα demonstrates that IκBα levels drop with etoposide treatment as a result of protein dissociation from NF-κB and subsequent ubiquitination and degradation. This fails to occur in DNIκBα H157 cells. (**e**) Loss of NF-κB activity in DNIκBα H157 cells results in more rapid and more aggressive tumor growth in nude mouse xenografts. We injected DNIκBα and WT H157 cells into the posterior flanks of nude mice to assess *in vivo* growth characteristics. DNIκBα H157 cells grow more rapidly and to a larger maximal volume over a growth period of 31 days with P decreasing below 0.005 by day 17. Means are from volumes of 38 individual tumors while error bars are s.e.m. (**f**) The aggressive growth pattern of DNIκBα H157 cells in nude mouse xenografts is not the result of a shortened cell cycle. Growth curves for WT H157, DNIκBα H157 and vector alone H157 cells are comparable, demonstrating that the accelerated rate of growth and aggressive tumor phenotype of DNIκBα H157 cells in nude mouse xenografts is not the result of an altered cell cycle. Means displayed are from duplicate samples of two independent experiments

grow with a comparable but somewhat slower doubling time relative to WT H157 cells (Figure 1f).

NF-κB is required for genotoxin but not paclitaxel-induced apoptosis

Treatment of WT H157 cells with 300 nM doxorubicin resulted in 32% apoptosis over 48 h. This is inhibited by almost 50% in DNIκBα H157 cells with an apoptotic index of 17% after a similar treatment with doxorubicin (not shown). This is comparable apoptotic suppression as was seen with 100 μM etoposide treatment (Figure 1a). However, to determine the specificity of NF-κB in genotoxin induced apoptosis, we treated cells with the microtubule toxin paclitaxel. Paclitaxel induces apoptosis primarily through phosphorylation and subsequent inactivation of Bcl-2. The phosphorylation renders Bcl-2 unable to sequester proapoptotic Bcl-2 family members such as Bax which induce mitochondria release of cytochrome *c* (Srivas-

tava *et al.*, 1999; Strobel *et al.*, 1996). Figure 2a shows the response of WT and DNIκBα H157 cells exposed to 30 nM and 300 nM paclitaxel for 24 h. Fifty to 52% of WT H157 cells are apoptotic after 24 h for both paclitaxel doses while 40% and 46% of DNIκBα H157 cells are apoptotic after 30 and 300 nM paclitaxel treatment, respectively. Paclitaxel-induced apoptosis was not significantly dependent on NF-κB activation, whereas loss of NF-κB activation in DNIκBα expressing cells resulted in significant resistance to both etoposide and doxorubicin.

In agreement with the *in vitro* results, analysis of xenografts in nude mice indicated sensitivity of WT H157 and DNIκBα H157 cell-derived tumors to treatment with paclitaxel (Figure 2b,c). The result with paclitaxel is in sharp contrast to the etoposide resistance of DNIκBα H157 cells *in vitro* as well as in xenografts. Wild type H157 xenograft growth is suppressed with etoposide treatment with a separation of growth curves reaching statistical significance by day 21 (Figure 2d). In contrast, DNIκBα xenografts are resistant to etoposide (Figure 2e). Despite treatment with etoposide, DNIκBα xenografts continue to grow at the same rate as untreated DNIκBα expressing tumors. These findings indicate that inhibition of NF-κB function in H157 cells results in a more aggressive tumor that is refractory to treatment with etoposide, similar to the anti-apoptosis and chemo-resistance of DNIκBα expressing H157 cells assayed *in vitro* (Figure 1a).

Etoposide induces surface expression of TRAIL and DR5

Increased cell surface expression of TRAIL is a general response to etoposide in both lung and breast epithelium (Figure 3). Using non-transformed, non-immortalized primary human airway epithelium (HAEC) and primary human mammary epithelium (HMEC) in conjunction with A549 lung adenocarcinoma, MDA-231 breast carcinoma, and ZR-75-1 breast caricinoma cells, we measured cell surface expression of TRAIL in response to 24 h of 100 μM etoposide. All five unstimulated cell lines had no detectable surface TRAIL expression (left column). Reproducible increases of 1.6–3.1-fold (middle and right column) were demonstrated after etoposide treatment. Bar graphs display the relative fluorescence for each cell line with and without etoposide (right column).

The chemo-resistance of DNIκB expressing H157 cells *in vitro* and *in vivo* indicates a major change in apoptotic potential resulting from loss of NF-κB signaling. We had previously shown that TRAIL and DR5 expression in different cell types was NF-κB

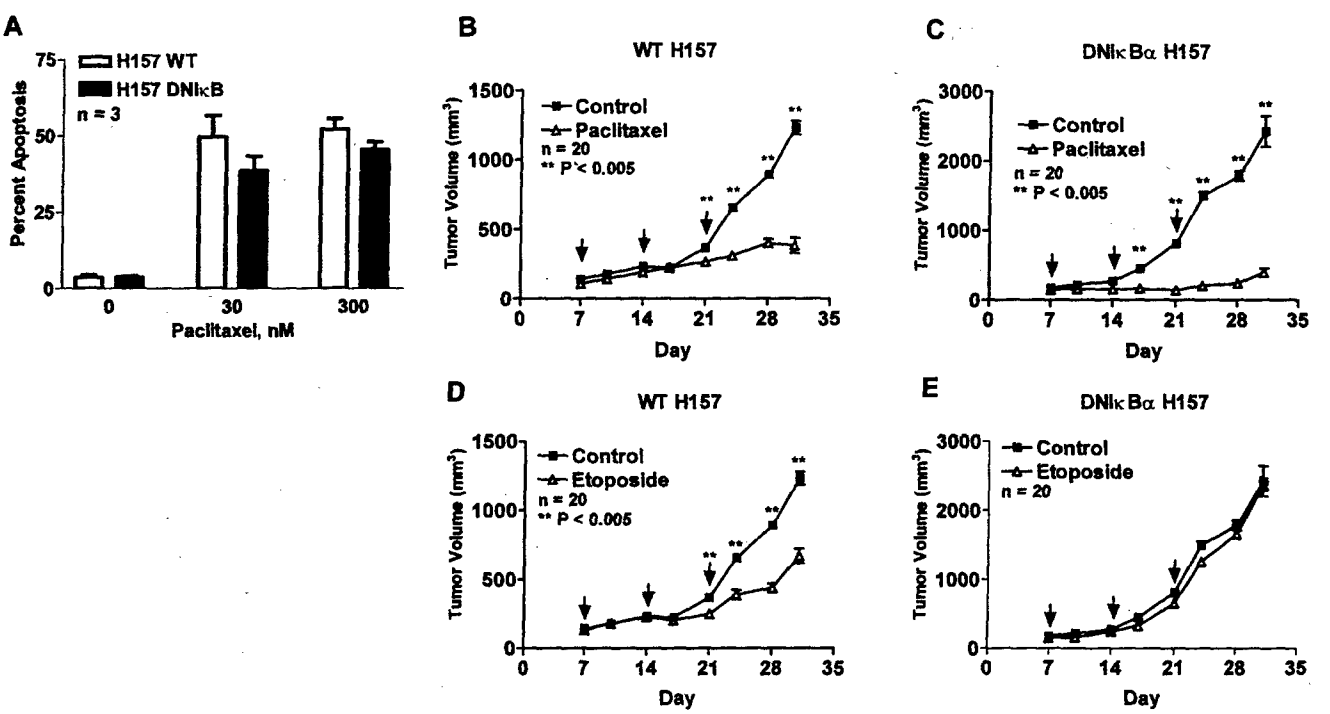

Figure 2 NF-κB inhibition causes genotoxin-specific chemo-resistance in lung tumors. (**a**) DNIκBα does not protect against the microtubule toxin paclitaxel. Treatment of WT and DNIκBα H157 cells for 24 h with the indicated doses of paclitaxel induces apoptosis to similar levels. Means displayed are from duplicate samples of three independent experiments. To validate these results, we xenografted WT and DNIκBα H157 cells into nude mice and treated with etoposide or paclitaxel. Arrows indicate days of treatment with paclitaxel (**b** and **c**) or etoposide (**d** and **e**). (**b**) WT H157 xenografts fail to grow when treated with paclitaxel chemotherapy ($P<0.005$ by day 21, $n=20$ tumors). (**c**) DNIκBα H157 xenografts also respond to paclitaxel chemotherapy with blunted tumor growth curves ($P<0.005$ by day 17, $n=20$ tumors). (**d**). Etoposide treatment of WT H157 xenografts inhibits tumor growth ($P<0.005$ by day 21, $n=20$ tumors). (**e**) DNIκBα xenografts grow despite treatment with etoposide (P = NS between vehicle and etoposide treated animals, $n=20$ tumors). DNIκBα xenografts demonstrate etoposide chemo-resistance

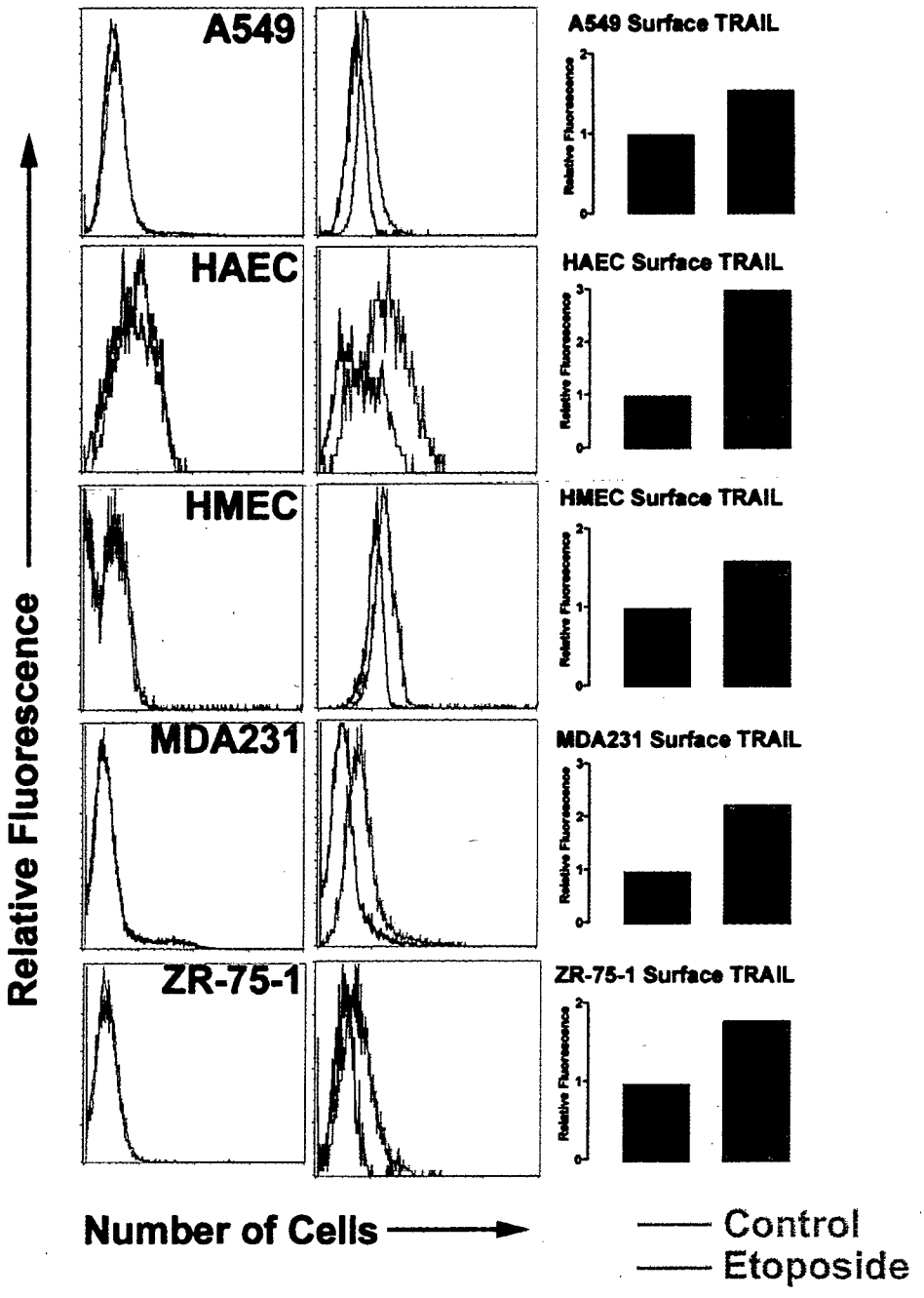

Figure 3 Etoposide induces surface expression of TRAIL. Primary human mammary (HMEC) and lung epithelial cells (HAEC), A549 and H157 lung carcinoma cells, MDA-231 and ZR-75-1 breast carcinoma cells were analysed for TRAIL surface expression in response to 24 h of 100 μM etoposide treatment. The left column indicates cell surface expression of TRAIL (blue line) versus background fluorescence (black line) of unstimulated cells. The middle column contains histograms of TRAIL surface expression (red line) compared to background fluorescence (black line) after 24 h of etoposide treatment. Relative fluorescences for each cell type in unstimulated (blue bars) and etoposide treated (red bars) are depicted in the graphs in the right column. All signals are normalized to background and set to one; therefore a relative fluorescence of one indicates no detectable surface protein

dependent (Gibson *et al*., 2000), therefore, we predicted that a loss in the surface expression of TRAIL or its death promoting receptors, DR4 and DR5, could account for the loss in genotoxin sensitivity we observed in DNIκB expressing H157 cells. To test this hypothesis, WT and DNIκBα H157 cells were treated with 100 μM etoposide for 24 h and subjected to flow cytometric analysis for measurement of DR4, DR5 and TRAIL cell surface expression. Figure 4a and b depict the surface expression of DR4 in WT H157 and DNIκBα H157 cells with and without etoposide treatment. Figure 4c shows this data in bar graph format in order to display the relative DR4 expression with and without etoposide treatment of cells. WT H157 cells

demonstrate DR4 surface expression of 15.3 ± 0.6 and 18.1 ± 1.7 ($n=3$, $P<0.05$) times greater than background with and without etoposide treatment, respectively. No significant difference in DR4 surface expression is seen in DNIκBα H157 cells, which demonstrate comparable DR4 surface expression ratios of 12.2 ± 0.9 and 17.0 ± 0.5 ($n=3$, $P<0.05$) with and without etoposide treatment, respectively. The levels of DR4 expression correlates with RNase protection assays measuring DR4 transcript (data not shown). Although DR4 surface expression levels decrease in both WT and DNIκBα H157 cells in response to etoposide, the magnitude of change being less than 50% stands in direct contrast to DR5.

DR5 surface expression increases with etoposide treatment in WT H157 cells, and this induction of surface expression is inhibited in DNIκBα H157 cells (Figure 4d, e, and f). Basal levels of DR5 in WT H157 cells drop from a relative surface expression of 13.1 ± 0.5 in wild type to 9.2 ± 0.3 ($n=3$, $P<0.001$) in DNIκBα H157 cells. More importantly, etoposide induced expression of DR5 with a surface expression ratio of 24.5 ± 2.3 in wild type cells drops significantly to 6.8 ± 0.2 ($n=3$, $P<0.0005$) in DNIκBα H157 cells (Figure 4f).

TRAIL surface expression in WT H157 cells treated with etoposide is also up-regulated as seen in Figure 4g and i. While WT H157 cells treated with etoposide induce surface expression of TRAIL 1.6-fold, this induction is absent in DNIκBα H157 cells (Figure 4h and i). The surface expression of TRAIL is relatively low but highly reproducible in its induction by etoposide ($n=3$, $P<0.01$). Etoposide therefore induces increased surface expression of TRAIL and one of its death promoting receptors, DR5. This is a NF-κB dependent response, as DNIκBα H157 cells lack the ability to increase the surface expression of both TRAIL and DR5 in response to etoposide.

Profiling the genotoxin response of H157 cells

NF-κB activation in several cell types appears to promote cell survival not apoptosis as observed with H157 cells (Baeuerle and Baltimore, 1996; Basu *et al.*, 1998; Lin *et al.*, 1998). The expression of the inhibitors of apoptosis, or IAPs, inhibit specific

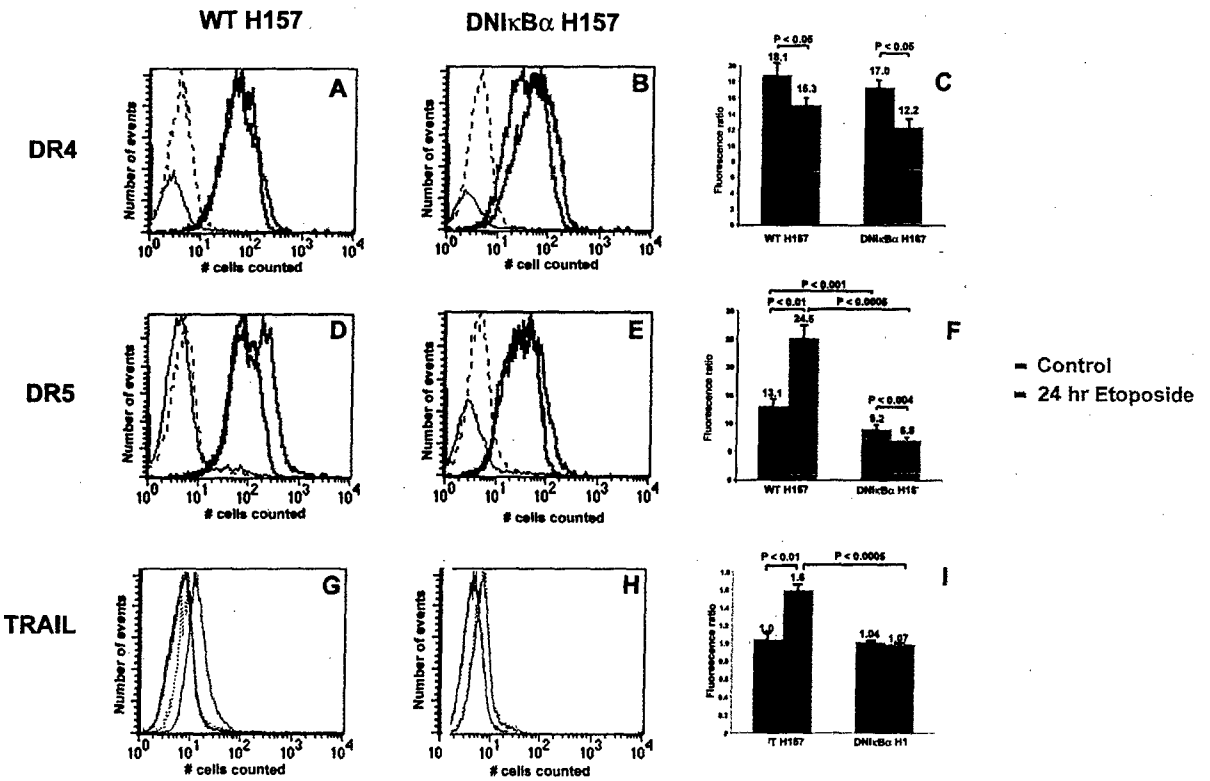

Figure 4 NF-κB induces the surface expression of DR5 and TRAIL. To determine if NF-κB mediates changes in DR4, DR5, or TRAIL surface protein expression, flow cytometry was conducted on WT (**a, d, g**) or DNIκBα H157 cells (**b, e, h**) to assess for DR4 (**a, b**), DR5 (**d, e**), and TRAIL (**g, h**) proteins. Solid black lines represent control background fluorescence; dashed black lines represent etoposide background fluorescence. Untreated cells (blue lines) were compared with cells treated with etoposide for 24 h at 100 μM (red lines). Figures **c, f,** and **i** depict data obtained in their respective rows in bar graph format. Numbers correspond to the relative fluorescence indicative of surface protein. This flow cytometry data demonstrates that etoposide induces the surface expression of DR5 and TRAIL in WT H157 cells (**f, i**). DNIκBα cells demonstrate a diminished basal level of DR5 as well as a loss of DR5 induction with etoposide treatment (**f**). Etoposide-induced TRAIL expression is also lost in DNIκBα cells compared with WT H157 cells (**i**). Histograms represent one experiment of three; means of these experiments are depicted in the bar graphs with error bars demonstrating s.e.m.

caspases and have been shown to be positively regulated by NF-κB. Thus, in addition to TRAIL and DR5, NF-κB is capable of regulating pro-survival genes. To define NF-κB regulated genes that contribute to pro- or anti-apoptotic signaling in response to genotoxins in cancer, gene profiling was conducted with total RNA isolated from WT and DNIκBα H157 cells. H157 cells stably expressing DNIκBα and DNIκBα-adenovirus infection of H157 cells were used for analysis with similar results in profiling the gene expression response to etoposide treatment. Hu6800 Affymetrix gene chips compared mRNA levels of 7129 genes between WT and DNIκBα expressing H157 cells treated for 0, 12, or 24 h with either 100 μM etoposide or DMSO treated control cells. Using this approach we were able to define genes whose expression is dependent on NF-κB transcriptional activity in the presence or absence of etoposide.

Figure 5 presents the list of genes regulated in a NF-κB dependent mechanism in response to etoposide. Database review revealed that 33% (17/52) of the 52 genes identified as NF-κB-dependent have been previously identified as regulated by NF-κB. This percentage is likely higher as many of the genes have no information regarding the role of NF-κB in controlling their expression. From a total of 52 genes dependent on NF-κB activation for regulation of their expression, 13 etoposide inducible genes were readily identified that have previously characterized functions that can clearly promote or inhibit apoptosis (Figure 5a). The values listed in Figures 5a and b indicate the etoposide induced fold change in WT cells that was absent in DNIκBα expressing cells. Two etoposide induced genes, A20 (Cooper *et al.*, 1996; Krikos *et al.*, 1992) and manganese superoxide dismutase (SOD2) (Jones *et al.*, 1997) are well defined in their regulation by NF-κB. Three genes having strong anti-apoptotic functions, the inhibitors of apoptosis (cIAP-1, cIAP-2 and XIAP), are induced by etoposide treatment. Forkhead FREAC-1 is a lung specific forkhead transcription factor and whose mRNA was increased sixfold in response to etoposide in an NF-κB-dependent mechanism (Hellqvist *et al.*, 1996; Mahlapuu *et al.*, 1998; Pierrou *et al.*, 1994). Specific forkhead transcription factors have been implicated in regulating pro-apoptotic gene expression including Fas ligand (Brunet *et al.*, 1999). Trefoil factor is a cytokine known to promote cell survival (Chen *et al.*, 2000; Suemori *et al.*, 1991; Taupin *et al.*, 2000; Thim, 1989), as is cell adherence to the extracellular matrix protein, fibronectin (Sakai *et al.*, 2001; Zhang *et al.*, 1995). The expression of both trefoil factor and fibronectin was NF-κB dependent and markedly inhibited in response to etoposide. Overall, of the 13 genes whose function has been clearly associated with survival and/or apoptosis, 11 were up-regulated and two down-regulated in response to etoposide in a NF-κB dependent mechanism.

Granted many other genes are regulated in response to etoposide (Figure 5b) or by NF-κB independent of etoposide (Figure 5c) that may regulate cell survival. In addition, genes not represented in the array may have significant roles in the response to genotoxin. Despite these limitations, the gene profiles identified in Figure 5a argue for an orchestrated response of cells exposed to etoposide that promotes survival versus the paracrine death response mediated by TRAIL. Genotoxins such as etoposide, in addition to inhibiting DNA replication, also generate oxygen radicals that cause cellular damage and can themselves induce apoptosis (Verhaegen *et al.*, 1995). Reactive oxygen species activate NF-κB (Wang *et al.*, 1999) and a compensatory SOD2 expression results in oxygen radical metabolism and protection from further cellular damage. A20 inhibits receptor activation of NF-κB and is well characterized in its ability to inhibit TNF-induced apoptosis (Opipari *et al.*, 1992). A20 expression would be predicted to protect cells from genotoxins by suppressing death receptor signaling. The strong induction of cIAP-1 and cIAP-2 would inhibit the caspases that drive cells down the apoptotic pathway (Chu *et al.*, 1997; Wang *et al.*, 1998). In contrast, the induction of TRAIL and DR5 would stimulate caspases that drive the apoptotic response. Induction of TNF receptor expression may also contribute to a pro-apoptotic response. Clearly, the NF-κB-dependent response to etoposide is complex and shows a response that allows cells to survive or die. NF-κB-dependent gene expression in response to etoposide is neither pro-survival nor anti-survival but rather allows a decision process for cell fate.

Validation of mRNA expression profiling

The NF-κB dependent changes in mRNA expression were confirmed for four genes, two with clear functions in apoptosis and two in controlling cell cycle or signaling. cIAP-1 and 2, cyclin D2 and MEK5c expression was monitored by relative reverse transcription PCR (RT–PCR). Results shown in Figure 6 depicts the fold-changes in RNA levels by Sybr-green RT–PCR analysis of total RNA harvested after 24 h treatment with etoposide in WT and DNIκBα H157 cells. RNA concentrations were controlled with internal 18S RNA standardized curves. The induction of cIAP-1 and cIAP-2 was blocked in DNIκBα H157 cells compared with WT H157 such that WT cells had 11 ± 3.7 and 37 ± 21-fold higher levels of cIAP-1 and cIAP-2 respectively. Changes in expression of cyclin D2 and MEK5c were similarly confirmed, indicating the general validity of the expression profiles shown in Figure 5.

IAP expression promotes H157 cell survival

Because IAPs are strongly induced by genotoxin treatment, we chose to examine whether expression of the IAP proteins cIAP-1 and cIAP-2 could inhibit etoposide-induced apoptosis. Expression vectors containing the sequences for cIAP-1 and cIAP-2 were generated in IRES vectors encoding green fluorescent

A **Etoposide regulated genes associated with apoptosis or cell survival**

Etoposide Induced Fold Change in WT H157 Cells	Gene Name
30	cIAP-1
27	cIAP-2
6	Forkhead transcription factor FREAC
5.3	TNFR
3.4	NFkB2
3	DR5*
2.7	A20
2.5	Rel B
2.4	Manganese superoxide dismutase
2	XIAP
2	TRAIL*
-42	Fibronectin
-30	Trefoil factor

B **Other etoposide regulated genes**

Etoposide Induced Fold Change in WT H157 Cells	Gene Name	Etoposide Induced Fold Change in WT H157 Cells	Gene Name
30	ICAM-1	-23.7	RGS4
14.3	Cyclin D2	-14.3	MEK5c
12.8	MDA-7	-6.7	C1 inhibitor
9	Pentaxin	-5.1	Gelsolin
9	Groα	-3.7	Apolipoprotein E
6.4	Osteonidogen	-3.7	IFNγ receptor 2
6.2	B94 protein	-3.6	Carbonic anhydrase IX
4.6	HREV107 tumor suppressor	-3.5	Dual specificity phosphatase 4
4.5	Bloom syndrome protein	-3.1	IRS-1
4.3	GTP cyclohydrolase	-3	Plectin
2.8	CD3-associated protein	-2.8	Transgelin
2.5	E6-AP oncogene	-2.8	Histone H4
2.4	Homeotic protein PL2	-2.6	NADH ubiquinone oxidoreductase
2	BRCA1 associated protein	-2.3	Sortilin 1
		-2.3	Glioma pathogenesis related protein
		-2.2	CRABP II

C **NFkB-regulated genes in the absence of etoposide**

Fold change: ratio WT/DNIkB H157 cells	Gene Name	Fold change: ratio WT/DNIkB H157 cells	Gene Name
3	Cytidine deaminase	-10.5	Collagen type XV
2.7	IL-11	-6.8	Predicted osteoblast protein
2.6	MHC class 1 polypeptide	-6.8	GS3955 serine/threonine kinase
2.6	TEA domain family member 4		
2	KIAA0018 gene product		

Figure 5 Gene-profiling identifies NF-κB as a regulator of both pro- and anti-apoptotic signaling. Only genes whose expression was similar across all three time points and whose fold change was two or greater by both GeneChip and GeneSpring mathematical algorithms are included in the final gene lists. (**a**) Gene profiling identifies important apoptotic mediators whose expression is dependent upon NF-κB in the presence of etoposide. The asterisk on TRAIL and DR5 indicate they are not on the Hu6800 gene chip. RNase protection assays with probes for TRAIL and DR5 were performed on the RNA samples and quantitated in response to etoposide. (**b**) Etoposide also altered expression of other genes in an NF-κB dependent manner. (**c**) NF-κB also regulates genes independent of etoposide. Individual analysis of gene profiles with GeneChip and GeneSpring software identifies additional NF-κB dependent proteins with both pro- and anti-apoptotic roles in response to genotoxin insult

protein (GFP) for selection by flow cytometry. H157 cell populations selected for GFP expression demonstrated overexpression of cIAP-1 and cIAP-2 greater than 10-fold compared with H157 cells harboring empty IRES-GFP vector and wild type H157 cells as determined by Sybr-green RT–PCR (data not shown). Figure 7 shows the results of apoptosis assays for the various H157 cell lines when exposed to 100 μM etoposide for 24 h. Wild type H157 cells and H157 cells harboring empty vector had $23\pm1.2\%$ and $21\pm1.4\%$ of the cell population apoptotic following etoposide treatment, respectively. Overexpression of cIAP-1 or cIAP-2 resulted in a significantly ($P<0.05$) inhibited apoptotic response to etoposide with $10\pm2.8\%$ and $12\pm1.8\%$ of the cells undergoing apoptosis, respectively. Thus, increased expression of IAPs results in a 50% diminution in apoptosis in H157 cells treated with etoposide. The results indicate that induction of IAPs would have a survival function in response to etoposide. Etoposide therefore induces expression of several genes that influence cell survival including TRAIL and its death receptor, DR5, and IAPs. The cumulative action of these proteins dictate cell survival.

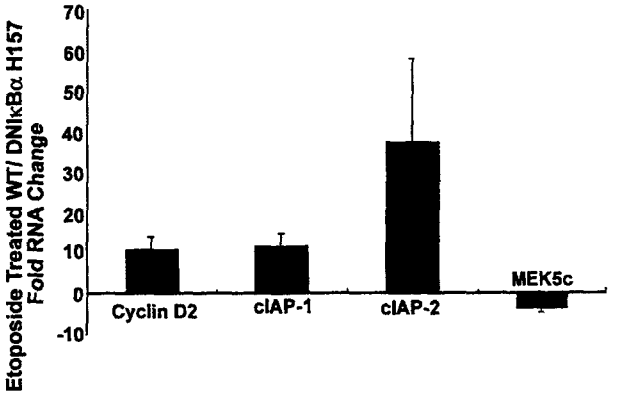

Figure 6 Gene profiling validations confirm the importance of endogenous apoptotic mediators in genotoxin-induced apoptosis. To further validate identified gene profiles, Sybr-green relative RT–PCR was performed with total RNA obtained from WT H157 and DNIκBα H157 cells using primers corresponding to cyclin D2, cIAP-1, cIAP-2 and MEK5c. The graph represents the mean RNA fold change between WT H157 and DNIκBα H157 cells treated with etoposide from two independent experiments performed in triplicate while error bars are s.e.m.

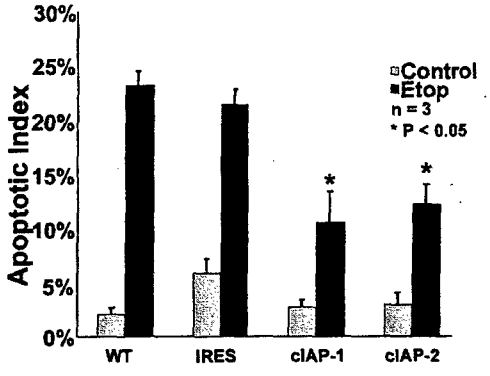

Figure 7 NF-κB-mediated induction of DR5/TRAIL overcomes the endogenous activity of cIAP-1 and cIAP-2. H157 cells stably expressing cIAP-1 or -2 were made to determine if IAP over expression counteracts the death receptor apoptotic response to etoposide. WT H157 cells or H157 cells stably harboring IRES vector alone, cIAP-1, or cIAP-2 expression vectors were treated with or without etoposide and apoptosis was quantitated. Expression of cIAP-1 and -2 blunted the apoptotic response of H157 cells to etoposide by 50%. Data bars indicate the mean of three independent experiments performed in duplicate while error bars are s.e.m.

Suppression of TRAIL death receptor signaling leads to chemo-resistance

Induction of TRAIL expression in response to genotoxins strongly correlates with the magnitude of apoptosis that is observed in normal lung and breast epithelium and carcinoma (Figure 8a). Cell surface TRAIL expression correlates with the apoptotic response to etoposide for primary human airway epithelium, H157 lung squamous carcinoma cells, A549 lung adenocarcinoma cells, ZR-75-1, and MDA-231 human breast adenocarcinoma cells. To test the prediction that cell surface TRAIL expression is an important autocrine or paracrine response to genotoxin-induced cell death, we stably expressed in H157 cells the GPI-linked decoy receptor, DcR1, which binds TRAIL but does not signal caspase activation (Sheridan *et al.*, 1997). DcR1 expression functions to bind TRAIL and effectively block TRAIL-induced apoptosis. The etoposide dose response curves seen in Figure 8b demonstrate that as the dose of genotoxin increases, the degree of apoptosis also increases in WT H157 cells. With etoposide doses ranging from 1–100 μM with 48 h treatment, WT H157 cells displayed apoptotic responses ranging from 18–52%. Two separate stable clones of H157 cells expressing DcR1, as confirmed by flow cytometry analysis of cell surface expression (data not shown), suppress etoposide-induced apoptosis relative to control H157 cells. H157 cells expressing DcR1 suppress etoposide induced apoptosis rates by greater than 50% to levels of 6–24% over the same dose range used with WT H157 cells ($n=3$, $P<0.05$ at all doses). DcR1 expression has a strong protective effect against etoposide induced cell death, consistent with a significant role for TRAIL in the death response and diminished TRAIL signaling in chemo-resistance to etoposide. Figure 8c demonstrates that DcR1 protects against doxorubicin induced apoptosis as well. WT H157 cells increased from 4 ± 1% to 35 ± 3% apoptosis with 300 nM and 37 ± 2% apoptosis with 1 μM doxorubicin treatment. Two separate stable clones of H157 cells expressing DcR1 suppressed the doxorubicin induced apoptosis at 300 nM (22 ± 0% for clone 1, 11 ± 4% for clone 2, $P<0.05$ vs WT) and at 1 μM (20 ± 1% for clone 1, 16 ± 4% for clone 2, $P<0.05$ vs WT). A similar effect of DcR1 is seen in MDA-231 breast adenocarcinomas (not shown), demonstrating the protective role of DcR1 against genotoxins is a general function of the decoy receptor and not a unique response in H157 cells. The protective effect of DcR1 expression is selective for genotoxins such as etoposide and doxorubicin and is not seen with paclitaxel-induced H157 cell death (Figure 8d), confirming a significant role for TRAIL expression in the apoptotic response to specific genotoxins but not microtubule toxins. Paclitaxel induced apoptosis to similar levels in WT and two separate DcR1 clones; 30 nM induced 52 ± 6% in WT vs 58 ± 1% in clone 1 vs 47 ± 1% in clone 2 while 300 nM induced 52 ± 4% in WT vs 62 ± 1% in clone 1 vs 51 ± 5% in clone 2.

Discussion

Two different but converging experimental lines of study are defining the importance of TRAIL-mediated death signaling in cancer. Several studies have begun to define mutations in the death receptors for TRAIL in different cancers. In metastatic breast cancer (Han *et al.*, 2001), head and neck squamous cell cancer (Fisher *et al.*, 2001; Ozoren *et al.*, 2000; Pai *et al.*, 1998), lung cancer (Fisher *et al.*, 2001; Lee *et al.*, 1999; Wu *et al.*, 2000), and non-Hodgkin's lymphoma (Lee *et al.*, 2001) mutations have been defined in the death receptors for TRAIL. In numerous other cancers changes in the expression profile of TRAIL death receptors has also

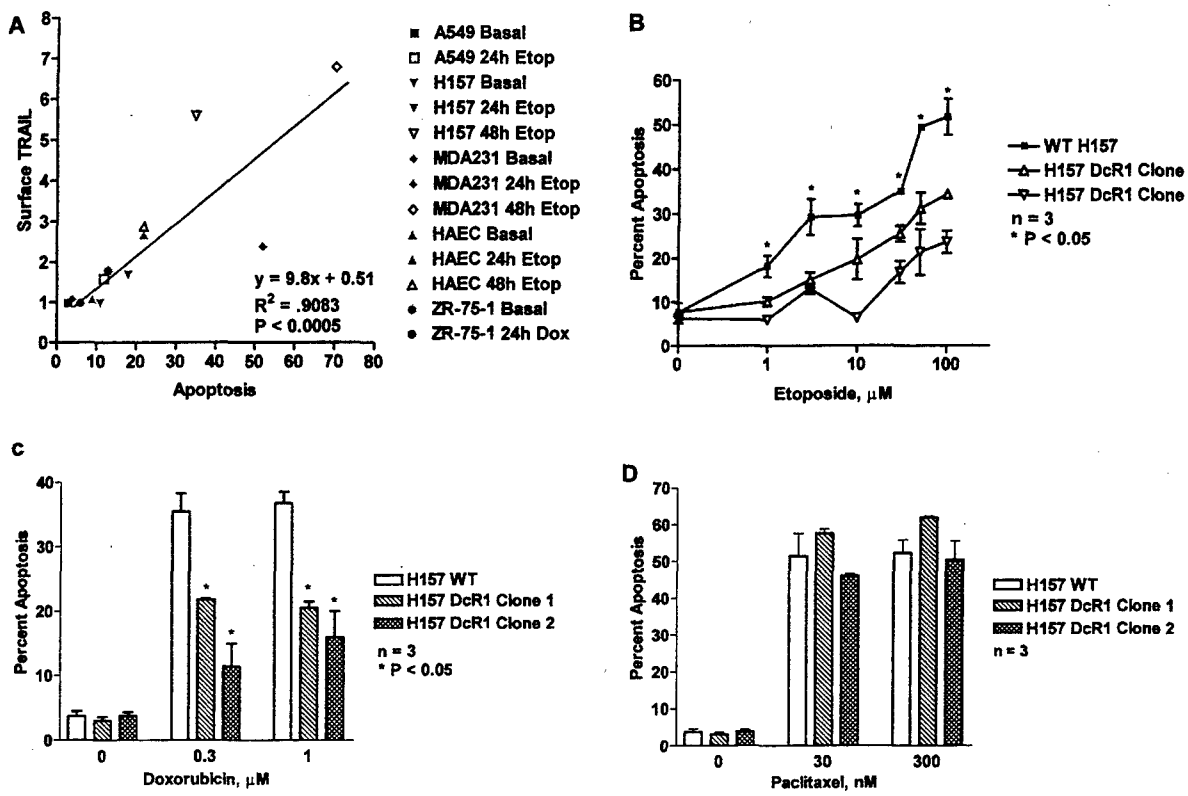

Figure 8 TRAIL mediates genotoxin-specific apoptosis. (**a**) Genotoxin-induced apoptosis correlates with TRAIL surface expression. Primary human lung airway epithelial cells (HAEC), A549 and H157 lung carcinoma cells, MDA-231 and ZR-75-1 breast carcinoma cells were analysed for TRAIL surface expression and degree of apoptosis with and without etoposide or doxorubicin. A linear correlation between surface expression of TRAIL and per cent apoptosis is seen in these cell lines with $R^2 = 0.903$, demonstrating that genotoxins induce TRAIL expression with a concomitant induction in apoptotic response. (**b**) Stable expression of DcR1 in H157 cells results in chemo-resistance to etoposide-induced apoptosis in a dose-dependent fashion. WT H157 or H157 stably expressing surface DcR1 cells were treated with a range of etoposide doses and assessed for apoptosis. Data points represent the means of duplicate samples from two independent experiments while error bars are s.e.m. (**c**, **d**). DcR1 expression correlates with chemo-resistance to doxorubicin (**c**), but not paclitaxel (**d**). Apoptosis assays demonstrate that DcR1 suppresses doxorubicin-induced apoptosis, but is unable to inhibit paclitaxel-induced apoptosis. The apoptotic pathway affected by DcR1-induced chemo-resistance is specific for etoposide and doxorubicin, suggesting an alternate paclitaxel-specific apoptotic pathway. For **c** and **d**, means are from duplicate samples of experiments done on three separate occasions while error bars are s.e.m.

been defined. Cumulatively, these studies indicate that expression or function of receptors that signal TRAIL-induced apoptosis is altered at frequencies approaching 50% in some cancers. Although the significance of these mutations is presently unclear, their frequency and potential survival advantage suggests they may contribute to tumorigenesis and possibly metastasis. TRAIL also has been shown to be decreased in oligodendrogliomas (Nakamura *et al.*, 2000). Our work and that of others are defining an involvement of a paracrine action for TRAIL-induced apoptosis in chemotherapy (Altucci *et al.*, 2001; Gibson *et al.*, 2000). Paracrine TRAIL-induced apoptosis is important for genotoxins like etoposide and doxorubicin but less important for the apoptotic response to microtubule toxins. Mutations that inhibit TRAIL receptor signaling or diminish TRAIL expression should promote resistance to chemotherapy.

What is the evidence that a paracrine TRAIL-induced apoptosis response is important in chemotherapy? Flow cytometric analysis clearly demonstrates that etoposide and doxorubicin stimulate cell surface expression of TRAIL in normal epithelium and multiple epithelia-derived carcinoma cell lines. The use of a soluble DR4:Fc fusion protein that binds TRAIL effectively suppresses genotoxin-induced apoptosis (Gibson *et al.*, 2000). This finding demonstrates that surface TRAIL expression contributes to genotoxin-induced cell death. Similarly, reovirus-induced apoptosis involves expression of TRAIL in epithelial-derived tumor cell lines that is inhibited by DR4:Fc fusion proteins or anti-TRAIL antibodies (Clarke *et al.*, 2000). In both studies the use of TNFα or Fas ligand protein traps or antibodies did not inhibit cell death, demonstrating the specificity of TRAIL in both genotoxin and virus-induced apoptosis. We have also used an alternative strategy, namely the expression of the TRAIL decoy receptor, DcR1, to inhibit genotoxin but not paclitaxel-induced apoptosis. DcR1, DR4:Fc and anti-TRAIL antibody suppression of genotoxin-induced apoptosis all demonstrate the importance of cell surface expression of TRAIL in specific apoptotic responses in epithelial-derived carcinomas. Interestingly, both geno-

toxin- and reovirus-induced expression of TRAIL is dependent on functional NF-κB signaling and inhibited by DNIκB. It was also recently shown that retinoic acid-induced apoptosis of acute promyelocytic leukemia cells is mediated by a paracrine TRAIL action (Altucci *et al.*, 2001). Cumulatively, the findings indicate paracrine TRAIL-induced apoptosis is a major contributing mechanism to the action of different drugs and viral-induced apoptosis of tumor cells.

Profiling the NF-κB-dependent response to etoposide demonstrates the induction of many genes including TRAIL and the IAPs. The IAPs are markedly induced in response to genotoxins and have the ability to significantly inhibit etoposide-mediated cell killing. We did not observe a significant change in expression of Bcl-X_L or any other Bcl-2 family member in H157 cells. Furthermore, the use of paclitaxel, a microtubule toxin that induces apoptosis primarily through phosphorylation and inactivation of Bcl-2 (Srivastava *et al.*, 1999; Strobel *et al.*, 1996), did not depend on NF-κB activity for initiating programmed cell death. At least in H157 lung squamous carcinoma cells, our studies would argue that NF-κB-dependent IAP expression is a significant mechanism for the survival function of NF-κB signaling. These findings indicate that activation of NF-κB in response to genotoxins stimulates a TRAIL death response and an IAP survival response. In different cancers, the magnitude of TRAIL expression for paracrine-mediated apoptosis versus IAP expression for survival is going to influence the chemo-sensitivity of the tumor. For example, tumor cells that lose the TRAIL paracrine response may be particularly chemo-resistant. Clinically, the administration of recombinant TRAIL concurrent with genotoxin based chemotherapy may help tilt the balance of NF-κB mediated signaling towards tumor cell apoptosis.

Materials and methods

Generation of stable clones

The cDNA for DNIκBα was excised from a CMV hIκBα 32S/32A vector and cloned into the *Hind*III/*Xba*I sites of pcDNA3.1(+). H157 cells were transfected with lipofectamine (Gibco BRL) and selected for neomycin resistance. Clones were screened for IκBα over-expression by Western blot and gel shift assay for loss of NF-κB DNA binding with nuclear extracts from cells treated with and without PMA. DcR1 stable cell lines were similarly generated with pcDNA3.1(+)/DcR1. After the clones grew to acceptable numbers, flow cytometry for surface expression of DcR1 was performed to verify G418 resistant clones over-expressing DcR1, cIAP-1, cIAP-2, and cIAP-1-AS stable clones were generated by cloning into the *Eco*R1 site of IRES vector (Clontech), selecting for G418 resistance, and performing flow cytometry to confirm GFP expression. IAP expression was confirmed by RT–PCR.

Acridine orange staining

H157 and DNIκBα H157 cells were treated with 100 μM etoposide, 30 nM paclitaxel, 300 nM paclitaxel, or 1 mM doxorubicin. At the given time points, 50 μl of a PBS solution containing 100 μg/ml acridine orange and 100 μg/ml ethidium bromide was added to pelleted cells. Cells were visualized on a fluorescent inverted microscope using a 40 × LWD lens and a high pass FITC filter to allow for nuclear visualization. At least 300 cells per plate were counted in a double blinded fashion. Only cells with both condensed chromatin and membrane blebbing were scored as apoptotic.

Flow cytometry for detection of surface expressed TRAIL, DR4, DR5 and DcR1

Anti-TRAIL, anti-DR4, anti-DR5, and anti-DcR1 antibodies were a kind gift from Immunex corporation. Flow cytometry was performed as previously described (Sedger *et al.*, 1999). Cells were analysed using a FACScan flow cytometer (Becton Dickinson) running Cell Quest Software (Becton Dickinson).

Western blotting

Western blotting was performed as previously described (Gibson *et al.*, 2000). IκBα antibody was used at a concentration of 1 : 500 (Santa Cruz).

Xenograft implantation

1×10^6 cells per 100 μl 1 × PBS and 100 μl growth factor reduced matrigel were injected on athymic nude mice posterior flanks. Tumor volumes were measured twice a week, and tumor volumes were calculated using the formula volume = length^2*width*π/6. Treated mice were given 15 mg/kg etoposide or 15 mg/kg paclitaxel intraperitoneally on days 7, 14 and 21.

Affymetrix gene chip profiling

Total RNA was isolated per manufacturer's recommendation with RNAzol (Tel-Test) from WT H157 cells and DNIκBα H157 cells treated for 0, 12, or 24 h with 100 μm etoposide (Sigma chemicals). Probes were generated per Affymetrix recommendations. Hu6800 probe arrays were then read with an argon laser in the HP GeneArray™ Scanner.

Gene profile analysis

Raw data was normalized separately in both GeneChip and GeneSpring to maximize sensitivity and specificity by using two different mathematical algorithms. All genes identified in the lists had a twofold or greater change in expression between WT H157 and Time zero, 12 h, and 24 h time points with or without etoposide treatment were treated as replicate experiments. Only genes whose expression profiles were consistent across these time points were included in the final gene lists. Further stringency was applied by excluding genes identified as absent in both groups by GeneChip.

Sybr green RT–PCR

RNA was isolated with RNAzol (Tel-Test). RNA samples were additionally treated with DNAse for 15 min at 37°C. PCR primers for amplification were selected utilizing Primer Express™ software (PE Applied Biosystems). All samples were normalized utilizing 18 s rRNA as an endogenous control. Each amplification was replicated in triplicate with total RNA isolated from three separate experiments.

References

Altucci L, Rossin A, Raffelsberger W, Reitmair A, Chomienne C and Gronemeyer H. (2001). *Nat. Med.*, **7**, 680–686.

Ashkenazi A and Dixit VM. (1999). *Curr. Opin. Cell. Biol.*, **11**, 255–260.

Baeuerle PA and Baltimore D. (1996). *Cell*, **87**, 13–20.

Basu S, Rosenzweig KR, Youmell M and Price BD. (1998). *Biochem. Biophys. Res. Commun.*, **247**, 79–83.

Brunet A, Bonni A, Zigmond MJ, Lin MZ, Juo P, Hu LS, Anderson MJ, Arden KC, Blenis J and Greenberg ME. (1999). *Cell*, **96**, 857–868.

Chaudhary PM, Eby M, Jasmin A, Bookwalter A, Murray J and Hood L. (1997). *Immunity*, **7**, 821–830.

Chen YH, Lu Y, De Plaen IG, Wang LY and Tan XD. (2000). *Biochem. Biophys. Res. Commun.*, **274**, 576–582.

Chu ZL, McKinsey TA, Liu L, Gentry JJ, Malim MH and Ballard DW. (1997). *Proc. Natl. Acad. Sci. USA*, **94**, 10057–10062.

Clarke P, Meintzer SM, Gibson S, Widmann C, Garrington TP, Johnson GL and Tyler KL. (2000). *J. Virol.*, **74**, 8135–8139.

Cooper JT, Stroka DM, Brostjan C, Palmetshofer A, Bach FH and Ferran C. (1996). *J. Biol. Chem.*, **271**, 18068–18073.

Fisher MJ, Virmani AK, Wu L, Aplenc R, Harper JC, Powell SM, Rebbeck TR, Sidransky D, Gazdar AF and El-Deiry WS. (2001). *Clin. Cancer Res.*, **7**, 1688–1697.

Gibson SB, Oyer R, Spalding AC, Anderson SM and Johnson GL. (2000). *Mol. Cell. Biol.*, **20**, 205–212.

Han J-Y, Shin M, Kim H, Lee S, Park W, Lee J, Yoo N, Kang J, Hong Y, Park C, Kim H-K and Lee K. (2001). *Proc. ASCO.*, **20**, Abstract 1657.

Hellqvist M, Mahlapuu M, Samuelsson L, Enerback S and Carlsson P. (1996). *J. Biol. Chem.*, **271**, 4482–4490.

Jones PL, Ping D and Boss JM. (1997). *Mol. Cell. Biol.*, **17**, 6970–6981.

Jurgensmeier JM, Xie Z, Deveraux Q, Ellerby L, Bredesen D and Reed JC. (1998). *Proc. Natl. Acad. Sci. USA*, **95**, 4997–5002.

Kasibhatla S, Brunner T, Genestier L, Echeverri F, Mahboubi A and Green DR. (1998). *Mol. Cell*, **1**, 543–551.

Kaufmann SH and Earnshaw WC. (2000). *Exp. Cell. Res.*, **256**, 42–49.

Krikos A, Laherty CD and Dixit VM. (1992). *J. Biol. Chem.*, **267**, 17971–17976.

Lee SH, Shin MS, Kim HS, Lee HK, Park WS, Kim SY, Lee JH, Han SY, Park JY, Oh RR, Jang JJ, Han JY, Lee JY and Yoo NJ. (1999). *Cancer Res.*, **59**, 5683–5686.

Lee SH, Shin MS, Kim HS, Lee HK, Park WS, Kim SY, Lee JH, Han SY, Park JY, Oh RR, Kang CS, Kim KM, Jang JJ, Nam SW, Lee JY and Yoo NJ. (2001). *Oncogene*, **20**, 399–403.

Li H, Zhu H, Xu CJ and Yuan J. (1998). *Cell*, **94**, 491–501.

Lin KI, DiDonato JA, Hoffmann A, Hardwick JM and Ratan RR. (1998). *J. Cell. Biol.*, **141**, 1479–1487.

Luo X, Budihardjo I, Zou H, Slaughter C and Wang X. (1998). *Cell*, **94**, 481–490.

Mahlapuu M, Pelto-Huikko M, Aitola M, Enerback S and Carlsson P. (1998). *Dev. Biol.*, **202**, 183–195.

Muzio M, Chinnaiyan AM, Kischkel FC, O'Rourke K, Shevchenko A, Ni J, Scaffidi C, Bretz JD, Zhang M, Gentz R, Mann M, Krammer PH, Peter ME and Dixit VM. (1996). *Cell*, **85**, 817–827.

Nakamura M, Rieger J, Weller M, Kim J, Kleihues P and Ohgaki H. (2000). *Acta. Neuropathol (Berl.)*, **99**, 1–6.

Opipari Jr AW, Hu HM, Yabkowitz R and Dixit VM. (1992). *J. Biol. Chem.*, **267**, 12424–12427.

Ozoren N, Fisher MJ, Kim K, Liu CX, Genin A, Shifman Y, Dicker DT, Spinner NB, Lisitsyn NA and El-Deiry WS. (2000). *Int. J. Oncol.*, **16**, 917–925.

Pai SI, Wu GS, Ozoren N, Wu L, Jen J, Sidransky D and El-Deiry WS. (1998). *Cancer Res.*, **58**, 3513–3518.

Pierrou S, Hellqvist M, Samuelsson L, Enerback S and Carlsson P. (1994). *EMBO J.*, **13**, 5002–5012.

Ravi R, Bedi GC, Engstrom LW, Zeng Q, Mookerjee B, Gelinas C, Fuchs EJ and Bedi A. (2001). *Nat. Cell. Biol.*, **3**, 409–416.

Sakai T, Johnson KJ, Murozono M, Sakai K, Magnuson MA, Wieloch T, Cronberg T, Isshiki A, Erickson HP and Fassler R. (2001). *Nat. Med.*, **7**, 324–330.

Schneider P, Bodmer JL, Thome M, Hofmann K, Holler N and Tschopp J. (1997). *FEBS Lett.*, **416**, 329–334.

Sedger LM, Shows DM, Blanton RA, Peschon JJ, Goodwin RG, Cosman D and Wiley SR. (1999). *J. Immunol.*, **163**, 920–926.

Sheridan JP, Marsters SA, Pitti RM, Gurney A, Skubatch M, Baldwin D, Ramakrishnan L, Gray CL, Baker K, Wood WI, Goddard AD, Godowski P and Ashkenazi A. (1997). *Science*, **277**, 818–821.

Srivastava RK, Mi QS, Hardwick JM and Longo DL. (1999). *Proc. Natl. Acad. Sci. USA*, **96**, 3775–3780.

Strobel T, Swanson L, Korsmeyer S and Cannistra SA. (1996). *Proc. Natl. Acad. Sci. USA*, **93**, 14094–14099.

Suemori S, Lynch-Devaney K and Podolsky DK. (1991). *Proc. Natl. Acad. Sci. USA*, **88**, 11017–11021.

Sun XM, MacFarlane M, Zhuang J, Wolf BB, Green DR and Cohen GM. (1999). *J. Biol. Chem.*, **274**, 5053–5060.

Taupin DR, Kinoshita K and Podolsky DK. (2000). *Proc. Natl. Acad. Sci. USA*, **97**, 799–804.

Thim L. (1989). *FEBS Lett.*, **250**, 85–90.

Tzung SP, Kim KM, Basanez G, Giedt CD, Simon J, Zimmerberg J, Zhang KY and Hockenbery DM. (2001). *Nat. Cell. Biol.*, **3**, 183–191.

Verhaegen S, McGowan AJ, Brophy AR, Fernandes RS and Cotter TG. (1995). *Biochem. Pharmacol.*, **50**, 1021–1029.

Wang CY, Mayo MW, Korneluk RG, Goeddel DV and Baldwin Jr AS. (1998). *Science*, **281**, 1680–1683.

Wang S, Leonard SS, Castranova V, Vallyathan V and Shi X. (1999). *Ann. Clin. Lab. Sci.*, **29**, 192–199.

Wu WG, Soria JC, Wang L, Kemp BL and Mao L. (2000). *Anticancer Res.*, **20**, 4525–4529.

Yang J, Liu X, Bhalla K, Kim CN, Ibrado AM, Cai J, Peng TI, Jones DP and Wang X. (1997). *Science*, **275**, 1129–1132.

Zha J, Harada H, Yang E, Jockel J and Korsmeyer SJ. (1996). *Cell*, **87**, 619–628.

Zhang Z, Vuori K, Reed JC and Ruoslahti E. (1995). *Proc. Natl. Acad. Sci. USA*, **92**, 6161–6165.

Zou H, Li Y, Liu X and Wang X. (1999). *J. Biol. Chem.*, **274**, 11549–11556.

JOURNAL OF VIROLOGY, Mar. 2002, p. 2585–2594 Vol. 76, No. 6
0022-538X/02/$04.00+0 DOI: 10.1128/JVI.76.6.2585–2594.2002

Reovirus-Induced Alterations in Gene Expression Related to Cell Cycle Regulation

George J. Poggioli,[1] Roberta L. DeBiasi,[2,3] Ryan Bickel,[3] Robert Jotte,[4,5] Aaron Spalding,[4] Gary L. Johnson,[4,6,7] and Kenneth L. Tyler[1,3,8,9,10]*

Departments of Neurology,[3] Pediatrics,[2] Medicine,[8] Hematology and Oncology,[5] Microbiology,[1] Pharmacology,[4] and Immunology,[9] University of Colorado Health Sciences Center, and Neurology Service, Denver Veterans Affairs Medical Center,[10] Denver, Colorado 80220, and Program in Molecular Signal Transduction[6] and Division of Basic Sciences,[7] National Jewish Center for Immunology and Respiratory Medicine, Denver, Colorado 80206

Received 9 July 2001/Accepted 30 November 2001

Mammalian reovirus infection results in perturbation of host cell cycle progression. Since reovirus infection is known to activate cellular transcription factors, we investigated alterations in cell cycle-related gene expression following HEK293 cell infection by using the Affymetrix U95A microarray. Serotype 3 reovirus infection results in differential expression of 10 genes classified as encoding proteins that function at the G_1-to-S transition, 11 genes classified as encoding proteins that function at G_2-to-M transition, and 4 genes classified as encoding proteins that function at the mitotic spindle checkpoint. Serotype 1 reovirus infection results in differential expression of four genes classified as encoding proteins that function at the G_1-to-S transition and three genes classified as encoding proteins that function at G_2-to-M transition but does not alter any genes classified as encoding proteins that function at the mitotic spindle checkpoint. We have previously shown that serotype 3, but not serotype 1, reovirus infection induces a G_2-to-M transition arrest resulting from an inhibition of cdc2 kinase activity. Of the differentially expressed genes encoding proteins regulating the G_2-to-M transition, chk1, wee1, and GADD45 are known to inhibit cdc2 kinase activity. A hypothetical model describing serotype 3 reovirus-induced inhibition of cdc2 kinase is presented, and reovirus-induced perturbations of the G_1-to-S, G_2-to-M, and mitotic spindle checkpoints are discussed.

Perturbation of cell cycle regulation is a characteristic of infection by viruses belonging to a diverse group of viral families. The reasons viruses stimulate proliferation or induce cell cycle arrest are not completely understood. In some cases, virus replication may depend on the availability of host cell precursors, whose abundance varies in a cell cycle-specific manner. In other cases, kinases critical in regulating cell cycle progression may be essential for phosphorylating viral proteins (reviewed in reference 58).

Reoviruses infect a variety of mammalian hosts and serve as an important experimental system for studying the molecular bases of viral pathogenesis (reviewed in reference 80). Reoviruses also provide a valuable model for studying virus-induced perturbations in cell cycle regulation, since reovirus infection has been associated with G_1 arrest, G_2/M arrest, and disruption of the mitotic spindle apparatus (see below). Inhibition of host cell DNA synthesis is one of the earliest cytopathic effects observed following serotype 3 reovirus infection in cultured cells (reviewed in reference 53). It was originally suggested that serotype 3 reovirus-induced inhibition of cellular proliferation resulted from inhibition of the initiation of DNA replication (14, 27, 68). However, the degree of cell culture synchronization prior to infection was either incomplete or not specified in these studies, impeding accurate identification of the cell cycle phase affected (14, 68).

Serotype 3 prototype strains type 3 Dearing (T3D) and type 3 Abney (T3A) inhibit cellular DNA synthesis to a greater extent than the serotype 1 prototype strain type 1 Lang (T1L) in a variety of cell lines (20, 23, 75, 82). Studies using T1L × T3D and T1L × T3A reassortant viruses indicate that the serotype 3 S1 gene is the primary determinant of differences in the capacity of reovirus strains to inhibit DNA synthesis (75, 82). The reovirus S1 gene segment is bicistronic, encoding the viral attachment protein, σ1, and a non-virion-associated protein, σ1s, from overlapping, alternative open reading frames (53).

Studies using purified recombinant serotype 3 σ1 protein and an anti-idiotype antibody (87.92.6) generated against the T3D σ1-specific monoclonal antibody 9BG5 suggest that inhibition of DNA synthesis in some cells may result from engagement of a cell surface receptor by σ1 (23, 70–72). For example, treatment of R1.1 thymoma cells with purified T3D σ1 results in a reversible G_1-to-S transition arrest (70, 71). The mechanism for T3D σ1-induced G_1-to-S arrest is not clear but may involve inhibition of $p21^{ras}$ (Ha-ras), since overexpression of Ha-ras prevents T3D σ1-induced G_1-to-S transition arrest (71, 72).

We have shown that reovirus infection inhibits cellular proliferation by inducing a G_2/M phase cell cycle arrest in a variety of cell types (63). T3A and T3D induce G_2/M phase cell cycle arrest to a greater extent than T1L (63). Like strain-specific differences in the capacity of reovirus to inhibit DNA synthesis (82), strain-specific differences in the capacity of reovirus to induce G_2/M phase cell cycle arrest are determined by the serotype 3 S1 gene (63). The S1-encoded σ1s protein is both necessary and sufficient to induce G_2/M arrest, since a σ1s-

* Corresponding author. Mailing address: Department of Neurology (B-182), University of Colorado Health Sciences Center, 4200 E. 9th Ave., Denver, CO 80262. Phone: (303) 393-2874. Fax: (303) 393-4686. E-mail: Ken.Tyler@UCHSC.edu.

deficient reovirus mutant fails to induce G_2/M arrest and inducible expression of σ1s results in accumulation of cells in the G_2/M phase of the cell cycle (63).

G_2-to-M transition requires the formation and activation of the $p34^{cdc2}$/cdk1 (cdc2)-cyclin B heterodimeric complex (reviewed in references 38 and 55). Activation of the cdc2-cyclin B complex is regulated by inhibitory phosphorylation of cdc2 (76). We showed that cdc2 kinase activity is inhibited following serotype 3, not serotype 1, reovirus infection (62). Inhibition of cdc2 kinase activity is, in part, due to serotype 3 σ1s-dependent phosphorylation of cdc2 (62). However, the pathway(s) leading to cdc2 kinase inhibition following serotype 3 reovirus infection remains unclear.

Since G_2 phase arrest cannot easily be distinguished from M phase arrest by flow cytometry using DNA intercalating dyes, it is possible that both G_2-to-M checkpoint arrest and mitotic spindle checkpoint arrest contribute to reovirus-induced G_2/M phase cell cycle arrest. Electron microscopic studies have shown that reovirus particles align along parallel arrays of microtubules and have the capacity to bind microtubules in vitro (3). Serotype 3 reovirus particles associate with microtubules of the mitotic spindle apparatus in infected cells (15) and require microtubule stability for fast axonal transport (81). In addition to association with microtubules, reovirus infection results in progressive disruption and reorganization of the vimentin (intermediate) filament network (74). The binding of reovirus to microtubules and the disruption of vimentin filaments may lead to changes in microtubule tension or binding to the kinetochore. Reovirus-induced disruption of the microtubule-kinetochore association could lead to activation of the mitotic spindle checkpoint and M phase cell cycle arrest (2, 78).

Serotype 3 reovirus infection activates the cellular transcription factors NF-κB (4, 13) and c-Jun (P. Clarke, personal communication). Activation of transcription factors following reovirus infection suggests that gene expression is critical in reovirus-induced pathogenesis. To identify potential pathways leading to serotype 3 reovirus-induced inhibition of proliferation, we conducted experiments to investigate the transcriptional response following serotype 3 and serotype 1 reovirus infections. High-throughput screening of more than 12,000 genes using oligonucleotide microarrays has identified potential reovirus-induced signaling pathways involved in cell cycle control. Of the genes differentially expressed following reovirus infection, several encode regulators of the critical G_2-to-M transition kinase cdc2.

MATERIALS AND METHODS

Infection. Human embryonic kidney (HEK293) cells (ATCC CRL1573) were plated in T75 flasks (Becton Dickinson, Franklin Lakes, N.J.) at a density of 5×10^6 cells per flask in a volume of 12 ml of Dulbecco's modified Eagle's medium supplemented to contain 10% heat-inactivated fetal bovine serum, 2 mM L-glutamine (Gibco-BRL, Gaithersburg, Md.), 1 mM sodium pyruvate (Gibco-BRL), and 100 U of penicillin per ml and 100 μg of streptomycin per ml (Gibco-BRL). After 24 h of incubation, when cells were 60 to 70% confluent, the medium was removed, and cells were infected with viral strain T3A at a multiplicity of infection (MOI) of 100 PFU per cell in a volume of 2 ml at 37°C for 1 h. A high MOI was used to ensure that all susceptible cells were infected, and studies in our laboratory indicate that a high MOI enhances the reproducibility of gene expression studies. Following infection, 10 ml of Dulbecco's modified Eagle's medium was added and flasks were incubated at 37°C. Cells used for control infections were inoculated with a virus-free cell lysate control. In order to identify differentially regulated transcripts important for serotype 3 reovirus-induced cell cycle perturbation, an identical experiment using T1L was performed. UV light-inactivated virus was generated for reverse transcription-PCR (RT-PCR) experiments, by exposing T3A virion stocks to short-wave (254-nm) UV light under conditions sufficient to generate an intensity of 560 $\mu W/cm^2$ for 15 min (energy level determined with a Blak-Ray J-225 short-wave UV intensity meter). These conditions produce inactivated virus stocks devoid of infectious virus, as determined by plaque assay (<10 PFU/ml). The inoculum of UV virus used was calculated based on the number of infectious particles present in T3A stock prior to UV inactivation.

cRNA target preparation and hybridization. Cells were harvested at 6, 12, and 24 h postinfection and washed with phosphate-buffered saline, and total RNA was isolated by using the RNeasy Mini Kit (Qiagen, Valencia, Calif.). Ten micrograms of RNA was converted to cDNA by using SuperScript Choice (Gibco-BRL), substituting high-performance liquid chromatography-purified T7-oligo-$d(T)_{24}$ for random primers. Second-strand synthesis was performed using T4 DNA polymerase, and cDNA was isolated by phenol-chloroform extraction using phase lock gels. Isolated cDNA was in vitro transcribed by using the BioArray High Yield RNA Transcript Labeling Kit (Enzo Biochem, New York, N.Y.) supplied with biotin-labeled UTP and CTP to produce biotin-labeled cRNA. Labeled cRNA was isolated by using an RNeasy Mini Kit column (Qiagen) and quantified for purity and yield. cRNA was fragmented in 100 mM potassium acetate–30 mM magnesium acetate–40 mM Tris-acetate (pH 8.1) for 35 min at 94°C, and hybridization performance was analyzed by using Test 2 arrays (Affymetrix, Santa Clara, Calif.). Target cRNA was hybridized to the U95A microarray (Affymetrix) according to Affymetrix protocols. Briefly, 15 μg of fragmented cRNA was hybridized for 16 h at 45°C with constant rotation (60 rpm). Microarrays were washed and stained with streptavidin-conjugated phycoerythrin (SAPE) by using the Affymetrix GeneChip Fluidic Station 400. Staining intensity was antibody amplified by using a biotinylated anti-streptavidin antibody at a concentration of 3 μg per ml followed by a second SAPE stain and was visualized at 570 nm. All hybridization steps were performed at the University of Colorado Health Sciences Center (UCHSC) Cancer Center Microarray Facility.

Data analysis. Each gene on the U95A array is represented by 20 different 25-base cDNA oligonucleotides complementary to a cRNA target transcript (perfect match). As a hybridization specificity control, an oligonucleotide containing a single base substitution corresponding to each perfect-match cDNA oligonucleotide (mismatch) is represented on the array. The combination of perfect-match and mismatch cDNA oligonucleotides for each gene is termed a probe set. By using Affymetrix-defined absolute mathematical algorithms describing perfect-match and mismatch intensities, each gene was defined as absent or present and assigned a value. Binding intensity values were scaled to evaluate differential expression following reovirus infection. By using Affymetrix-defined comparison mathematical algorithms, a reovirus-induced transcript was classified as not changed, marginally increased, marginally decreased, increased, or decreased, and a fold change in expression was calculated. Nucleotide accession numbers for transcripts cited in the text that were not changed appear in Table 2. Since each condition was performed in duplicate, we used two additional criteria, as follows, to classify a gene as significantly up- or downregulated following reovirus infection. (i) Reovirus-induced expression of a gene at each time point must be classified as increased or marginally increased (or decreased or marginally decreased) in each virus-infected condition compared to each mock-infected condition. (ii) The mean fold change in reovirus-induced gene expression must be greater than 2. Mean transcriptional expression of a given gene at a given time point was calculated as the sum of the fold change in gene expression for each virus-infected condition compared to each mock-infected condition divided by 4. Standard errors in mean transcriptional expression of a gene were also calculated.

RT-PCR. HEK293 cells were infected as described above. Additional cells were infected with UV-inactivated T3A virus (replication incompetent) as a control to assess whether active replication was required for the effects observed with T3A-infected cells (see "Infection" above for description of UV-inactivated T3A virus). Cells were harvested at 12 and 24 h postinfection and washed with phosphate-buffered saline, and RNA was isolated. Five micrograms of RNA was converted to cDNA by using the SuperScript Preamplification System (Gibco-BRL) supplied with oligo-$d(T)_{12-18}$ primer. Reverse transcription was performed at 42°C for 1 h. PCR was performed using primers generated against chk1 (AF016582) (forward primer, 5′-CTG AAG AAG CAG TCG CAG TG-3′; reverse primer, 5′-TTC CAC AGG ACC AAA CAT CA-3′), wee1 (U10564) (forward primer, 5′-AAC CTC AAT CCC AAA TGC TG-3′; reverse primer, 5′-TTG CCA TCT GTG CTT TCT TG-3′), the growth arrest and DNA damage-inducible protein 45 (GADD45) (M60974) (forward primer, 5′-TGC GAG AAC

GAC ATC AAC AT-3'; reverse primer, 5'-TCC CGG CAA AAA CAA ATA AG-3'), and β-actin (BC004251) (forward primer, 5'-GAA ACT ACC TTC AAC TCC ATC-3'; reverse primer, 5'-CGA GGC CAG GAT GGA GCC GCC-3'), yielding product sizes of 495, 506, 200, and 219 bp, respectively. PCR cycle conditions were 94°C for 30 s, 55°C for 30 s, and 72°C for 1 min for 25 cycles. Dilutions of cDNA were performed to determine the linear range for each primer pair. PCR products were resolved on a 2% agarose gel containing ethidium bromide and were visualized with UV light. Densitometric analysis was performed using a FluorS MultiImager System and Quantity One software (Bio-Rad, Hercules, Calif.).

RESULTS

Reovirus-induced alterations in gene expression. Previous work has established that serotype 3, not serotype 1, reovirus infection induces perturbations in cell cycle regulation in multiple cell lines, including HEK293 cells. To identify potential pathways exploited by serotype 3 reovirus to deregulate the host cell cycle, we evaluated the profile of HEK293 cellular gene expression following T3A infection at 6, 12, and 24 h by using the Affymetrix U95A microarray. We found that serotype 3 reovirus infection induced significant changes in the expression of 25 genes encoding proteins regulating cell cycle progression. Ten genes (40%) were classified as encoding proteins that function at the G_1-to-S transition, 11 genes (44%) were classified as encoding proteins that function at the G_2-to-M transition, and 4 genes (16%) were classified as encoding proteins that function at the mitotic spindle checkpoint (Table 1). Twenty cell cycle-related transcripts were increased following serotype 3 reovirus infection, and five transcripts were decreased. Four of the five downregulated genes were classified as transcripts encoding proteins regulating G_2-to-M transition. No cell cycle-related genes were differentially expressed at 6 h postinfection. At 12 h, five cell cycle-related genes were found to be differentially expressed following serotype 3 reovirus infection, two were upregulated, and three were downregulated. Four of the five genes altered at 12 h postinfection were classified as transcripts encoding proteins regulating the G_2-to-M transition. At 24 h postinfection, 23 cell cycle-related genes were found to be differentially expressed, 19 were upregulated, and 3 were downregulated. One transcript found to be upregulated and one found to be downregulated at 12 h post-T3A infection were increased and decreased at 24 h postinfection, respectively. Histone H1, histone H2A, and wee1 were represented twice on the array, and histone H2B was represented six times. Fold changes in gene expression for replicates and for multiple representations of a gene were highly reproducible.

To identify differentially regulated transcripts important for serotype 3 reovirus-induced cell cycle perturbation, we compared the profile of HEK293 cellular gene expression following T1L infection at 24 h postinfection using the Affymetrix U95A microarray. We found that serotype 1 reovirus infection induced significant changes in the expression of six genes encoding proteins regulating cell cycle progression. Three genes (50%) were classified as encoding proteins that function at the G_1-to-S transition, and three genes (50%) were classified as encoding proteins that function at the G_2-to-M transition (Table 1). T1L infection did not alter any genes classified as encoding proteins that function at the mitotic spindle checkpoint at 24 h postinfection (Table 1). Each cell cycle-related transcript that was differentially regulated following serotype 1 reovirus infection was increased. T1L infection resulted in differential regulation of 23% of transcripts differentially regulated by T3A at 24 h postinfection. The transcript encoding E2F6 was the only cell cycle-related transcript differentially regulated by T1L infection that was not differentially regulated by T3A infection. Of the nine T3A-regulated transcripts encoding proteins that function at the G_1-to-S transition at 24 h postinfection, two (22%) were differentially regulated by T1L. Of the nine T3A-regulated transcripts encoding proteins that function at the G_2-to-M transition at 24 h postinfection, three (33%) were differentially regulated by T1L. These results indicate that serotype 3 reovirus infection perturbs the differential expression of genes encoding proteins that regulate the G_1-to-S, G_2-to-M, and mitotic spindle checkpoints and that T1L infection results in differential regulation of a subset of these transcripts. In addition, the earliest detectable changes in gene expression following T3A infection were for genes encoding G_2-to-M regulatory proteins, suggesting that deregulation of the G_2-to-M transition is an early event following serotype 3 reovirus infection.

Reovirus-induced alterations in genes encoding proteins that regulate G_1-to-S progression. Treatment of specific cell types, including R1.1 thymoma cells, with purified T3D σ1 protein leads to a reversible G_1-to-S transition arrest that depends on the inhibition of Ha-ras (70–72). Ten genes encoding proteins that function at the G_1-to-S transition were altered following serotype 3 reovirus infection. The level of Ha-ras gene expression was not changed following reovirus infection. Expression of the gene encoding N-ras was also not inhibited and was, in fact, increased 2.1-fold ± 0.2-fold in serotype 3 reovirus-infected cells at 24 h postinfection (Table 1).

The G_1-to-S transition requires activation of cyclin-dependent kinases (cdk) (57). cdk2, -4, and -6 kinase activity results in phosphorylation of the retinoblastoma protein (pRb) and the pRb-related proteins p107 and p130. Phosphorylation of pRb leads to activation of the transcription factor E2F (31). The level of cdk4 gene expression was not changed following reovirus infection (Table 2). cdk2 and -6 were not represented on the U95A microarray. Levels of pRb, p107, p130, and E2F1, -2, -4, -5, and -6 gene expression were not changed following reovirus infection (Table 2), except for the transcript encoding E2F6, which was upregulated 2.1-fold ± 0.1-fold following T1L infection (Table 1). Activation of cdk2, -4, or -6 requires binding to cyclin E or cyclin D (31). Cyclin E expression was reduced 2.8-fold ± 0.1-fold in serotype 3 reovirus-infected cells. However, the level of cyclin E2 (a cyclin E isoform) gene expression was increased 2.1-fold ± 0.2-fold in serotype 3 reovirus-infected cells (Table 1). Levels of cyclin D1, -2, and -3 expression were not changed following reovirus infection (Table 2).

Activation of cdk2 depends on its phosphorylation state (57). The level of protein phosphatase 2C (PP2C) gene expression at 24 h after infection with T3A was 5.3-fold ± 0.4-fold greater than that for a mock-infected control. cdk-cyclin complex activity is known to be inhibited by cdk inhibitors (CDKI) (29, 31). Levels of CDKI expression, including $p21^{WAF1/CIP1}$, $p27^{KIP1}$, $p57^{KIP2}$, $p16^{INK4a}$, $p15^{INK4b}$, and $p19^{INK4d}$ were not changed following reovirus infection (Table 2). Since active cdk2, -4, or -6 kinase results in E2F-dependent transcription, the transcriptional level of E2F-responsive genes necessary for

TABLE 1. Reovirus-induced alterations in expression of genes known to regulate the cell cycle

Gene[a]	Accession no.[b]	Fold change in expression[c] at the indicated time after infection with:		
		T3A		TIL (24 h)
		12 h	24 h	
G_1-S checkpoint				
N-Ras	X02751		2.1 ± 0.2	
Cyclin E	M73812		−2.8 ± 0.1	
Cyclin E2	AF091433		2.1 ± 0.2	
PP2C-α	AF070670		5.3 ± 0.4	
C-1[d]	U41816		2.2 ± 0.1	
ANA[e]	D64110		2.9 ± 0.1	2.5 ± 0.1
E2F6	AF041381			2.1 ± 0.1
Histone H1	X03473[f]		2.7 ± 0.1	2.3 ± 0.2
			3.1 ± 0.2	2.1 ± 0.2
Histone H2A	LI9779[g]		2.0 ± 0.1	
	AI885852		2.2 ± 0.1	
Histone H2B	X00088[g]		2.0 ± 0.1	
	Z80782		2.8 ± 0.1	
	Z80780		3.1 ± 0.3	
	Z80779		3.2 ± 0.2	
	AA873858		5.8 ± 0.6	
Histone H4	X00038	4.7 ± 0.5		
G_2-M checkpoint				
wee-1	U10564[g]		2.4 ± 0.1	1.9 ± 0.1[h]
	X62048		2.5 ± 0.1	2.0 ± 0.1
chk-1	AF016582		3.2 ± 0.1	
GADD45	M60974	3.3 ± 0.2	4.9 ± 0.1	4.4 ± 0.1
B56-β subunit of PP2A	L42374	−3.1 ± 0.3		
SG2NA	U17989		2.4 ± 0.2	2.5 ± 0.2
FRP1	U49844		−2.1 ± 0.1	
PCTAIRE-2	X66360		2.6 ± 0.1	
Trap	AB025254[i]		2.0 ± 0.3	
C-2K	X80230	−2.1 ± 0.1		
SAK	Y13115		3.8 ± 0.5	
Ki-67 antigen[j]	X65550	−1.9 ± 0.0	−2.3 ± 0.2	
Mitotic spindle checkpoint				
BUB-3	AF047472		2.2 ± 0.1	
MPP11	X98260		2.0 ± 0.1	
HZWINT1	AF067656		2.6 ± 0.0	
Nuc-2[k]	S78234		2.1 ± 0.2	

[a] Genes that are not addressed in the text are described in footnotes.
[b] Corresponds to the nucleotide accession number assigned to the Affymetrix probe set on the U95A microarray.
[c] Values are means ± standard errors of the means from two independent experiments. A negative number indicates that the transcript was downregulated. Where no value is given, there was no change.
[d] A possible transcription factor with activity at the G_1-to-S transition (37).
[e] Overexpression leads to retardation of cell cycle progression through the G_1 phase (85).
[f] Represented twice on the U95A microarray.
[g] Represented multiple times on the U95A microarray.
[h] This gene was not considered upregulated as defined in Materials and Methods, because it was found to be increased in three of four analyses.
[i] Affymetrix-assigned GenBank accession number refers to partial coding sequence for Trap. The complete coding sequence is at AB030644.
[j] General marker of proliferation; may be regulated by cdc2 (reviewed in references 18 and 73).
[k] An APC component (reviewed in reference 59); may also play a role in the G_1-to-S transition (8, 44).

the G_1-to-S transition, including cyclin E, cyclin A, cdc2, cdc25C, $p21^{WAF1/CIP1}$, c-*myc*, B-myb, p107, E2F1, E2F2, dihydrofolate reductase, thymidine kinase, DNA polymerase α, histone H2A, and cdc6, serve as a measure of cdk2, -4, or -6 kinase activity (26). Levels of these E2F-responsive transcripts were not changed following reovirus infection except for cyclin E, c-*myc*, and DNA polymerase α, which were downregulated 2.8-fold ± 0.1-fold, 2.0-fold ± 0.0-fold, and 2.5-fold ± 0.2-fold following serotype 3 reovirus infection, respectively, and histone H2A and cdc2, which were upregulated 2.0-fold ± 0.1-fold or 2.2-fold ± 0.1-fold and 1.8-fold in serotype 3 reovirus compared to mock-infected cells. The failure to detect a coherent pattern of gene expression encoding key G_1-to-S checkpoint control proteins is consistent with our observation that reovirus infection does not induce G_1 arrest in HEK293 cells. However, we did find changes in the expression of genes encoding histones, cyclin E and E2, and some E2F-responsive transcripts following serotype 3 reovirus infection.

Reovirus-induced alterations in genes encoding proteins that regulate the G_2-to-M progression. We have previously shown that serotype 3 reovirus-induced G_2/M phase cell cycle arrest is due to inhibitory phosphorylation of cdc2 (62). Eleven genes encoding proteins that function at the G_2-to-M transition were altered following serotype 3 reovirus infection. These

TABLE 2. Nucleotide accession numbers for genes mentioned in the text that were not changed following T3A or T1L infection

Gene	Accession number[a]
ATM	U26455
B-myb	X13293
BUB1	AF053305
cdc25C	M34065
cdc6	U77949
cdk4	U37022
Cyclin A	X51688, U66838[b]
Cyclin B	M25753
Cyclin D1	M64349
Cyclin D2	X68452
Cyclin D3	M92287
Dihydrofolate reductase	J00146, J00140, J00139[b]
E2F1	U47677, M96577[b]
E2F2	L22846
E2F4	S75174
E2F5	U15642
E2F6	AF041381
Ha-ras	J00277
MAD2	AJ000186, U65410[b]
MAD3	AF053306
pRb	M15400, L49219, L49229, L41913, L41870[b]
p107	L14812
p130	X74594, X76061[b]
$p15^{INK4b}$	AF004819, L36844[b]
$p16^{INK4a}$	U26727
$p19^{INK4d}$	U40343
$p21^{WAF1/CIP1}$	U03106
$p27^{KIP1}$	U10906
$p57^{KIP2}$	D64137, U22398[b]
Thymidine kinase	K02581, M15205, U80628[b]

[a] Corresponds to the nucleotide accession number assigned to an Affymetrix probe set on the U95A microarray.
[b] Represented multiple times on the U95A microarray.

changes were among the earliest changes in gene expression identified in serotype 3 reovirus-infected cells. The level of cdc2 gene expression at 24 h post-T3A infection was 1.8-fold greater than that in a mock-infected control. We have not reproducibly detected changes in levels of cdc2 protein in reovirus-infected cells; however we have consistently found an increase in the proportion of hyperphosphorylated cdc2 following serotype 3 reovirus infection (62). An increase in cdc2 phosphorylation could result from an increase in wee1 kinase activity, which directly phosphorylates and inactivates cdc2 (60). wee1 was determined to be upregulated at 24 h postinfection by using the U95A microarray (Table 1). Levels of wee1 gene expression at 24 h post-T3A infection were 2.4-fold ± 0.1-fold (for accession number U10564) and 2.5-fold ± 0.1-fold (for accession number X62048) greater than those for a mock-infected control. Levels of wee1 gene expression at 24 h post-T1L infection were 1.9-fold ± 0.1-fold (for accession number U10564) and 2.0-fold ± 0.1-fold (for accession number X62048) greater than those for a mock-infected control. The increases in wee1 gene expression following T3A and T1L infection were confirmed by RT-PCR and were 2.3- and 2.4-fold greater, respectively, than those for a mock-infected control at 24 h postinfection (Fig. 1). RT-PCR analysis of UV-inactivated T3A-infected cells, demonstrated a small but measurable increase in wee1 transcripts compared that for to mock-infected cells (a 1.6-fold increase), indicating that active viral replication is not necessary but may augment the expression of wee1 in reovirus-infected cells (Fig. 1). Increased levels of wee1 kinase may result in inhibitory phosphorylation of cdc2 following serotype 3 reovirus infection, but increases in wee1 are not sufficient for serotype 3 reovirus-induced phosphorylation of cdc2, since T1L infection results in similar increases in wee1 gene expression.

Increased inhibitory phosphorylation of cdc2 following reovirus infection could also result from inactivation of the cdc2-specific phosphatase cdc25C (reviewed in reference 38). Following reovirus infection, the level of cdc25C gene expression was not changed (Table 2). The kinase chk1 can enhance wee1 kinase activity (56) and inhibit cdc25C phosphatase activity (22). The level of chk1 gene expression at 24 h post-T3A infection was 3.2-fold ± 0.1-fold greater than that for a mock-infected control and was unchanged in T1L-infected cells (Table 1). The increase in chk1 gene expression following T3A infection was confirmed by RT-PCR and was 3.6-fold greater than that for a mock-infected control at 24 h postinfection (Fig. 1). In contrast, chk1 transcripts were not altered following T1L infection, as assessed by RT-PCR. chk1 transcripts were slightly increased in UV-inactivated T3A-infected cells compared to mock-infected cells (1.6-fold increase), again suggesting that active viral replication is not required but may augment differential expression of chk1 following T3A infection (Fig. 1). These results suggest that increased levels of chk1 kinase may result in inhibitory phosphorylation of cdc25C on Ser-216 and activation of wee1 following serotype 3 reovirus infection.

In addition to the inhibition of cdc2 by phosphorylation, serotype 3 reovirus-induced G_2/M phase cell cycle arrest could result from dissociation of cdc2 from cyclin B. The level of cyclin B gene expression was not changed following reovirus infection (Table 2), consistent with our studies suggesting that changes in the level of cyclin B protein are not responsible for reovirus-induced G_2-to-M transition arrest (62).

GADD45 is known to inhibit cdc2 kinase activity by physically dissociating cdc2 kinase from cyclin B (87). To determine whether GADD45 could be responsible for reovirus-induced inactivation of cdc2, we analyzed the transcriptional expression of GADD45 following serotype 3 reovirus infection. Levels of GADD45 gene expression at 12 and 24 h after infection with T3A were 3.3-fold ± 0.2-fold and 4.9-fold ± 0.1-fold greater than those for a mock-infected control, respectively (Table 1). The increase in GADD45 gene expression following T3A infection was confirmed by RT-PCR and was 4.5-fold greater than that for a mock-infected control at 24 h postinfection (Fig. 1). The level of GADD45 gene expression at 24 h after infection with T1L was 4.4-fold ± 0.1-fold greater than that for a mock-infected control, and this increase was confirmed by RT-PCR (5.2-fold increase [Fig. 1]). A small but measurable increase in the level of GADD 45 transcripts was noted by RT-PCR analysis in cells infected with UV-inactivated T3A compared to mock-infected cells (1.3-fold increase [Fig. 1]). This suggests that increased levels of GADD45 may result in inhibition of cdc2 by physically dissociating cdc2 from cyclin B following serotype 3 reovirus infection, but increases in GADD45 are not sufficient for serotype 3 reovirus-induced phosphorylation of cdc2, since T1L infection results in a sim-

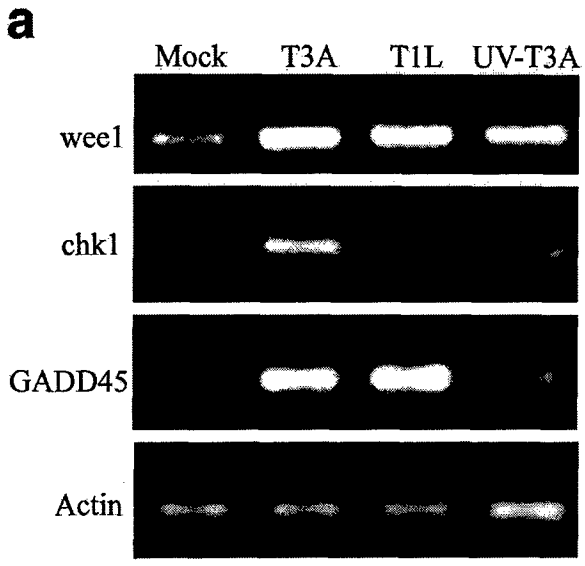

FIG. 1. wee1, chk1, and GADD45 transcripts are increased following reovirus infection. (a) HEK293 cells were either mock infected or infected with T3A, T1L, or UV-inactivated T3A at an MOI of 100 PFU per cell. mRNA was collected at 24 h postinfection and analyzed for chk1, wee1, and GADD45 transcripts by RT-PCR to confirm microarray analyses and also to assess the importance of replication competence for the observed changes in gene expression. β-Actin was used as a control in each RT-PCR to ensure matched total mRNA and equivalent amplication conditions for each experimental sample. (b) Quantitative densitometric analysis of specific mRNA abundance in each sample.

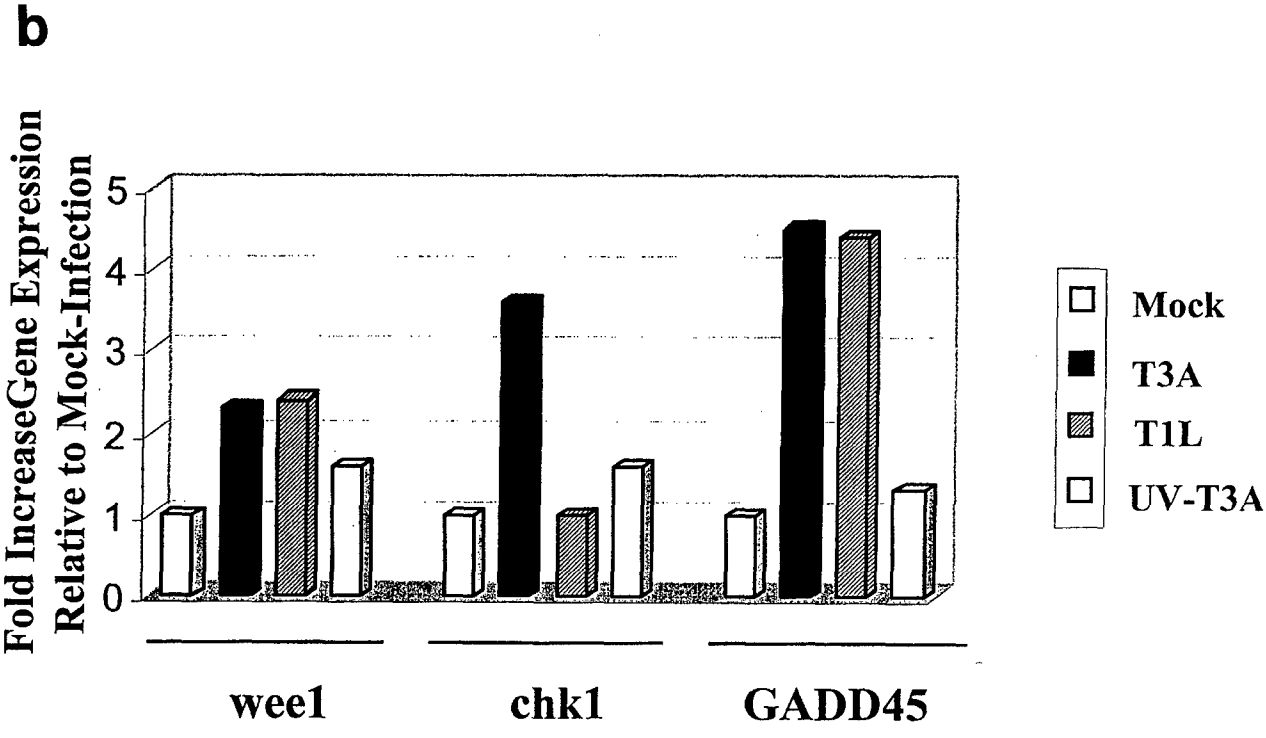

ilar increase in GADD45 gene expression. Thus, we found that reovirus infection induces changes in expression levels of genes encoding key proteins regulating cdc2 kinase activity, including wee1, chk1, and GADD45, which is consistent with the findings of our previous studies suggesting a central role for cdc2 inhibition in serotype 3 reovirus-induced G_2/M phase cell cycle arrest (63).

Reovirus-induced alterations in genes encoding proteins that regulate mitotic spindle checkpoint signaling. Reovirus particles are capable of binding microtubules, and infection results in progressive disruption of vimentin filaments. Changes in microtubule tension or binding to the kinetochore could lead to reovirus-induced mitotic arrest. Four genes encoding proteins that function at the mitotic spindle checkpoint were altered following reovirus infection. The transcriptional levels of mitotic spindle checkpoint components that monitor spindle abnormalities, including MAD2, MAD3, and BUB1, were not changed following reovirus-infection (Table 2). The level of BUB3 gene expression at 24 h after infection with T3A was 2.2-fold ± 0.1-fold greater than that for a mock-infected control (Table 1). Activation of the mitotic spindle checkpoint leads to inhibition of the anaphase-promoting complex (APC) and M phase cell cycle arrest (2, 78). Expression of the gene encoding Nuc2, an APC component, was 2.1-fold ± 0.2-fold greater than that for a mock-infected control (Table 1). These

results suggest that serotype 3 reovirus-induced alterations in gene expression may induce M phase cell cycle arrest.

DISCUSSION

The use of DNA microarray technology following reovirus infection has identified several genes encoding proteins that may play a role in serotype 3 reovirus-induced disruption of the cell cycle. The results presented here provide a comprehensive overview of alterations in expression of genes encoding proteins that regulate cell cycle progression following reovirus infection. Although these alterations are likely to reflect changes in gene expression, it should be noted that DNA microarray technology assesses changes in steady-state levels of specific mRNAs rather than transcriptional activity.

G_1-to-S checkpoint: reovirus-induced alterations in G_1-to-S restriction checkpoint control. Treatment with purified T3D σ1 protein leads to a reversible G_1-to-S phase transition arrest in R1.1 thymoma cells that is dependent on Ha-ras inhibition (70–72). However, G_1-to-S arrest is not a universal feature of reovirus infection and does not occur in reovirus-infected HEK293 cells (63). We were unable to detect changes in expression of $p21^{ras}$-related genes involved in G_1-to-S regulation, and we found that gene expression of the $p21^{ras}$ isoform, N-ras, was selectively increased following serotype 3 reovirus infection.

G_1-to-S transition arrest following serotype 3 reovirus infection could result from inactivation of the G_1-to-S cyclin dependent kinase cdk2, -4, or -6 by the protein phosphatase PP2C-α. PP2C-α is known to dephosphorylate activating phosphates on cdk2 (9), which may result in inhibition of cdk2 kinase activity. Decreased expression of the cdk2 regulatory cyclin, cyclin E, was counterbalanced by an increase in the expression of the cyclin E isoform, cyclin E2, suggesting that G_1 cyclin expression does not play a significant role in regulating serotype 3 reovirus-induced G_1-to-S progression. Alterations in histone synthesis and alterations in the relative levels of histone proteins could alter G_1-to-S progression, but no clear model has been elucidated (19). Collectively, these findings indicate that serotype 3 reovirus-induced alterations in gene expression are not consistent with G_1-to-S arrest in HEK293 cells.

G_2-to-M checkpoint: reovirus-induced inhibition of cdc2 by phosphorylation. Serotype 3 reovirus-induced G_2/M phase cell cycle arrest results from a reduction in cdc2 kinase activity due to inhibitory phosphorylation, which has been demonstrated in infection of multiple cell lines, including HEK293, MDCK, C127, and HeLa cells (62). An increase in hyperphosphorylated cdc2 could be due either to increases in cdc2-specific kinase activity or to decreases in cdc2-specific phosphatase activity, or to both. The kinases wee1 and myt1 and the phosphatase cdc25C regulate the phosphorylation state of cdc2 (reviewed in reference 38). Following serotype 3 reovirus infection, levels of wee1 transcripts are elevated, suggesting that this kinase may play a role in inhibiting cdc2 (Fig. 2). However, an elevation in wee1 transcript levels is not sufficient for serotype 3 reovirus-induced inhibitory phosphorylation of cdc2, since the transcript encoding wee1 kinase is similarly upregulated following T1L infection. The activity of the cdc2-specific phosphatase cdc25C is regulated by phosphorylation. Hyperphosphorylation of cdc25C results in active phosphatase activity capable of removing inhibitory phosphates from cdc2 kinase (reviewed in reference 38). Following reovirus infection, cdc25C is inhibited by dephosphorylation (62). It is suggested that the HIV Vpr protein can inhibit cdc2 kinase activity (30, 64) through mechanisms requiring wee1 and involving the inactivation of cdc25C (35, 48).

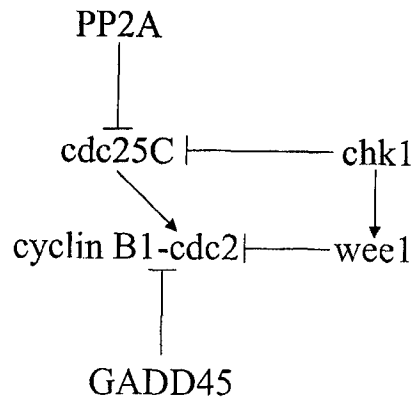

FIG. 2. Proposed model for serotype 3 reovirus-induced G_2-to-M transition arrest. cdc2 kinase activity is required for entry into mitosis. Active cdc2 kinase is complexed with cyclin B and dephosphorylated at Thr14/Tyr15. Following reovirus infection, cdc2 is inhibited, in part, by phosphorylation. The increase in phosphorylated cdc2 may be due to upregulation of the kinases chk1 and wee1 and/or localization to the nucleus of the phosphatase PP2A, which can inhibit the cdc2-activating phosphatase cdc25C. cdc2 kinase activity may also be inhibited by dissociation of cyclin B by GADD45. Arrows indicate activation; blunted lines indicate inhibition.

PP2A or PP2A-like activity is capable of negatively regulating cdc25C by removing activating phosphates (12, 42, 45). HIV Vpr is reported to inactivate cdc25C by physically targeting PP2A to the nucleus and enhancing the recruitment and dephosphorylation of cdc25C though association with the PP2A-B55 regulatory subunit (35). Following serotype 3 reovirus infection, we found selective decreased expression of the PP2A–B56-β regulatory subunit. Since the B56-β regulatory subunit is known to localize PP2A to the cytoplasm (50), downregulation of B56-β production may lead to increased nuclear localization of PP2A following reovirus infection (Fig. 2). Furthermore, upregulation of S/G_2 nuclear antigen (SG2NA) may target PP2A to the nucleus following serotype 3 reovirus infection, since SG2NA is known both to localize to the nucleus (52) and to interact with the C subunit of PP2A (51). However, an elevation in SG2NA transcript levels is not sufficient for serotype 3 reovirus-induced dephosphorylation of cdc25C, since the transcript encoding SG2NA is similarly upregulated following T1L infection. Nonetheless, it is possible that reovirus-induced nuclear localization of PP2A could inhibit cdc25C, which is consistent with the cdc2 hyperphosphorylation and G_2/M phase cell cycle arrest found following serotype 3 reovirus infection.

cdc25C activity is also inhibited following phosphorylation by the kinases chk1 and chk2 (22, 69). Phosphorylation of cdc25C on Ser-216 by chk1 or chk2 leads to 14-3-3 protein binding, which results in sequestration of cdc25C into the cytoplasm (47, 61). Export to the cytoplasm physically separates cdc25C from cdc2 kinase. We have found that reovirus infec-

tion is associated with increased expression of chk1, suggesting that this kinase plays a role in reovirus-induced inhibition of cdc25C (Fig. 2). chk1 kinase activity is also suggested to regulate wee1 subcellular localization, such that cdc2 kinase is phosphorylated and inactivated (56) (Fig. 2). This suggests that serotype 3 reovirus infection may selectively increase the level of chk1 kinase activity to modulate the activities of kinases and phosphatases directly responsible for regulating cdc2 activity.

G_2-to-M checkpoint: reovirus-induced inhibition of cdc2 by physical dissociation from cyclin B. An alternative mechanism for cdc2 inhibition is by physical interaction with GADD45. GADD45 inhibits cdc2 kinase by physically dissociating cdc2 from cyclin B (83, 87). Physical dissociation of cdc2 kinase from its regulatory cyclin results in elimination of cdc2 kinase activity and G_2-to-M checkpoint arrest (24, 55). Serotype 3 reovirus induces an increase in GADD45 expression, suggesting that GADD45 plays a role in reovirus-induced G_2-to-M checkpoint arrest (Fig. 2). However, an elevation in GADD45 transcript levels is not sufficient for serotype 3 reovirus-induced inhibition of cdc2 kinase activity, since the transcript encoding GADD45 is similarly upregulated following T1L infection. Interestingly, it is possible that GADD45-induced inhibition of cdc2 kinase activity results in accumulation of cells in the G_2/M phase of the cell cycle following infection with a herpes simplex virus (HSV) restricted to expressing the infected-cell polypeptide ICP0, since this virus induces an increase in GADD45 protein levels (34). The capacity of GADD45 to regulate cdc2 activity is a function of protein concentration (83). GADD45 transcription is regulated by p53 (41, 87) and Brca1 (28, 39). We have preliminary data suggesting that serotype 3 reovirus infection may result in increased expression of Brca1 protein. Reovirus-induced increases in Brca1 activity may result from changes in the activity of ATM or ATM-related kinases (46). Although we did not detect changes in expression of the gene encoding ATM, the expression of FRP1, a kinase with significant homology to ATM kinases (11), was selectively increased following serotype 3 reovirus infection.

The data presented in this report and our previous studies are consistent with a model in which reovirus-induced phosphorylation of cdc2 results in G_2/M phase cell cycle arrest that is dependent on σ1s expression (63). σ1s is a highly basic protein (16, 17) that is present in the nuclei of serotype 3-infected cells (7, 67), where it could directly interact with cdc2 or proteins regulating cdc2 kinase activity. However, the role of σ1s in serotype 3 reovirus-induced G_2/M phase cell cycle arrest has not yet been determined.

Mitotic spindle checkpoint: reovirus-induced alterations in spindle checkpoint signaling. Reovirus-induced disruption of the microtubule-kinetochore association may contribute to G_2/M arrest by activating the mitotic spindle checkpoint, which inhibits the APC and results in M phase arrest (2, 78). Selective expression of several genes encoding proteins with putative roles in regulating the mitotic spindle checkpoint were altered following serotype 3 reovirus infection. For example, Bub3 is an integral component of mitotic spindle checkpoint signaling, localizes to unattached kinetochores, and phosphorylates and complexes with Bub1 (6, 40, 66, 79). The functions of MPP11 and HZWINT1 are not completely understood but have been speculated to contribute to mitotic spindle checkpoint regulation, since they localize to mitotic structures, including kinetochores (49, 65, 77). These results suggest that deregulation of mitotic spindle checkpoint proteins may also contribute to serotype 3 reovirus-induced G_2/M phase cell cycle arrest.

Other proteins functioning in G_2 or M. Several genes encoding proteins that influence both the G_2-to-M and mitotic spindle checkpoints were selectively differentially regulated following serotype 3 reovirus infection. For example, polo-like kinase activity is important in regulating G_2-to-M transition events by activating cdc25C and in regulating M phase events including APC regulation, centrosome maturation, and bipolar spindle formation (25, 54). SAK, a polo-like kinase (36), was found to be upregulated following serotype 3 reovirus infection; however, the role of SAK in cell cycle regulation is not clear. Interestingly, expression of murine SAK-a is cell cycle regulated, with levels peaking in M phase, which is consistent with a role in the latter portion of the cell cycle (21). This suggests that serotype 3 reovirus may perturb both the G_2-to-M transition and the mitotic spindle checkpoint to ensure host cell cycle arrest in the G_2/M phase.

Serotype 3 reovirus infection also selectively altered the expression of genes encoding proteins with cdc2-related serine/threonine kinase activity, including C-2k (5) and PCTAIRE-2 (33). This suggests that serotype 3 reovirus may require cdc2-like kinase activity to posttranslationally modify a viral protein in a manner similar to the phosphorylation of varicella-zoster virus glycoprotein gI (84), Epstein-Barr virus EBNA-LP (43), hepatitis E virus ORF3 (86), and herpes simplex virus ICP0 (1) by cdc2. Alternatively, cdc2-like kinase activity may be responsible for alterations in cytoskeletal structure following serotype 3 reovirus infection. As discussed earlier, reovirus infection leads to disruption and reorganization of vimentin filaments into viral inclusions. Vimentin organization is regulated by cdc2-related kinase activity (10). PCTAIRE-2 kinase activity may regulate cytoskeletal protein distribution (33). Thus, alterations in PCTAIRE-2 and Trap (tudor repeat associator with PCTAIRE-2 [32]) following reovirus infection may lead to cytoskeletal changes necessary for viral inclusion formation. These results suggest that the reovirus life cycle may require modulation of cdc2-like kinase activity.

The present experiments shed light on the kinetics of key cellular processes that may directly influence reovirus-induced G_2/M arrest. The lack of differential expression of key transcripts prior to 12 h postinfection is consistent with prior findings, which showed no alteration in the activities of several key regulators of cell cycle progression (including cdc2 kinase) at 6 h postinfection (62). It is important to note that the lack of detectable altered gene expression at 6 h postinfection in these experiments does not preclude either early activation of cell cycle regulators at the protein level or altered expression of cell cycle-regulatory genes not represented on the U95A microarray. It is interesting that UV-inactivated (replication-incompetent) virus induced small but detectable changes in gene expression in the direction of those seen with infectious virus. This suggests that while viral replication may not be required, it substantially augments the expression of cellular regulators of cell cycle progression. Since the reovirus replication cycle is approximately 24 h in HEK293 cells, the requirement for viral replication for maximal alteration in gene expression may account for the lack of detectable alterations at the earliest time point postinfection.

In conclusion, reovirus infection alters a limited subset of transcripts encoding proteins that function to regulate cell cycle progression. Transcripts encoding proteins that function at the G_1-to-S, G_2-to-M, and mitotic spindle checkpoints were altered following serotype 3 reovirus infection. Of this group, genes encoding proteins regulating the G_2-to-M cell cycle transition were among the earliest to show changes in expression. This is consistent with the findings of our previous studies indicating that serotype 3 reovirus infection of HEK293 cells induces a G_2/M phase cell cycle arrest (63). We recently showed that G_2/M arrest results from inhibition of the key G_2-to-M transition kinase cdc2 (62). Consistent with these findings, we found changes in expression of kinases, phosphatases, and GADD proteins that directly and indirectly influence cdc2 kinase activity. These results have enabled us to provide a hypothetical model for modulation of cdc2 kinase activity in serotype 3 reovirus-infected cells.

ACKNOWLEDGMENTS

G. J. Poggioli and R. L. DeBiasi contributed equally to this work.

This work was supported by Public Health Service award AG14071 from the National Institute on Aging, Merit and REAP grants from the Department of Veterans Affairs, a U.S. Army Medical Research Acquisition Activity Grant (DAMD17-98-1-8614) (to K.L.T.), and an Infectious Diseases Society of America Young Investigator Award (to R.L.D.).

REFERENCES

1. **Advani, S. J., R. R. Weichselbaum, and B. Roizman.** 2000. The role of cdc2 in the expression of herpes simplex virus genes. Proc. Natl. Acad. Sci. USA **97**:10996–11001.
2. **Amon, A.** 1999. The spindle checkpoint. Curr. Opin. Genet. Dev. **9**:69–75.
3. **Babiss, L. E., R. B. Luftig, J. A. Weatherbee, R. R. Weihing, U. R. Ray, and B. N. Fields.** 1979. Reovirus serotypes 1 and 3 differ in their in vitro association with microtubules. J. Virol. **30**:863–874.
4. **Barton, E. S., J. C. Forrest, J. L. Connolly, J. D. Chappell, Y. Liu, F. J. Schnell, A. Nusrat, C. A. Parkos, and T. S. Dermody.** 2001. Junction adhesion molecule is a receptor for reovirus. Cell **104**:441–451.
5. **Best, J. L., D. H. Presky, R. A. Swerlick, D. K. Burns, and W. Chu.** 1995. Cloning of a full-length cDNA sequence encoding a cdc2-related protein kinase from human endothelial cells. Biochem. Biophys. Res. Commun. **208**:562–568.
6. **Brady, D. M., and K. G. Hardwick.** 2000. Complex formation between Mad1p, Bub1p and Bub3p is crucial for spindle checkpoint function. Curr. Biol. **10**:675–678.
7. **Ceruzzi, M., and A. J. Shatkin.** 1986. Expression of reovirus p14 in bacteria and identification in the cytoplasm of infected mouse L cells. Virology **153**:35–45.
8. **Chen, P. L., Y. C. Ueng, T. Durfee, K. C. Chen, T. Yang-Feng, and W. H. Lee.** 1995. Identification of a human homologue of yeast nuc2 which interacts with the retinoblastoma protein in a specific manner. Cell Growth Differ. **6**:199–210.
9. **Cheng, A., P. Kaldis, and M. J. Solomon.** 2000. Dephosphorylation of human cyclin-dependent kinases by protein phosphatase type 2Cα and β2 isoforms. J. Biol. Chem. **275**:34744–34749.
10. **Chou, Y. H., J. R. Bischoff, D. Beach, and R. D. Goldman.** 1990. Intermediate filament reorganization during mitosis is mediated by $p34^{cdc2}$ phosphorylation of vimentin. Cell **62**:1063–1071.
11. **Cimprich, K. A., T. B. Shin, C. T. Keith, and S. L. Schreiber.** 1996. cDNA cloning and gene mapping of a candidate human cell cycle checkpoint protein. Proc. Natl. Acad. Sci. USA **93**:2850–2855.
12. **Clarke, P. R., I. Hoffmann, G. Draetta, and E. Karsenti.** 1993. Dephosphorylation of cdc25-C by a type-2A protein phosphatase: specific regulation during the cell cycle in *Xenopus* egg extracts. Mol. Biol. Cell **4**:397–411.
13. **Connolly, J. L., S. E. Rodgers, P. Clarke, D. W. Ballard, L. D. Kerr, K. L. Tyler, and T. S. Dermody.** 2000. Reovirus-induced apoptosis requires activation of transcription factor NF-κB. J. Virol. **74**:2981–2989.
14. **Cox, D. C., and J. E. Shaw.** 1974. Inhibition of the initiation of cellular DNA synthesis after reovirus infection. J. Virol. **13**:760–761.
15. **Dales, S.** 1963. Association between the spindle apparatus and reovirus. Proc. Natl. Acad. Sci. USA **50**:268–275.
16. **Dermody, T. S., M. L. Nibert, R. Bassel-Duby, and B. N. Fields.** 1990. Sequence diversity in S1 genes and S1 translation products of 11 serotype 3 reovirus strains. J. Virol. **64**:4842–4850.
17. **Duncan, R., D. Horne, L. W. Cashdollar, W. K. Joklik, and P. W. Lee.** 1990. Identification of conserved domains in the cell attachment proteins of the three serotypes of reovirus. Virology **174**:399–409.
18. **Endl, E., and J. Gerdes.** 2000. The Ki-67 protein: fascinating forms and an unknown function. Exp. Cell Res. **257**:231–237.
19. **Ewen, M. E.** 2000. Where the cell cycle and histones meet. Genes Dev. **14**:2265–2270.
20. **Fajardo, E., and A. J. Shatkin.** 1990. Expression of the two reovirus S1 gene products in transfected mammalian cells. Virology **178**:223–231.
21. **Fode, C., C. Binkert, and J. W. Dennis.** 1996. Constitutive expression of murine Sak-a suppresses cell growth and induces multinucleation. Mol. Cell. Biol. **16**:4665–4672.
22. **Furnari, B., N. Rhind, and P. Russell.** 1997. Cdc25 mitotic inducer targeted by chk1 DNA damage checkpoint kinase. Science **277**:1495–1497.
23. **Gaulton, G. N., and M. I. Greene.** 1989. Inhibition of cellular DNA synthesis by reovirus occurs through a receptor-linked signaling pathway that is mimicked by antiidiotypic, antireceptor antibody. J. Exp. Med. **169**:197–211.
24. **Gautier, J., J. Minshull, M. Lohka, M. Glotzer, T. Hunt, and J. L. Maller.** 1990. Cyclin is a component of maturation-promoting factor from *Xenopus*. Cell **60**:487–494.
25. **Glover, D. M., I. M. Hagan, and A. A. Tavares.** 1998. Polo-like kinases: a team that plays throughout mitosis. Genes Dev. **12**:3777–3787.
26. **Grana, X., J. Garriga, and X. Mayol.** 1998. Role of the retinoblastoma protein family, pRB, p107 and p130 in the negative control of cell growth. Oncogene **17**:3365–3383.
27. **Hand, R., and I. Tamm.** 1974. Initiation of DNA replication in mammalian cells and its inhibition by reovirus infection. J. Mol. Biol. **82**:175–183.
28. **Harkin, D. P., J. M. Bean, D. Miklos, Y. H. Song, V. B. Truong, C. Englert, F. C. Christians, L. W. Ellisen, S. Maheswaran, J. D. Oliner, and D. A. Haber.** 1999. Induction of GADD45 and JNK/SAPK-dependent apoptosis following inducible expression of BRCA1. Cell **97**:575–586.
29. **Harper, J. W.** 1997. Cyclin dependent kinase inhibitors. Cancer Surv. **29**:91–107.
30. **He, J., S. Choe, R. Walker, P. Di Marzio, D. O. Morgan, and N. R. Landau.** 1995. Human immunodeficiency virus type 1 viral protein R (Vpr) arrests cells in the G_2 phase of the cell cycle by inhibiting $p34^{cdc2}$ activity. J. Virol. **69**:6705–6711.
31. **Herwig, S., and M. Strauss.** 1997. The retinoblastoma protein: a master regulator of cell cycle, differentiation and apoptosis. Eur. J. Biochem. **246**: 581–601.
32. **Hirose, T., M. Kawabuchi, T. Tamaru, N. Okumura, K. Nagai, and M. Okada.** 2000. Identification of tudor repeat associator with PCTAIRE 2 (Trap). A novel protein that interacts with the N-terminal domain of PCTAIRE 2 in rat brain. Eur. J. Biochem. **267**:2113–2121.
33. **Hirose, T., T. Tamaru, N. Okumura, K. Nagai, and M. Okada.** 1997. PCTAIRE 2, a Cdc2-related serine/threonine kinase, is predominantly expressed in terminally differentiated neurons. Eur. J. Biochem. **249**:481–488.
34. **Hobbs, W. E., and N. A. DeLuca.** 1999. Perturbation of cell cycle progression and cellular gene expression as a function of herpes simplex virus ICP0. J. Virol. **73**:8245–8255.
35. **Hrimech, M., X. J. Yao, P. E. Branton, and E. A. Cohen.** 2000. Human immunodeficiency virus type 1 vpr-mediated G_2 cell cycle arrest: vpr interferes with cell cycle signaling cascades by interacting with the B subunit of serine/threonine protein phosphatase 2A. EMBO J. **19**:3956–3967.
36. **Hudson, J. W., L. Chen, C. Fode, C. Binkert, and J. W. Dennis.** 2000. Sak kinase gene structure and transcriptional regulation. Gene **241**:65–73.
37. **Iijima, M., Y. Kano, T. Nohno, and M. Namba.** 1996. Cloning of cDNA with possible transcription factor activity at the G_1-S phase transition in human fibroblast cell lines. Acta Med. Okayama **50**:73–77.
38. **Jackman, M. R., and J. N. Pines.** 1997. Cyclins and the G_2/M transition. Cancer Surv. **29**:47–73.
39. **Jin, S., H. Zhao, F. Fan, P. Blanck, W. Fan, A. B. Colchagie, A. J. Fornace, and Q. Zhan.** 2000. BRCA1 activation of the GADD45 promoter. Oncogene **19**:4050–4057.
40. **Kalitsis, P., E. Earle, K. J. Fowler, and K. H. Choo.** 2000. Bub3 gene disruption in mice reveals essential mitotic spindle checkpoint function during early embryogenesis. Genes Dev. **14**:2277–2282.
41. **Kastan, M. B., Q. Zhan, W. S. el Deiry, F. Carrier, T. Jacks, W. V. Walsh, B. S. Plunkett, B. Vogelstein, and A. J. Fornace.** 1992. A mammalian cell cycle checkpoint pathway utilizing p53 and GADD45 is defective in ataxia telangiectasia. Cell **71**:587–597.
42. **Kinoshita, N., H. Ohkura, and M. Yanagida.** 1990. Distinct, essential roles of type 1 and 2A protein phosphatases in the control of the fission yeast cell division cycle. Cell **63**:405–415.
43. **Kitay, M. K., and D. T. Rowe.** 1996. Cell cycle stage-specific phosphorylation of the Epstein-Barr virus immortalization protein EBNA-LP. J. Virol. **70**: 7885–7893.
44. **Kumada, K., S. Su, M. Yanagida, and T. Toda.** 1995. Fission yeast TPR-family protein nuc2 is required for G_1-arrest upon nitrogen starvation and is an inhibitor of septum formation. J. Cell Sci. **108**:895–905.
45. **Lee, T. H., M. J. Solomon, M. C. Mumby, and M. W. Kirschner.** 1991. INH,

a negative regulator of MPF, is a form of protein phosphatase 2A. Cell **64**:415–423.
46. **Li, S., N. S. Ting, L. Zheng, P. L. Chen, Y. Ziv, Y. Shiloh, E. Y. Lee, and W. H. Lee.** 2000. Functional link of BRCA1 and ataxia telangiectasia gene product in DNA damage response. Nature **406**:210–215.
47. **Lopez-Girona, A., B. Furnari, O. Mondesert, and P. Russell.** 1999. Nuclear localization of Cdc25 is regulated by DNA damage and a 14-3-3 protein. Nature **397**:172–175.
48. **Masuda, M., Y. Nagai, N. Oshima, K. Tanaka, H. Murakami, H. Igarashi, and H. Okayama.** 2000. Genetic studies with the fission yeast *Schizosaccharomyces pombe* suggest involvement of *wee1*, *ppa2*, and *rad24* in induction of cell cycle arrest by human immunodeficiency virus type 1 Vpr. J. Virol. **74**:2636–2646.
49. **Matsumoto-Taniura, N., F. Pirollet, R. Monroe, L. Gerace, and J. M. Westendorf.** 1996. Identification of novel M phase phosphoproteins by expression cloning. Mol. Biol. Cell **7**:1455–1469.
50. **McCright, B., A. M. Rivers, S. Audlin, and D. M. Virshup.** 2089. 1996. The B56 family of protein phosphatase 2A (PP2A) regulatory subunits encodes differentiation-induced phosphoproteins that target PP2A to both nucleus and cytoplasm. J. Biol. Chem. **271**:22081–22082.
51. **Moreno, C. S., S. Park, K. Nelson, D. Ashby, F. Hubalek, W. S. Lane, and D. C. Pallas.** 2000. WD40 repeat proteins striatin and S/G_2 nuclear autoantigen are members of a novel family of calmodulin-binding proteins that associate with protein phosphatase 2A. J. Biol. Chem. **275**:5257–5263.
52. **Muro, Y., E. K. Chan, G. Landberg, and E. M. Tan.** 1995. A cell-cycle nuclear autoantigen containing WD-40 motifs expressed mainly in S and G_2 phase cells. Biochem. Biophys. Res. Commun. **207**:1029–1037.
53. **Nibert, M. L., L. A. Schiff, and B. N. Fields.** 1996. Reoviruses and their replication, p. 1557–1596. *In* B. N. Fields, D. M. Knipe, and P. M. Howley (ed.), Fields virology, 3rd ed. Lippincott-Raven Publishers, Philadelphia, Pa.
54. **Nigg, E. A.** 1998. Polo-like kinases: positive regulators of cell division from start to finish. Curr. Opin. Cell Biol. **10**:776–783.
55. **Nurse, P.** 1990. Universal control mechanism regulating onset of M-phase. Nature **344**:503–508.
56. **O'Connell, M. J., J. M. Raleigh, H. M. Verkade, and P. Nurse.** 1997. Chk1 is a wee1 kinase in the G_2 DNA damage checkpoint inhibiting cdc2 by Y15 phosphorylation. EMBO J. **16**:545–554.
57. **O'Connor, P. M.** 1997. Mammalian G_1 and G_2 phase checkpoints. Cancer Surv. **29**:151–182.
58. **Op, D. B., and P. Caillet-Fauquet.** 1997. Viruses and the cell cycle. Prog. Cell Cycle Res.**3**:1–19.
59. **Page, A. M., and P. Hieter.** 1997. The anaphase promoting complex. Cancer Surv. **29**:133–150.
60. **Parker, L. L., S. Atherton-Fessler, and H. Piwnica-Worms.** 1992. $p107^{wee1}$ is a dual-specificity kinase that phosphorylates $p34^{cdc2}$ on tyrosine 15. Proc. Natl. Acad. Sci. USA **89**:2917–2921.
61. **Peng, C. Y., P. R. Graves, R. S. Thoma, Z. Wu, A. S. Shaw, and H. Piwnica-Worms.** 1997. Mitotic and G_2 checkpoint control: regulation of 14-3-3 protein binding by phosphorylation of Cdc25C on serine-216. Science **277**:1501–1505.
62. **Poggioli, G. J., T. S. Dermody, and K. L. Tyler.** 2001. Reovirus-induced σ1s-dependent G_2/M phase cell cycle arrest is associated with inhibition of $p34^{cdc2}$. J. Virol. **75**:7429–7434.
63. **Poggioli, G. J., C. Keefer, J. L. Connolly, T. S. Dermody, and K. L. Tyler.** 2000. Reovirus-induced G_2/M cell cycle arrest requires σ1s and occurs in the absence of apoptosis. J. Virol. **74**:9562–9570.
64. **Re, F., D. Braaten, E. K. Franke, and J. Luban.** 1995. Human immunodeficiency virus type 1 Vpr arrests the cell cycle in G_2 by inhibiting the activation of $p34^{cdc2}$-cyclin B. J. Virol. **69**:6859–6864.
65. **Resto, V. A., O. L. Caballero, M. R. Buta, W. H. Westra, L. Wu, J. M. Westendorf, J. Jen, P. Hieter, and D. Sidransky.** 2000. A putative oncogenic role for MPP11 in head and neck squamous cell cancer. Cancer Res. **60**: 5529–5535.
66. **Roberts, B. T., K. A. Farr, and M. A. Hoyt.** 1994. The *Saccharomyces cerevisiae* checkpoint gene BUB1 encodes a novel protein kinase. Mol. Cell. Biol. **14**:8282–8291.
67. **Rodgers, S. E., J. L. Connolly, J. D. Chappell, and T. S. Dermody.** 1998. Reovirus growth in cell culture does not require the full complement of viral proteins: identification of a σ1s-null mutant. J. Virol. **72**:8597–8604.
68. **Roner, M. R., and D. C. Cox.** 1985. Cellular integrity is required for inhibition of initiation of cellular DNA synthesis by reovirus type 3. J. Virol. **53**:350–359.
69. **Sanchez, Y., C. Wong, R. S. Thoma, R. Richman, Z. Wu, H. Piwnica-Worms, and S. J. Elledge.** 1997. Conservation of the Chk1 checkpoint pathway in mammals: linkage of DNA damage to Cdk regulation through Cdc25. Science **277**:1497–1501.
70. **Saragovi, H. U., A. Bhandoola, M. M. Lemercier, G. K. Akbar, and M. I. Greene.** 1995. A receptor that subserves reovirus binding can inhibit lymphocyte proliferation triggered by mitogenic signals. DNA Cell Biol.**14**:653–664.
71. **Saragovi, H. U., N. Rebai, G. M. Di Guglielmo, R. Macleod, J. Sheng, D. H. Rubin, and M. I. Greene.** 1999. A G_1 cell cycle arrest induced by ligands of the reovirus type 3 receptor is secondary to inactivation of $p21^{ras}$ and mitogen-activated protein kinase. DNA Cell Biol.**18**:763–770.
72. **Saragovi, H. U., N. Rebai, E. Roux, M. Gagnon, X. Zhang, B. Robaire, J. Bromberg, and M. I. Greene.** 1998. Signal transduction and antiproliferative function of the mammalian receptor for type 3 reovirus. Curr. Top. Microbiol. Immunol. **233**:155–166.
73. **Scholzen, T., and J. Gerdes.** 2000. The Ki-67 protein: from the known and the unknown. J. Cell. Physiol. **182**:311–322.
74. **Sharpe, A. H., L. B. Chen, and B. N. Fields.** 1982. The interaction of mammalian reoviruses with the cytoskeleton of monkey kidney CV-1 cells. Virology **120**:399–411.
75. **Sharpe, A. H., and B. N. Fields.** 1981. Reovirus inhibition of cellular DNA synthesis: role of the S1 gene. J. Virol. **38**:389–392.
76. **Solomon, M. J., M. Glotzer, T. H. Lee, M. Philippe, and M. W. Kirschner.** 1990. Cyclin activation of $p34^{cdc2}$. Cell **63**:1013–1024.
77. **Starr, D. A., R. Saffery, Z. Li, A. E. Simpson, K. H. Choo, T. J. Yen, and M. L. Goldberg.** 2000. HZwint-1, a novel human kinetochore component that interacts with HZW10. J. Cell Sci. **113**:1939–1950.
78. **Straight, A. F.** 1997. Cell cycle: checkpoint proteins and kinetochores. Curr. Biol. **7**:R613–R616.
79. **Taylor, S. S., E. Ha, and F. McKeon.** 1998. The human homologue of Bub3 is required for kinetochore localization of Bub1 and a Mad3/Bub1-related protein kinase. J. Cell Biol. **142**:1–11.
80. **Tyler, K. L., and B. N. Fields.** 1996. Reoviruses, p. 1597–1623. *In* B. N. Fields, D. M. Knipe, and P. M. Howley (ed.), Fields virology, 3rd ed. Lippincott-Raven Publishers, Philadelphia, Pa.
81. **Tyler, K. L., D. A. McPhee, and B. N. Fields.** 1986. Distinct pathways of viral spread in the host determined by reovirus S1 gene segment. Science **233**: 770–774.
82. **Tyler, K. L., M. K. Squier, A. L. Brown, B. Pike, D. Willis, S. M. Oberhaus, T. S. Dermody, and J. J. Cohen.** 1996. Linkage between reovirus-induced apoptosis and inhibition of cellular DNA synthesis: role of the S1 and M2 genes. J. Virol. **70**:7984–7991.
83. **Wang, X. W., Q. Zhan, J. D. Coursen, M. A. Khan, H. U. Kontny, L. Yu, M. C. Hollander, P. M. O'Connor, A. J. Fornace, Jr., and C. C. Harris.** 1999. GADD45 induction of a G_2/M cell cycle checkpoint. Proc. Natl. Acad. Sci. USA **96**:3706–3711.
84. **Ye, M., K. M. Duus, J. Peng, D. H. Price, and C. Grose.** 1999. Varicella-zoster virus Fc receptor component gI is phosphorylated on its endodomain by a cyclin-dependent kinase. J. Virol. **73**:1320–1330.
85. **Yoshida, Y., S. Matsuda, N. Ikematsu, J. Kawamura-Tsuzuku, J. Inazawa, H. Umemori, and T. Yamamoto.** 1998. ANA, a novel member of the Tob/BTG1 family, is expressed in the ventricular zone of the developing central nervous system. Oncogene **16**:2687–2693.
86. **Zafrullah, M., M. H. Ozdener, S. K. Panda, and S. Jameel.** 1997. The ORF3 protein of hepatitis E virus is a phosphoprotein that associates with the cytoskeleton. J. Virol. **71**:9045–9053.
87. **Zhan, Q., M. J. Antinore, X. W. Wang, F. Carrier, M. L. Smith, C. C. Harris, and A. J. Fornace, Jr.** 1999. Association with cdc2 and inhibition of cdc2/cyclin B1 kinase activity by the p53-regulated protein GADD45. Oncogene **18**:2892–2900.

Cell Death and Differentiation (2002) 9, 926–933

www.nature.com/cdd

Reovirus-induced apoptosis requires both death receptor- and mitochondrial-mediated caspase-dependent pathways of cell death

DJ Kominsky[1], RJ Bickel[1], and KL Tyler*[,1,2,3]

[1] Department of Neurology, University of Colorado Health Science Center, Denver, Colorado 80262, USA
[2] Department of Medicine, Microbiology, and Immunology, University of Colorado Health Science Center, Denver, Colorado 80262, USA
[3] Denver Veteran's Affairs Medical Center, Denver, Colorado 80220, USA
* Corresponding author: KL Tyler, Department of Neurology (B-182), University of Colorado Health Science Center, 4200 E. 9th Avenue, Denver, CO 80262, USA. Tel: (303) 393-2874; Fax: (303) 393-4686; E-mail: Ken.Tyler@uchsc.edu.

Received 17.10.01; revised 14.1.02; accepted 6.2.02
Edited by CJ Thiele

Abstract

Apoptosis plays an important role in the pathogenesis of many viral infections. Despite this fact, the apoptotic pathways triggered during viral infections are incompletely understood. We now provide the first detailed characterization of the pattern of caspase activation following infection with a cytoplasmically replicating RNA virus. Reovirus infection of HEK293 cells results in the activation of caspase-8 followed by cleavage of the pro-apoptotic protein Bid. This initiates the activation of the mitochondrial apoptotic pathway leading to release of cytochrome *c* and activation of caspase-9. Combined activation of death receptor and mitochondrial pathways results in downstream activation of effector caspases including caspase-3 and caspase-7 and cleavage of cellular substrates including PARP. Apoptosis is initiated by death receptor pathways but requires mitochondrial amplification producing a biphasic pattern of caspase-8, Bid, and caspase-3 activation.
Cell Death and Differentiation (2002) **9,** 926–933. doi:10.1038/sj.cdd.4401045

Keywords: apoptosis; reovirus; caspase; death receptor; mitochondria

Abbreviations: JAM, junction adhesion molecule; TNF, tumor necrosis factor; TRAIL, TNF-related apoptosis-inducing ligand; DR, death receptor; DISC, death-inducing signaling complex; FADD, Fas-associated death domain; DEVD-AFC, Asp-Glu-Val-Asp-7-amino-4-methyl coumarin; PARP, poly(ADP-ribose) polymerase; Ac-YVAD-CHO, Ac-Tyr-Val-Ala-Asp-CHO; Ac-DEVD-CHO, Ac-Asp-Glu-Val-Asp-CHO; Ac-IETD-CHO, Ac-Ile-Asp-Thr-Glu-CHO

Introduction

Apoptosis is a particular type of cell death that is characterized by distinctive changes in cellular morphology, including cell shrinkage, zeiosis, nuclear condensation, chromatin margination and subsequent degradation that are associated with inter-nucleosomal DNA fragmentation. Apoptosis may be initiated by a wide variety of cellular insults, including death receptor stimulation, γ-radiation, and cytotoxic compounds. Induction or inhibition of apoptosis is an important feature of many types of viral infection, both *in vitro* and *in vivo*. Despite this fact, the mechanisms of virus-induced apoptosis remain largely unknown. This is particularly true for RNA viruses, the majority of which have cytoplasmic intracellular sites of replication and do not require nuclear integrity for successful propogation.

Mammalian reoviruses are non-enveloped double-stranded RNA viruses whose replication occurs exclusively in the cytoplasm. Reoviruses induce apoptosis in a wide variety of cultured cells *in vitro*.[1–3] Apoptosis also plays a critical role during reovirus infection *in vivo*, and is the mechanism of virus-induced tissue injury in key target organs, including the central nervous system and heart.[1,4,5] Inhibition of apoptosis dramatically reduces the extent of reovirus-induced tissue injury *in vivo*.[5]

It has been shown recently that reovirus-induced apoptosis requires interaction with its cell surface receptors including junction adhesion molecule (JAM).[6] Apoptosis involves the tumor necrosis factor (TNF) superfamily of cell surface death receptors, specifically DR4, DR5 and their ligand, TNF-related apoptosis-inducing ligand (TRAIL),[7] and is inhibited by anti-TRAIL antibodies or soluble forms of DR4 or DR5 which inhibit interaction of TRAIL with functional cell surface DR4 and DR5.[7] The contribution of mitochondrial apoptotic pathways to this process has been unknown, as has the exact nature of the caspase cascades activated and their inter-relationship.

Apoptosis induced by activation of cell surface death receptors ('extrinsic pathway') involves the formation of a death-induced signaling complex (DISC) that recruits and activates caspase-8.[8] Activated caspase-8 can, in turn, activate downstream effector caspases including caspases-3 and -7. Mitochondria play a central role in an 'intrinsic' pathway of apoptosis. In this pathway, apoptotic stimuli enhance mitochondrial membrane permeability and permit the translocation of cytochrome *c* and other pro-apoptotic molecules from the mitochondria into the cytosol.[9–12] A cytosolic complex including cytochrome *c* and Apaf-1 (apoptosome) activates caspase-9.[13] Activated caspase-9, like activated caspase-8, can activate additional downstream effector caspases including caspase-3. The intrinsic and extrinsic pathways are linked by Bid, a pro-apoptotic

Bcl-2 family member. Caspase-8-dependent cleavage of Bid allows this protein to translocate to the mitochondrion, where it directly or indirectly facilitates cytochrome *c* release.[14–18] The importance of the mitochondrial apoptotic pathway in augmenting death-receptor initiated apoptosis can be assessed by studying the pattern of caspase activation and the effects of Bcl-2 expression. Death receptor-initiated, mitochondrial-dependent apoptosis is generally associated with early low level activation of caspase-8 and is inhibitable by Bcl-2.[19,20] Conversely, mitochondrial-independent, death receptor-initiated apoptosis is associated with more robust caspase-8 activation and is not inhibited by Bcl-2 expression.[19,20]

In this paper we provide the first comprehensive characterization of the pattern of caspase activation following infection with a cytoplasmically replicating RNA virus. We show that reovirus infection results in the activation of death receptor- and mitochondrial-associated initiator caspases, caspase-8 and caspase-9. Activation of these initiator caspases is followed by activation of the effector caspases caspase-3 and caspase-7. Caspase-8-dependent cleavage of the Bid provides a linkage between the death receptor and mitochondrial pathways of apoptosis following reovirus infection. Inhibition of caspase-8 activation prevents the cleavage of Bid, and the subsequent activation of the mitochondrial pathway. Both the mitochondrial and death receptor-initiated pathways are essential for reovirus-induced apoptosis as inhibition of death receptor pathways by over-expression of dominant negative FADD (FADD-DN) or of mitochondrial pathways by over-expression of Bcl-2 prevents reovirus-induced effector caspase activation. Consistent with this model, cell permeable inhibitors of both group II caspases (caspase-2, -3, and -7) and group III caspases (caspase-6, -8, and -9) but not of group I caspases (caspase-1, -4, and -5) inhibit reovirus-induced caspase-3 activation. These studies provide not only a comprehensive profile of caspase activation following virus infection, but also the first demonstration that both death receptor and mitochondrial pathways can play an essential role in virus-induced apoptosis.

Results

Caspase-8 is activated following reovirus infection

Apoptosis initiated via TNF receptor superfamily cell death receptors involves the adaptor molecule FADD and subsequent activation of caspases, starting with the initiator caspase, caspase-8.[21] We therefore wanted to examine whether reovirus infection induced the activation of caspase-8. As shown in Figure 1a, reovirus infection induces the activation of caspase-8 as evidenced by the disappearance of the full-length proenzyme (seen as a 55/54 kD doublet). The reduction in caspase-8 immunoreactivity appeared to be biphasic. A first phase of activation was detectable as early as 8 h post-infection. A second, more intense phase of activation began at 22 h post-infection and continued through $\geqslant$34 h (Figure 1a,b). No cellular morphological changes were observed correlating with the early phase of caspase-8 activation.

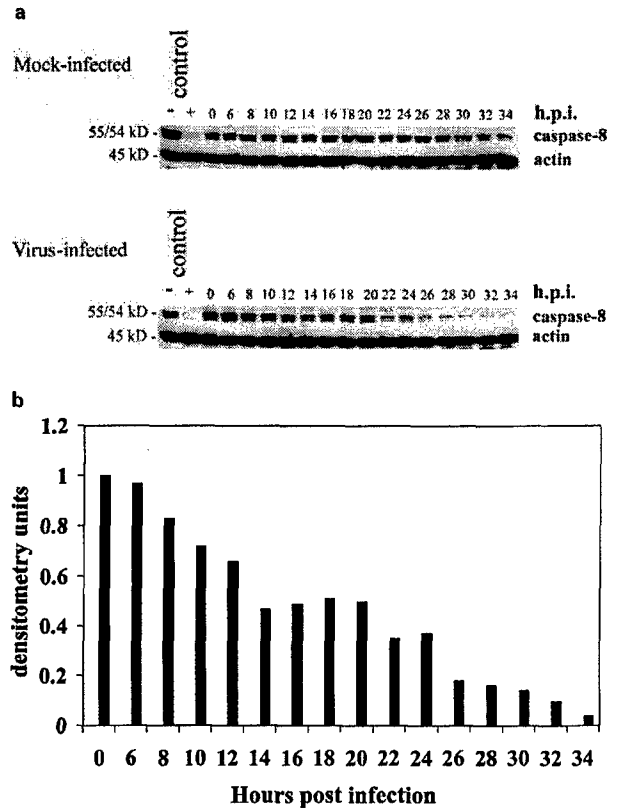

Figure 1 Reovirus infection induces the activation of caspase-8. HEK 293 lysates were prepared at the indicated times points from mock-infected or reovirus-infected cells and probed with anti-caspase-8 antibodies and anti-actin antibodies (**a**). Control lanes represent Jurkat cell lysates untreated (−) or treated (+) with activating anti-Fas antibody and harvested at 8 h post treatment. The Western is representative of two separate experiments. The graph displays densitometric analysis of the virus-infected Western blot analysis (**b**). Values are expressed as arbitrary densitometric units

Reovirus infection is associated with release of mitochondrial cytochrome *c* and activation of caspase-9

Reovirus-induced activation of caspase-8 revealed a biphasic pattern. This suggested that apoptosis signals initiated through the death receptor pathway might be amplified by other apoptotic pathways. We therefore looked for evidence that reovirus infection activated mitochondrial-associated apoptotic signaling pathways. We first wished to determine whether reovirus infection was associated with release of cytochrome *c* and activation of caspase-9. Mitochondria-free lysates were prepared from both mock- and reovirus-infected cells at the indicated time points and analyzed by Western blot for the presence of cytosolic cytochrome *c* (Figure 2). Blots were probed with antisera directed against the mitochondrial integral membrane protein cytochrome *c* oxidase (subunit II) to detect potential mitochondrial contamination of the samples. Cytosolic cytochrome *c* is detected in reovirus-infected cells at ~10 h post-infection (Figure 2a). In order to determine whether cytochrome *c* release was dependent on death receptor-initiated signaling, we also examined the

cellular localization of mitochondrial cytochrome *c* following reovirus infection in FADD-DN expressing cells. As shown in Figure 2b, cytochrome *c* is found at only trace levels in the cytoplasm of reovirus-infected FADD-DN expressing cells. These results indicate that caspase-8 activation occurs upstream of, and is required for, the release of cytochrome *c*. We next wished to determine whether caspase-9 was activated. Activation of caspase-9 involves the cleavage of the 46 kD pro-enzyme into a 37 kD active fragment. Activated caspase-9 was first detectable in reovirus-infected cells at 10 h post-infection (Figure 3), and was not detected in mock-infected cells. Activation increased steadily from 10 to 18 h and then persisted for $\geqslant$32 h.

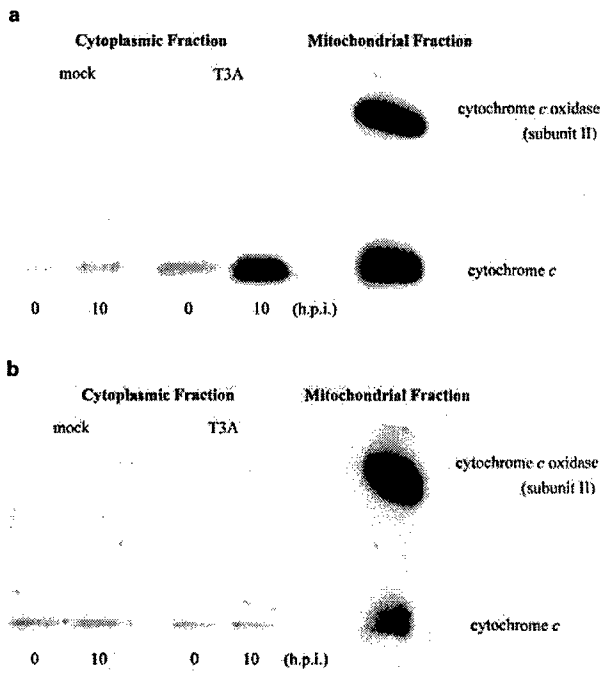

Figure 2 Cytochrome *c* is present in the cytosol of reovirus infected cells. HEK 293 cell lysates (**a**) and FADD-DN expressing HEK 293 cells lysates (**b**) were prepared at the indicated time points as described (see Materials and Methods) and resolved using SDS–PAGE. Western blot analysis was performed using anti-cytochrome *c* antibodies and anti-cytochrome *c* oxidase (subunit II) and are representative of three separate experiments

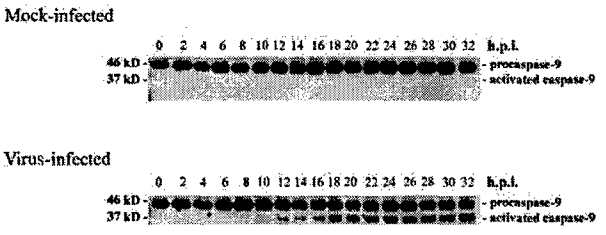

Figure 3 Caspase-9 is activated in reovirus-infected cells. HEK 293 cell lysates were prepared from mock-infected or reovirus-infected cells at the indicated time points and resolved by SDS–PAGE. Western blot analysis was performed using anti-caspase-9 antibodies and the blot is representative of three separate experiments

Bid is cleaved following reovirus infection

Bid is a pro-apoptotic member of the Bcl-2 protein family. Activation of both Fas receptor by Fas and DR4/DR5 by TRAIL can induce caspase-8 dependent cleavage of Bid.[15,17,18] Cleaved Bid can facilitate the release of cytochrome *c* from the mitochondrion and lead to subsequent apoptosome-mediated activation of caspase-9.[16] We wished to determine whether Bid was cleaved following reovirus infection, and if this cleavage depended on caspase-8 activation. Western blot analysis revealed that full-length Bid levels remain relatively unchanged in mock-infected cells (Figure 4a). However, following reovirus infection there was a biphasic pattern of Bid cleavage, analogous to that seen with caspase-8 (Figure 4a). Loss of the full length immunoreactive Bid was first detected as early as 10 h post-infection. A second phase of Bid cleavage began at 26 h post-infection and continued through $\geqslant$40 h (Figure 4a,b). In order to determine whether Bid cleavage was dependent on caspase-8 activation, we examined levels of immunoreactive Bid in cells in which caspase-8 activation was blocked by stable expression of DN-FADD. FADD-DN expression completely inhibited reovirus-induced Bid cleavage, indicating that Bid cleavage is caspase-8 dependent (Figure 4c).

Reovirus infection is associated with activation of caspase-3 and caspase-7

Effector caspases, including caspases-3, -6 and -7, form part of the final common pathway for death receptor and mitochondrial apoptotic pathways. Having shown that reovirus infection resulted in activation of both death receptor and mitochondrion-associated initiator caspases we next wished to determine which effector caspases were activated. Caspase-3 activation was evaluated by Western blot, using an antibody specific for the activated form of the enzyme. Activation of caspase-3 is associated with the appearance of specific cleavage product at ~20 kD representing the large subunit of active caspase-3. As shown in Figure 5a, this fragment appears beginning at ~8 h post-infection in reovirus infected cells, but not in the mock infected controls. There is a biphasic activation profile, with the initial activation phase beginning at 8 h post-infection and a second, more intense activation phase beginning at 24 h post-infection (Figure 5a). A similar pattern of caspase activation was seen in fluorogenic substrate assays using a caspase-3 specific substrate (DEVD-AFC) (see Figure 6c). An initial phase of activation at 6–12 h was followed by a rapid activation peak 12–18 h. Activated caspase-3 cleaves a variety of cellular substrates to induce the morphological hallmarks of apoptosis. We therefore examined the cleavage of PARP. PARP is cleaved by caspase-3 from the full-length 116 kD protein to an 85 kD inactive fragment. As shown in Figure 5b, PARP cleavage exceeding that seen in mock-infected cells was first detectable at 14 h post-infection and persisted until $\geqslant$20 h post-infection. These experiments established that reovirus infection results in activation of the effector caspase, caspase-3 and is associated with cleavage of cellular substrates of caspase-3.

Other effector caspases may also be activated downstream of caspase-8 and caspase-9. Therefore, we

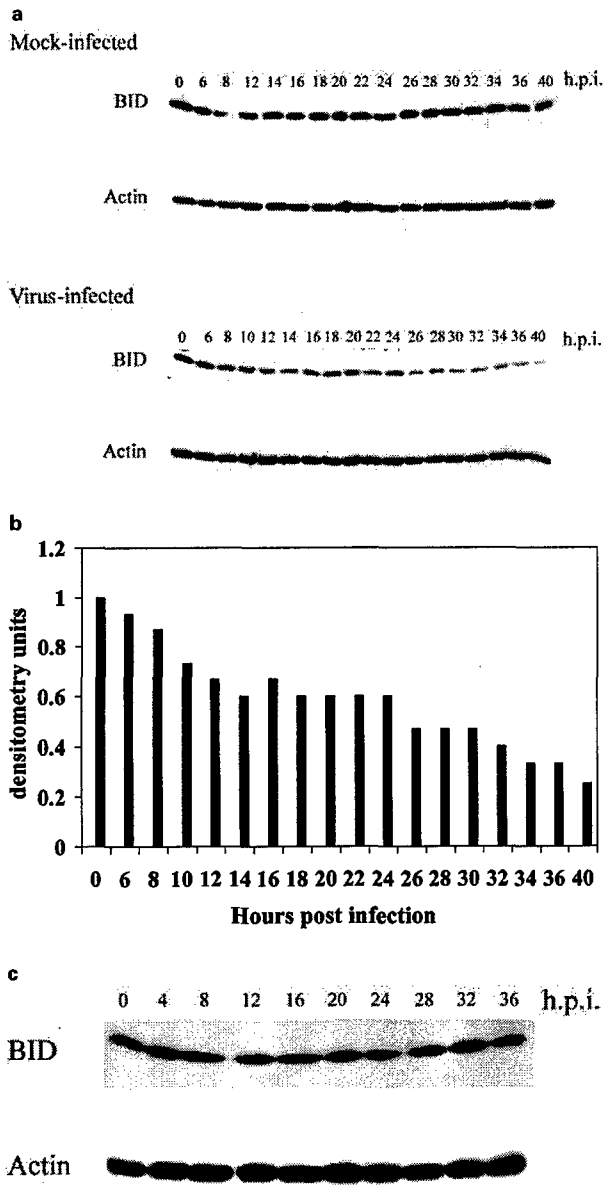

Figure 4 Reovirus infection leads to cleavage of full-length Bid. Lysates were prepared at the indicated time points from mock-infected or reovirus-infected HEK 293 cells (**a**) and reovirus infected FADD-DN expressing HEK 293 cells (**c**) and probed with anti-Bid antibodies and anti-actin antibodies. Each Western blot is representative of two separate experiments. The graph displays densitometric analysis of the virus-infected Western blot analysis (**b**). Values are expressed as arbitrary densitometric units

examined the activation state of two other effector caspases, caspase-6 and caspase-7. We found no evidence by immunoblot of caspase-6 activation in reovirus-infected cells (data not shown). Caspase-7 is activated in infected cells as evidenced by the detection of the 20 kD large subunit of active caspase-7 (Figure 5C). However, caspase-7 activation appears to occur later than activation of caspase-3, and the amount of activation appears less.

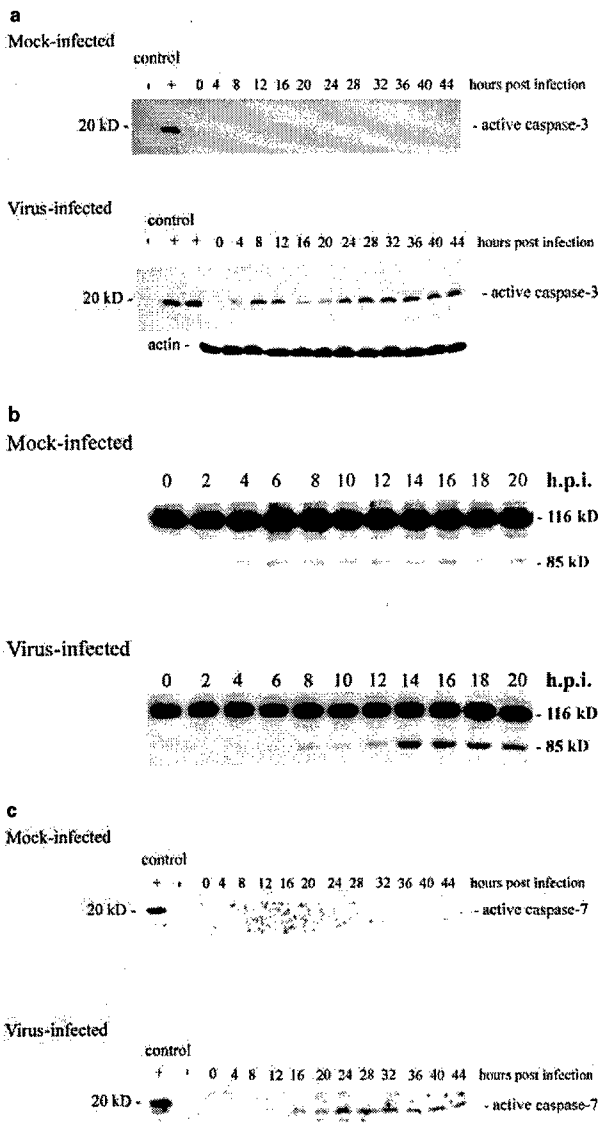

Figure 5 Reovirus infection leads to activation of caspase-3. Western blot analysis was performed using HEK 293 lysates harvested at the indicated time points from mock-infected and reovirus-infected cells and probed with anti-caspase-3 antibodies (**a**), anti-PARP antibodies (**b**), or anti-caspase-7 antibodies (**c**). Control lanes represent Jurkat cell lysates untreated (−) or treated (+) with activating anti-Fas antibody and harvested at 8 h post treatment. Each Western is representative of two separate experiments

In order to determine whether activation of effector caspases was completely dependent on the initial activation of death-receptor mediated pathways, we examined effector caspase activation in cells stably expressing DN-FADD. As shown in Figure 6a, the activation of both caspase-3 and caspase-7 is blocked in cells stably expressing DN-FADD. Caspase-3 activity, as measured in a fluorogenic substrate assay, is almost completely inhibited in these cells (Figure 6c). This suggests that activation of death-receptor initiated apoptotic signaling pathways is required for reovirus-induced effector caspase activation and apoptosis.

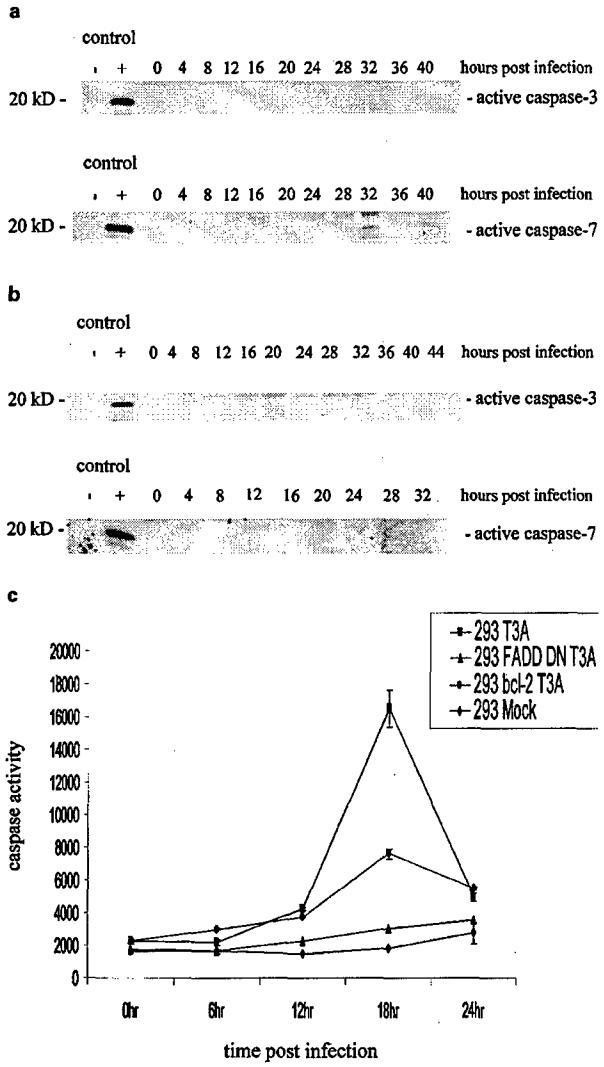

Figure 6 Effector caspase activation in inhibited in FADD-DN and Bcl-2 over-expressing cells. Western blot analysis was performed using cell lysates prepared from reovirus-infected FADD-DN over-expressing cells (**a**) or Bcl-2 overexpressing cells (**b**) at the indicated time points and probed with anti-caspase-3 antibodies and anti-caspase-7 antibodies. Control lanes represent Jurkat cell lysates untreated (−) or treated (+) with activating anti-Fas antibody and harvested at 8 h post treatment. Western blots are representative of two separate experiments. Fluorogenic substrate assays (**c**) were performed in triplicate. Error bars represent standard error of the mean. Fluorescence is expressed as arbitrary units

Bcl-2 overexpression inhibits effector caspase activation following reovirus infection

Experiments with FADD-DN indicated that death-receptor pathways were necessary for reovirus-induced apoptosis. Activation of both caspase-8 and Bid showed a biphasic pattern with an early activation phase at 8–10 h followed by a later activation phase. Reovirus-induced initiation of mitochondrial apoptotic pathways occurred downstream of caspase-8 activation, began slightly later following infection, and was not biphasic. This suggested that mitochondrial apoptotic pathways might play a central role in amplifying death receptor-initiated signaling. The capacity of Bcl-2 to inhibit apoptosis has been used as evidence suggesting an essential role for mitochondrial apoptotic pathways.[19,20] We wished to determine whether Bcl-2 over-expression in HEK cells inhibited caspase activation. Caspase activation was examined using both Western blot analysis and fluorogenic substrate assays. As shown in Figure 6b, activation of both caspase-3 and caspase-7 is inhibited in cells over-expressing Bcl-2. The late phase of caspase-8 activation was also inhibited in these cells although the low level early phase of caspase-8 activation was preserved (data not shown). Caspase-3 activity, as measured in a fluorogenic substrate assay, is also significantly reduced in these cells (Figure 6c). However, the pattern of inhibition differs from that seen in cells stably expressing DN-FADD. In Bcl-2 expressing cells there is some residual caspase-3 activation suggesting that death receptor-mediated apoptotic pathways can induce low levels of effector caspase activation, but full induction requires augmentation by mitochondrial apoptotic pathways. This low level of caspase-3 activation in Bcl-2 overexpressing cells was not reflected in cellular morphology.

Effects of synthetic caspase peptide inhibitors on caspase-3 activation

Caspases can be categorized into three major groups based on their pattern of substrate specificity.[22,23] Group I includes caspase-1, -4, and 5; group II includes caspase-2, -3, and 7; group III includes caspase-6, -8 and -9. Cell permeable, reversible, peptide caspase inhibitors have been developed based on these caspase substrate profiles.[22,23] We tested the capacity of three reversible cell permeable caspase inhibitors with specificity for group I (Ac-YVAD-CHO), group II (Ac-DEVD-CHO), and group III (Ac-IETD-CHO) caspases to inhibit reovirus-induced caspase-3 activation at 18 h post-infection. As shown in Figure 7, the group II inhibitor Ac-DEVD-CHO completely inhibited reovirus-induced caspase-3 activity at a concentration of 10 μM. The group I inhibitor (Ac-YVAD-CHO) had no effect on caspase-3 activation, consistent with a lack of involvement of caspases-1, -4 or -5 in reovirus-induced apoptosis. The group III inhibitor Ac-IETD-CHO achieved maximal inhibition of reovirus-induced caspase-3 activation at a concentration of 5 μM. However, the maximum degree of inhibition (65%) was not as high as that seen with the group II inhibitor. These data suggest that while the activation of group III caspases, including caspase-8 and -9, is critically important to reovirus-induced apoptosis that other as yet unidentified caspases may also contribute to caspase-3 activation. However, the fact that expression of DN-FADD was as effective as treatment with the group II inhibitor Ac-DEVD-CHO in blocking caspase-3 activation, suggests that the apical caspases that contribute to caspase-3 activation all depend on an initial death-receptor initiated caspase activation signal.

Discussion

Understanding the mechanisms of virus-induced apoptosis is crucial to understanding how viruses injure target tissues and

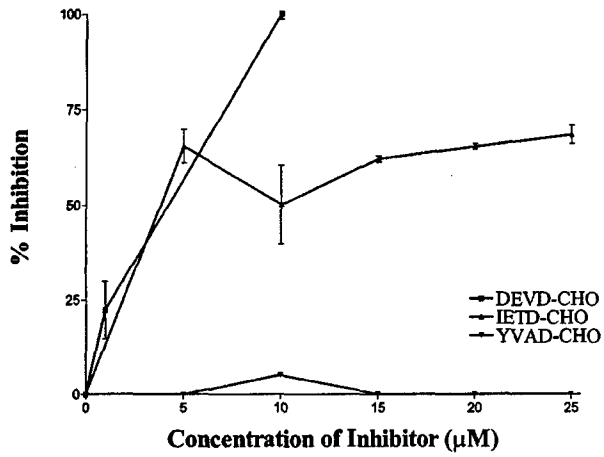

Figure 7 Synthetic peptide inhibition of DEVD-specific caspase activation. HEK 293 cells were pretreated with the synthetic peptide inhibitors at the concentrations shown for 1 h prior to reovirus infection (M.O.I. 100). Fluorogenic substrate assays were performed at 18 h post infection. Values are expressed as per cent inhibition where untreated reovirus-infected cells represent 0% inhibition and mock-infected cells represent 100% inhibition

induce disease. The exact pathways leading to virus-induced apoptosis are still incompletely understood. Since caspases play a central role in virtually all known apoptotic signaling pathways, it is not surprising that they have been implicated in virus-induced apoptosis. Pancaspase peptide inhibitors have been shown to inhibit apoptosis induced by viruses as diverse as Sindbis,[24,25] HIV-1,[26,27] Herpes simplex virus type 1,[28] influenza,[29] Sendai,[30] and TGEV.[31]

The events that initiate caspase activation in virus-infected cells are still incompletely understood. Activation of caspase-8 plays an important role in apoptosis induced by HIV-1,[26] influenza,[29] Sendai,[30] and Sindbis,[24] suggesting that death-receptor initiated processes may be important in apoptosis induced by these viruses.

Many forms of virus-induced apoptosis are inhibited by anti-apoptotic members of the Bcl-2 family.[32–35] One of the most thoroughly investigated mechanisms for the anti-apoptotic actions of Bcl-2 involves its inhibition of the release of cytochrome *c* from mitochondria.[36,37] Abnormalities of mitochondrial transmembrane potential and release of cytochrome *c* have been described following infection with HIV,[38] TGEV,[31] chicken anemia virus,[39] and herpes simplex virus.[28] These studies suggest that both mitochondrial and death-receptor mediated pathways may play an important role in virus-induced apoptosis.

Reovirus-induced apoptosis involves the DR4/DR5/TRAIL system of cell surface death receptors.[7] In this study we found that caspase-8 was activated within 8 h of reovirus infection. The activation of caspase-8 occurs in two distinct phases, consistent with a model in which initial death-receptor mediated activation of caspase-8 is subsequently augmented by activation of caspase-9 or other caspases (discussed below). Following activation, caspase-8 cleaves Bid, a pro-apoptotic Bcl-2 family protein. Cleaved Bid provides an essential link between reovirus-induced death-receptor mediated caspase-8 activation and activation of mitochondrial pathways. Inhibition of caspase-8 activation by over-expression of DN-FADD prevented Bid cleavage, suggesting that reovirus infection also activated the mitochondrial apoptotic pathway. Cytochrome *c* was found to be present in the cytoplasm of infected cells at ~10 h post infection. Additionally, cytochrome *c* release was blocked in FADD-DN expressing cells suggesting that this event requires caspase-8. We also found that caspase-9 is activated at ~12 h post infection.

Having shown that reovirus infection was associated with activation of both death-receptor and mitochondrial-associated initiator caspases, we next wished to determine which effector caspases were subsequently activated. Here we show that the effector caspase, caspase-3 is activated beginning at ~8 h post infection and peaking at ~18 h post infection. Additionally, caspase-7 was activated in reovirus-infected cells, although this event occurs later than caspase-3 activation. Another effector caspase, caspase-6, was not activated in reovirus-infected cells.

There is evidence that although mitochondrial cytochrome *c* release and caspase-9 activation occur downstream of death receptor stimulation, that these events are not necessarily required for all forms of death-receptor initiated apoptosis.[19,20] Therefore we examined the effects of Bcl-2 overexpression on effector caspase activation following reovirus infection. Bcl-2 overexpression inhibits the activation of both caspase-3 and caspase-7, as well as the second phase of caspase-8 activation. This data is consistent with earlier studies suggesting that reovirus-induced apoptosis could be inhibited in MDCK cells over-expressing Bcl-2.[2] This provides conclusive evidence of the importance of the mitochondrial apoptotic pathway in reovirus-induced cell death.

Caspases can be broadly grouped into three categories based on their pattern of substrate specificity.[22,23] A group II caspase inhibitor completely blocked reovirus-induced caspase-3 activity at low concentrations. This result is consistent with the known activation of caspases-3 and -7 in reovirus infection. A group I caspase inhibitor had no effect, even at high concentrations. This suggested that caspases-1, -4 and -5 do not play a significant role in reovirus-induced apoptosis. A group III caspase inhibitor significantly reduced caspase-3 activity, but its effect was only partial when compared to the group II inhibitor. This result was consistent with our observation that caspase-8 and -9 were involved in reovirus-induced caspase-3 activation. The lack of complete inhibition of caspase-3 activation by the group III inhibitor suggests that additional, as yet unidentified, caspases may also contribute to reovirus-induced caspase-3 activation. However, the complete inhibition of caspase-3 activation seen in cells expressing DN-FADD suggests that death receptor activation is the key initiating event in all reovirus-induced caspase activation cascades that ultimately contribute to effector caspase activation.

Our data provides the first comprehensive model of the events leading to apoptosis when cells are infected with a non-enveloped RNA virus whose replication cycle occurs entirely within the cytoplasm (Figure 8). Apoptosis is initiated through cell surface death receptors leading to

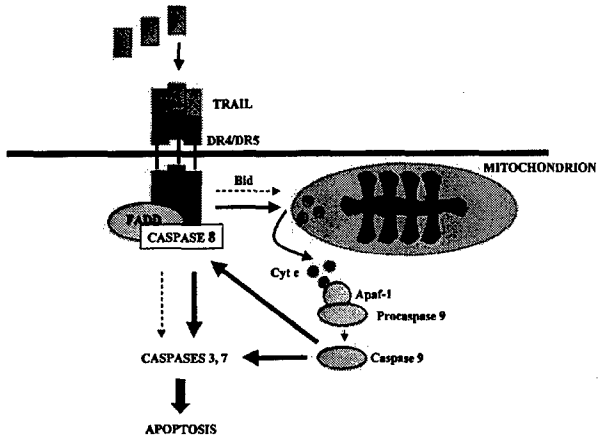

Figure 8 Schematic representation of reovirus-induced apoptosis pathways. Reovirus infection promotes release of cell-associated TRAIL and DR4/DR5-dependent apoptosis. An early phase of caspase-8 activation leads to cleavage of Bid and low level activation of caspase-3 (dashed arrows). This is followed by a second phase of caspase activation in which release of cytochrome *c* activates caspase-9 inducing further caspase-8 activation (solid arrows). Caspase-8 and caspase-9 contribute to effector caspase activation

the activation of caspase-8. Caspase-8 activation is essential for virus-induced apoptosis, and inhibition of this activation in cells stably expressing DN-FADD completely inhibits reovirus-induced effector caspase activation. Caspase-8 activation results in cleavage of Bid and activation of mitochondrial apoptotic pathways. Activation of caspase-8 in the absence of augmentation from the mitochondrial pathway, as occurs in cells stably expressing Bcl-2, results in only low levels of effector caspase activation. These results are consistent with the biphasic pattern of activation of caspase-8, Bid, and caspase-3. Early activation of caspase-8 and Bid induces the mitochondrial pathway which in turn amplifies caspase-8 and Bid activation allowing full expression of apoptosis.

Materials and Methods

Reagents

Anti-cytochrome *c* (7H8.2C12) (1:1000), anti-PARP (C2-10) (1:2000), anti-caspase-6 (B93-4) (1:1000), anti-caspase-8 (B9-2) (1:2000), and anti-caspase-9 (1:1000) antibodies were purchased from Pharmingen (San Diego, CA, USA). Anti-caspase-3 (1:1000) and anti-caspase-7 (1:1000) were purchased from Cell Signaling Technology (Beverly, MA, USA). Anti-Bid antibodies (1:1000) were from Trevigen (Gaithersburg, MD, USA). Anti-actin antibodies (JLA20) (1:5000) were from Calbiochem (Darmstadt, Germany). Anti-human cytochrome *c* oxidase (subunit II) antibodies (12C4-F12) (1:1000) were from Molecular Probes (Eugene, OR, USA). Anti-Fas antibody (CH-11) was from Upstate Biotechnology (Lake Placid, NY, USA). Caspase synthetic peptide inhibitors used were caspase-3 Inhibitor I (cell permeable), caspase-8 Inhibitor I (cell permeable), and caspase-1 Inhibitor I (cell permeable) (Calbiochem, Darmstadt, Germany). ApoAlert caspase-3 fluorometric assay kit was purchased from Clontech (Palo Alto, CA, USA).

Cells, virus, and DNA constructs

HEK293 cells (ATCC CRL1573) were grown in Dulbecco's modified Eagle's medium (DMEM) supplemented with 100 U/ml each of penicillin and streptomycin and containing 10% fetal bovine serum. Jurkat cells were a gift of Dr. John Cohen and were grown in RPMI supplemented with 100 U/ml each of penicillin and streptomycin and containing 10% fetal bovine serum. FADD-DN cells were a gift of Dr. Gary Johnson and express amino acids 80–208 of the FADD cDNA (with the addition of an AU1 epitope tag at the N-terminus) from the CMV promoter of pcDNA3 (Invitrogen, Carlsbad, CA, USA). HEK 293 cells stably over-expressing Bcl-2 were provided by Dr. Gary Johnson. The cell line was constructed by cloning full-length Bcl-2 into the pLXSN vector and transfecting cells via retroviral transduction. Reovirus (Type 3 Abney, T3A) is a laboratory stock, which has been plaque purified and passaged (twice) in L929 cells (ATCC CCL1) to generate working stocks.[40] All experiments were performed using an M.O.I. of 100. High M.O.I.s were chosen to insure synchronized infection of all susceptible cells, and to maximize the apoptotic stimulus.

Western blot analysis

Reovirus-infected cells were harvested at the indicated times, pelleted by centrifugation, washed with ice-cold phosphate-buffered saline, and lysed by sonication in 150 μl of lysis buffer (1% NP40, 0.15 M NaCl, 5.0 mM EDTA, 0.01 M Tris (pH 8.0), 1.0 mM PMSF, 0.02 mg/ml leupeptin, 0.02 mg/ml trypsin inhibitor). Lysates were cleared by centrifugation (20 000 × *g*, 2 min), mixed 1:1 with SDS sample buffer, boiled for 5 min, and stored at −70°C. To prepare mitochondrial-free extracts, cells were pelleted, washed twice in ice-cold PBS, and incubated on ice for 30 min in buffer containing 220 mM mannitol, 68 mM sucrose, 50 mM PIPES-KOH (pH 7.4), 50 mM KCl, 5 mM EGTA, 2 mM $MgCl_2$, 1 mM DTT, and protease inhibitors (complete cocktail, Boehringer Mannheim, Indianapolis, IN, USA). Cells were lysed using 40 strokes in a Dounce homogenizer (B pestle). Lysates were centrifuged at 14 000 × *g* for 15 min at 4°C to remove debris. Supernatants and mitochondrial pellets were prepared for electrophoresis as above. Proteins were separated by SDS–PAGE electrophoresis and transferred to Hybond-c extra nitrocellulose membrane (Amersham, Buckinghamshire, UK) for immunobloting. Blots were then probed with the specified antibodies at the dilutions described above. Proteins were visualized using the ECL detection system (Amersham, Buckinghamshire, UK). Densitometric analysis was performed using a FluorS Multilmager system and Quantity One software (Bio-Rad, Hercules, CA, USA).

Caspase-3 activation assays

Caspase-3 activation assays were performed using a kit obtained from Clontech (Palo Alto, CA, USA). Experiments were performed using 1×10^6 cells/time point. Cells were centrifuged at 200 × *g*, supernatants were removed, and the cell pellets were frozen at −70°C until all the time points were collected. Assays were performed in 96-well plates and analyzed using a fluorescent plate reader (CytoFluor 4000, PerSeptive Biosystems, Framingham, MA, USA). Cleavage of DEVD-AFC, a synthetic caspase-3 substrate, was used to determine caspase-3 activation. Cleavage after the second Asp residue produces free AFC. The amount of fluorescence detected is directly proportional to amount of caspase-3 activity. Because all of the fluorogenic substrate assay experiments were performed at the same time, both the mock and reovirus-induced caspase-3 activation profiles are the same in all of these experiments and are included in each figure to facilitate comparisons. Results of all experiments are reported as means ± S.E.M.

Acknowledgements

This work was supported by Public Health Service grant 1RO1AG14071 from the National Institute of Aging, Merit and REAP grants from the Department of Veterans Affairs, and a US Army Medical Research and Material Command grant (DAMD179818614). Tissue culture media was obtained from the UCHSC Cancer Center Media Core.

References

1. Oberhaus SM, Dermody TS and Tyler KL (1998) Apoptosis and the cytopathic effects of reovirus. Curr. Top. Microbiol. Immunol. 233: 23–49
2. Rodgers SE, Barton ES, Oberhaus SM, Pike B, Gibson CA, Tyler KL and Dermody TS (1997) Reovirus-induced apoptosis of MDCK cells is not linked to viral yield and is blocked by Bcl-2. J. Virol. 71: 2540–2546
3. Tyler KL, Squier MK, Rodgers SE, Schneider BE, Oberhaus SM, Grdina TA, Cohen JJ and Dermody TS (1995) Differences in the capacity of reovirus strains to induce apoptosis are determined by the viral attachment protein sigma 1. J. Virol. 69: 6972–6979
4. Oberhaus SM, Smith RL, Clayton GH, Dermody TS and Tyler KL (1997) Reovirus infection and tissue injury in the mouse central nervous system are associated with apoptosis. J. Virol. 71: 2100–2106
5. DeBiasi RL, Edelstein CL, Sherry and Tyler KL (2001) Calpain inhibition protects against virus-induced apoptotic myocardial injury. J. Virol. 75: 351–361
6. Barton ES, Forrest JC, Connolly JL, Chappell JD, Liu Y, Schnell FJ, Nusrat A, Parkos CA and Dermody TS (2001) Junction adhesion molecule is a receptor for reovirus. Cell 104: 441–451
7. Clarke P, Meintzer SM, Gibson S, Widmann C, Garrington TP, Johnson GL and Tyler KL (2000) Reovirus-induced apoptosis is mediated by TRAIL. J. Virol. 74: 8135–8139
8. Ashkenazi A and Dixit VM (1998) Death receptors: signaling and modulation. Science 281: 1305–1308
9. Li P, Nijhawan D, Budihardjo I, Srinivasula SM, Ahmad M, Alnemri ES and Wang X (1997) Cytochrome c and dATP-dependent formation of Apaf-1/caspase-9 complex initiates an apoptotic protease cascade. Cell 91: 479–489
10. Verhagen AM, Ekert PG, Pakusch M, Silke J, Connolly LM, Reid GE, Moritz RL, Simpson RJ and Vaux DL (2000) Identification of DIABLO, a mammalian protein that promotes apoptosis by binding to and antagonizing IAP proteins. Cell 102: 43–53
11. Du C, Fang M, Li Y, Li L and Wang X (2000) Smac, a mitochondrial protein that promotes cytochrome c-dependent caspase activation by eliminating IAP inhibition. Cell 102: 33–42
12. Joza N, Susin SA, Daugas E, Stanford WL, Cho SK, Li CY, Sasaki T, Elia AJ, Cheng Hy, Ravagnan L, Ferri KF, Zamzami N, Wakeham A, Hakem R, Yoshida H, Kong YY, MakTW, Zuniga-Pflucker JC, Kroemer G and Penninger JM (2001) Essential role of the mitochondrial apoptosis-inducing factor in programmed cell death. Nature 410: 549–554
13. Zou H, Li Y, Liu X and Wang X (1999) An APAF-1-cytochrome c multimeric complex is a functional apoptosome that activates procaspase-9. J. Biol. Chem. 274: 11549–11556
14. Gross A, Yin XM, Wang K, Wei MC, Jockel J, Milliman C, Erdjument-Bromage H, Tempst P and Korsmeyer SJ (1999) Caspase cleaved BID targets mitochondria and is required for cytochrome c release, while BCL-XL prevents this release but not tumor necrosis factor-R1/Fas death. J. Biol. Chem. 274: 1156–1163
15. Li H, Zhu H, Xu CJ and Yuan J (1998) Cleavage of BID by caspase 8 mediates the mitochondrial damage in the Fas pathway of apoptosis. Cell 94: 491–501
16. Luo X, Budihardjo I, Zou H, Slaughter C and Wang X (1998) Bid, a Bcl2 interacting protein, mediates cytochrome c release from mitochondria in response to activation of cell surface death receptors. Cell 94: 481–490
17. Yamada H, Tada-Oikawa S, Uchida A and Kawanishi S (1999) TRAIL causes cleavage of bid by caspase-8 and loss of mitochondrial membrane potential resulting in apoptosis in BJAB cells. Biochem. Biophys. Res. Commun. 265: 130–133
18. Yin XM, Wang K, Gross A, Zhao Y, Zinkel S, Klocke B, Roth KA and Korsmeyer SJ (1999) Bid-deficient mice are resistant to Fas-induced hepatocellular apoptosis. Nature 400: 886–891
19. Scaffidi C, Schmitz I, Zha J, Korsmeyer SJ, Krammer PH and Peter ME (1999) Differential modulation of apoptosis sensitivity in CD95 type I and type II cells. J. Biol. Chem. 274: 22532–22538
20. Scaffidi C, Fulda S, Srinivasan A, Friesen C, Li F, Tomaselli K,J Debatin KM, Krammer PH and Peter ME (1998) Two CD95 (APO-1/Fas) signaling pathways. EMBO J. 17: 1675–1687
21. Hu S, Vincenz C, Ni J, Gentz R and Dixit VM (1997) I-FLICE, a novel inhibitor of tumor necrosis factor receptor-1- and CD- 95-induced apoptosis. J. Biol. Chem. 272: 17255–17257
22. Thornberry NA, Rano TA, Peterson EP, Rasper DM, Timkey T, Garcia-Calvo M, Houtzager VM, Nordstrom PA, Roy S, Vaillancourt JP, Chapman KT and Nicholson DW (1997) A combinatorial approach defines specificities of members of the caspase family and granzyme B. Functional relationships established for key mediators of apoptosis. J. Biol. Chem. 272: 17907–17911
23. Talanian RV, Quinlan C, Trautz S, Hackett MC, Mankovich JA, Banach D, Ghayur T, Brady KD and Wong WW (1997) Substrate specificities of caspase family proteases. J. Biol. Chem. 272: 9677–9682
24. Nava VE, Rosen A, Veliuona MA, Clem RJ, Levine B and Hardwick JM (1998) Sindbis virus induces apoptosis through a caspase-dependent, CrmA- sensitive pathway. J. Virol. 72: 452–459
25. Jan JT, Chatterjee S and Griffin DE (2000) Sindbis virus entry into cells triggers apoptosis by activating sphingomyelinase, leading to the release of ceramide. J. Virol. 74: 6425–6432
26. Stewart SA, Poon B, Song JY and Chen IS (2000) Human immunodeficiency virus type 1 vpr induces apoptosis through caspase activation. J. Virol. 74: 3105–3111
27. Biard-Piechaczyk M, Robert-Hebmann V, Richard V, Roland J, Hipskind RA and Devaux C (2000) Caspase-dependent apoptosis of cells expressing the chemokine receptor CXCR4 is induced by cell membrane-associated human immunodeficiency virus type 1 envelope glycoprotein (gp120). Virology 268: 329–344
28. Galvan V, Brandimarti R, Munger J and Roizman B (2000) Bcl-2 blocks a caspase-dependent pathway of apoptosis activated by herpes simplex virus 1 infection in HEp-2 cells. J. Virol. 74: 1931–1938
29. Takizawa T, Tatematsu C, Ohashi K and Nakanishi Y (1999) Recruitment of apoptotic cysteine proteases (caspases) in influenza virus-induced cell death. Microbiol. Immunol. 43: 245–252
30. Bitzer M, Prinz F, Bauer M, Spiegel M, Neubert WJ, Gregor M, Schulze-Osthoff K and Lauer U (1999) Sendai virus infection induces apoptosis through activation of caspase- 8 (FLICE) and caspase-3 (CPP32). J. Virol. 73: 702—708
31. Eleouet JF, Chilmonczyk S, Besnardeau L and Laude H (1998) Transmissible gastroenteritis coronavirus induces programmed cell death in infected cells through a caspase-dependent pathway. J. Virol. 72: 4918–4924
32. O'Brien V (1998) Viruses and apoptosis. J. Gen. Virol. 79: 1833–1845
33. Razvi ES, Welsh RM (1995) Apoptosis in viral infections. Adv. Virus Res. 45: 1–60
34. Teodoro JG and Branton PE (1997) Regulation of apoptosis by viral gene products. J. Virol. 71: 1739–1746
35. Shen Y and Shenk TE (1995) Viruses and apoptosis. Curr. Opin. Genet. Dev. 5: 105–111
36. Adams JM and Cory S (1998) The Bcl-2 protein family: arbiters of cell survival. Science 281: 1322–1326
37. Reed JC (1998) Bcl-2 family proteins. Oncogene 17: 3225–3236
38. Ferri KF, Jacotot E, Blanco J, Este JA, Zamzami N, Susin SA, Xie Z, Brothers G, Reed JC, Penninger JM and Kroemer G (2000) Apoptosis control in syncytia induced by the HIV type 1-envelope glycoprotein complex: role of mitochondria and caspases. J. Exp. Med. 192: 1081–1092
39. Danen-van Oorschot AA, Der Eb AJ and Noteborn MH (2000) The chicken anemia virus-derived protein apoptin requires activation of caspases for induction of apoptosis in human tumor cells. J. Virol. 74: 7072–7078
40. Tyler KL, Squier MK, Brown AL, Pike B, Willis D, Oberhaus SM, Dermody TS and Cohen JJ (1996) Linkage between reovirus-induced apoptosis and inhibition of cellular DNA synthesis: role of the S1 and M2 genes. J. Virol. 70: 7984–7991

ELSEVIER

Journal of Clinical Virology 25 (2002) S5–S11

JOURNAL OF CLINICAL VIROLOGY

www.elsevier.com/locate/jcv

Use of PCR for the diagnosis of herpesvirus infections of the central nervous system

Roberta L. DeBiasi [a,b,*], B.K. Kleinschmidt-DeMasters [b,c], Adriana Weinberg [a,f,g], Kenneth L. Tyler [b,d,e,f]

[a] *Department of Pediatrics, University of Colorado Health Sciences Center, 4200 East Ninth Avenue, Denver, CO 80262, USA*
[b] *Department of Neurology, University of Colorado Health Sciences Center and The Denver Veterans Administration Hospital, 4200 East Ninth Avenue, Denver, CO 80262, USA*
[c] *Department of Pathology, University of Colorado Health Sciences Center, 4200 East Ninth Avenue, Denver, CO 80262, USA*
[d] *Department of Microbiology, University of Colorado Health Sciences Center, 4200 East Ninth Avenue, Denver, CO 80262, USA*
[e] *Department of Immunology, University of Colorado Health Sciences Center, 4200 East Ninth Avenue, Denver, CO 80262, USA*
[f] *Department of Medicine, University of Colorado Health Sciences Center, 4200 East Ninth Avenue, Denver, CO 80262, USA*
[g] *The Clinical Virology Laboratory, University of Colorado Health Sciences Center, 4200 East Ninth Avenue, Denver, CO 80262, USA*

Abstract

Polymerase chain reaction (PCR) analysis of cerebrospinal fluid (CSF) has revolutionized the diagnosis of nervous system viral infections, particularly those caused by human herpesviruses (HHV). The PCR technique allows the detection of minute quantities of DNA or RNA in body fluids and tissues. Both fresh-frozen and formalin-fixed tissues may be utilized for PCR assays, with the latter making archival studies possible. CSF PCR has now replaced brain biopsy as the gold standard for the diagnosis of herpes simplex virus (HSV) encephalitis. PCR analysis of both CSF and nervous system tissues has also broadened our understanding of the spectrum of disease caused by HSV-1 and -2, cytomegalovirus (CMV), Epstein–Barr virus (EBV), varicella zoster virus (VZV) and HHV-6. PCR results obtained from tissue specimens must be interpreted cautiously, since this highly sensitive technique may detect portions of viral genomic material that may be present even in the absence of active viral infection. Tissue PCR results in particular must be corroborated with clinical and neuropathologic evidence of central nervous system (CNS) infection. In several neurological diseases, negative PCR results have provided evidence against a role for herpesviruses as the causative agents. This review summarizes the role of CSF PCR in the diagnosis and therapeutic management of herpesvirus infections of the nervous system, particularly those caused by HSV and VZV.

Keywords: Polymerase chain reaction; Viral infections; Nervous system; Cerebrospinal fluid; Herpes simplex virus; Varicella zoster virus; Cytomegalovirus; Epstein–Barr virus

* Corresponding author. Tel.: +1-303-393-4684; fax: +1-303-393-5271
E-mail address: roberta.debiasi@uchsc.edu (R.L. DeBiasi).

1386-6532/02/$ - see front matter
PII: S1386-6532(02)00028-8

1. Polymerase chain reaction (PCR): background and technical issues

PCR can be applied to the diagnosis of any disease in which nucleic acid (e.g. DNA, RNA) or their expression as messenger RNA (mRNA) plays a role. PCR techniques allow the in vitro synthesis of millions of copies of a specific gene segment of interest, allowing the rapid detection of as few as one to 10 copies of the target DNA from the original sample. The widespread availability of an in-house test in most hospitals, or ready access to a reference laboratory has led to the incorporation of PCR testing on cerebrospinal fluid (CSF) and body fluids into medical practice in the United States and other developed countries.

In infectious diseases, PCR is ideally suited for identifying fastidious organisms that may be difficult or impossible to culture (DeBiasi and Tyler, 1999). The technique can be performed rapidly and inexpensively, with a turnaround time of 24 h or less rather than the standard minimum of 1–28 days required for viral culture. Unlike the traditional culture methods that may yield negative results after patient receives even small doses of antiviral drugs, CSF PCR retains its sensitivity after short courses of antiviral therapy or passive immunization. This allows the prompt initiation of empiric therapy when a patient first presents with suspected meningitis or encephalitis, without potentially compromising definitive diagnostic tests. PCR is also preferable to serological testing, which often requires 2–4 weeks after acute infection for the development of a diagnostic rise in antibody titers, and is of limited value for viruses with high basal seroprevalence rates. In contrast to serologic testing, CSF PCR yields positive results during acute infection, when the amount of replicating virus is maximal. Finally, CSF PCR is substantially less invasive than brain biopsy, which was previously the gold standard for the diagnosis of many central nervous system (CNS) herpesvirus infections.

The exquisite sensitivity of PCR is both its greatest virtue and greatest potential limitation. A positive CSF PCR result indicates the presence of viral nucleic acid and is, in general, a marker of recent or ongoing active CNS viral infection by that particular pathogen, especially in an immunocompetent individual (Tyler, 1994). False-positive CSF PCR results, in which a positive result does not indicate active CSF infection, can occur due to inadvertent contamination of specimens or failure to properly confirm the specificity of the amplified product. It is theoretically possible that positive CSF PCR results in patients with systemic disease and traumatic lumbar punctures or breakdown of the blood–brain barrier may reflect their systemic infection rather than CNS disease, although data on this point are lacking.

Replicating virus and viral DNA do not persist indefinitely, so that the CSF PCR test becomes negative over time, especially in immunocompetent patients (Haanpaa et al., 1998). While most CSF testing in the clinical setting of suspected meningitis or meningoencephalomyelitis is performed within 1–2 days following the onset of neurological symptoms, positive test results can persist for 2–4 weeks after the onset of clinical disease depending on the virus and the treatment initiated (Weber et al., 1996). False-negative tests can occur if PCR inhibitors are present in CSF. However, modest CSF xanthochromia, high protein levels, or high white blood cell counts do not generally have a negative impact on CSF PCR testing.

CSF PCR testing may be performed on fresh or frozen samples. Refrigeration for a few hours or even days does not appear to significantly reduce the yield of the test (Weinberg, personal communication). However, viral DNA is relatively more stable than RNA in archived samples. The exquisite sensitivity of the technique allows the use of small volumes of CSF for analysis (i.e. 30 μl), although laboratories generally request at least 0.5 ml.

Quantitative PCR by several techniques is increasingly being applied to clinical samples. One technique involves the use of internal oligonucleotides—labeled at one end with a fluorescent dye and at the other end with a quencher dye—along with the PCR primers during amplification. Fluorescence emitted during PCR is measured and directly correlated to the number of copies of the target nucleic acid in the original sample. Several

studies have suggested that nucleic acid copy number ("viral load") may be a marker for the severity of disease or may help predict the outcome, although it remains to be determined whether this is true for all herpesvirus infections (Domingues et al., 1998).

2. Our clinical virology laboratory's experience

The UCHSC clinical virology laboratory performs CSF PCR for herpesviruses (herpes simplex virus, HSV; Epstein–Barr virus, EBV; cytomegalovirus, CMV; and varicella zoster virus, VZV) three times a week, which makes clinically useful data rapidly available for the management of patients with presumed diagnoses of herpesvirus encephalitis, and reduces unnecessary therapeutic interventions. Upon receipt of CSF specimens are stored at −70 °C in 30 μl aliquots. DNA is extracted from each aliquot with InstaGene purification matrix (Boehringer Mannheim, Mannheim, Germany). Amplification is carried out in 50 μl mixtures containing 20 μl of extracted DNA, 1.25 U of PfuI (Stratagene LaJolla, California, USA), 100 μM of each four deoxynucleoside triphosphates, and 1 μM of each primer in PfuI buffer (Stratagene). Samples are amplified in duplicate for 45 cycles. Amplified DNAs are separated according to molecular weight using agarose gel electrophoresis and transferred to nylon membranes. The identity of the DNA bands is confirmed by hybridization with a digoxigenin-labeled probe (Boehringer Mannheim), followed by an anti-digoxigenin antibody conjugated to alkaline phosphatase and CSPD® chemiluminescent substrate (Tropix, Bedford, MA, USA). Each assay includes a negative water control and two positive sensitivity controls. Tests are considered valid if controls yield the expected results and if patient replicates agree.

Our HSV PCR detects ≥ 2 genomic equivalents per reaction. Upon review of 2214 CSF specimens received at our institution for HSV PCR analysis between 1997 and 2001, 79 specimens (3.6%) yielded positive results. The prevalence of other herpesviruses based on the review of all herpesvirus PCRs performed at our institution is as follows: EBV 7.4% (39/528 samples between 1995 and 2001), VZV 3.9% (22/569 samples between 1998 and 2002), and CMV 2.3% (11/483 samples between 1999 and 2002).

3. Use of PCR for the diagnosis of specific CNS herpesvirus infections

CSF PCR testing has played a critical role in establishing the frequency and distribution of herpesvirus infections in immunocompetent populations. Detection of HSV-1, HSV-2, CMV, and VZV DNA correlates strongly with specific clinical syndromes of encephalitis/myelitis and meningitis. Occasional immunocompetent or immunocompromised patients have more than one herpesvirus detected in CSF by PCR, and EBV has been the most frequent agent associated with a dual positive result. In a large series of 662 patients, mostly immunocompetent, detection of human herpesviruses (HHV)-6 and EBV by CSF PCR did not correlate clinically in several individuals with the presence of a CNS infection known to be caused by that virus (Studahl et al., 2000). Similarly, in a large study of immunocompromised (HIV-infected) individuals, conducted to assess the diagnostic reliability of CSF PCR by comparison with biopsy or autopsy diagnoses, the most frequent false-positive herpesvirus detected was HHV-6 (Cinque et al., 1996). Additional large studies are necessary to determine the extent of false-positive PCR results for herpesviruses, especially with regard to HHV-6 and EBV in immunocompromised hosts.

3.1. HSV

3.1.1. HSV-1

Despite the high prevalence of seropositivity to HSV in the general population and the fact that the virus becomes latent in dorsal root ganglia of most humans, HSV DNA is not detected in CSF of HSV-seropositive individuals who are neurologically normal or who have other types of non-HSV CNS infections (Tyler, 1994). The sensitivity and specificity of CSF PCR exceeds 95% for HSV encephalitis (Lakeman and Whitley, 1995), and as

a result, CSF PCR has replaced brain biopsy as the diagnostic test of choice for HSV encephalitis. The high sensitivity and specificity of CSF PCR means that in patients with a low pre-test probability of HSV encephalitis an appropriately performed negative test essentially excludes the diagnosis. Conversely, in patients with a high pre-test probability of HSV encephalitis, a negative test, although dramatically decreasing the likelihood of HSV encephalitis, does not entirely exclude it. A positive CSF PCR for HSV in the appropriate clinical setting is initially diagnostic of HSV encephalitis (Tebas et al., 1998) The use of HSV CSF PCR has also led to the identification of mild or atypical forms of encephalitis that were formerly attributed to other viruses, often in the absence of brain biopsy (Domingues et al., 1997) and that may account for 17% of total cases of HSV encephalitis (Fodor et al., 1998). CSF PCR has established the diagnosis and role of HSV-1 in brainstem encephalitis (Tyler et al., 1995), myelitis (Studahl et al., 2000), multifocal or diffuse encephalitis without temporal lobe involvement in children (Schlesinger et al., 1995a), and neonatal encephalitis. In children, symptoms of HSV encephalitis may recur after antiviral therapy. These "relapses" have been attributed both to residual active infection and post-infectious immune-mediated processes. CSF PCR may help distinguish between these possibilities (Ito et al., 2000). Quantitative CSF PCR in cases of pediatric HSV encephalitis is currently being studied as a method for monitoring response to antiviral drugs (Ando et al., 1993).

3.1.2. HSV-2

CSF PCR has helped clinicians to recognize that HSV-2 may cause aseptic meningitis even in the absence of genital herpetic lesions (Schlesinger et al., 1995b), and established HSV-2 as the most common cause of benign recurrent lymphocytic meningitis, including many cases previously diagnosed as Mollaret's meningitis (Tedder et al., 1994). CSF viral cultures are typically negative during recurrent episodes of HSV-2 meningitis. However, CSF PCR is positive in patients with recurrent episodes of HSV-2 meningitis. CSF PCR has illustrated that immunocompetent adults may develop HSV-2-induced meningoencephalitis and meningitis (Studahl et al., 2000), as well as rare cases of HSV-2 brainstem encephalitis and recurrent thoracic myelitis.

3.2. VZV

CSF PCR for VZV has considerably broadened the understanding of the neurologic complications due to VZV infection. VZV infection can involve virtually every part of the central and peripheral nervous system (Kleinschmidt-DeMasters and Gilden, 2001). The combination of serological studies and CSF PCR for VZV has been particularly helpful in identifying cases of VZV CNS infections without associated rash (*sine herpete*) (Bergstrom, 1996). Since the virus can only rarely be cultured from CSF, the diagnosis of meningitis or meningoencephalitis previously depended on the presence of a characteristic vesicular erythematous rash before, during, or after CNS infection, and VZV-mediated neurologic diseases were under-recognized. CSF PCR for VZV has shown that aseptic meningitis and brainstem encephalitis due to this virus may occur in immunocompetent hosts (Haanpaa et al., 1998; Studahl et al., 2000). In HIV-infected patients, CSF PCR for VZV DNA may have utility in monitoring therapeutic response and in predicting the outcome of VZV meningoencephalitis. For example, in a series of 516 HIV-infected patients, PCR became negative in patients treated with antivirals whose clinical conditions improved, but remained positive despite appropriate therapy in several patients who subsequently died (Cinque et al., 1997). In addition, patients with detectable CSF VZV DNA, which was considered an indicator of subclinical reactivation of VZV antecedent to clinical disease, who were treated with antiviral agents, had improved outcome. Monitoring of CSF PCR allowed for the effective use of prophylactic therapy in this patient population.

PCR on both CSF and fluid from auricular vesicles has confirmed that VZV causes Ramsay Hunt syndrome, the second most common cause of seventh nerve facial paralysis after Bell's palsy (Murakami et al., 1998). Ramsay Hunt syndrome can be difficult to recognize since the rash is

hidden in the ear or mouth, and the rash may be delayed, particularly in pediatric patients. PCR on endoneurial fluids and posterior auricular muscle samples collected during decompressive facial nerve surgery for Bell's palsy identified HSV-1 DNA in 79% of patients and confirmed that neither EBV or VZV is an important cause of idiopathic Bell's palsy. A subsequent study using PCR identified a subset of patients with acute peripheral facial palsy that has zoster *sine herpete* (Furuta et al., 2000). VZV was responsible for a significant percentage of the total number of cases of facial palsy (29%), and an even higher percentage of reactivations (88%) in HSV-seronegative patients. Hence, PCR has verified a role for herpesviruses in both of the common causes of facial nerve paralysis and has distinguished which virus is causative in clinically confusing cases.

PCR testing on fresh, frozen, or archival-fixed and paraffin-embedded CNS tissues has allowed the detection of VZV nucleic acid, even from small or imperfectly preserved specimens. Tissue PCR of cerebral arteries has established a direct role for VZV in cases of large-vessel and small-vessel vasculopathy (Melanson et al., 1996). In a patient with waxing and waning VZV vasculitis, the detection of VZV DNA by PCR led to the discovery that VZV antigen was also present, indicating a productive infection in blood vessels as the cause of the disease. Brain tissues may be positive for VZV DNA by PCR even when the virus is no longer detectable by other methods, such as light microscopy for viral inclusions, immunohistochemistry, or in situ hybridization.

3.3. EBV

CSF PCR testing has been found to be nearly 100% sensitive as a tumor marker for EBV-related CNS lymphoma, and has changed the way in which clinicians diagnose CNS lymphoma in immunocompromised individuals (Landgren et al., 1994). In a study of AIDS patients with CNS mass lesions, a positive EBV CSF PCR correctly identified all 17 CNS lymphoma cases and was positive in only one of 68 AIDS patients with non-CNS lymphoma mass lesions (Cinque et al., 1996). CSF PCR for EBV is also positive during the acute phase of the illness in children with infectious mononucleosis and neurological complications such as transverse myelitis, meningoencephalitis, and aseptic meningitis (Weber et al., 1996). CSF PCR is not positive in EBV-seropositive individuals in the absence of CNS infection. However, positive EBV PCR may be seen in patients with evidence of other viral or non-viral CNS infection, raising the possibility that these infections may trigger viral reactivation. Studies are currently in progress to determine whether quantitative PCR will be useful for distinguishing different types of EBV CNS infections or for identifying the causative agent in cases in which there is evidence for dual infection with EBV and another pathogen (Weinberg et al., in press).

3.4. CMV

CSF PCR is a useful technique for detecting CMV CNS infections in immunodeficient hosts, with a reported sensitivity of 82% and specificity of 99% in AIDS patients (Cinque et al., 1995). The clinical utility of the test in the setting of congenital CMV infection is being investigated, particularly with respect to correlating neurologic outcome with CSF viral load (Whitley, personal communication). CMV viral load has also been monitored in peripheral blood leukocytes as a method to predict which immunosuppressed patients might develop end-organ disease.

3.5. HHV-6, HHV-7 and HHV-8

CSF PCR testing has corroborated the role of HHV-6 in febrile seizures, meningitis, encephalitis, and encephalopathy in immunocompetent and immunocompromised individuals (Yoshikawa and Asano, 2000). HHV-6 genome has been demonstrated in CSF from up to 57% of children younger than 1 year of age who have febrile seizures and has also been seen in children with recurrent febrile convulsions. The role of HHV-7 in neurological disease is unclear, although the detection of HHV-7 DNA in CSF and serum of children with exanthem subitum and encephalopathy has been reported (Torigoe et al., 1996). Encephalitis in immunocompromised individuals

associated with HHV-8 has been described, but this awaits additional confirmation. HHV-8 DNA has been detected in primary CNS lymphomas in some studies but not others. In the study in which HHV-8 was detected, the virus was surmised to play an indirect role in the development of primary CNS lymphoma, and was thought be present in the adjacent non-neoplastic lymphocytes but not the lymphoma cells (Corboy et al., 1998).

4. Use of tissue PCR to exclude herpesvirus as etiologic agents of nervous system disease

Given the protean manifestations of herpesvirus-mediated infections of the central and peripheral nervous system, efforts have been made to detect these viruses by PCR on tissues from several disease entities characterized by arteritis and/or inflammation. PCR testing of various tissue specimens has made it unlikely that VZV plays an etiologic role in giant cell arteritis and has provided no evidence that VZV, CMV, EBV, or HSV play a role in childhood multifocal encephalomalacia. Negative PCR results have also made it unlikely that HSV plays a causative role in Meniere's disease. A survey of a variety of peripheral nerve diseases, including inflammatory peripheral neuropathies, revealed no HSV DNA by PCR in peripheral nerves, making it unlikely that HSV plays a significant role in these disorders (Kleinschmidt-DeMasters et al., 2001).

The significance of the detection of HSV in CNS tissues is uncertain. HSV viral genome was first detected in human brain tissue using nucleic acid hybridization techniques in 1979 and 1981. Since then, PCR has confirmed the presence of HSV DNA in brainstem, olfactory bulbs and limbic areas of individuals without CNS disease (Baringer and Pisani, 1994). Since HSV has never been isolated by culture from normal human brain tissue, the presence of the viral genome, as detected by PCR, is of uncertain significance. Further studies are needed to determine whether the entire viral genome is present, and if so, if this represents latent virus or virus potentially capable of reactivation. Positive PCR results may instead represent the presence of random viral sequences or fragments of virus in neurons or other CNS cells. Tissue PCR remains a research technique that requires further study prior to its potential use as a clinical diagnostic method.

Acknowledgements

Research support has been provided by the Reuler–Lewin Family Professorship of Neurology and the US Army (Medical Research Grant DAMD 17-98-1-8614). We thank Erich Schmidt for his assistance in compiling data from the UCHSC Clinical Virology Laboratory databases.

References

Ando Y, Kimura H, Miwata H, Kudo T, Shibata M, Morishima T. Quantitative analysis of herpes simplex virus DNA in cerebrospinal fluid of children with herpes simplex encephalitis. J Med Virol 1993;41:170–3.

Baringer JR, Pisani P. Herpes simplex virus genomes in human nervous system tissue analyzed by polymerase chain reaction. Ann Neurol 1994;36:823–9.

Bergstrom T. Polymerase chain reaction for diagnosis of varicella zoster virus central nervous system infections without skin manifestations. Scand J Infect Dis Suppl 1996;100:41–5.

Cinque P, Baldanti F, Vago L, Terreni MR, Lillo F, Furione M, Castagna A, Monforte AD, Lazzarin A, Linde A. Ganciclovir therapy for cytomegalovirus (CMV) infection of the central nervous system in AIDS patients: monitoring by CMV DNA detection in cerebrospinal fluid. J Infect Dis 1995;171:1603–6.

Cinque P, Bossolasco S, Vago L, Fornara C, Lipari S, Racca S, Lazzarin A, Linde A. Varicella-zoster virus (VZV) DNA in cerebrospinal fluid of patients infected with human immunodeficiency virus: VZV disease of the central nervous system or subclinical reactivation of VZV infection? Clin Infect Dis 1997;25:634–9.

Cinque P, Vago L, Dahl H, Brytting M, Terreni MR, Fornara C, Racca S, Castagna A, Monforte AD, Wahren B, Lazzarin A, Linde A. Polymerase chain reaction on cerebrospinal fluid for diagnosis of virus-associated opportunistic diseases of the central nervous system in HIV-infected patients. AIDS 1996;10:951–8.

Corboy JR, Garl PJ, Kleinschmidt-DeMasters BK. Human herpesvirus 8 DNA in CNS lymphomas from patients with and without AIDS. Neurology 1998;50:335–40.

DeBiasi RL, Tyler KL. Polymerase chain reaction in the diagnosis and management of central nervous system infections. Arch Neurol 1999;56:1215–9.

Domingues RB, Lakeman FD, Mayo MS, Whitley RJ. Application of competitive PCR to cerebrospinal fluid samples from patients with herpes simplex encephalitis. J Clin Microbiol 1998;36:2229–34.

Domingues RB, Tsanaclis AM, Pannuti CS, Mayo MS, Lakeman FD. Evaluation of the range of clinical presentations of herpes simplex encephalitis by using polymerase chain reaction assay of cerebrospinal fluid samples. Clin Infect Dis 1997;25:86–91.

Fodor PA, Levin MJ, Weinberg A, Sandberg E, Sylman J, Tyler KL. Atypical herpes simplex virus encephalitis diagnosed by PCR amplification of viral DNA from CSF. Neurology 1998;51:554–9.

Furuta Y, Ohtani F, Kawabata H, Fukuda S, Bergstrom T. High prevalence of varicella-zoster virus reactivation in herpes simplex virus-seronegative patients with acute peripheral facial palsy. Clin Infect Dis 2000;30:529–33.

Haanpaa M, Dastidar P, Weinberg A, Levin M, Miettinen A, Lapinlampi A, Laippala P, Nurmikko T. CSF and MRI findings in patients with acute herpes zoster. Neurology 1998;51:1405–11.

Ito Y, Kimura H, Yabuta Y, Ando Y, Murakami T, Shiomi M, Morishima T. Exacerbation of herpes simplex encephalitis after successful treatment with acyclovir. Clin Infect Dis 2000;30:185–7.

Kleinschmidt-DeMasters BK, Gilden DH. Varicella-zoster virus infections of the nervous system: clinical and pathologic correlates. Arch Pathol Lab Med 2001;125:770–80.

Kleinschmidt-DeMasters BK, DeBiasi RL, Tyler KL. Polymerase chain reaction as a diagnostic adjunct in herpesvirus infections of the nervous system. Brain Pathol 2001;11:452–64.

Lakeman FD, Whitley RJ. Diagnosis of herpes simplex encephalitis: application of polymerase chain reaction to cerebrospinal fluid from brain-biopsied patients and correlation with disease. National Institute of Allergy and Infectious Diseases Collaborative Antiviral Study Group. J Infect Dis 1995;171:857–63.

Landgren M, Kyllerman M, Bergstrom T, Dotevall L, Ljungstrom L, Ricksten A. Diagnosis of Epstein–Barr virus-induced central nervous system infections by DNA amplification from cerebrospinal fluid. Ann Neurol 1994;35:631–5.

Melanson M, Chalk C, Georgevich L, Fett K, Lapierre Y, Duong H, Richardson J, Marineau C, Rouleau GA. Varicella-zoster virus DNA in CSF and arteries in delayed contralateral hemiplegia: evidence for viral invasion of cerebral arteries. Neurology 1996;47:569–70.

Murakami S, Nakashiro Y, Mizobuchi M, Hato N, Honda N, Gyo K. Varicella-zoster virus distribution in Ramsay Hunt syndrome revealed by polymerase chain reaction. Acta Otolaryngol 1998;118:145–9.

Schlesinger Y, Buller RS, Brunstrom JE, Moran CJ, Storch GA. Expanded spectrum of herpes simplex encephalitis in childhood. J Pediatr 1995a;126:234–41.

Schlesinger Y, Tebas P, Gaudreault-Keener M, Buller RS, Storch GA. Herpes simplex virus type 2 meningitis in the absence of genital lesions: improved recognition with use of the polymerase chain reaction. Clin Infect Dis 1995b;20:842–8.

Studahl M, Hagberg L, Rekabdar E, Bergstrom T. Herpesvirus DNA detection in cerebral spinal fluid: differences in clinical presentation between alpha-, beta-, and gamma-herpesviruses. Scand J Infect Dis 2000;32:237–48.

Tebas P, Nease RF, Storch GA. Use of the polymerase chain reaction in the diagnosis of herpes simplex encephalitis: A decision analysis model. Am. J. Med. 1998;105:287–95.

Tedder DG, Ashley R, Tyler KL, Levin MJ. Herpes simplex virus infection as a cause of benign recurrent lymphocytic meningitis. Ann Intern Med 1994;121:334–8.

Torigoe S, Koide W, Yamada M, Miyashiro E, Tanaka-Taya K, Yamanishi K. Human herpesvirus 7 infection associated with central nervous system manifestations. J Pediatr 1996;129:301–5.

Tyler KL. Polymerase chain reaction and the diagnosis of viral central nervous system diseases. Ann Neurol 1994;36:809–11.

Tyler KL, Tedder DG, Yamamoto LJ, Klapper JA, Ashley R, Lichtenstein KA, Levin MJ. Recurrent brainstem encephalitis associated with herpes simplex virus type 1 DNA in cerebrospinal fluid. Neurology 1995;45:2246–50.

Weber T, Frye S, Bodemer M, Otto M, Luke W. Clinical implications of nucleic acid amplification methods for the diagnosis of viral infections of the nervous system. J Neurovirol 1996;2:175–90.

Weinberg A, Li S, Palmer M, Tyler KL. Use of quantitative CSF PCR in the analysis of Epstein–Barr virus infection of the central nervous system. Ann. Neurol. (in press).

Yoshikawa T, Asano Y. Central nervous system complications in human herpesvirus-6 infection. Brain Dev 2000;22:307–14.

tapraid5/ay-aon/ay-aon/ay1202/ay0678d02a | martink | S=6 | 7/18/02 | 9:20 | Art: 0341R

Quantitative CSF PCR in Epstein–Barr Virus Infections of the Central Nervous System

Adriana Weinberg, MD,[1,2] Shaobing Li, MD,[1] Megan Palmer, MD,[1] and Kenneth L. Tyler, MD[2–5]

Acute Epstein–Barr virus (EBV) infection of the central nervous system (CNS) is associated with meningoencephalitis and other neurological syndromes in immunocompetent hosts and with CNS lymphomas (CNSLs) in immunocompromised hosts. Diagnosis is based on serological studies and more recently on detection of EBV DNA in cerebrospinal fluid (CSF) by polymerase chain reaction (PCR). We measured EBV DNA by quantitative PCR and EBV mRNA by RT-PCR in the CSF in patients with EBV-associated neurological disorders. EBV was identified as the cause of CNS infection in 28 patients: 14 with CNSL, 10 with encephalitis, and 4 with postinfectious neurological complications. CSF analysis showed that patients with CNSL had high EBV load (mean ± standard error of 4.8 ± 0.2 $\log_{10}$ DNA copies/ml) and low leukocyte counts (22 ± 7 cells/μl); encephalitis was characterized by high EBV load (4.2 ± 0.3 $\log_{10}$ DNA copies/ml) and high leukocyte counts (143 ± 62 cells/μl); and patients with postinfectious complications showed low EBV load (3.0 ± 0.2 $\log_{10}$ DNA copies/ml) with high leukocyte counts (88 ± 57 cells/μl). Lytic cycle EBV mRNA, a marker of viral replication, was identified in 10 CSF samples from patients with CNSL and encephalitis. To our knowledge, this is the first application of quantitative CSF PCR and the first demonstration of the presence of lytic cycle EBV mRNA in CSF of patients with EBV-associated neurological disease.

AQ: 1

Ann Neurol 2002;52:000–000

Fu

Central nervous system (CNS) complications of Epstein–Barr virus (EBV) infection occur in 1 to 18% of patients with infectious mononucleosis and include encephalitis, meningitis, cerebellitis, polyradiculomyelitis, transverse myelitis, cranial and peripheral neuropathies, and psychiatric abnormalities.[1–7] EBV infections of the CNS can occur in the absence of infectious mononucleosis.[6] EBV has been associated with cranial and peripheral neuropathies, and serological evidence of active EBV infection has been reported in up to 29% of childhood cases of Guillain–Barré syndrome and 19% of childhood cases of facial palsy.[6,7] EBV-associated lymphomas represent another important cause of EBV-related CNS disease.[8–13] These disorders are particularly common in immunocompromised hosts including patients with acquired immune deficiency syndrome and transplant recipients.

Until recently, diagnosis of EBV-associated CNS disease depended predominantly on demonstration of the presence of antibodies in cerebrospinal fluid (CSF) and/or serum, because virs is only rarely isolated from CSF.[14–18] A role for EBV in the pathogenesis of CNS lymphomas (CNSLs) was established by demonstrating the presence of EBV genome and/or antigen in tumor cells using in situ hybridization or immunohistochemistry.[8] More recently, amplification of EBV DNA in the CSF by PCR has become an important method for diagnosis of EBV CNS infections and CNSL.[19–21]

In this study, we report the first use of quantitative EBV PCR and RT-PCR for a lytic cycle EBV mRNA in a large series of patients with EBV CNS infections.

AQ: 2

Patients and Methods

Study Design and Definitions

CSF specimens containing EBV DNA detected by PCR were identified in the Diagnostic Virology Laboratory at the University of Colorado Health Sciences Center between October 1995 and March 2001. Clinical, laboratory, and follow-up information was obtained through a questionnaire submitted to the attending physician and/or neurology consultant, and from medical records review. Patients were grouped into the following diagnostic categories: (1) CNSL, defined by typical histopathology or by a typical radiographic exam and consistent clinical presentation in the absence of an alternate diag-

From the Departments of [1]Pediatrics, [2]Medicine, [3]Microbiology and Immunology, and [4]Neurology, University of Colorado Health Sciences Center and [5]Denver Veterans Affairs Medical Center, Denver, CO.

Received Apr 16, 2002, and in revised form May 28. Accepted for publication May 29, 2002.

Published online XX Month 2002, in Wiley InterScience (www.interscience.wiley.com). DOI: 10.1002/ana.10321

Address correspondence to Dr Weinberg, University of Colorado Health Sciences Center, Campus Box C227, Denver, CO 80262. E-mail: Adriana.Weinberg@uchsc.edu

nosis; (2) encephalitis, defined by the presence of fever, altered mental status, and focal neurological signs or symptoms indicative of parenchymal brain involvement, in the absence of other potential pathogenic agents; and (3) postinfectious complications, including cases of Guillain–Barré syndrome, acute demyelinating encephalitis, transverse myelitis, and polyradiculomyelitis, after acute EBV infection.

Qualitative Epstein–Barr Virus Polymerase Chain Reaction

Qualitative EBV PCR was performed as previously described[21,22] using duplicates of CSF aliquots stored at −70°C. Each assay included two negative water controls and two positive controls of EBV-producing B95-8 cell culture supernatant. The tests were considered valid if the controls yielded the expected results and if the replicates were concordant.

Quantitative Epstein–Barr Virus Polymerase Chain Reaction

Quantitative EBV PCR was performed using a competitive method adapted from a previously described assay.[23] The internal standard (IS) was synthesized by amplification of a 304bp fragment in the EBV region BMLF1 3501 to 3804, followed by deletion of an 81bp internal segment. The resultant 233bp IS was PCR-amplified and inserted in the vector PCR-Script SK+ (Stratagene, La Jolla, CA). *Escherichia coli* XL10-Gold Kan Ultracompetent cells (Stratagene) transformed with the IS-containing plasmid was grown in Luria–Bertani medium (Gibco BRL, Gaithersburg, MD) and selected with an ampicillin marker. The plasmid DNA was purified with a Qiagen tip 500 (Qiagen, Chatsworth, CA) and quantitated with a spectrophotometer (CECIL CE2401). The number of IS copies was confirmed by coamplification with known amounts of EBV B95-8 DNA quantitative standards (ABI). The PCR products were separated by agarose gel electrophoresis, stained with Vista Green, scanned with a Storm instrument (Molecular Dynamics, Sunnyvale, CA), and quantitated using ImageQuant software. Using 1,000 IS copies per reaction tube and dilutions of the quantitative standards, a linear relationship between input and measured DNA was identified between 1,000 to 1,000,000 copies EBV DNA per milliliter of specimen. DNA, extracted from clinical specimens, coamplified with 1,000 copies of IS per reaction tube, and quantitated by Storm. Positive and negative controls were run with each clinical specimen.

RNA Methods

EBV transcription of the early lytic cycle gene *BZLF1* was detected by RT-PCR as previously described.[24,25] CSF nucleic acids, purified with QIAamp viral RNA mini kit (Qiagen), were reverse transcribed and amplified using primers Z1 and Z2. Amplicon was detected by Southern blot using Z2B as a probe.

The BZLF1 target area was selected because the primers Z1 and Z2 anneal to exon 1 and exon 3, respectively. Therefore, RT-PCR typically generates two bands of 252 and 450kb molecular weight, corresponding to the cDNA and the genomic DNA, respectively. The presence of genomic DNA amplicon was used as an internal sensitivity control. The presence of both 450 and 252kb bands was interpreted as evidence of BZLF1 transcription. The presence of the 450kb band in the absence of the 252 one was interpreted as absence of BZLF1 transcription. The absence of both 450 and 252kb bands was interpreted as lack of homology between the primer pair and the clinical strains or insufficient nucleic acid template in the sample.

Statistical Analysis

Statistical analysis was performed using StatView 5.0.1 software (SAS Institute, Cary, NC).

Results

Description of the Patient Population

Of 528 CSF samples tested for EBV by PCR, 39 had positive results (7.4%). Eleven cases were excluded because other pathogenic agents in addition to EBV may have contributed to their illnesses. Demographic features of the 28 patients remaining in the study are shown in the Table. Twenty-two patients had primary or acquired immunocompromising conditions, including human immunodeficiency virus (HIV; n = 16), solid organ transplantation (n = 5), and common variable immunodeficiency (n = 1).

Central Nervous System Lymphoma

CNSL was diagnosed in 14 patients whose underlying disorders included advanced HIV infection (12) and transplantation (2). The presenting signs and symptoms included behavioral changes, seizures, aphasia, motor weakness, sensory abnormalities, and ataxia. Loss of developmental milestones was seen in children. Thirteen patients had computed tomography (CT) or magnetic resonance imaging studies of the CNS, which were abnormal in all but one case (PID 10). PID 10 had a normal noncontrast CT accompanying aphasia and new-onset seizures. An magnetic resonance imaging was not performed. This patient had a lymph node biopsy, which showed non-Hodgkin lymphoma. Single-photon emission CT scans were positive in three cases and negative in one.

Histopathological diagnosis was made by brain biopsy in three patients. Three additional patients (PIDs 2, 10, and 13) had lymphoma diagnosed on biopsies from sites other than CNS, and one patient had both CNS and lymph node biopsy. Only the pediatric patients had EBV-specific serology performed at CNSL diagnosis: one consistent with acute infection and one with past infection.

Laboratory examination of the CSF (Fig) showed pleocytosis in 10 of 14 patients, erythrocytes in 6 cases, and elevated protein in all cases. Glucose concentration was normal in all but one patient who had 23μg/dl of glucose in the CSF. The $\log_{10}$ EBV DNA copies per

Table. Selected Clinical and Laboratory Characteristics of Patients with EBV-Associated Neurological Disorders

PID	Diagnosis	Gender	Age (yr)	Race	CSF EBV DNA (copies/ml)	CSF mRNA	Underlying Conditions/ Treatment	EBV-Specific Therapy	Outcome
1	CNSL	M	26	H	4,100	nd	HIV/−	—	Fatal
2	CNSL[a]	M	32	H	10,000	nd	HIV/−	—	Fatal
3	CNSL[b]	M	37	W	15,000	nd	HIV/HAART	—	Fatal
4	CNSL[a]	M	56	H	25,540	+	HIV/HAART	ACV	Fatal
5	CNSL	M	38	W	28,000	+	HIV/ART	ACV	Fatal
6	CNSL	M	2	W	50,000	nd	Heart Tx/ ↓ IS	GCV	Fatal
7	CNSL[b]	M	33	W	50,000	nd	HIV/ART	ACV	Fatal
8	CNSL[b]	M	65	H	58,700	+	HIV/HAART	—	Stable
9	CNSL	M	45	H	92,000	nd	HIV/−	ACV	Fatal
10	CNSL[a,b]	M	48	W	115,000	+	HIV/HAART	—	Indeterminate[c]
11	CNSL	M	25	W	152,000	nd	HIV/HAART	ACV	Improved
12	CNSL	M	32	W	270,000	+	HIV/ART	ACV/GCV	Fatal
13	CNSL[a,b]	M	7	W	298,300	nd	Renal Tx/ ↓ IS	—	Improved
14	CNSL	M	38	W	605,000	nd	HIV/−	—	Fatal
15	Encephalitis	M	55	W	500	nd	NONE	ACV	Improved
16	Encephalitis	M	29	W	900	nd	HIV/HAART	—	Improved
17	Encephalitis	F		W	8,000	−	NONE	—	Improved
18	Encephalitis	M	47	W	8,900	nd	HIV/HAART	—	Improved
19	Encephalitis	M	71	W	17,900	−	Renal Tx/−	—	Improved
20	Encephalitis	M	43	W	29,000	+	HIV/HAART	ACV	Improved
21	Encephalitis	F	35	B	40,800	+	HIV/HAART	ACV	Improved
22	Encephalitis	M	19	W	64,400	+	Renal Tx/ ↓ IS	FOS	Improved
23	Encephalitis	M	18	W	77,000	+	NONE	ACV	Improved
24	Encephalitis	F	58	W	216,000	+	Renal Tx/ ↓ IS	ACV	Improved
25	ADEM	M	2	H	500	nd	NONE	ACV	Fatal
26	TRM	M	7	W	500	nd	NONE	—	Improved
27	PRM[d]	F	43	W	1,904	nd	CVID/IVIG	GCV	Improved
28	Guillain–Barré	M	55	W	2,000	nd	NONE	ACV	Stable

EBV = Epstein–Barr virus; CSF = cerebrospinal fluid; CNSL = central nervous system lymphoma; H = Hispanic; nd = not done; HIV = human immunodeficiency virus infection; W = white; HAART = highly active ART with three or more drugs including a protease inhibitor or nonnucleoside analog; ACV = acyclovir; Tx = transplantation; IS = immunosuppression; GCV = ganciclovir; ART = antiretroviral therapy with one or more nucleoside analogs; ADEM = acute demyelinating encephalitis; TRM = transverse myelitis; PRM = polyradiculomyelitis; CVID = combined variable immunodeficiency; IVIG = intravenous immunoglobulin.

[a]Patients with systemic lymphoma including the central nervous system.
[b]Patients treated with chemotherapy and/or radiation therapy.
[c]Outcome indeterminate because of insufficient follow-up (2 months).
[d]A detailed description of this case can be found in Maydi and colleagues,[26] Case 4.

milliliter of CSF varied between 3.6 and 5.8 with a mean ± standard error (SE) of 4.8 ± 0.2.

Clinical management of CNSL patients varied (see Table). Only 8 of the 12 HIV-infected patients received antiretroviral therapy. In addition, six received anti-EBV antivirals and five were treated with chemotherapy and/or radiotherapy. The clinical management of the two transplant recipients consisted of decreased immunosuppression and antivirals or chemotherapy. Clinical conditions improved or remained stable after 2 or more years of follow-up in two HIV-infected patients and one transplant recipient. There was no association between outcome and EBV viral load (p = 0.37, unpaired t test).

Epstein–Barr Virus Encephalitis

There were 10 patients with encephalitis (see Table). Seven had impaired immunity (four HIV infections and three transplantations). Signs and symptoms included fever, headache, seizures, aphasia, localized muscle weakness, and numbness or hyperesthesia. CT or magnetic resonance imaging were abnormal in all cases. Typical magnetic resonance findings included single or multiple areas of increased T_2 signal, often with gadolinium enhancement and associated edema in the cerebral hemispheres and cerebellum. One patient, a renal graft recipient (PID 22) who developed clinical and radiological abnormalities in the context of acute EBV infection by serological criteria underwent a brain biopsy, which showed areas of parenchymal and perivascular inflammation with polyclonal T-cell infiltrates, establishing the diagnosis of encephalitis.

The CSF (see Fig) leukocyte counts were elevated in all the patients with encephalitis and invariably showed a predominance of mononuclear cells. Reactive and atypical lymphocytes were each described in one pa-

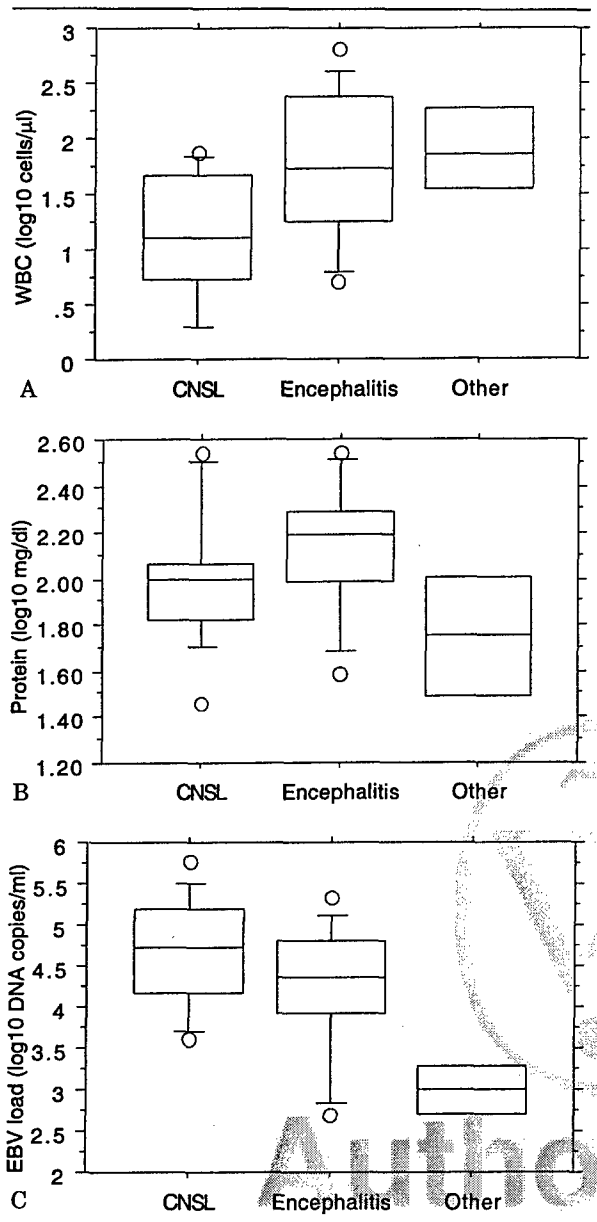

Fig. Cerebrospinal fluid analysis of patients with Epstein–Barr virus (EBV) infection of the central nervous system (CNS). Data were derived from 14 patients with CNS lymphoma (CNSL), 10 with encephalitis, and 4 with postinfectious complications (other). Leukocyte counts (A) were significantly different between CNSL and encephalitis patients ($p = 0.02$) *but not for any other group comparisons* ($p > 0.1$). *Protein concentrations (B) were not statistically different among groups* ($p > 0.1$). *EBV load (C) was significantly lower in patients with postinfectious complications compared with encephalitis or CNSL* ($p < 0.01$). *The difference between CNSL and encephalitis did not quite reach statistical significance* ($p = 0.07$). *WBC = white blood cell (leukocyte)*

tient. Erythrocytes were present in five cases. The CSF protein was elevated and glucose was normal in all cases. The EBV load in the CSF varied between 2.7 and 5.3 $\log_{10}$ DNA copies per milliliter with mean ± SE of 4.2 ± 0.3 $\log_{10}$ copies per milliliter.

Six patients received EBV-specific antiviral therapy. The use of antivirals tended to be more common in patients with higher viral loads ($p = 0.09$, Mann–Whitney U test). This suggests an association between severity of disease and viral load, if we assume that the sicker patients were more likely to receive EBV-specific therapy. Among treated patients, signs of recovery began 2 to 7 days after initiating therapy. Two patients treated with anti-EBV antivirals, who had repeat measurements of EBV load in the CSF 7 and 14 days into therapy, respectively, showed greater than or equal to 1 $\log_{10}$ decreases of the viral load. Two HIV-infected patients with encephalitis had been receiving highly active antiretroviral therapy for 4 years when they developed EBV encephalitis and two started highly active antiretroviral therapy after the diagnosis of EBV infection. Management of immunosuppressive regimens in the three transplant recipients varied. All patients with EBV encephalitis improved clinically, regardless of underlying conditions, use of EBV-specific antiviral therapy, or EBV load.

Postinfectious Complications

Four patients experienced postinfectious complications, one each with Guillain–Barré syndrome, acute demyelinating encephalitis, polyradiculomyelitis, or transverse myelitis (see Table).

CSF examinations showed elevated leukocyte and protein in three cases each, erythrocyte and normal glucose in all cases. The EBV load varied between 2.7 and 3.3 $\log_{10}$ EBV DNA copies per milliliter (mean ± SE, 3 ± 0.2 $\log_{10}$ DNA copies/ml). PIDs 25 and 26 had serological evidence of acute EBV infection.

All patients received immunomodulators (corticosteroids or intravenous immunoglobulin). Three patients also received antivirals. PID 25 died of EBV-associated hemophagocytic syndrome soon after the diagnosis of acute demyelinating encephalitis was established. The other patients improved or remained stable.

Comparative Analysis of Cerebrospinal Fluid Findings in Patients with Epstein–Barr Virus–Associated Central Nervous System Infections

To identify correlations between CSF abnormalities and EBV-associated neurological disorders, the results of EBV quantitative PCR, leukocyte, and protein were compared among the three diagnostic categories. EBV load in the CSF was significantly higher in patients with CNSL and encephalitis versus postinfectious complications ($p < 0.01$). The difference in EBV load between patients with CNSL and encephalitis was not significant, although patients with CNSL had fewer CSF leukocyte ($p = 0.02$). Protein levels were statistically similar among all groups.

Regression analysis was used to determine correlations of EBV load in the CSF with leukocyte counts. There was a significant inverse correlation between EBV load and leukocyte across all diagnostic categories ($p = 0.04$), which argues against the hypothesis that EBV in CSF resulted solely from latent viral DNA present in infiltrating lymphocytes. When patients with encephalitis were separately analyzed, the inverse correlation between EBV load and leukocyte almost reached significance ($p = 0.08$), suggesting that the inflammatory infiltrate might contribute to viral clearance.

Identification of mRNA Corresponding to a Lytic Cycle Gene in the Cerebrospinal Fluid

Twelve CSF samples were tested by RT-PCR for transcription of the lytic cycle gene *BZLF1*. Ten samples, equally distributed between CNSL and encephalitis patients, which contained 4.5 to 5.8 $\log_{10}$ EBV DNA copies per milliliter, showed evidence of mRNA synthesis indicating active EBV replication in the CNS. In the remaining two samples, both DNA and RNA amplification failed, indicating decreased sequence homology between the primers the template and/or DNA copy number below the analytical sensitivity of the test.

Discussion

EBV PCR of the CSF established the association of neurological disorders with EBV in the absence of acute EBV infection. Most descriptions of the neurological complications of EBV are based on children with acute EBV infection.[1–7] In contrast, only 17% of our patients were children, despite the fact that users of the laboratory for EBV PCR include a similar number of adult and pediatric health care facilities. This preponderance of EBV CNS infections in adults, which differs from previous reports, could be partially ascribed to the high number of immunocompromised patients in our study. However, all three immunocompetent patients with EBV encephalitis were older than 18 years of age. Other investigators have also recently described isolated cases of EBV encephalomyelitis in adults with serological evidence of EBV reactivation.[27–29]

AQ: 6

CSF analysis showed significant differences among diagnostic categories for EBV load and leukocytes. Patients with CNSL had high CSF EBV load in the presence of low leukocyte counts. Patients with encephalitis also had relatively high EBV load, but this was associated with higher leukocyte than in patients with CNSL. Patients with postinfectious complications of EBV infection had a low EBV load associated with a relatively high leukocyte. These CSF patterns suggest the following pathogenic scenarios: rapid cellular and viral turnover with limited inflammatory response in CNSL, intense viral replication and vigorous inflammation associated with encephalitis, and low viral replication and vigorous inflammation associated with postinfectious complications.

Antivirals active against EBV were used in some patients, but their use did not affect the outcome of the disease. However, a selection bias favoring the use of antivirals in the sickest population might have occurred. This is suggested by the fact that, among patients with encephalitis, the use of acyclovir and ganciclovir was more common in individuals with high viral loads. This observation also might indicate an association between high CSF EBV load and severity of clinical manifestations, if we assume that physicians were more likely to treat sicker patients. Of note, the CSF EBV load decreased in the two encephalitis patients whose CSF was tested after 7 and 14 days of treatment, respectively, suggesting that the drugs inhibited the viral replication.

The presence of lytic cycle mRNA in the CSF in all 10 patients in whom this could be analyzed indicated that EBV was actively replicating in the CNS. This result is consistent with a lack of correlation between CSF EBV viral load and CSF leukocyte, which strongly suggests that the EBV DNA detected by PCR was from actively replicating virus and not just latent EBV DNA carried in inflammatory cells. Actively replicating EBV in the CNS may have resulted from either de novo infection or reactivation of latent virus. Because EBV does not become latent in neurons or other nonlymphoid cells, if CNS infection follows EBV reactivation, it is likely that this occurs at extraneural sites with subsequent spread of virus to CNS by infected lymphocytes.

It has been suggested previously that EBV encephalitis was a consequence of cytotoxic T-lymphocyte–mediated tissue destruction.[30] In this series, two patients with encephalitis had CSF atypical lymphocytes, consistent with cytotoxic T lymphocytes. Furthermore, EBV load decreased with higher leukocyte counts, suggesting a role of the inflammatory cells in viral clearance. These data taken collectively indicate that patients with severe EBV encephalitis might benefit from combined antiviral and T-cell immunosuppressive therapy.

This study was supported by grants from National Institute of Child Health and Human Development and AIDS Clinical Trials Group (A.W.) and by grants from the Department of Defense, Department of Veterans Affairs, and the Reuler-Lewin Family Professorship of Neurology (K.L.T.).

We thank Drs Judith Anderson, Asad Ansari, Michelle Barron, William Burman, David Cohn, Steven Johnson, Marie Landry, Joseph Nania, and Wheat Williams for referring the patient specimens and providing the clinical information, and Dr Myron Levin for critical review of the manuscript.

AQ: 7

References

1. Connelly KP, DeWitt LD. Neurologic complications of infectious mononucleosis. Pediatr Neurol 1994;10:181–184.
2. Cotton MF, Reiley T, Robinson CC, et al. Acute aqueductal stenosis in a patient with Epstein-Barr virus infectious mononucleosis. Pediatr Infect Dis J 1994;13:224–227.
3. Anderson MD, Kennedy CA, Lewis AW. Retrobulbar neuritis complicating acute Epstein-Barr virus infection. Clin Infect Dis 1994;18:799–801.
4. Tsutsumi H, Kamazaki H, Nakata S, et al. Sequential development of acute meningoencephalitis and transverse myelitis caused by Epstein-Barr virus during infectious mononucleosis. Pediatr Infect Dis J 1994;13:665–667.
5. Connolly M, Junker AK, Chan KW, et al. Cranial neuropathy, polyneurophathy and thrombocytopenia with Epstein-Barr virus infection. Dev Med Child Neurol 1994;36:1010–1015.
6. Grose C, Henle W, Henle G, et al. Primary Epstein-Barr virus infections in acute neurologic diseases. N Engl J Med 1975; 292:392–395.
7. Alpert G, Fleisher GR. Complications of infection with Epstein-Barr virus during childhood: a study of children admitted to the hospital. Pediatr Infect Dis J 1984;3:304–307.
8. Hochberg IH, Miller G, Schooley RT, et al. Central-nervous-system lymphoma related to Epstein-Barr virus. N Engl J Med 1983;309:745–748.
9. Cinque P, Brytting M, Vago L, et al. Epstein-Barr virus DNA in cerebrospinal fluid from patients with AIDS-related primary lymphoma of the central nervous system. Lancet 1993;342: 398–401.
10. Meerbach A, Gruhn B, Egerer R, et al. Semiquantitative PCR analysis of Epstein Barr virus DNA in clinical samples of patients with EBV-associated diseases. J Med Virol 2001;65: 348–357.
11. Jones JL, Hanson DL, Dworkin MS, et al. Effect of antiretroviral therapy on recent trends in selected cancers among HIV-infected persons. J Acquir Immune Defic Syndr 1999; 21(suppl):11–17.
12. Buchbinder SP, Holmberg SD, Scheer S, et al. Combination antiretroviral therapy and incidence of AIDS-related malignancies. J Acquir Immune Defic Syndr 1999;21(suppl):23–25.
13. Palella FP Jr, Delaney KM, Moorman AC, et al. Declining morbidity and mortality among patients with advanced human immunodeficiency virus infection. New Engl J Med 1998;338: 853–860.
14. Halsted CC, Chang RS. Infectious mononucleosis and encephalitis: recovery of EB virus from spinal fluid. Exp Reason 1979;64:257–258.
15. Schiff JA, Schaefer JA, Robinson JE. Epstein-Barr virus in cerebrospinal fluid during infectious mononucleosis encephalitis. Yale J Biol Med 1982;55:59–63
16. Joncas JH, Chicoine L, Thivierge R, et al. Epstein-Barr virus antibodies in the cerebrospinal fluid: a case of infectious mononucleosis with encephalitis. Am J Dis Child 1974;127: 282–285.
17. Bray PF, Culp KW, McFarlin DE, et al. Demyelinating disease after neurologically complicated primary Epstein-Barr virus infection. Neurology 1992;42: 278–282.
18. Paskavitz JF, Anderson CA, Filley CM, et al. Acute arcuate fiber demyelinating encephalopathy following Epstein-Barr virus infection. Ann Neurol 1995;38:127–131.
19. Cinque, P, Vago L, Dahl H, et al. Polymerase chain reaction on cerebrospinal fluid for diagnosis of virus-associated opportunistic diseases of the central nervous system in HIV-infected patients. AIDS 1996;10:951–958.
20. D'Arminio Monforte A, Cinque P, Vago L, et al. A comparison of brain biopsy and CSF-PCR in the diagnosis of CNS lesions in AIDS patients. J Neurol 1997;244:35–39.
21. Pedneault L, Katz BZ, Miller G. Detection of Epstein-Barr virus in the brain by the polymerase chain reaction. Ann Neurol 1992;32:184–192.
22. Weinberg A, Spiers D, Cai GY, et al. Evaluation of a commercial polymerase chain reaction kit for the diagnosis of CMV infection of the central nervous system. J Clin Microbiol 1998; 11:3382–3384.
23. Weinberg A, Hodges TN, Li S, et al. A comparison of polymerase chain reaction, antigenemia and rapid blood culture for the detection and prevention of cytomegalovirus disease after lung transplantation. J Clin Microbiol 2000;38:768.
24. Zhang JX, Chen HL, Zong YS, et al. Epstein-Barr virus expression within keratinizing nasopharyngeal carcinoma. J Med Virol 1998;55:227–233.
25. Chen HL, Lung ML, Chan KH, et al. Tissue distribution of Epstein-Barr virus genotypes. J Virol 1996;70:7301–7305.
26. Majid A, Galett SL, Sweeney CJ, et al. Epstein-Barr virus myeloradiculitis and ecephalomyeloradiculitis. Brain 2002;125: 159–165.
27. Imai S, Usui N, Sugiura M, et al. Epstein-Barr virus genomic sequences and specific antibodies in cerebrospinal fluid in children with neurologic complications of acute and reactivated EBV infections. J Med Virol 1993;40:278–284.
28. Bray PF, Culp KW, McFarlin DE, et al. Demyelinating disease after neurologically complicated primary Epstein-Barr virus infection. Neurology 1992;42:278–282.
29. Tselis, A, Duman R, Storch GA, et al. Epstein-Barr virus encephalomyelitis diagnosed by polymerase chain reaction: detection of the genome in the CSF. Neurology 1997;48: 1351–1355.
30. Lehrnbecher T, Chittka B, Nanan R, et al. Activated T lymphocytes in the cerebrospinal fluid of a patient with Epstein-Barr virus-associated meningoencephalitis. Pediatr Infect Dis J 1996;15:631–632.